AD NUMBER: AD0103963
LIMITATION CHANGES
TO: Approved for public release; distribution is unlimited.
FROM: Distribution authorized to U.S. Gov't. agencies and their contractors; Administrative/Operational Use; 1 Oct 1955. Other requests shall be referred to the Air Force Wright Air Development Center, Wright-Patterson AFB, OH 45433.
AUTHORITY
PB130358, 21 SEP 1977

WADC TECHNICAL REPORT 55-294

FC

A STUDY OF CANOPY SHAPES AND STRESSES FOR PARACHUTES IN STEADY DESCENT

A. D. TOPPING
J. D. MARKETOS
N. C. COSTAKOS

GOODYEAR AIRCRAFT CORPORATION
AKRON, OHIO

OCTOBER 1955

WRIGHT AIR DEVELOPMENT CENTER

WADC TECHNICAL REPORT 55-294

A STUDY OF CANOPY SHAPES AND STRESSES FOR PARACHUTES IN STEADY DESCENT

A. D. TOPPING

J. D. MARKETOS

N. C. COSTAKOS

GOODYEAR AIRCRAFT CORPORATION

AKRON, OHIO

GER 7071

OCTOBER 1955

EQUIPMENT LABORATORY

CONTRACT No. AF 33(616)-2445

PROJECT No. 6065

TASK No. 61512

WRIGHT AIR DEVELOPMENT CENTER

AIR RESEARCH AND DEVELOPMENT COMMAND

UNITED STATES AIR FORCE

WRIGHT-PATTERSON AIR FORCE BASE, OHIO

Carpenter Litho & Prtg. Co., Springfield, O.

100 - September 1956

FOREWORD

This report was prepared by Goodyear Aircraft Corporation, Akron, Ohio; on USAF Contract No. AF33(616)-2445. The contract was initiated under Project No. 6065-61512, "Study of Parachute Canopy Shapes and Stresses", and was administered under the direction of the Parachute Branch of the Equipment Laboratory of Wright Air Development Center, with Mr. A. M. Hegele acting as project engineer.

The work was coordinated at Goodyear Aircraft Corporation by Dr. R. S. Ross and Mr. F. J. Stimler of the Research and Development Department. The authors, members of the Structural Analysis Department, were assisted in the detailed solutions and numerical calculations by Mr. S. L. Gugleta, Mr. A. H. Jaffe, Mr. R. L. Swart and Mrs. G. L. Whitlock, also of the Structural Analysis Department.

Valuable assistance to this project has been given by Dr. H. G. Heinrich and Mr. G. E. Aichinger of WADC.

ABSTRACT

Analytical solutions for the fully inflated shapes of the circular canopies of flat, extended skirt, conical, personnel guide surface, and conical ring slot parachutes in steady descent are given. The solution for the flat canopy uses as a first approximation the Taylor curve, and after taking into account the fullness of the gores, yields a shape having a rounded apex rather than the flat top characteristic of the Taylor curve. The solution for the flat canopy is found to be adaptable to all the other canopies except the conical, even though both the conical ring slot and the personnel guide surface canopies are conical. An entirely new solution is developed for the conical canopy by obtaining a first approximation that neglects gore fullness and then altering this by taking fullness into account. Several representative dimensions obtained from each analytical solution agree with corresponding dimensions obtained from a photograph within 9% — within about 4% for the flat canopy, the only type analyzed which has been given previous theoretical study. The earlier theory differs from the flat canopy photograph by as much as 8.8%. These discrepancies are probably due only in part to theoretical inaccuracies.

Cord tensions and cloth stresses consistent with the analytically determined shapes are calculated. The effects of varying such parameters as the suspension line length, number of gores, and cone angle, as well as the effect of design details such as shortness of lines over the canopy, extra gore fullness at the vent, bias gores, and reinforcement details, are studied.

PUBLICATION APPROVAL

This report has been reviewed and is approved.

FOR THE COMMANDER

ROBERT A. BARRERE
Colonel, USAF
Chief, Equipment Laboratory

TABLE OF CONTENTS

Section		Page
	Introduction and Review of Literature	1
1.	Basic Theoretical Shapes and Cord Tensions	9
1.1	Shape of Flat Canopy from Apex to Maximum Inflated Radius . .	10
1.2	Non-Dimensional Cartesian Coordinates x/x_m and z/x_m of the Points of Taylor's Curve Given by the Equation $x = x_m \sqrt{\sin \phi}$	21
1.3	Portion of Cord Between Maximum Inflated Radius and Skirt . .	24
1.4	Complete Solution for the Shape of the Cord and Suspension Line of a Flat Canopy	30
1.5	Effect of Variation of the Parameter a_m on Flat Canopy Cord Shape	36
1.6	Extended Skirt Canopy	45
1.7	Equation of the Cords for the Conical Canopy - First Approximation	49
1.8	Equation of the Cords for the Conical Canopy - Second Approximation	65
1.9	Personnel Guide Surface Canopy	95
1.10	Conical Ring Slot Canopy	106
1.11	Comparison of Cord Shapes of Five Different Canopies in the Fully Inflated Equilibrium Condition Holding the Parameters l_c, l_s' and N Constant	111
1.12	Calculated Cord Tensions of Five Canopy Types with Common l_c, l_s', N, and Differential Pressure p	119
2.	Comparison of Theoretical with Photographically Determined Canopy Shapes	124
2.1	Comparison of the Theoretical with the Photographically Determined Shape of a Fully Inflated Flat Canopy. (Type D_o = 28 ft, N = 28, l_c = 14 ft, l_s = 22 ft 10 in)	126

Section		Page
2.2	Comparison of the Theoretical with the Photographically Determined Shape of a Fully Inflated Extended Skirt Canopy. (Type T-10, D_o = 35 ft, N = 30, l_c = 17.90 ft, l_s = 25.5 ft)	136
2.3	Comparison of the Theoretical with the Photographically Determined Shape of a Fully Inflated Conical Canopy. (N = 24, β = 30°, l_c = 14 ft, l_s = 22 ft 10 in)	144
2.4	Comparison of the Theoretical with the Photographically Determined Shape of a Fully Inflated Personnel Guide Surface Canopy. (Type C-11, D_o = 30 ft, N = 24, β = 30°, l_c = 13.857 ft, l_s = 30 ft)	150
2.5	Comparison of the Theoretical with the Photographically Determined Shape of a Fully Inflated Conical Ring Slot Canopy. (D_o = 22 ft, N = 32, β = 25°, l_c = 11.55 ft, l_s = 22 ft) .	156
2.6	Comparison of Taylor Shape with Present Theory and with the Photographically Determined Shape of a Fully Inflated Flat Type Canopy Holding l_c and l'_s Constant	162
2.7	Analysis of the Tension and Loading in the Cord of the Flat Canopy Using the Intrinsic Equation of Equilibrium for Heavy Cords	166
3.	Effects of Various Parameters on Canopy Shapes and Stresses .	171
3.1	Effect of Suspension Line Length on the Cord Shape of a Flat Canopy	172
3.2	Effects of Cone Angle Variation on the Canopy Shape and Stresses of a Conical Canopy	177
3.3	Effect on Canopy Shapes and Stresses of Cloth Fullness at the Vent of Six Different Canopies	188
3.4	Effect of Shortness of Cords on Cord Shape and Fabric Stresses of a Flat Canopy	193
3.5	Effect of Rib, Skirt and Vent Reinforcement, and Shortness of Vent Lines on Canopy Shape and Stresses	195
3.6	Effect of Number of Gores on Canopy Shape	202

TABLE OF CONTENTS (CONT)

Section		Page
4.	Cloth Stresses	207
4.1	Variation of Cloth Stresses with Distance from the Apex for Five Canopy Shapes	208
4.2	Effect of Cloth Stress in Straight and Bias Gores	219
4.3	Experimental Determination of Stress-Strain Relations in Cloth and Fabric	225
4.4	Effect of Cloth Stresses on Porosity	242
5.	Conclusions, Recommendations, and References	252
5.1	Summary and Conclusions	252
5.2	Recommendations	256
5.3	References	258

LIST OF ILLUSTRATIONS

Figure		Page
1	. . . . .	4
1.1.1	. . . . .	12
1.1.2	. . . . .	13
1.1.3	. . . . .	14
1.1.4	. . . . .	15
1.1.5	. . . . .	17
1.1.6	Cord Curve for a Flat Canopy from Apex to Maximum Inflated Radius	20
1.2.1	. . . . .	21
1.3.1	. . . . .	24
1.4.1	Cord Shape of a Flat Canopy	35
1.5.1	Variation of L/r_1 vs ϕ for Various Values of sin α_m	37
1.6.1	. . . . .	45
1.7.1	. . . . .	49
1.7.2	. . . . .	50
1.7.3	. . . . .	50
1.7.4	. . . . .	51
1.7.5	. . . . .	60
1.7.6	Graphical Solution of Equation (1.7.28) - $\phi_B = 72.65°$	63
1.7.7	Cord Shape of a Conical Canopy. First Approximation. N = 24, $\beta = 30°$, $l_c/l_s' = .6$	64
1.8.1	. . . . .	65
1.8.2	. . . . .	65
1.8.3	. . . . .	66
1.8.4	. . . . .	66

Figure		Page
1.8.5	. . . . .	66
1.8.6	. . . . .	68
1.8.7	. . . . .	69
1.8.8	. . . . .	69
1.8.9	. . . . .	73
1.8.10	. . . . .	77
1.8.11	Intersection of Curve OH_1F with the Straight Lines (1.8.15) . . .	79
1.8.12	. . . . .	83
1.8.13	Cord Shape of a Conical Canopy - First and Second Approximations ($N = 24$, $l_c/l_s = .6$, common x_m)	94
1.9.1	. . . . .	95
1.9.2	. . . . .	95
1.9.3	. . . . .	97
1.9.4	Variation of α vs ϕ	101
1.9.5	. . . . .	102
1.10.1	. . . . .	106
1.11.1	Comparison of Theoretical Cord Shapes of Five Different Canopy Types in Fully Inflated Equilibrium Condition with Constant l_c, l_s' and N ($N = 24$, $l_c/l_s' = .6$ for all five types)	118
1.12.1	Cord Tensions in Five Canopy Types having Common $l_c = 10$ ft, $l_s' = 10/.6$ ft, $N = 24$ and Differential Pressure p	123
2.1.1	. . . . .	126
2.1.2	. . . . .	129
2.1.3	. . . . .	131
2.1.4	Representative Photograph of a Fully Inflated Flat Canopy (T-7) .	134
2.1.5	Comparison of Theoretical with Photographically Determined Shape of a Fully Inflated Flat Canopy. (Type T-7 $D_o = 28$ ft, $N = 28$, $l_c = 14$ ft, $l_s = 22$ ft 10 in.)	135

Figure		Page
2.2.1	. . . . .	136
2.2.2	. . . . .	136
2.2.3	. . . . .	139
2.2.4	Representative Photograph of a Fully Inflated Extended Skirt Canopy (T-10)	142
2.2.5	Comparison of Theoretical with Photographically Determined Shape of a Fully Inflated Extended Skirt Canopy. (Type T-10, D_o = 35 ft, N = 30, l_c = 17.90 ft, l_s = 25.5 ft)	143
2.3.1	. . . . .	146
2.3.2	Representative Photograph of a Fully Inflated Conical Canopy . . .	148
2.3.3	Comparison of Theoretical with Photographically Determined Shape of a Fully Inflated Conical Canopy (N = 24, β = 30°, l_c = 14 ft, l_s = 22 ft 10 in.)	149
2.4.1	. . . . .	150
2.4.2	. . . . .	151
2.4.3	Representative Photograph of a Fully Inflated Personnel Guide Surface Canopy (C-11)	154
2.4.4	Comparison of Theoretical with Photographically Determined Shape of a Fully Inflated Personnel Guide Surface Canopy (Type C-11, D_o = 30 ft, N = 24, β = 30°, l_c = 13.857 ft, l_s = 30 ft) . . .	155
2.5.1	Representative Photograph of a Fully Inflated Conical Ring Slot Canopy	160
2.5.2	Comparison of Theoretical with Photographically Determined Shape of a Fully Inflated Conical Ring Slot Canopy (N = 32, β = 25°, l_c = 11.55 ft, l_s = 22 ft)	161
2.6.1	. . . . .	162
2.7.1	. . . . .	167
3.1.1	Cord Shapes of a Flat Canopy with Different Ratios l_c/l_s' but with the same l_c	176
3.2.1	Cord Curves for Various Cone Angles β	179
3.3.1	. . . . .	188

Figure		Page
3.3.2	Effect of 10% Extra Fullness on Cloth Stress	192
3.5.1	Section Normal to Parachute Axis (One Gore)	195
3.5.2	Sketches of Vent Reinforcements for a 28-Foot Flat Canopy . . .	196
3.5.3	Sketches of Vent Reinforcements for a 35-Foot Extended Skirt Canopy	197
3.5.4	Fullness and Circumferential Stresses at the Vent	198
3.5.5	Sketch Showing Stresses Acting on a Strip of Vent Reinforcement Between two Adjacent Cords. (Air Pressure is not shown) . . .	199
3.5.6	Sketch of Vent Strip of Figure 3.5.5 above with and without Fullness and Cord Shortness	199
3.6.1	. . . . .	202
3.6.2	Comparison of Cord Shape for Flat Canopies with Same T/p and Showing the Effect of the Number of Gores on Cord Shape and Angle of Suspension Lines	205
3.6.3	Effect of Number of Gores on Maximum Inflated Radius in a Flat Canopy	206
4.1.1	. . . . .	209
4.1.2	Variation of Cloth Stresses with Distance from the Apex for Five Canopy Shapes	218
4.2.1	Plots of $\tan \alpha \tan \beta = \sigma_1 / \sigma_2$	223
4.2.2	Stress-Strain Conditions at Centerline of Gore	224
4.3.1	Close up of GAC Small Biaxial Tester Used for Testing of Nylon Parachute Cloth	229
4.3.2	GAC Small Biaxial Tester for Fabric and Its Allied Instrumentation	230
4.3.3	GAC Fabric Strain Micrometer with Sketch Showing Construction and Operating Principles	231
4.3.4	Normal Characteristics of Rip-Stop Nylon Cloth	232
4.3.5	Normal Characteristics of Rip-Stop Nylon Cloth	233

Figure		Page
4.3.6		234
4.3.7	Normal Characteristics of Tow-Target Cloth	235
4.3.8	Normal Characteristics of Tow-Target Cloth	236
4.3.9	Roller Type Elongation Indicator (RTEI)	237
4.3.10	Roller Type Elongation Indicator, Deflected	238
4.3.11	Strain Measurements in Parachute Cloth	239
4.3.12	Strain Measurements in Parachute Cloth	240
4.3.13	Strain Measurements in Airship Fabrics	241
4.4.1	Thread Extension	242
4.4.2	Thread Shear	244
4.4.3	Thread Shear with $\sigma_1/\sigma_2 = 3$	245
4.4.4	Location of Panels for Canopy	248
4.4.5	Spherical Cloth Shape	249

LIST OF TABLES

Table		Page
1.1.1	Values of L/r_1 for Various Values of ϕ	17
1.1.2	Values of x/x_m and z/x_m for Various Values of ϕ	19
1.2.1	Values of x/x_m and z/x_m vs ϕ for a Taylor Curve	23
1.3.1	Values of $f(n) = 2n + (n^2 - 1) \log \frac{n+1}{n-1}$ vs n	29
1.4.1	Cord Coordinates from Apex to MIR	34
1.4.2	Cord Coordinates from MIR to Skirt	34
1.5.1	Values of the Ratio L/r_1 vs ϕ ($0 \leq \phi \leq 45°$)	38
1.5.2	Values of the Ratio L/r_1 vs ϕ ($45° \leq \phi \leq 90°$)	39
1.5.3	Values of x/x_m and z/x_m vs ϕ ($0 \leq \phi \leq 45°$) for a Flat Canopy with $\sin \alpha_m = .9, .8$ and $.7$	42
1.5.4	x/x_m and z/x_m for $\phi = \pi/4$ and Various Values of $\sin \alpha_m$	44
1.6.1	Values of x/x_m and z/x_m vs ϕ	46
1.7.1	Values of x/x_m, s/x_m, s/x_m vs ϕ for a Conical Canopy - First Approximation	58
1.7.2	Values of $\frac{.6}{\cos \phi}$ and $\frac{2\,\widehat{OC} - \widehat{OB}}{x_B}$ vs ϕ	62
1.8.1	Values of x_1, z_1, ϕ_1 ($N = 24$)	71
1.8.2	Values of H_1 G_1 and Coordinates x_2, z_2 vs ϕ	75
1.8.3	Values of $K = G_1F/x_m$ vs ϕ	80
1.8.4	Values of α vs ϕ	82
1.8.5	Values of I_A, I_B, Q and x/x_m vs ϕ	87
1.8.6	Values of z/x_m and s/x_m vs ϕ	91

Table		Page
1.9.1	Values of α vs ϕ	100
1.11.1	Coordinates of Several Points of the Parabolic Arc. Z's are Measured from MIR Downward	115
1.11.2	Coordinates of Several Points of the Cord of a Conical Canopy with 24 Gores, $l_c/l_s' = .6$ and $l_c = 10$ ft	116
1.11.3	Coordinates of Several Points of the Cords of Flat, Extended Skirt, Ring Slot, and Personnel Guide Surface Canopies Having N = 24, $l_c/l_s' = .6$, and $l_c = 10$ ft	117
1.12.1	Values of T/p vs s for a Conical Canopy in the 1st Approximation	122
2.1.1	Coordinates of Several Points of the Parabolic Portion	128
2.1.2	Non-Dimensional and Absolute Coordinates of Several Points on the Cord from Apex to Skirt	128
2.1.3	Coordinates of Gore Centerline for $0 \leq \phi \leq 45°$	132
2.1.4	Coordinates of Gore Centerline for $43° 52' \leq \phi_g \leq 90°$	133
2.2.1	Cord Coordinates from Apex to MIR	137
2.2.2	Coordinates of Several Points of the Parabolic Portion	138
2.2.3	Coordinates of Gore Centerline for $0 \leq \phi \leq 45°$	141
2.2.4	Coordinates of Gore Centerline for $43° 56' \leq \phi_g \leq 90°$	141
2.3.1	Cord Coordinates for a Conical Canopy	145
2.3.2	Coordinates of the Theoretical Gore Centerline	147
2.4.1	Cord Coordinates for a Personnel Guide Surface Canopy	151
2.4.2	Coordinates for Gore Centerline for $0 \leq \phi \leq 45°$	153
2.4.3	Coordinates of Gore Centerline for $43° 43' \leq \phi_g \leq 90°$	153
2.5.1	Cord Coordinates for a Conical Ring Slot Canopy	157
2.5.2	Coordinates for Gore Centerline for $0 \leq \phi \leq 45°$	159
2.5.3	Coordinates for Gore Centerline for $44° \leq \phi_g \leq 90°$	159

Table		Page
2.6.1	Cord Coordinates for Taylor Curves and Flat Canopy with Common l_c and l_s'	165
3.1.1	Values of θ and x_m vs l_c/l_s' of a Flat Canopy with l_c = 10 ft	172
3.1.2	Coordinates of Points of Cord on a Parabolic Arc for Different Values of l_c/l_s' for a Flat Canopy	173
3.1.3	Actual Values of Coordinates of the Cord with Different Values of l_c/l_s'	174
3.2.1	Coordinates of Cord for Various Cone Angles β	178
3.2.2	Values of s/x_m vs ϕ for Several Cone Angles	182
3.2.3	Values of T and f_1 vs ϕ and Absolute Coordinates x and z of a Conical Canopy for Several Cone Angles β. N = 24, l_c = 14 ft, l_c/l_s' = .6	185
3.3.1	The Angle ξ''	189
3.3.2	Values of r_{1_v} and r_1 for Three Canopies	191
3.3.3	r_1 for a Flat Canopy, Type T-7	192
4.1.1	Values of r_1 vs ϕ ($45° \leq \phi \leq 90°$) for a Flat Canopy (T-7)	209
4.1.2	Values of r_1 vs ϕ ($45° \leq \phi \leq 90°$) for a Extended Skirt Canopy (T-10)	210
4.1.3	Values of f_1/p and s vs ϕ for a Conical Canopy in the First Approximation	211
4.1.4	Values of s and r_1 vs ϕ for a Conical Canopy	213
4.1.5	Values of r_1 vs ϕ ($45° \leq \phi \leq 90°$) for a Conical Ring Slot Canopy	214
4.1.6	Values of r_1 vs ϕ ($45° \leq \phi \leq 90°$) for a Personnel Guide Surface Canopy	215
4.1.7	Values of s vs ϕ for a T-7, T-10, Ring Slot, and Personnel Guide Surface Canopies	217
4.4.1	Porosity Measurements on a Canopy of 1.1 oz. Nylon Rip-Stop Spec MIL-C-7020 Type I. (Reference 26)	247

Table		Page
4.4.2	Cloth Stress During Porosity Test	251
5.1.1	Deviations of Theoretical Inflated Canopy Dimensions from Their Photographically Determined Values	252
5.1.2	Comparison of Load-Carrying Capacity of Five Theoretical Canopy Shapes	253
5.1.3	Comparison of Drag Characteristics of Five Canopy Shapes . .	254

LIST OF SYMBOLS,

ABBREVIATIONS, AND DEFINITIONS

Axis of Parachute	The axis of symmetry (assumed vertical) of the surface of revolution containing the cords.
Plane P_1	Any plane formed by the normals erected at two points equidistant from the apex on adjacent cords and passing through the axis of the canopy.
A_{sk}	Projected area of one gore on the horizontal plane at the skirt.
D_o	Nominal diameter, that is the diameter of any design of parachute canopy based upon a circle having an area equal to the cloth area.
f_1	Tensile force per unit length in the section of the canopy cut by a plane P_1.
f_2	Tensile force per unit length in the direction of a line determined by the intersection of the canopy with an axial plane.
$f(n)$	$2n + (n^2 - 1) \log \frac{n + 1}{n - 1}$
dF	Increment of tensile force collinear with f_1 along a canopy strip corresponding to a length ds of the cord.
F_t	Tensile strength of the cloth per unit length.
k_a	Non-dimensional ratio l_a/x_m

k_c	Non-dimensional ratio l_c/x_m
k'_s	Non-dimensional ratio l'_s/x_m
k_{sk}	Non-dimensional ratio x_{sk}/x_m
l_a	Length of the cord from the apex to the maximum inflated radius.
l_b	Length of the cord from the maximum inflated radius to the skirt.
l_c	Length of the cord from the apex to the skirt.
l_s	Length of the suspension line, that is of that portion of the cord between the skirt and the upper point of the riser.
l'_s	The distance from the skirt to the axis of the canopy measured along the tangent to the cord at the skirt.
n	csc θ
N	Number of suspension lines.
p	Differential pressure between inside and outside of the parachute canopy.
r_1	Radius of curvature of the line which results as the intersection of one inflated gore by a plane P_1.
r_{1v}	Value of r_1 when the plane P_1 passes through the edge of the vent.
r_2	Radius of curvature of the line of intersection of the inflated canopy by an axial plane.

r_{sk}	Boundary value of r_1 for a plane P_1 passing through the skirt.
R	Load per unit cord length normal to the cord.
s	Distance from the apex measured along the cord line to a point on the cord.
s_o	Length of that straight portion of the cord over the canopy of an inflated conical solid parachute.
s_g	Distance to a point on the canopy measured from the apex along the plane curve formed by the intersection of the canopy with the axial plane bisecting the inflated gore.
s_m	Distance along the cord from the apex to the MIR.
s_{gm}	Distance from the apex measured along the centerline of the gore to the point most distant from the apex.
s_v	Distance from the apex measured along the cord to the edge of the vent.
T	Tensile force in the cord.
W	Total weight of suspended load and parachute.
W_b	Weight of suspended load.
x, z	Rectangular coordinates of points on the cord.
x_m = MIR	Maximum inflated radius of cord (MIR), i.e. maximum value of x.

x_g, z_g	Rectangular coordinates of points on the centerline of the gore.
x_{gm}	Maximum value of x_g.
x_{sk}	Value of x at the skirt.
$x_{sk}^{(T)}$	Value of x_{sk} for a theoretical cord shape.
$x_{sk}^{(P)}$	Value of x_{sk} for a photographical cord shape.
x_v	Value of x at the edge of the vent.
z_m	Vertical distance from apex to MIR.
z_{sk}	Value of z at the skirt.
X, Z	Cartesian coordinates of that portion of the cord below MIR with respect to a set of axes X, Z, whose origin is the point (x_m, z_m).
α	The half-angle formed by the extreme radii of curvature of a plane curve determined by the intersection of one inflated gore with a plane P_1.
α_m	Value of α corresponding to the MIR.
α_{sk}	Value of α corresponding to the skirt.
β	Constructed cone angle of a conical canopy.
θ	The angle between suspension lines and the axis of canopy.
$\theta^{(P)}$	Value of θ for a photographical cord shape.
$\theta^{(T)}$	Value of θ for a theoretical cord shape.

2λ	The angle between the tangents of two adjacent cords at points equidistant from the apex.
2ξ	The angle of a flat gore.
$2\xi'$	The angle between two adjacent cords on the conical surface formed by the uninflated canopy of a conical parachute.
ρ	Radius of curvature of the cord.
ρ_m	Value of ρ at the MIR.
σ_1, σ_2	Principal stresses in a gore (lbs/in).
ϕ	Angle formed by the normal at any point on a cord line and the canopy axis.
ω	Angular measurement about the vertical axis.

NOTE: Secondary symbols not listed above are defined in the text where they are introduced.

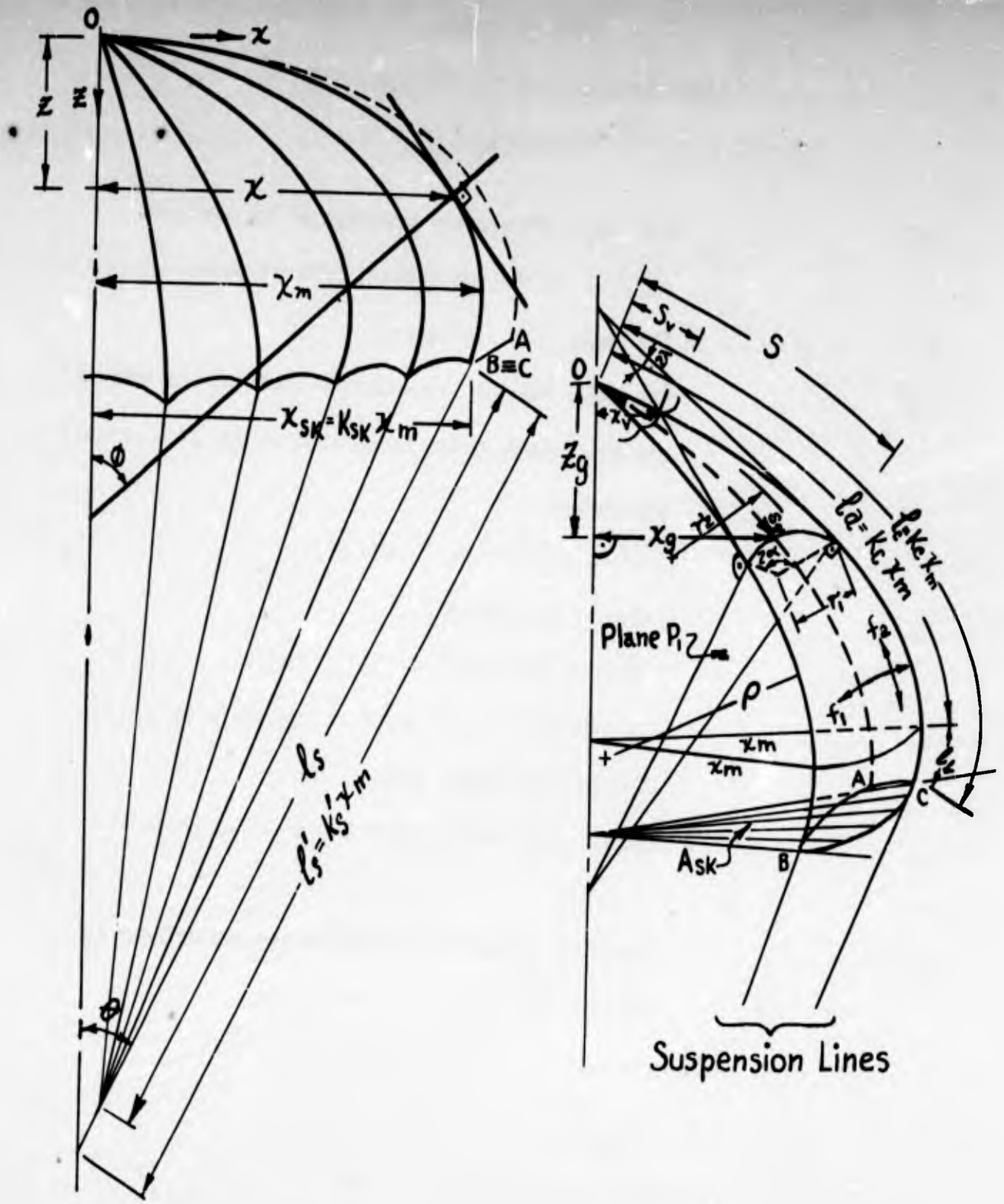

Schematic Definition of Terms used in Stress Analysis of the Canopy

INTRODUCTION AND REVIEW OF LITERATURE

The importance of knowing the stress distribution in parachutes and its relation to parachute strength lies, as in all airborne structures and equipment, in the necessity for minimizing weight, since stress analysis is an indispensable element in light-weight design where strength is a factor. The need for minimum weight is emphasized by the fact that personnel escape parachutes may be used only once (if at all) in the life of many aircraft, and are merely dead weight most of the time. Paratroop tactics and the widening utilization of parachutes for stabilization, missile recovery, parabrakes, and cargo dropping, as well as in devices for escape from aircraft at extreme speeds and altitudes, make the problem one of major importance.

The development of parachutes to meet the new needs has proceeded chiefly along empirical lines, but, as more than one scientist has pointed out, experiments do not lead to understanding except when they test the validity of a previously developed theory. Parachute technology has now advanced to the point where empirical methods need to be supplemented by analytical treatments.

The determination of stresses in a parachute is essentially an aeroelastic problem (insofar as the cloth and cords may be said to be elastic), and experience with structural failures in parachutes, as well as measurements of snatch and opening shock forces, indicate that the critical stresses occur during the opening process. The steady state problem is of interest, nevertheless, because the maximum stresses in the infinite mass case, which approximates conditions of deployment for braking applications, seem to occur when the parachute

is fully, or almost fully, opened. The steady descent problem may also serve as a helpful preliminary to the more difficult and important problem of the determination of critical transient stresses during opening by indicating the probable influence of some of the parameters.

The stresses in a parachute canopy are dependent upon the inflated shape, which in turn depends on the stress distribution so that the two things are inseparable; however, it is possible to get visual checks on the shape while the stress distribution can be observed only indirectly and with some difficulty. In fact, in the case of parachute canopies, no such experimental data is as yet available. Much of the present work therefore consists of calculating shapes from assumed stress distributions.

There is an imposing array of parameters which influence canopy shapes and stresses; for example, gore pattern, number of gores, size, the ratio of suspension line length to canopy cord length, stress-strain properties of the cloth and cords, cloth weave, direction of cloth warp, and design details such as seam and vent reinforcements. While the present work does not attempt to account for all such factors in one all-enveloping analysis, consideration is given to as many as possible, and it is chiefly in this respect that the present study goes beyond previous work in the field.

The earliest analytical studies of parachute canopy shapes seem to have been made by the British investigators Taylor, Southwell, Griffiths, Jones, and Williams, at the Royal Aircraft Establishment in 1919. This work was summarized, together with some other work, by Jones in 1923 (Reference 1). The first theoretical canopy shape, upon which all other British work has been based, was obtained by Taylor, and is called the Taylor shape. The British approach, as

presented by Jones, does not attempt to analyze a given canopy; instead it attempts to solve the problem "What shape of parachute will have the least weight?" It is first assumed that there are a very large number of suspension lines, and that the canopy pattern is flat. When the canopy is inflated, the cloth bulges out between the cords. As the number of cords, N, increases, the radius of the bulge in a plane normal to the cords, r_1, decreases. In a membrane, the relation

$$p = f_1/r_1 + f_2/r_2 \qquad (1)$$

holds. Since r_2 is very large compared to r_1, ignore f_2/r_2.

Then

$$f_1 = pr_1 \qquad (2)$$

But as N increases, r_1 decreases, whence in the limit $f_1 = 0$. It is therefore reasoned that the excess material between cords could be removed without changing the basic inflated shape of the canopy, to achieve a minimum weight design. The argument as given by Jones is somewhat more complex, but amounts to the same thing. It should not escape notice that from here on, Jones is necessarily talking about a surface of revolution. By expressing r_1 and r_2 in terms of x and ϕ, it is then shown that the equation of the generator of this surface is

$$\sin \phi = x^2/x_m^2 \qquad (3)$$

which is called the equation of the Taylor curve.

Equation (3) is the solution of Equations (1) and (2) provided that the differential pressure p in Equation (2) is constant. Jones also gives the shape when the differential pressure p is equal to $A\left[B + (m-1)(r/x_m)^n\right]$, where A and B are constants and m and n are non-dimensional parameters, for the cases B = 1, m and n having preassigned values, and for B = 0, m = 2, and n having pre-

assigned values. He shows that these shapes may be derived from the Taylor shape.

In addition, the effect of introducing a circumferential tension, $f_1 \neq 0$, while the differential pressure is held constant is investigated. By arbitrarily varying f_2, shapes corresponding more closely to actual canopy shapes than does the Taylor shape are obtained. This approach may be regarded as a method of accounting for gore fullnesses with $\alpha \neq \pi/2$.

In 1942, the basic analysis was re-examined by Stevens and Johns (Reference 2). They were interested in the case where the number of lines is finite. It will be worth considering their analysis in detail. See Figure 1.

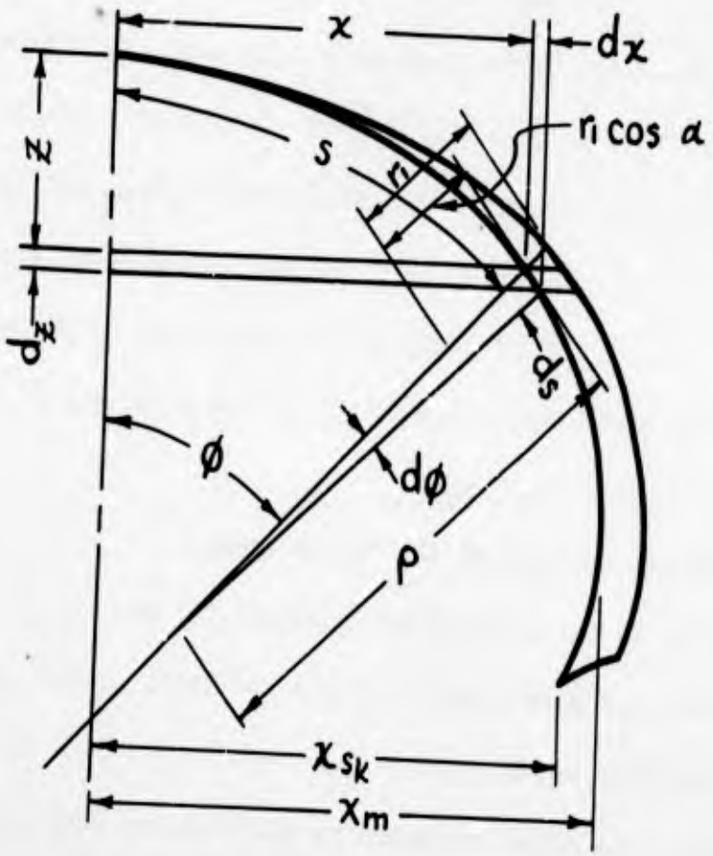

Figure 1

For equilibrium of a strip of cloth between two planes a distance ds apart, summing forces normal to the cord line,

$$T d\phi = 2p\pi x \, ds/N \tag{4}$$

(approximately) Also

$$dx = ds \cos \phi \tag{5}$$

Dividing Equations (4) by (5)

$$T \, d\phi/dx \quad 2\pi px/N \cos \phi \tag{6}$$

Separating the variables and integrating yields (assuming, as usual, that p is constant)

$$N \int T \cos \phi \, d\phi = \pi px^2 \tag{7}$$

But equilibrium of vertical forces on that portion of the canopy above the plane requires that

$$NT \sin \phi \cong p\pi x^2 \tag{8}$$

Obviously, T must be constant and equal to

$$T = p\pi x_s^2/N \tag{9}$$

Substituting this in Equations (7) or (8) yields Equation (3), the equation of the Taylor curve. Further, since T is constant, there can be no shear between cloth and cord lines, the cloth tensions must be normal to the corus. The approach given here is again somewhat different than the original authors', but yields the same conclusions.

An interesting thing about Stevens and Johns' result is that they find the cloth stresses to be only circumferential (contrary to a statement in Reference 3, p. 116), while the original Taylor shape was found by assuming that only meridional stress exists. The original analysis leads to infinite stresses at the

apex; Stevens and Johns' does not. Incidentally, an analysis made by Duncan, Stevens, and Richards (Reference 4) shows that the stress at the apex of the Taylor parachute is not infinite if the elasticity of the fabric is taken into account.

German work on parachute stresses has dealt with surfaces of revolution. Beck (Reference 5) produced expressions for the membrane stresses in a variety of shells of revolution for pressures both constant and linearly varying.

Reagan (Reference 6) in the United States has also considered parachutes as surfaces of revolution. Finally, an investigation of conical ribbon parachutes by Jaeger, Culver, and Della-Vedova of Lockheed Aircraft Corporation (Reference 7) should be mentioned.

As a basis for further work, the most helpful of these analyses is that of Stevens and Johns (Reference 2). These points are to be noted, however:

1) Their cord shape is independent of the canopy pattern.

2) Comparison with photographs indicates that the Taylor shape is flatter than any actual inflated canopy.

3) There are three inaccuracies in the development:

   a) The area between cords on which the pressure acts in Equation (4) is greater than $2\pi x\, ds/N$ except near the maximum inflated radius, where it is less.

   b) The slope at the center line of gore is smaller than the corresponding slope of the cords.

   c) The projected area on which the pressure acts in Equation (8) is greater than πx^2.

In the present study, analysis of five specific circular canopy designs is attempted; namely,

1) Flat

2) Extended Skirt

3) Conical

4) Personnel Guide Surface

5) Conical Ring Slot

All except No. 5 are solid cloth types, and it may be noted that No. 4 is a conical type. Only pressure distributions uniform over the canopy will be considered. This is justified by experimental work on parachute models reported by Jones (Reference 1), which indicated very nearly constant differential pressures over the canopies, with the maximum variation (about 10%) occurring at the pressure tap nearest the skirt in every case.

The report is divided into four main sections. In Section 1, Basic Theoretical Shapes and Cord Tensions, solutions for the flat and conical canopies are developed which serve also as important parts of the solutions for extended skirt, personnel guide surface, and conical ring slot canopies. Some other approaches are investigated and the variation of cord tensions between skirt and apex is compared for the theoretical canopies as well as the relative magnitudes of these tensions.

In Section 2, Comparison of Theoretical with Photographically Determined Canopy Shapes, the various theoretical canopy shapes are compared with shapes obtained from actual photographs. The flat canopy shape is also compared with the Taylor curve.

In Section 3, Effects of Various Parameters on Canopy Shapes and Stresses, the influence of such factors as suspension line length, cone angle variation, and various design details such as shortness of cords over the canopy, and vent, rib, and skirt reinforcements are investigated.

In Section 4, Cloth Stresses, the variation of cloth stress at the cord with distance from the apex is shown and the effect of biaxial stresses in straight and bias gores is investigated. Some experimental data on biaxial stress properties of fabric are discussed and the kind of stress-strain data needed is pointed out. In the final section, the relation between stress and porosity in parachute canopies is studied.

SECTION 1 - BASIC THEORETICAL SHAPES AND CORD TENSIONS

INTRODUCTION

Sections 1.1 to 1.5 deal with the cord and canopy shape of the flat canopy. In Section 1.1 a cord shape is determined by modifying Taylor's equation in accordance with assumptions concerning the shape of the gore. This gives a cord shape that is too deep; consequently, in Section 1.4, it is coupled with the Taylor curve whose coordinates are given in Section 1.2. The portion of the cord below the Maximum Inflated Radius (MIR) is assumed to be a parabolic arc. Section 1.3 gives equations by which the parameters of the parabolic arc may be determined. The three portions of the cord are summarized in Section 1.4. In Section 1.1 one of the parameters is chosen arbitrarily. This choice is further examined in Section 1.5.

Sections 1.6 and 1.7 give the first and second approximations to the conical canopy. In the first approximation sections of the gore cut by horizontal planes are assumed to be polygons and the cord curve is assumed to be symmetrical about the MIR. Using the cord shape of the first approximation and taking into account gore fullness new cord coordinates are derived as the second approximation.

Sections 1.8 and 1.9 give solutions of the extended skirt and conical ring slot canopies which are based on the flat canopy. The personnel guide surface canopy shape is solved in Section 1.10 by considering the effect of the pockets on the shape of a flat canopy.

Sections 1.11 and 1.12 give the cord shapes and tensions for the five canopy types discussed when the parameters l_c, l_s' and N and the differential pres-

sure, p, are held constant for all types.

1.1 Shape of Flat Canopy from Apex to Maximum Inflated Radius

Stevens and Johns (Reference 2) arrive at the Taylor equation

$$x^2 = x_m^2 \sin \phi \qquad (1.1.1)$$

for the shape of the surface formed by the cord lines without any considerations of the uninflated canopy pattern. From this result, they evolve a design which has come to be called the Exeter type parachute. Since it has been observed that the cord lines do not actually take the Taylor shape for all parachutes, the assumptions and approximations used were examined to see which ones would be affected by pattern geometry. It appears that the most important one is an assumption that the projected differential area on which the pressure is assumed to act has the area $2\pi x\, ds/N$. The actual projected area normal to the canopy surface between two planes corresponding to $x = x$ and $x = x + dx$ is not rectangular but instead is bounded on two sides by curves, so that this area is greater than assumed by Stevens and Johns. The shape of the boundary curves is a function of the canopy pattern. In the case of the flat canopy, the Taylor shape may be regarded as a first approximation to the actual shape of the inflated canopy, or rather of the curve formed by the cords over the canopy. This fact can be made use of to obtain a second approximation, and this corrected curve could be used as the basis of a third approximation, and so forth.

The steps in such a procedure are as follows:

1) In Figure 1.1.1a the cords are assumed to be Taylor curves, $x^2 = x_m^2 \sin \phi$, as a first approximation.
2) The distance between cords at points equidistant (points A and B) from the apex is $2x \sin \pi/N$. See Figure 1.1.1a.

3) The distance between corresponding points in the flat pattern is $2s \sin \pi/N$. See Figure 1.1.1b.

4) The fullness of the line AB is $2 (s - x) \sin \pi/N$, or directly proportional to the fullness $(s - x)$ of the cords.

5) Based on step 4 the line AB is also assumed to be a Taylor curve $u^2 = b^2 \sin \xi$ where u and ξ are coordinates of the points of the curve AB on the inflated canopy, corresponding to x and ϕ respectively of the cord. At the point A of the Taylor curve AB the coordinate ξ is assumed equal to the coordinate ϕ of the cord curve. See Figures 1.1.1a and d. Thus $u/b = x/x_m$.

6) Assume that the plane P_1 formed by the normals OA and OB intersects the gore in a circular arc of length s_1. See Figures 1.1.1a and c.

7) At the maximum inflated radius, assume that $\alpha_m = \pi/2$ (see Section 1.5 for justification and discussion of this assumption). As a consequence of this and step 5, $u\phi = 90° = b = r_1$ or $u^2 = r_1^2 \sin \phi$. Thus the Taylor curve AB is always the same Taylor curve independent of x or ϕ. The only variable quantity is the portion of the Taylor curve that applies at each point (x, ϕ) of the cord. At the MIR the Taylor curve is complete; at the apex it degenerates to a point. In between, the point A is determined by the angle ϕ.

8) Since from step 7 the Taylor curve AB is always part of the same Taylor curve $u^2 = r_1^2 \sin \phi$ it seems that it is reasonable to assume that the circular arc is always part of the same circle of the radius r_1. Only the half-angle α varies. At point A, $r_1 \sin \alpha = x \sin \pi/N = u = r_1 \sqrt{\sin \phi}$. Therefore $\sin \alpha = \sqrt{\sin \phi} = x/x_m$. (1.1.2)

9) Assume that the surface of the gore from the circle to the horizontal section of the canopy through points A and B is circularly cylindrical with radius r_1. The axis of this cylinder passes through the canopy axis and lies in a plane tangent to the surface of revolution generated by the cord curves at that point midway between points A and B. With this assumption the circular arc of radius r_1 and central angle 2α projects on a horizontal plane as an ellipse of semi-minor axis r_1 and semi-major axis $r_1 \csc \phi$. (A better approximation would be to assume a conical surface.)

10) This horizontal ellipse projects onto the tangential plane of step 9 as another ellipse with semi-axes r_1 and $r_1 \cot \phi$.

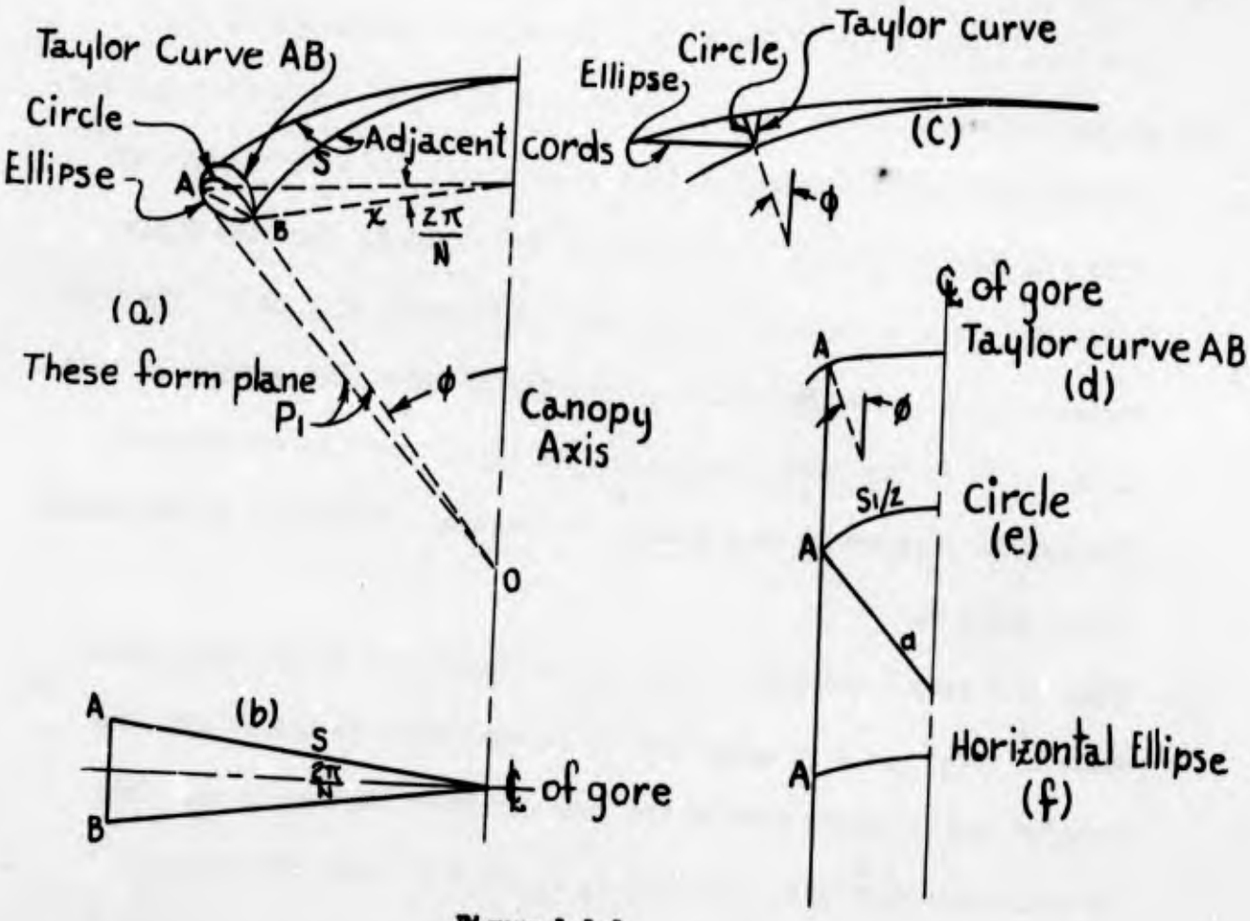

Figure 1.1.1

Figure 1.1.2a is a somewhat enlarged view of Figure 1.1.1.c. Figure 1.1.2b is a view of the circular arc of central angle 2α while Figure 1.1.2c is a view of the ellipse ACB projected onto the tangential plane of step 9 by the horizontal ellipse that is projected by the circular arc. Let L be the length of the ellipse ACB. Two cases arise when $\phi < 45°$ and $\phi < 45°$. In the first case r_1 is the semi-minor axis and in the second case r_1 is the semi major-axis. Stevens and Johns used $2\pi\alpha/N$ for the length L. Here we will use the actual length L.

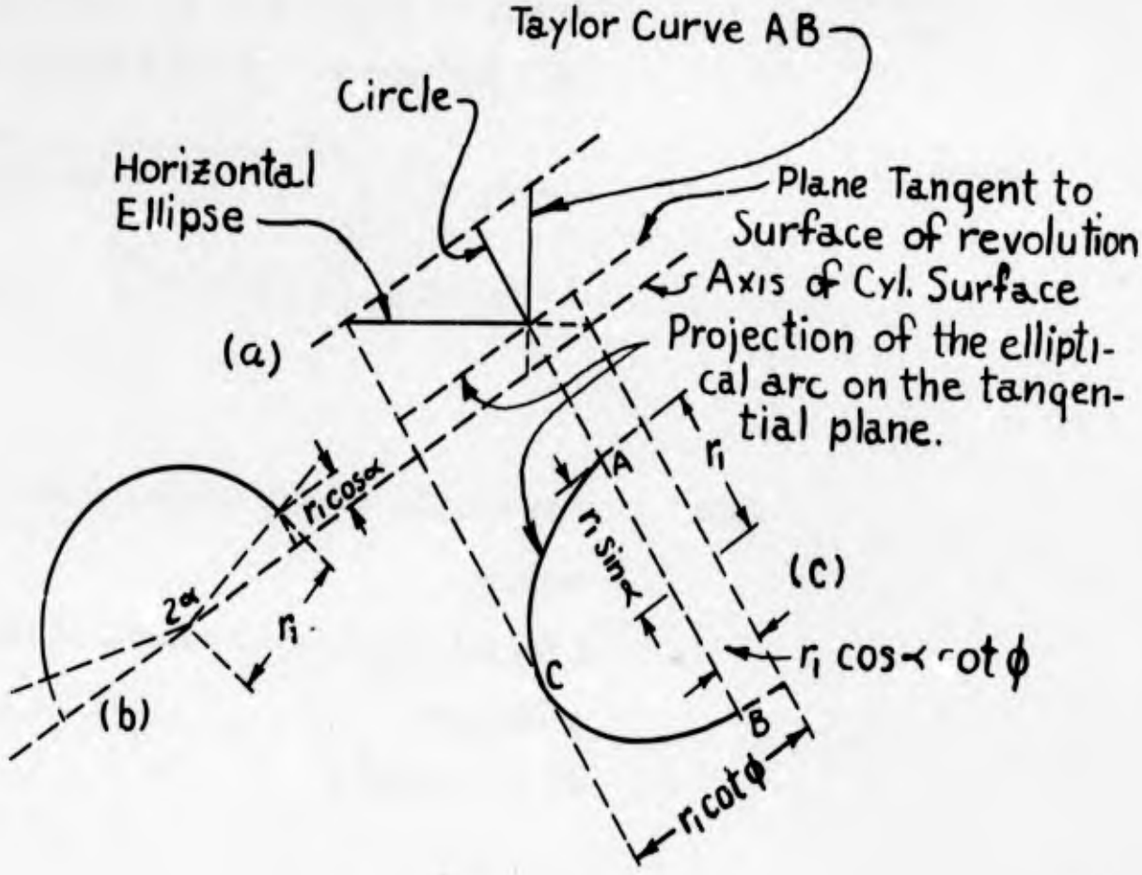

Figure 1.1.2

First Case $\phi < 45°$ ($\cot\phi > 1$; $r_1 \cot\phi > r_1$ Hence r_1 = minor semi-axis)

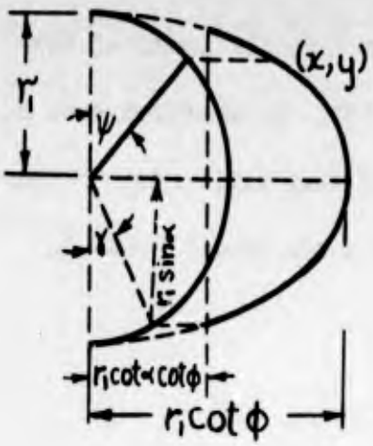

Figure 1.1.3

ψ = angle parameter (dummy variable)

Limits of ψ: $\pi/2$, γ = arc cos $(\sqrt{\sin\phi})$

Parametric equations of the ellipse:

$$\begin{cases} x = r_1 \cot\phi \sin\psi \\ y = r_1 \cos\psi \end{cases}$$

$$dL = \sqrt{dx^2 \times dy^2}$$

$$dx = r_1 \cot\phi \cos\psi \, d\psi, \quad dy = -r_1 \sin\psi \, d\psi$$

$$dL^2 = \left[r_1^2 \sin^2\psi + r_1^2 \cot^2\phi \cos^2\psi \right] d\psi^2$$

$$L = 2r_1 \cot\phi \int_{\gamma}^{\pi/2} \sqrt{1 - (1 - \tan^2\phi) \sin^2\psi} \, d\psi$$

$$L = 2r_1 \cot\phi \left[E - E(k, \gamma) \right] \qquad (1.1.3)$$

where E is complete elliptic integral of the second kind

$E(k, \gamma)$ is an elliptic integral of the second kind

$k^2 = 1 - \tan^2\phi$

Second Case $\phi > 45°$ ($\cot\phi < 1$, $r_1 \cot\phi < r_1$, r_1 = major semi-axis)

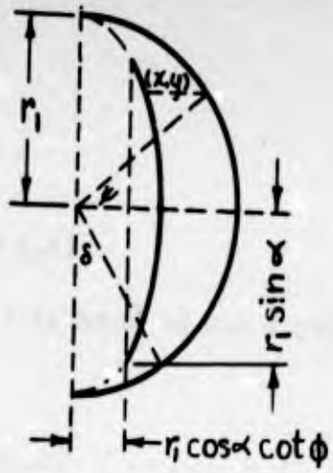

Figure 1.1.4

ψ = angle parameter (dummy variable)

Limits of ψ: 0 and $\pi/2 - \delta = \pi/2$

$- \arccos(\sqrt{\sin\phi})$

Parametric equations of the ellipse:

$$\begin{cases} x = r_1 \cot\phi \cos\psi \\ y = r_1 \sin\alpha \end{cases}$$

$dx = -r_1 \cot\phi \sin\psi \, d\psi$, $dy = r_1 \cos\psi \, d\psi$

$$dL^2 = r_1^2 \left[1 - (1 - \cot^2\phi) \sin^2\psi\right] d\psi^2$$

$$L = 2r_1 \int_0^{\pi/2 - \delta} \sqrt{1 - (1 - \cot^2\phi) \sin^2\psi} \, d\psi$$

$$= 2r_1 E(k, \pi/2 - \delta) \qquad (1.1.4)$$

where $E(k, \pi/2 - \delta)$ is an elliptic integral of the second kind

$k^2 = (1 - \cot^2\phi)$

Thus the length, L of the elliptical projection of the horizontal section of the canopy on the tangential plane is given by either one of the elliptic integrals of the second kind; Equations (1.1.3) or (1.1.4) depending upon ϕ.

Stevens and Johns' Equation (3) is

$$Td\phi = 2p\pi x \, ds/N \qquad (1.1.5)$$

The factor $2\pi x/N$ is replaced here by L. Thus Equation (1.1.5) becomes

$$T d\phi = pL ds$$

Since $dx = ds \cos \phi$ (see Figure 1.1.1a)

$$T \cos \phi \, d\phi = pL \, dx$$

which can be written as

$$T \frac{d(\sin \phi)}{L} = p \, dx \qquad (1.1.6)$$

Equation (1.1.6) can be integrated if the length L can be found as a function of $\sin \phi$; i.e.,

$$L = r_1 f(\sin \phi) \qquad (1.1.7)$$

Table 1.1.1 shows values of L/r_1 for various values of ϕ and in Figure 1.1.5 these values are plotted. These data may be approximated by an equation of second degree to give an easily integrable expression.

$$f(\sin \phi) = a \sin^2 \phi + b \sin \phi + c \qquad (1.1.8)$$

The values of a, b and c are determined by the values of L/r_1 at $\phi = 0°$, 45° and 90°. Except for $\phi = 0°$, the values of L/r_1 can be obtained from from Table 1.1.1. At $\phi = 0$, L/r_1 yields the indeterminate form $\infty \times 0$; however, by applying L'Hospital's rule once it can be shown that the

$$\lim_{\phi \to 0} L/r_1 = 1$$

Using the values of L/r_1 at $\phi = 0°$, 45° and 90° the constants a, b and c become $a = -1.367$, $b = 2.367$, and $c = 1$. Equation (1.1.8) then is

$$f(\sin \phi) = -1.367 \sin^2 \phi + 2.367 \sin \phi + 1$$

Table 1.1.1 Values of L/r_1 for various values of ϕ.

ϕ	L/r_1 from Eq. (1.1.3)	ϕ	L/r_1 from Eq. (1.1.4)
10	1.38	45	1.99
20	1.65	50	2.029
30	1.82	60	2.082
40	1.94	70	2.055
45	1.99	80	2.026
		90	2.000

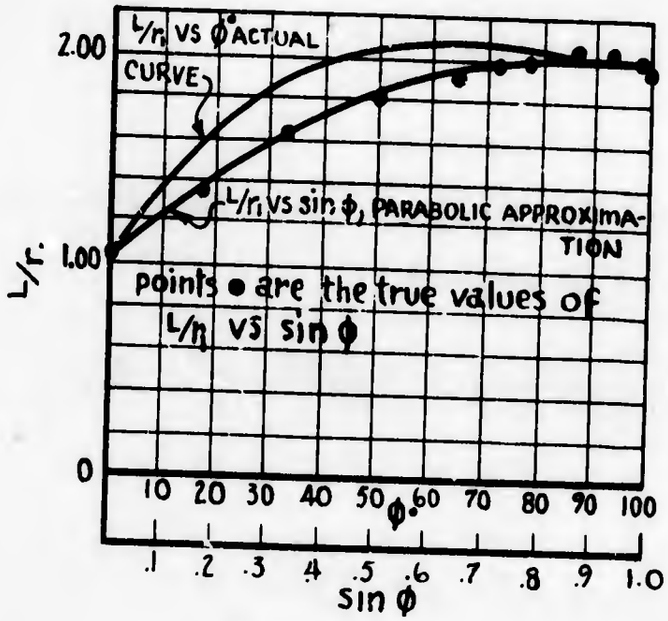

Figure 1.1.5

Using the above values of a, b and c and Equation (1.1.7) in Equation (1.1.6) the following results:

$$\frac{pr_1}{T}\,dx = \frac{d(\sin\phi)}{-1.367\sin^2\phi + 2.367\sin\phi + 1}$$

which integrates to

$$\frac{pr_1}{T} x = .3005 \log A \frac{.351 + \sin \phi}{2.083 - \sin \phi} \qquad (1.1.9)$$

The constant A is evaluated by noting that $x = 0$ when $\phi = 0$. Hence Equation (1.1.12) becomes

$$\frac{pr_1}{T} x = .3005 \log 5.84 \frac{.351 + \sin \phi}{2.083 - \sin \phi} \qquad (1.1.10)$$

At $\phi = 90°$ and $x = x_m$, Equation (1.1.10) gives

$$\frac{pr_1}{T} = \frac{.59674}{x_m} \qquad (1.1.11)$$

Therefore substituting Equation (1.1.11) into Equation(1.1.10) results in

$$x = .5036\, x_m \log 5.85 \frac{.351 + \sin \phi}{2.083 - \sin \phi} \qquad (1.1.12)$$

From Figure 1.1.1a, $dz = \tan \phi\, dx$.

Differentiating Equation (1.1.12) with respect to ϕ and substituting into Equation (1.1.13) the following results:

$$dz = .5036\, x_m \left(\frac{\sin \phi}{.351 + \sin \phi} + \frac{\sin \phi}{2.083 - \sin \phi} \right) d\phi$$

Integration yields

$$z = .5036\, x_m \left[2.28 \tan^{-1} \frac{2.083 \tan \phi/2 - 1}{1.827} \right.$$

$$\left. -.375 \log \frac{.351 \tan \phi/2 + .064}{.351 \tan \phi/2 + 1.936} - .138 \right] \qquad (1.1.14)$$

The constant of integration -.138 is obtained by noting that $z = 0$ when $\phi = 0$. The length of the cord curve from apex to any arbitrary value of ϕ may be obtained from

$$s = \int ds = \int_0^{\phi} dx/\cos\phi \qquad (1.1.15)$$

or

$$s/xn = .5512 \tan^{-1} (1.140 \tan \phi/2 - .5473) + .5378 \log \left[(.351 \tan \phi/2 + .064) (.351 \tan \phi/2 - 1.936)^{-1} \right] + 2.1073 \qquad (1.1.16)$$

Table 1.1.2 Values of x/x_m and s/x_m for Various Values of ϕ

ϕ	x/x_m (Eq. 1.1.12)	s/x_m (Eq. 1.1.14)
0	0	0
2	.04814	.00094
4	.10034	.00342
6	.14910	.00775
8	.19489	.01348
10	.23814	.02040
20	.42480	.07014
30	.57612	.14042
40	.70183	.22859
45	.75640	.27836
50	.80574	.33235
60	.88868	.45091
70	.94971	.58169
80	.98729	.72191
90	1.00000	.86731

The coordinates of Table 1.1.2 are plotted in Figure 1.1.6. This shape when compared with photographs of inflated flat canopies is too deep; i.e., the Taylor shape, which is too flat, has been over-corrected. Since the Taylor curve is most in error near the apex, a combination solution is worked out in Section 1.4. For this purpose and for comparison, the coordinates of the Taylor curve are needed. These coordinates are calculated in the following section.

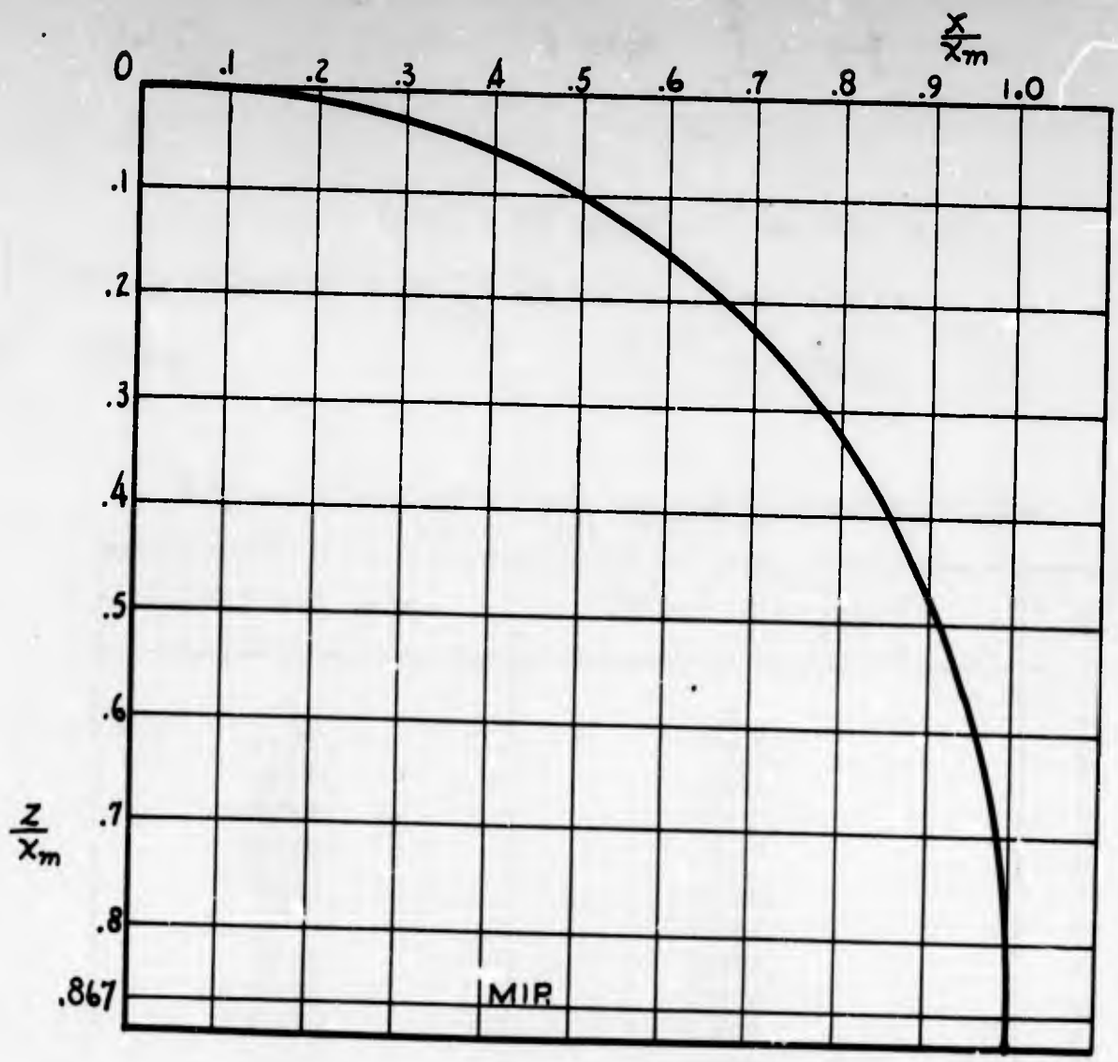

Parametric Equations of Cord

$$x/x_m = .5036 \log 5.85 \frac{.351 + \sin\phi}{2.083 - \sin\phi} \qquad \text{EQ 1.1.16}$$

and

$$z/x_m = .5036 \left[2.28 \tan^{-1} \frac{2.083 \tan\frac{\phi}{2} - 1}{1.827} - .375 \log \frac{.351 \tan\frac{\phi}{2} + .064}{.351 \tan\frac{\phi}{2} + 1.936} - .138 \right] \qquad \text{EQ 1.1.19}$$

Figure 1.1.6 - Cord Curve for a Flat Canopy from Apex to Maximum Inflated Radius

1.2 Non-Dimensional Cartesian Coordinates x/x_m and z/x_m of the Points of Taylor's Curve Given by the Equation $x = x_m \sqrt{\sin \phi}$

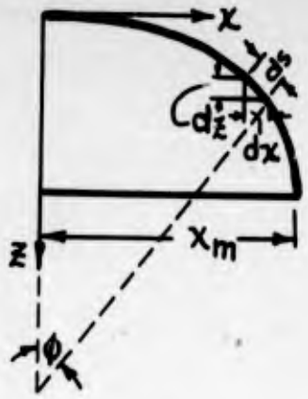

Figure 1.2.1

Differentiating equation

$$x = x_m \sqrt{\sin \phi}$$

with respect to ϕ and taking equation

$$dz = dx \tan \phi$$

into account

$$dz = (x_m/2) \sqrt{\sin \phi} \; d\phi \text{ is obtained,}$$

from which

$$z = x_m/2 \int_0^{\phi} \sqrt{\sin \phi} \; d\phi. \qquad (1.2.1)$$

Substituting cos t for sin ϕ in the integral of Equation(1.2.1) the integral $\int_0^{\phi} \sqrt{\sin \phi} \; d\phi$ becomes $\int_{t_1}^{t_2} \frac{-2 \cos^2 t \, dt}{\sqrt{1 + \cos^2 t}}$ where $t_1 = \pi/2$, $t_2 = \cos^{-1}\sqrt{\sin\phi}$

Finally Equation (1.2.1) becomes:

$$z = \frac{x_m}{\sqrt{2}} \left[2 (E - E(u)) - (K - u) \right] \qquad (1.2.2)$$

where E is the complete elliptic integral of second kind $\int_0^{90} \sqrt{1 - \tfrac{1}{2} \sin^2 t} \; dt$

E (u) is the elliptic integral of second kind $\int_0^{\cos^{-1}\sqrt{\sin\phi}} \sqrt{1 - \tfrac{1}{2} \sin^2 t} \; dt$

K is the complete elliptic integral of first kind $\int_0^{90} \frac{dt}{\sqrt{1 - \tfrac{1}{2} \sin^2 t}}$

and u is the elliptic integral of first kind $\int_0^{\cos^{-1}\sqrt{\sin\phi}} \frac{dt}{\sqrt{1 - \tfrac{1}{2} \sin^2 t}}$

Values of x/x_m and z/x_m given by the above parametric equations are tabulated in Table 1.2.1 for values of the parameter ϕ between 0° and 90°.

Table 1.2.1 - Values of x/x_m and z/x_m vs ϕ for a Taylor Curve

ϕ	sin ϕ	$x/x_m = \sqrt{\sin \phi}$	$\cos^{-1} \sqrt{\sin \phi}$	E	E (u)	2 [E-E(u)]	K	u	K-u	z/x_m
0°	.0000	.0000	90.000	1.3506	1.3506	.0000	1.8541	1.8541	.0000	.0000
4°	.0698	.2642	74.680	↑	1.1592	.3828	↑	1.4802	.3739	.0063
10°	.1736	.4167	65.373	↑	1.0378	.6256	↑	1.2624	.5917	.0240
20°	3420	.5848	54.210	↑	.8842	.9328	↑	1.0168	.8373	.0675
30°	.5000	.7071	45.000	↑	.7482	1.2048	↑	.8260	1.0281	.1249
40°	.6428	.8017	36.700	↑	.6198	1.4616	↑	.6626	1.1915	.1910
45°	.7071	.8409	32.767	↑	.5569	1.5874	↑	.5876	1.2665	.2269
50°	.7660	.8752	28.930	↑	.4945	1.7122	↑	.5158	1.3383	.2644
60°	.8660	.9306	21.470	↑	.3702	1.9608	↑	.3792	1.4749	.3436
70°	.9397	.9694	14.214	↑	.2466	2.2080	↑	.2495	1.6046	.4267
80°	.9848	.9924	7.055	↑	.1230	2.4552	↑	.1233	1.7308	.5122
84°	.9945	.9972	4.278	↑	.0746	2.5520	↑	.0747	1.7794	.5463
90°	1.0000	1.0000	.000	1.3506	.0000	2.7012	1.8541	.0000	1.8541	.5990

1.3 Portion of Cord Between Maximum Inflated Radius and Skirt

The portion of the canopy between the MIR and the skirt is difficult to analyze rigorously because of irregularities caused by the fact that the bottom of a gore takes an arc not in a horizontal plane, and the fact that it is near the skirt that non-uniformity of pressure is most likely to exist. Fortunately, the length of cord involved is not large except when l_c/l_s is abnormally large. Therefore, for simplicity, the cord curve in this region is assumed to be a parabolic arc. It is shown in Section 2.6 that the difference between the parabola and the Taylor curve in this region has a negligible effect on canopy shape, which is a further justification of the assumption. The equation of the parabolic arc is obtained as follows:

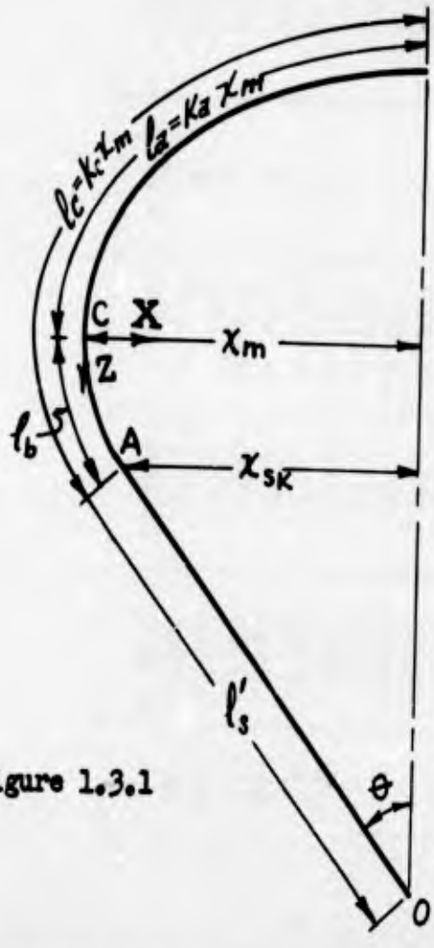

Figure 1.3.1

Assumptions:

1) The portion CA of the cord below the MIR is a parabolic arc with vertex of the parabola at C and axis along x_m.

2) The radius of curvature of the parabola at its vertex is equal to the radius of curvature of the curve above at the point C.

The equation of the parabola is (origin at C)

$$Z = c\sqrt{X} = c\sqrt{x_m - x} \qquad (1.3.1)$$

$$dZ/dX = c/(2\sqrt{X}) \qquad (1.3.2)$$

$$d^2Z/d^2X = -c/4X^{3/2} \qquad (1.3.3)$$

Radius of curvature of the parabola at C:

$$\rho = \rho_m = \left| \frac{\left[1 + \left(\frac{dZ}{dX}\right)^2\right]^{3/2}}{\frac{d^2Z}{dX^2}} \right| \qquad (1.3.4)$$

Substituting values from Equations (1.3.2) and (1.3.3) into Equation (1.3.4) results in

$$\rho_m = c^2/2 \qquad (1.3.5)$$

from which $$c = \sqrt{2\rho_m} \qquad (1.3.6)$$

Then Equation (1.3.1) becomes $$Z = x_m \sqrt{2\rho_m/x_m}\ \sqrt{1 - x/x_m} \qquad (1.3.7)$$

The length of this parabolic arc is given by

$$l_b = \int_0^{X_{ak}} \sqrt{1 + \left(\frac{dZ}{dX}\right)^2}\ dX \qquad (1.3.8)$$

where $$X_{ak} = x_m - x_{ak} \qquad (1.3.9)$$

Substituting $c^2/4X$ for $(dZ/dX)^2$ (from Equation (1.3.2)) into Equation (1.3.8) we get

$$l_b = \int_0^{X_{ak}} \sqrt{1 + c^2/4X}\ dX \qquad (1.3.10)$$

Equation (1.3.10) may be integrated by letting $\sqrt{1 + c^2/4X} = \cosh t$.

With this substitution we get

$$l_b = -\frac{c^2}{2}\int_{t_1}^{t_2} \frac{\cosh^2 t}{\sinh^3 t}\,dt = \frac{c^2}{2}\left[\frac{\cosh t}{2\sinh^2 t} + t \log \frac{\cosh t + 1}{\cosh t - 1}\right]\Bigg|_{t_1}^{t_2}$$

$$= \frac{c^2}{8}\left[\frac{2\sqrt{1 + c^2/4X_{sk}}}{c^2/4X_{sk}} + \log \frac{\sqrt{1 + c^2/4X_{sk}} + 1}{1 + c^2/4X_{sk} - 1}\right] \qquad (1.3.11)$$

Let $x_{sk} = k_{sk}x_m, \quad l_s' = k_s'x_m$ (1.3.12)

Then from triangle AOB Figure 1.3.1

$$\sin\theta = x_{sk}/l_s' = k_{sk}/k_s' = 1/n \qquad (1.3.13)$$

But $\cot\theta = (dZ/dX)_{X = X_{sk}} = \dfrac{c}{2\sqrt{x_m - x_{sk}}}$

and $\cot\theta = \dfrac{\sqrt{1 - \sin\theta}}{\sin\theta} = \dfrac{\sqrt{k_s'^2 - k_{sk}^2}}{k_{sk}} = \sqrt{n^2 - 1}$

Then $c = 2\cot\theta\sqrt{x_m - x_{sk}} = 2\dfrac{\sqrt{k_s'^2 - k_{sk}^2}}{k_{sk}}\sqrt{x_m}\sqrt{1 - k_{sk}}$

or $c^2 = \dfrac{4x_m(k_s'^2 - k_{sk}^2)(1 - k_{sk})}{k_{sk}^2}$ (1.3.14)

Using Equations (1.3.12) and (1.3.14) in Equation (1.3.11) we get

$$l_b = \frac{(1 - k_{sk})(k_s'^2 - k_{sk}^2)\, x_m}{2k_{sk}^2} \left[\frac{2\sqrt{1 + \dfrac{k_s'^2 - k_{sk}^2}{k_{sk}^2}}}{\dfrac{k_s'^2 - k_{sk}^2}{k_{sk}^2}} + \log \frac{\sqrt{1 + \dfrac{k_s'^2 - k_{sk}^2}{k_{sk}^2}} + 1}{\sqrt{1 + \dfrac{k_s'^2 - k_{sk}^2}{k_{sk}^2}} - 1} \right] \qquad (1.3.15)$$

But $l_b = l_c - l_a = x_m (k_c - k_a)$ (1.3.16)

Using Equation (1.3.16) in Equation (1.3.15) and after some simplifications the latter one becomes:

$$k_c - k_a = \frac{1 - k_{sk}}{2} \left[2n + (n^2 - 1) \log \frac{n + 1}{n - 1} \right] = \frac{1 - k_{sk}}{2} f(n) \qquad (1.3.17)$$

Equation (1.3.17) can be written $k_s' \frac{k_c}{k_s'} - k_a = \frac{1 - k_{sk}}{2} f(n)$ or

$nk_{sk} \frac{k_c}{k_s'} - k_a = \frac{1 - k_{sk}}{2} f(n)$. And solving for k_{sk} we obtain

$$k_{sk} = \frac{f(n) + 2k_a}{f(n) + 2n \frac{k_c}{k_s'}} \qquad (1.3.18)$$

Combining Equations (1.3.5) and (1.3.14) and solving for k_{sk} we obtain

$$k_{sk} = 1 - \frac{\frac{1}{2} \rho_m / x_m}{n^2 - 1} \qquad (1.3.19)$$

The quantities k_a and ρ_m/κ_m are determined by the shape of the cord above the maximum inflated radius. The ratio k_c/k_s' must be known for a given canopy. To determine k_{sk} we must assume values of n in order to find that value of n that will satisfy both Equation (1.3.18) and (1.3.19).

Table 1.3.1 gives values of the function f(n) for several values of n. By plotting f (n) vs. n from the values of Table 1.3.1 it can be shown that a straight line approximates the data well between n = 2 to n = 3.4. The equation of this line is

$$f(n) \simeq 4.240\, n - 1.184 \qquad (2 \leq n \leq 3.4) \tag{1.3.20}$$

Equation (1.3.20) may be extrapolated for values of $n > 3.4$ but not with the same accuracy of 0.1%.

Table 1.3.1 - Values of $f(n) = 2n + (n^2 - 1) \log \frac{n+1}{n-1}$ vs n

①	②	③	④	⑤	⑥	⑦	⑧	⑨	⑩
n	2n	n^2	$n^2 - 1$	n + 1	n - 1	$\frac{n+1}{n-1}$	$\log \frac{n+1}{n-1}$	④ · ⑧	f (n)
2.0	4.0	4.00	3.00	3.00	1.00	3.00000	1.09861	3.29583	7.29583
2.2	4.4	4.84	3.84	3.20	1.20	2.66667	.98083	3.76639	8.16639
2.4	4.8	5.76	4.76	3.40	1.40	2.42857	.88730	4.22355	9.02355
2.6	5.2	6.76	5.76	3.60	1.60	2.25000	.81093	4.67096	9.87096
2.8	5.6	7.84	6.84	3.80	1.80	2.11111	.74721	5.11092	10.71092
3.0	6.0	9.00	8.00	4.00	2.00	2.00000	.69315	5.54520	11.54520
3.1	6.2	9.61	8.61	4.10	2.10	1.95238	.66904	5.76043	11.96043
3.2	6.4	10.24	9.24	4.20	2.20	1.90909	.64663	5.97486	12.37486
3.4	6.8	11.56	10.56	4.40	2.40	1.83333	.60613	6.40073	13.20073

1.4 Complete Solution for the Shape of the Cord and Suspension Line of a Flat Canopy

Neither the solution of Section 1.1 nor the Taylor curve, Section 1.2, is good enough by itself to fit the photographic shapes available. The solution of Section 1.1 gives a shape that is too deep from apex to MIR while the Taylor shape is too flat, especially in the neighborhood of the apex. For these reasons the solution of Section 1.1 is used for the upper portion of the cord curve while the Taylor curve is used for the portion above and in the neighborhood of the MIR. A parabolic curve is used for the portion of the cord curve below the MIR because it is the simplest curve that fits the photographic shape and also satisfies the necessary boundary conditions.

The arbitrary angle 45° is chosen for the value of the parameter ϕ at which the solutions of Section 1.1 and Taylor's curve meet. Although a better value of ϕ could be found by matching radii of curvature, or by trial, the more complex solution resulting would not be justified by the small increase in accuracy. The given value of the ratio l_c/l_s' determines the end point of the cord curve below the MIR when used with the length of the cord from apex to MIR.

The portion of the cord curve from apex to MIR is determined such that the curve of Section 1.1 and Taylor's curve have the same x/x_m at $\phi = 45°$. At $\phi = 45°$ the Cartesian coordinates of the curve of Section 1.1 and Taylor's curve are $x/x_m = .7564$, $z/x_m = .2784$ and $x/x_m = .8409$, $z/x_m = .2269$ respectively. If both curves are to be continuous, have the same first derivatives at $\phi = 45°$, and also have a common origin, it is necessary to magnify the coordinates of the curve of Section 1.1 for $0 \leq \phi \leq 45°$ by the factor $.8409/.7564 = 1.1117$ and to add the difference $(.2784)(1.1117) - .2269 = .0826$ to the z/x_m coordinates of the Taylor curve for $45° \leq \phi \leq 90°$. With these modifications the parametric

equations for the coordinates of the cord curve from apex to MIR are:

For $0 \leq \phi \leq 45°$ - Equations (1.1.12) and (1.1.14)

$$x = 1.1117\ (.5036\ x_m)\ \log 5.85\ \frac{.351 + \sin\phi}{2.083 - .\sin\phi} \tag{1.4.1}$$

$$z = 1.1117\ (.5036\ x_m)\ \left[2.28\ \tan^{-1}\frac{2.083\ \tan\phi/2 - 1}{1.827} \right.$$

$$\left. - .375\ \log\ \frac{.351\ \tan\phi/2 + .064}{.351\ \tan\phi/2 + 1.936} - .138 \right] \tag{1.4.2}$$

For $45° \leq \phi \leq 90°$ - Equations (1.1.1) and (1.2.2)

$$x = x_m\ \sqrt{\sin\phi} \tag{1.4.3}$$

$$z = \frac{x_m}{\sqrt{2}}\ \left[2\ (E - E\ (u)) - (K - u) \right] + .0826\ x_m \tag{1.4.4}$$

From the MIR downward the cord curve is a parabola whose vertex is at the MIR. The radius of curvature of the parabola at its vertex is the same as that of the Taylor curve there, and its length is determined by the ratio l_c/l_s' and the length of the cord from apex to MIR. According to Section 1.3 these conditions are satisfied by Equations (1.3.18) and (1.3.19) which are given below.

$$k_{sk} = \frac{f(n) + 2k_c}{f(n) + 2n\ k_c/k_s'} \tag{1.4.5}$$

$$k_{sk} = 1 - \frac{\frac{1}{2}\ \rho_m/x_m}{n^2 - 1} \tag{1.4.6}$$

The quantity $k_a x_m$ is the length of the cord curve above MIR. This length is

$$l_a = .8324\ x_m + .4155\ x_m \tag{1.4.7}$$

in which the first factor of the first term is the length of the curve of Section

1.1 from $\phi = 0°$ to $\phi = 45°$. This length may be calculated from Equation 1.1.16 of Section 1.1 by substituting $\phi = 45°$ into that equation. The factor 1.1117 is the magnification factor mentioned above. The second term is the length of the Taylor curve from $\phi = 45°$ to $\phi = 90°$. This length is obtained by integration as follows: The Taylor curve is

$$x = x_m \sqrt{\sin \phi}$$

$$\text{length} = \int ds = \int \frac{dx}{\cos \phi} = \frac{x_m}{2} \int_{\pi/4}^{\pi/2} \frac{d\phi}{\sqrt{\sin \phi}} = \sqrt{2}\, x_m \int_0^{\cos^{-1} \frac{1}{\sqrt{2}}} \frac{dt}{\sqrt{1 - \frac{1}{2} \sin^2 t}} \qquad (1.4.8)$$

which is an elliptic integral of the first kind and hence its value is $.4155\, x_m$.

With $k_a = 1.3409$, $l_c/l_s' = k_c/k_s' = .56$, and $\rho_m = \left.\frac{ds}{d\phi}\right|_{\phi = 90°}$

$$\rho_m = \sec \phi \left.\frac{dx}{d\phi}\right|_{\phi = 90°} = \left.\frac{x_m}{2\sqrt{\sin \phi}}\right|_{0 = 90°} = \frac{x_m}{2} \qquad (1.4.9)$$

Equations (1.4.5) and (1.4.6) become

$$k_{sk} = \frac{f(n) + 2.6818}{f(n) + 1.12\, n}$$

$$k_{sk} = \frac{.25}{n^2 - 1}$$

These two equations are satisfied by $n = 2.8385$ which gives $k_{sk} = .96460$ and .96458 respectively. The angle $\theta = \csc^{-1} n = 20° 38'$. The coordinates of the parabola are then calculated using the equation of the parabola (Equation (1.3.7)).

$$z = z_m + x_m \sqrt{1 - \frac{x}{x_m}} \qquad (1.4.10)$$

where z_m is the z coordinate of the MIR the last point being obtained with

$$x_{sk}/x_m = k_{sk}$$

The result of combining the three portions of the cord curve are given in Tables 1.4.1 and 1.4.2 and plotted in Figure 1.4.1.

Table 1.4.1 - Cord Coordinates from Apex to MIR

	$0 \leq \phi \leq 45°$				$45° \leq \phi \leq 90°$			
	From Section 1.1		Magnified		Taylor's Curve		Translated	
	x/x_m	z/x_m	x/x_m	z/x_m	x/x_m	z/x_m	x/x_m	z/x_m
ϕ	Eq.(1.1.12)	Eq.(1.1.14)	Eq. (1.4.1)	Eq.(1.4.2)	Eq.(1.1.1)	Eq. (1.2.2)	Eq. (1.4.3)	Eq. (1.4.4)
0	0	0	0	0				
2	.0481	.0009	.0535	.0010				
4	.1003	.0034	.1115	.0038				
6	.1491	.0078	.1658	.0087				
8	.1949	.0135	.2167	.0150				
10	.2381	.0204	.2647	.0227				
20	.4248	.0701	.4723	.0779				
30	.5761	.1404	.6405	.1561				
40	.7018	.2286	.7802	.2541				
45	.7564	.2784	.8409	.3095				
50					.8409	.2269	.8409	.3095
60					.8752	.2644	.8752	.3470
70					.9306	.3436	.9306	.4262
80					.9694	.4267	.9694	.5093
90					.9924	.5122	.9924	.5948
					1.0000	.5990	1.0000	.6816

Table 1.4.2 - Cord Coordinates from MIR to Skirt

x/x_m	Z/x_m	z/x_m
	Eq.(1.3.7)	Eq.(1.4.10)
1.0000	0	.6816
.9929	.0843	.7659
.9858	.1192	.8008
.9787	.1460	.8276
.9716	.1685	.8501
.9646	.1881	.8697

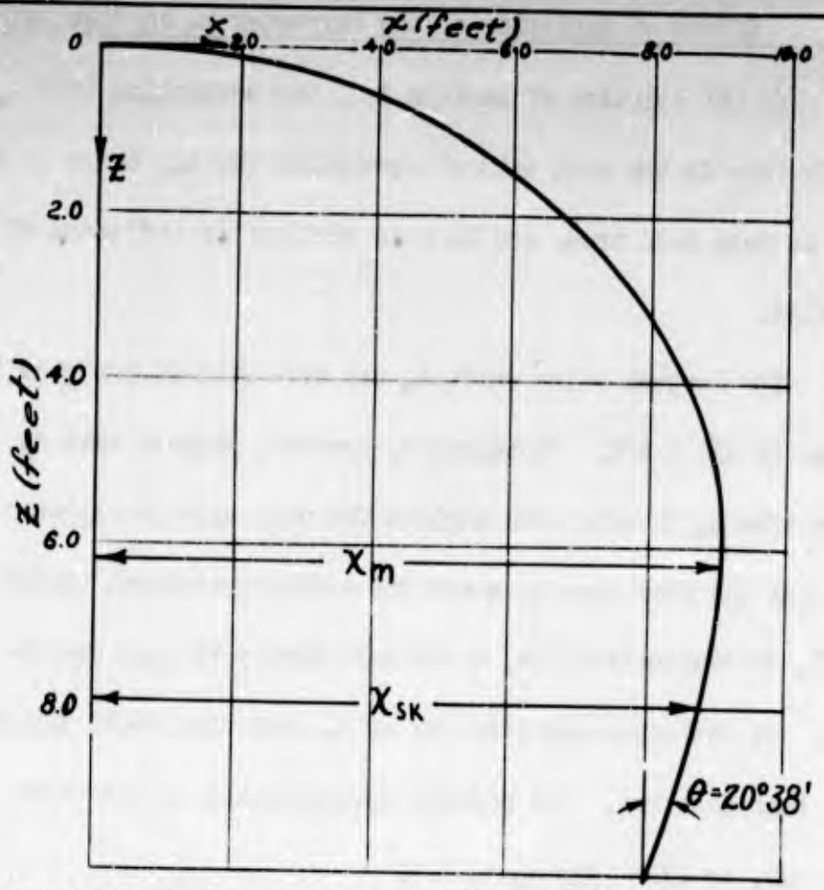

Equations of Cord

$$0 \leq \phi \leq 45° \quad \begin{cases} x = 1.1117\,(.5036)\,x_m \log 5.85\,\dfrac{.351 + \sin\phi}{2.083 - \sin\phi} \\ z = 1.1117\,(.5036\,x_m)\left[2.28\tan^{-1}\dfrac{2.083\tan\phi/2 - 1}{1.827} - .375\log\dfrac{.351\tan\phi/2 + .064}{.351\tan\phi/2 + 1.936} - .138\right] \end{cases}$$

$$45 \leq \phi \leq 90° \quad \begin{cases} x = x_m\sqrt{\sin\phi} \\ z = \dfrac{x_m}{\sqrt{2}}\left[2\,(E - E(u)) - (K - u)\right] + .0826\,x_m \end{cases}$$

$$\text{where} \quad u = \int_0^{\cos^{-1}\left(\sqrt{\sin\phi}\right)} \frac{dt}{\sqrt{1 - \frac{1}{2}\sin^2 t}}$$

$$\phi \geq 90° \quad \text{or} \quad x_m \geq x \geq .9646\,x_m \quad \left\{ z = .6816\,x_m + x_m\sqrt{1 - \frac{x}{x_m}} \right.$$

Figure 1.4.1 - Cord Shape of a Flat Canopy

1.5 Effect of Variation of the Parameter α_m on Flat Canopy Cord Shape

In the solution of Section 1.1, the assumption that $\alpha_m = \pi/2$ is made. While this is the most natural assumption for α_m, there is no obvious reason why it must hold true, and in this section the influence of this parameter is studied.

The largest value which α_m can have without one gore interfering with another is $\pi/2 + \pi/N$. Photographs, however, suggest that $\alpha_m < \pi/2$ is more probable than $\alpha_m > \pi/2$. The angle α for most canopies appears to be less than $\pi/2$ all the way from apex to skirt for ordinary designs, though by making the ratio l_c/l_s sufficiently large, α can undoubtedly be made greater than $\pi/2$ below the MIR. On the other hand, values of α_m less than about $\pi/3$ or possibly $\pi/4$, have not been observed. The present investigation is therefore limited to $\pi/4 < \alpha_m < \pi/2$. or $.7 < \sin \alpha_m < 1.0$.

The generalized analysis below corresponds to that of Section 1.1, and applies to flat canopies. Steps 1 to 6 of the argument remain unchanged; the remainder are generalized as follows:

7. $\alpha_m < \pi/2$, $u_\phi = \pi/2 = b = r_1 \sin \alpha_m$, the curve AB is still just one Taylor curve from apex to MIR but it is a smaller Taylor curve at the MIR than for $\alpha_m = \pi/2$.

8. The Taylor curve AB is changed to $u^2 = r_1^2 \sin^2 \alpha_m \sin \phi$. At point A, $r_1 \sin \alpha = x \sin \pi/N = u = r_1 \sin \alpha_m \sqrt{\sin \phi}$. Therefore $\sin \alpha_1 = \sin \alpha_m \sqrt{\sin \phi} = (x/x_m) \sin \alpha_m$.

9 & 10 are unchanged.

As before, it is necessary to determine the length L of the elliptical arc projected upon the tangential plane. Equations (1.1.3) and (1.1.4) are unchanged except for the limits of integration. These equations are

$$\begin{cases} L = 2r_1 \cot \phi \int_{\gamma}^{\pi/2} \sqrt{1 - (1 - \tan^2 \phi) \sin^2 \psi}\ d\psi \\ 0 \leq \phi \leq 45^\circ \\ \gamma = \cos^{-1} (\sin \alpha_m \sqrt{\sin \phi}) \end{cases} \qquad (1.5.1)$$

$$\begin{cases} L = 2r_1 \int_{0}^{\pi/2 - \delta} \sqrt{1 - (1 - \cot^2 \phi) \sin^2 \psi}\ d\psi \\ 45^\circ \leq \phi \leq 90^\circ \\ \delta = \cos^{-1} (\sin \alpha_m \sqrt{\sin \phi}) \end{cases} \qquad (1.5.2)$$

For $\phi = 0$, L/r_1 is again indeterminate, but by applying L'Hospital's Rule once

$$\lim_{\phi \to 0} L/r_1 = \sin^2 \alpha_m \qquad (1.5.3)$$

The values of α_m chosen were $\sin \alpha_m = 0.7$, 0.8, and 0.9. $\sin \alpha_m = 1.0$ is given in Section 1.1. With these three values of α_m three equations of the type

$$L/r_1 = f_i (\sin \phi) = a_i \sin^2 \phi + b_i \sin \phi + c_i \qquad (1.5.4)$$

were determined with $i = 1, 2, 3$ denoting $\sin \alpha_m = 0.7$, 0.8, 0.9 respectively. Tables 1.5.1 and 1.5.2 give values of L/r_1 for $0 \leq \phi \leq 45^\circ$ and $45^\circ \leq \phi \leq 90^\circ$ for the three values of α_m. These are plotted in Figure 1.5.1.

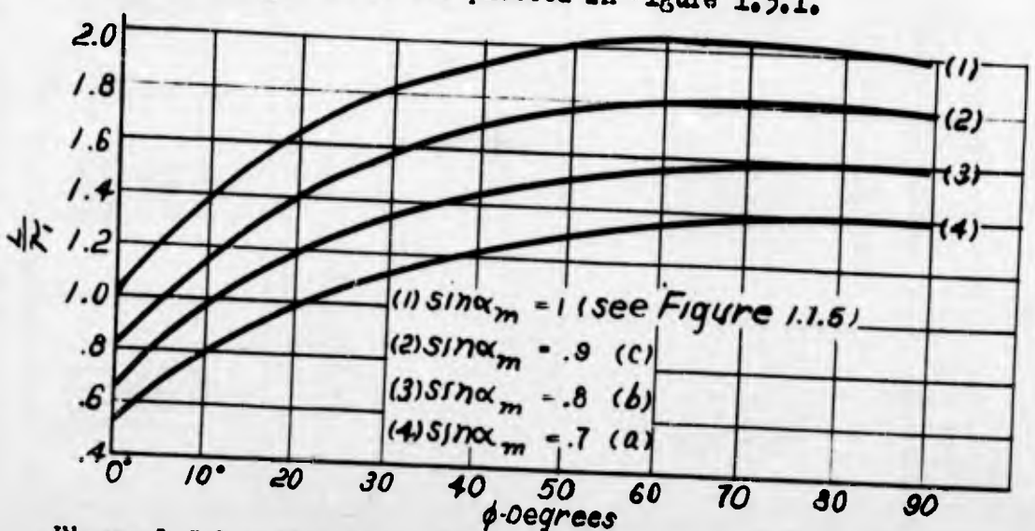

Figure 1.5.1 - Variation of L/r_1 vs ϕ for Various Values of $\sin \alpha_m$

Table 1.5.1 – Values of the Ratio L/r_1 vs ϕ ($0 \leq \phi \leq 45°$)

①	②	③	④	⑤	⑥	⑦ Arc cos [sin α_m · ③]		
ϕ	sin ϕ	$\sqrt{\sin \phi}$	tan ϕ	$\sqrt{1 - \tan^2\phi}$	Arc sin ⑤	sin α_m =.7	sin α_m =.8	sin α_m =.9
0°	–	–	–	–	–	–	–	–
10°	.17365	.41671	.17633	.98433	79° 50.6'	73° 2.43'	70° 31.59'	67° 58'
20°	.34202	.58482	.36397	.93141	68° 39.36'	65° 50.08'	62° 06.27'	58° 15'
30°	.50000	.70711	.57735	.81650	54° 44.18'	60° 19.12'	55° 33'	50° 31'
40°	.65279	.80174	.83910	.54398	32° 57.27'	55° 51.58'	50° 06.27'	43° 49'
45°	.70711	.84090	1.00000	.00000	00° 00'	53° 56.42'	47° 43.36'	40° 49'

⑧ E (α_1, γ') *			⑨ E (α, $\pi/2$) *			⑩ L/r_1 = [⑨ – ⑧] 2/ ④		
sin α_m =.7	sin α_m =.8	sin α_m =.9	sin α_m =.7	sin α_m =.8	sin α_m =.9	sin α_m =.7	sin α_m =.8	sin α_m =.9
–	–	–	–	–	–	.4900	.6400	.8100
.9709	.9553	.9377	1.0412	1.0412	1.0412	.7974	.9754	1.161
.9518	.9161	.8779	1.1306	1.1306	1.1306	.9825	1.1787	1.413
.9385	.8783	.8110	1.2612	1.2612	1.2612	1.1179	1.3264	1.559
.9357	.8453	.7443	1.4467	1.4467	1.4467	1.2180	1.4334	1.674
.9415	.8330	.7121	1.5708	1.5708	1.5708	1.2586	1.4756	1.7168

*Reference 8, pages 69 – 72

Table 1.5.2 – Values of the Ratio L/r_1 vs ϕ ($45° \leq \phi \leq 90°$)

①	②	③	④	⑤	⑥	⑦		
						δ = Arc cos [sin α_m · ③]		
ϕ	sin ϕ	$\sqrt{\sin \phi}$	cot ϕ	$\sqrt{1 - \cot^2 \phi}$	Arc sin ⑤	sin α_m =.7	sin α_m =.8	sin α_m =.9
45°	.70711	.84090	1.0000	.00000	00° 00'	53° 56.42'	47° 43.36'	40° 48'
50°	.76604	.87524	.83910	.54398	32° 57.27'	52° 23.04'	45° 33.48'	38° 01.62'
60°	.86603	.93061	.57735	.81650	54° 44.18'	49° 21.04'	41° 53.10'	33° 07'
70°	.93969	.96938	.36397	.93141	68° 39.36'	47° 16.08'	39° 09'	29° 16'
80	.98481	.99238	.17633	.98433	79° 50.60'	45° 59.95'	37° 26.12'	20° 44'
90°	1.0000	1.0000	.00000	1.0000	90° 00'	45° 34.38'	36° 52.18'	25° 50'

⑧			⑨			⑩		
$\pi/2 - \delta$			E (α, $\pi/2 - \delta$) *			L/r_1 = 2 ⑨		
sin α_m =.7	sin α_m =.8	sin α_m =.9	sin α_m =.7	sin α_m =.8	sin α_m =.9	sin α_m =.7	sin α_m =.8	sin α_m =.9
36° 3.18'	42° 16.64'	49° 12'	.6292	.7378	.8587	1.2584	1.4756	1.7168
37° 46.96'	44° 26.52'	51° 58.38'	.6462	.7547	.8748	1.2924	1.5094	1.750
40° 38.96'	48° 06.90'	56° 53'	.6719	.7788	.8955	1.3438	1.5576	1.791
42° 43.91'	50° 51'	60° 44'	.6883	.7923	.9020	1.3766	1.5846	1.804
44° 0.05'	52° 33.88'	63° 16'	.6972	.7986	.9012	1.3944	1.5972	1.8024
44° 25.62'	53° 07.82'	64° 10'	.7000	.8000	.9000	1.4000	1.6000	1.8000

* Reference 8, pages 69 – 72

As in Section 1.1 the constants a_i, b_i, and c_i of Equation (1.5.4) are determined by using the values of L/r_1 at $\phi = 0$, 45° and 90°. With these values of L/r_1 the parametric equations of the Cartesian coordinates x and z are determined and also the length s. The results are given below. The coordinates x/x_m and z/x_m are given in Table 1.5.3 for $0 \leq \phi \leq \pi/4$.

Equations of L/r_1, x/x_m, z/x_m and s/x_m for Various Values of α_m are:

$$L/r_1 = -.604 \sin^2\phi + 1.514 \sin\phi + .490 \quad (\sin\alpha_m = .7)$$

$$= -.757 \sin^2\phi + 1.717 \sin\phi + .640 \quad (\sin\alpha_m = .8)$$

$$= -.998 \sin^2\phi + 1.988 \sin\phi + .810 \quad (\sin\alpha_m = .9)$$

$$= -1.367 \sin^2\phi + 2.367 \sin\phi + 1.000 \quad (\sin\alpha_m = 1.0)$$

$$x/x_m = .5168 \log \left[9.639\,(.290 + \sin\phi)\,(2.796 - \sin\phi)^{-1}\right], (\sin\alpha_m = .7)$$

$$= .5291 \log \left[7.96\,(.326 + \sin\phi)\,(2.594 - \sin\phi)^{-1}\right], (\sin\alpha_m = .8)$$

$$= .5224 \log \left[6.74\,(.347 + \sin\phi)\,(2.338 - \sin\phi)^{-1}\right], (\sin\alpha_m = .9)$$

$$= .5036 \log \left[5.85\,(.351 + \sin\phi)\,(2.083 - \sin\phi)^{-1}\right], (\sin\alpha_m = 1.0)$$

$$z/x_m = 1.107 \tan^{-1}(1.071 \tan\phi/2 - .3829)$$
$$-.1566 \log \left[(.290 \tan\phi/2 + .043)\,(.290 \tan\phi/2 + 1.957)^{-1}\right] - .1934$$
$$(\sin\alpha_m = .7)$$

$$= 1.147 \tan^{-1}(1.084 \tan\phi/2 - .4178)$$
$$-.1824 \log \left[(.326 \tan\phi/2 + .055)\,(.326 \tan\phi/2 + 1.945)^{-1}\right] - .1977$$
$$(\sin\alpha_m = .8)$$

$$= 1.156 \tan^{-1}(1.106 \tan\phi/2 - .4731)$$
$$-.1933 \log \left[(.347 \tan\phi/2 + .062)\,(.347 \tan\phi/2 + 1.938)^{-1}\right] - .1543$$
$$(\sin\alpha_m = .9)$$

$$= 1.148 \tan^{-1}(1.140 \tan\phi/2 - .5473)$$
$$-.1888 \log \left[(.351 \tan\phi/2 + .064)\,(.351 \tan\phi/2 + 1.936)^{-1}\right] - .0695$$
$$(\sin\alpha_m = 1.0)$$

$$s/x_m = .3958 \tan^{-1} (1.071 \tan \phi/2 - .3829)$$
$$+.5400 \log \left[(.290 \tan \phi/2 + .043)(.290 \tan \phi/2 + 1.957)^{-1}\right] + 2.2064$$
$$(\sin \alpha_m = .7)$$
$$= .4421 \tan^{-1} (1.084 \tan \phi/2 - .4178)$$
$$+.5597 \log \left[(.326 \tan \phi/2 + .055)(.326 \tan \phi/2 + 1.945)^{-1}\right] + 2.1748$$
$$(\sin \alpha_m = .8)$$
$$= .4942 \tan^{-1} (1.106 \tan \phi/2 - .4731)$$
$$+.5570 \log \left[(.347 \tan \phi/2 + .062)(.347 \tan \phi/2 + 1.938)^{-1}\right] + 2.1348$$
$$(\sin \alpha_m = .9)$$
$$= .5512 \tan^{-1} (1.140 \tan \phi/2 - .5473)$$
$$+.5378 \log \left[(.351 \tan \phi/2 + .064)(.351 \tan \phi/2 + 1.936)^{-1}\right] + 2.1073$$
$$(\sin \alpha_m = 1.0)$$

Table 1.5.3 – Values of x/x_m and z/x_m vs ϕ ($0 \leq \phi \leq 45°$) for a Flat Canopy with $\sin \alpha_m = .9, .8$ and $.7$

①	②	③	④	⑤	⑥	⑦	⑧	⑨	⑩	⑪
0°	.00000	1.0000	1.0000	1.0000	.0000	.0000	.0000	.0000	.0000	.0000
2°	.03490	1.1173	1.1222	1.1344	.11093	.11529	.12610	.0579	.0610	.0652
4°	.06976	1.2381	1.2477	1.2723	.21359	.22131	.24082	.1116	.1171	.1245
6°	.10453	1.3620	1.3761	1.4130	.30895	.31926	.34571	.1614	.1689	.1787
8°	.13917	1.4898	1.5080	1.5573	.39866	.41080	.44295	.2083	.2174	.2289
10°	.17365	1.6210	1.6430	1.7046	.48304	.49652	.53333	.2523	.2627	.2756
15°	.25882	1.9631	1.9929	2.0851	.67452	.68958	.73482	.3524	.3649	.3798
20°	.34202	2.3257	2.3606	2.4825	.84402	.85891	.90926	.4409	.4544	.4699
25°	.42262	2.7071	2.7437	2.8941	.99587	1.00931	1.06267	.5202	.5340	.5492
30°	.50000	3.1048	3.1393	3.3165	1.13294	1.14400	1.19891	.5918	.6053	.6196
35°	.57358	3.5153	3.5436	3.7455	1.25712	1.26514	1.32056	.6567	.6694	.6825
40°	.64279	3.9338	3.9515	4.1756	1.36960	1.37409	1.42926	.7155	.7270	.7386
45°	.70711	4.3544	4.3574	4.6008	1.47119	1.47188	1.52623	.7685	.7788	.7888

① = ϕ

② = $\sin \phi$

③ = $6.7392\ (.3470 + ②)/(2.3385 - ②)$

④ = $7.9598\ (.3259 + ②)/(2.5941 - ②)$

⑤ = $9.639\ (.2901 + ②)/(2.7963 - ②)$

⑥ = log ③

⑦ = log ④

⑧ = log ⑤

⑨ = $x/x_m = .5224$ ⑥ for ($\sin \alpha_m = .9$)

⑩ = $x/x_m = .5291$ ⑦ for ($\sin \alpha_m = .8$)

⑪ = $x/x_m = .5168$ ⑧ for ($\sin \alpha_m = .7$)

Table 1.5.3 (cont)

(1) ø	(12)	(13)	(14)	(15)	(16)	(17)	(18)	(19) z/x_m sin α_m =.9	(20) z/x_m sin α_m =.8	(21) z/x_m sin α_m =.7
0	.00000	-.5107	-.4538	-.4047	.6651	.6518	.5977	.0000	.0000	.0000
2	.01746	-.4924	-.4353	-.3867	.6476	.6341	.5807	.0009	.0011	.0006
4	.03492	-.4737	-.4163	-.3683	.6319	.6182	.5656	.0039	.0042	.0039
6	.05241	-.4549	-.3973	-.3496	.6172	.6037	.5517	.0080	.0087	.0087
8	.06993	-.4354	-.3780	-.3306	.6037	.5902	.5390	.0140	.0145	.0150
10	.08749	-.4159	-.3583	-.3117	.5910	.5778	.5272	.0208	.0218	.0221
15	.13165	-.3658	-.3079	-.2627	.5630	.5500	.5014	.0429	.0444	.0453
20	.17633	-.3133	-.2555	-.2122	.5385	.5259	.4791	.0709	.0727	.0735
25	.22169	-.2589	-.2015	-.1600	.5169	.5047	.4598	.1037	.1055	.1064
30	.26795	-.2021	-.1454	-.1059	.4972	.4856	.4424	.1408	.1425	.1431
35	.31530	-.1429	-.0871	-.0502	.4793	.4680	.4265	.1821	.1832	[illegible]9
40	.36397	-.0814	-.0267	+.0074	.4627	.4520	.4119	.2270	.2276	.2259
45	.41421	-.0172	+.0357	+.0670	.4473	.4369	.3984	.2758	.2749	.2720

NOTE:

(1) = ø

(12) = $\tan ø/2$

(13) = $1.1558 \tan^{-1}[1.1062\ (12) - .4731]$

(14) = $1.1468 \tan^{-1}[1.0838\ (12) - .4178]$

(15) = $1.1068 \tan^{-1}[1.0708\ (12) - .3829]$

(16) = $-.1933 \log \dfrac{.3470\ (12) + .062}{.3470\ (12) + 1.938}$

(17) = $-.1824 \log \dfrac{.326\ (12) + .055}{.326\ (12) + 1.945}$

(18) = $-.1566 \log \dfrac{.290\ (12) + .043}{.290\ (12) + 1.957}$

(19) = (13) + (16) - .1543

(20) = (14) + (17) -.1977

(21) = (15) + (18) -.1934

The tabulation of x/x_m and z/x_m is restricted to the range $0 \leq \phi \leq \pi/4$ because this is the only part of the curve which is ultimately used in the combined solution of Section 1.4. The maximum difference in x/x_m and z/x_m for various values of α_m may be expected to occur at or near $\phi = \pi/2$, however, These values are tabulated below.

Table 1.5.4 - x/x_m and z/x_m for $\phi = \pi/4$ and Various Values of $\sin \alpha_m$

$\sin \alpha_m$	0.7	0.8	0.9	0.10
x/x_m	.7888	.7788	.7685	.7564
z/x_m	.2720	.2749	.2758	.2784

The maximum difference in x/x_m is 4.3% while in z/x_m the maximum difference is 2.35%. The maximum error in the cord line shape introduced by taking $\sin \alpha_m = 1.0$, accordingly, should be no more than 4 or 5%; in fact, since α_m in most cases seems to be greater than $\pi/3$, the error is probably less than 2%. The assumption in Section 1.1, that $\alpha_m = \pi/2$, therefore seems justified, since greater accuracy is not claimed for the solution.

1.6 Extended Skirt Canopy

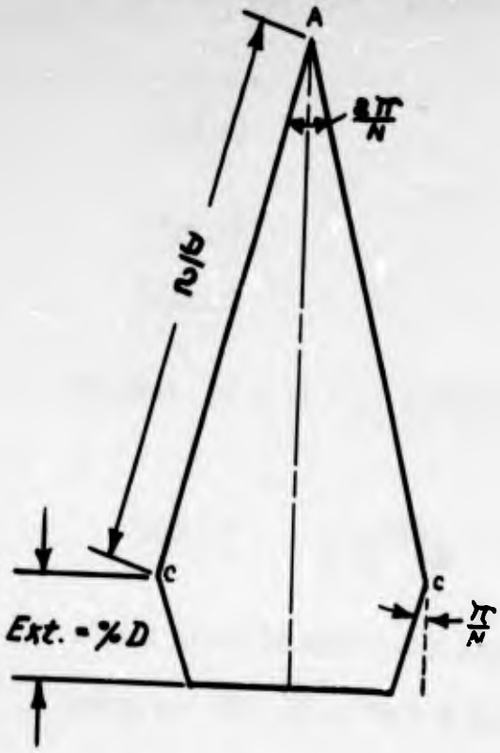

Figure 1.6.1

The extended skirt canopy is one in which the triangular gore is extended by means of a trapezoidal piece of fabric as indicated in Figure 1.6.1. Denoting by D/2 the length of the gore edge from the apex to the point where the fabric extension starts, the term "extension" of an extended skirt canopy is defined as the ratio of the geometric altitude of the trapezoid to the length D expressed as a percentag'. In extended skirt canopies in which the extension is 10% or 12.5%, the angle included between the extensions of the equal sides of the trapezoid is, according to current design practice, equal to the angle of the triangular gore portion.

In the analysis of the cord shape of an extended skirt canopy it is assumed that the points C (see Figure 1.6.1) are at the MIR in the inflated state, that is $D/2 = l_a$, and that the cord shape above the MIR is geometrically similar to that given in Section 1.4, while the cord portion below MIR follows a parabolic arc.

Representing by e the extension, expressed as a ratio, of an extended skirt canopy we have by definition

$$e = \frac{l_b \cos(\pi/N)}{D} \qquad (1.6.1)$$

Solving Equation (1.6.1) for l_b and taking equation $l_a = D/2$ into account we obtain

$$l_b = \frac{2el_a}{\cos(\pi/N)} \qquad (1.6.2)$$

From Section 1.4, $l_a = ka x_m = 1.3409\, x_m$; (1.6.3)

hence Equation (1.6.2) becomes $l_b \frac{2.6818\, x_m e}{\cos(\pi/N)}$ (1.6.4)

Substituting Equation (1.6.3) and (1.6.4) in the equation $l_c = l_a + l_b$ results in

$$l_c = 1.3409\, x_m + \frac{2.6818\, x_m e}{\cos\ \pi/N} = 1.3409\, x_m \left(1 + \frac{2e}{\cos\ \pi/N}\right) \qquad (1.6.5)$$

For the cord portion from apex to MIR the coordinates are those of Table 1.4.1. Table 1.6.1 gives the ratios x/x_m and z/x_m vs ϕ from $\phi = 0°$ to $\phi = 90°$ as given in Table 1.4.1

Table 1.6.1 : Values of x/x_m and z/x_m vs ϕ

ϕ	x/x_m	z/x_m
0	.0000	.0000
2	.0535	.0010
4	.1115	.0038
6	.1658	.0087
8	.2167	.0150
10	.2647	.0227
20	.4723	.0779
30	.6405	.1561
40	.7802	.2541
45	.8409	.3095
50	.8752	.3470
60	.9306	.4262
70	.9694	.5093
80	.9924	.5948
90	1.0000	.6816

The portion of the cord below MIR is assumed to be a parabolic arc as was done in Section 1.4. The determination of this parabolic arc is slightly different from that in Section 1.4 since the length of the parabolic arc is known from Equation (1.6.4).

From Section 1.3 the length of the cord from MIR to skirt is given by the expression $x_m \frac{1 - k_{sk}}{2} f(n)$; hence:

$$\frac{2.6818\, x_m e}{\cos(\pi/N)} = \frac{1 - k_{sk}}{2} f(n)\, x_m$$

or

$$\frac{2.6818e}{\cos(\pi/N)} = \frac{1 - k_{sk}}{2} f(n) \qquad (1.6.6)$$

But $k_{sk} = k'_s/n = (k_c/n)(k'_s/k_c) = \frac{1.3409}{n}\left(1 + \frac{2e}{\cos \pi/N}\right) k'_s/k_c$ (see Equation (1.6.5)).

Then Equation (1.6.6) gives

$$f(n) = \frac{4e}{\frac{\cos \pi/N}{1.3409} - \frac{1}{n}(\cos \pi/N + 2e)\, k'_s/k_c} \qquad (1.6.7)$$

For a particular extended skirt canopy the extension e and the ratio k'_s/k_c are known, and Equation (1.6.7) can be solved by trial and error for the unknown, n. The parabolic arc is given by the equation $Z = c\sqrt{X}$ (1.6.8)
in which Z's are measured from the MIR downward, $X = x_m - x$ and c is a constant determined as follows:

Differentiating Equation (1.6.8) results in $dZ/dX = c/2\sqrt{X}$ (1.6.9)

For $X = x_m - x_{sk} = x_m(1 - k_{sk})$, $dZ/dX = \frac{\sqrt{1 - (1/n)^2}}{1/n} = \sqrt{n^2 - 1}$; then Equation (1.6.9) gives

$$\sqrt{n^2 - 1} = \frac{c}{2\sqrt{x_m (1 - k_{sk})}} \quad \text{or} \quad c = 2\sqrt{(n^2 - 1)(1 - k_{sk})}\ \sqrt{x_m} \qquad (1.6.10)$$

Hence Equation (1.6.8) becomes

$$Z = 2\sqrt{(n^2 - 1)(1 - k_{sk})}\ \ x_m \sqrt{1 - x/x_m} \qquad (1.6.11)$$

The value of k_{sk} involved in Equation (1.6.11) can be determined from equation

$$k_{sk} = \frac{1.3409}{n} \left(1 + \frac{2e}{\cos \pi/N}\right) k_s'/k_c \qquad (1.6.12)$$

The equation for the shape of the cords for the extended skirt canopy with $N = 24$, $l_c/l_s' = 0.6$, and a 10% extension is worked out in Section 1.11 and plotted in Figure 1.11.8.

1.7 Equation on the Cords for the Conical Canopy - First Approximation

The Taylor shape is clearly not a good approximation to the shape of an inflated conical canopy. Culver, Jaeger, and Della-Vedowa (Reference 7), in investigating conical ribbon canopies, assume the cord shape to consist of a straight line from the apex plus a circular or elliptical arc tangent to this line and to another straight line below MIR. While this approach led to useful results, it was decided to attempt to obtain a solution having a more fundamental physical basis.

Two assumptions are introduced: (1) as a first approximation, the fullness of the gore of the inflated canopy is neglected and the sections of the canopy cut by horizontal planes are assumed to be regular polygons; (2) the cord below the maximum inflated radius is assumed to follow a curve symmetrical to a portion of the cord above the MIR, the symmetry being considered about the MIR.

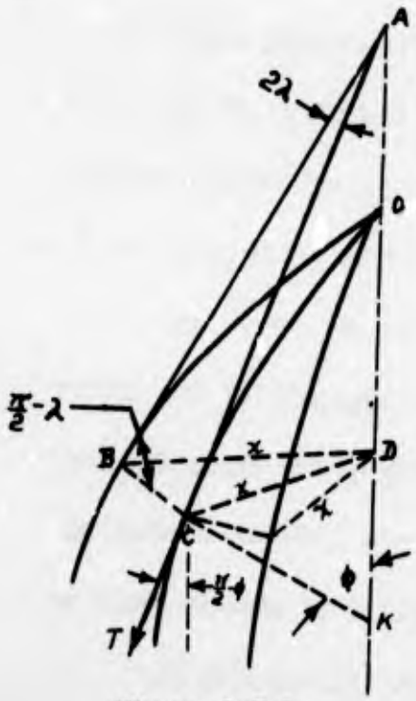

Figure 1.7.1

For any horizontal section of the canopy formed by cutting the cords at points x distant from the axis of canopy the equation of equilibrium of the upper free body is

$$N \tfrac{1}{2} x^2 p \sin(2\pi/N) = NT \sin\phi$$

or $$T \sin\phi = \tfrac{1}{2} x^2 p \sin(2\pi/N) \qquad (1.7.1)$$

Figure 1.7.2 shows an infinitesimal length ds of the cord as a free body under loading by the fabric.

The resultant fabric-cord force dF corresponding to a length ds of the cord is given by the equation.

$$dF = (ds \cos\lambda)\, f_1$$

Therefore the equilibrium of forces upon the

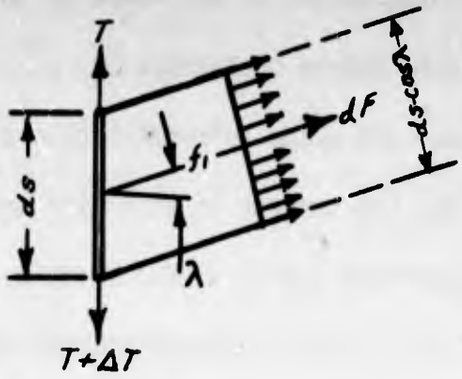

Figure 1.7.2

axis of T gives the equation

$$T + 2dF \cos(\pi/2 - \lambda) = T + \Delta T$$

$$\text{or} \quad \Delta T = 2f_1 ds \cos\lambda \sin\lambda \qquad (1.7.2)$$

But $ds = \sec\phi\, dx$; hence Equation (1.7.2) becomes

$$dT/dx = \frac{f_1 \sin 2\lambda}{\cos\phi} \qquad (1.7.3)$$

From the right triangle ACD of Figure 1.7.1

$$CD = CA \cos\phi$$

From the isosceles triangles BCD, BCA: $BC/2 = CD \sin\pi/N = CA \cos\phi$.

Dividing these two last equations we get $\sin\pi/N = \frac{\sin\lambda}{\cos\phi}$

$$\text{or} \quad \sin\lambda = \sin(\pi/N)\cos\phi \qquad (1.7.4)$$

$$\text{hence} \quad \cos\lambda = \sqrt{1 - \sin^2(\pi/N)\ \cos^2\phi} \qquad (1.7.5)$$

Determination of f_1

The resultant of the forces acting normal to the infinitesimal strip CE (Figure 1.7.3) is equated to the normal components, upon the plane of this strip, of the axial forces acting along the strips of the canopy on either side of CE.

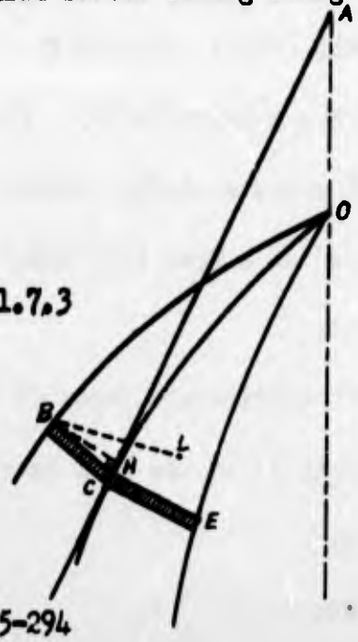

Figure 1.7.3

Normal force on CE = $2x\ p \sin(\pi/N) \cos\lambda\ ds$

Axial force in BC = $f_1 \cos\lambda\ ds$

To find the normal component of the latter force upon the plane of the strip CE, the trihedral solid angle C.ABE is considered from a different point of view in order to clarify the picture (Figure 1.7.4).

In Figure 1.7.4 BL is normal to the place ACE

BH is normal to the line CA

Then LH is normal to the line CA

μ = Angle (unknown) formed by BC and the normal CN to the plane ACE

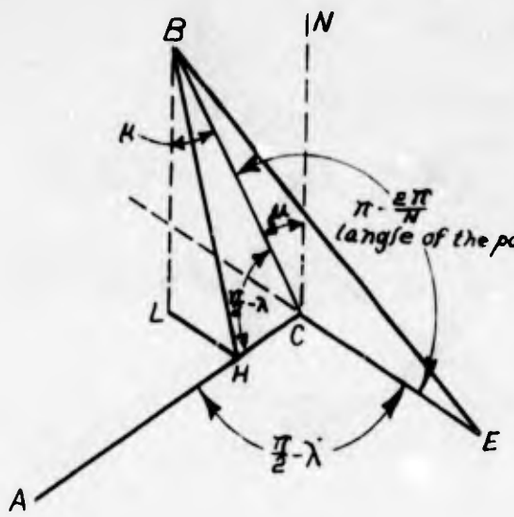

Figure 1.7.4

BL = BC cos μ = BH sin (Angle $\widehat{BHL}$)

But angle $\widehat{BHL}$ = 180° - B.AC.E where B.AC.E represents the dihedral angle formed by the planes BAC and EAC.

Then BL = BC cos μ = BH sin (B.AC.E)

(1.7.6)

But BH = BC sin $(\pi/2 - \lambda)$ = BC cos λ

Therefore Equation (1.7.6) becomes:

BC cos μ = BC cos λ sin (B.AC.E) or

$\cos\mu = \cos\lambda \sin$ (B.AC.E) (1.7.7)

From isosceles triangles BCE and BHE we have:

BE/2 = BC sin $(\pi/2 - \pi/N)$ = BC cos π/N

and BE/2 = BH sin $(\frac{1}{2}$ B.AC.E)

Then BC cos π/N = BH sin $(\frac{1}{2}$ B.AC.E) or

BC/BH cos π/N = sin $(\frac{1}{2}$ B.AC.E) (1.7.8)

But BC/BH = csc $(\pi/2 - \lambda)$ = sec λ

Hence Equation (1.7.8) becomes sec λ cos (π/N) = sin $(\frac{1}{2}$ B.AC.E)

Then $\sin$ (B.AC.E) = $\frac{2 \cos(\pi/N)}{\cos^2 \lambda} \sqrt{\cos^2\lambda - \cos^2(\pi/N)}$

and Equation (1.7.7) becomes:

$$\cos\mu = \frac{2\cos(\pi/N)}{\cos\lambda}\sqrt{\cos^2\lambda - \cos^2(\pi/N)} \qquad (1.7.9)$$

Then the component normal to the plane of the strip CE due to the axial forces acting along the two adjacent strips is $f_1 ds \cos\lambda \cos\mu$. Consequently the equation of equilibrium of the forces normal to the plane of the strip CE is:

$$2xp \sin(\pi/N) \cos\lambda \, ds = 2f_1 \cos\lambda \cos\mu \, ds$$

Substituting Equation (1.7.9) in the last equation results in

$$xp \tan(\pi/N) = \frac{2f_1}{\cos\lambda}\sqrt{\cos^2\lambda - \cos^2(\pi/N)} \qquad (1.7.10)$$

From Equation (1.7.5), $\cos^2\lambda = 1 - \sin^2(\pi/N)\cos^2\phi = \sin^2\phi + \cos^2\phi\cos^2(\pi/N)$

Thence Equation (1.7.10) becomes:

$$xp \tan(\pi/N) = \frac{2f_1}{\cos\lambda}\sqrt{1 - \sin^2(\pi/\lambda)\cos^2\phi - \cos^2(\pi/N)}$$

from which $$f_1 = \frac{xp\cos\lambda}{2\cos(\pi/N)\sin\phi} \qquad (1.7.11)$$

Substituting Equation (1.7.11) in Equation (1.7.3) results in

$$dT/dx = xp\tan(\pi/N)\left[1 - \sin^2(\pi/N)\cos^2\phi\right]\csc\phi \qquad (1.7.12)$$

Differentiating Equation (1.7.1) we obtain

$$T\cos\phi\, d\phi + \sin\phi\, dT = p\sin(2\pi/N)\, x\, dx \qquad (1.7.13)$$

Substituting Equation (1.7.1) and (1.7.12) in Equation (1.7.13) we get

$$dx/x = \frac{\cos^2(\pi/N)\cot\phi}{2\cos^2(\pi/N) - \left[1 - \sin^2(\pi/N)\cos^2\phi\right]}\, d\phi \qquad (1.7.14)$$

Integrating:

$$\log x = \cos^2(\pi/N)\int\frac{\cot\phi\, d\phi}{2\cos^2(\pi/N) - \left[1 - \sin^2(\pi/N)\cos^2\phi\right]} + C \qquad (1.7.15)$$

Performing the integration indicated in Equation (1.7.15) and taking into account the boundary condition $x = x_m$ for $\phi = 90°$, we obtain the following equation

$$x = x_m \frac{\sqrt{\cos(2\pi/N)}}{\sqrt{\cos^2(\pi/N)\cot^2\phi + \cos(2\pi/N)}} \qquad (1.7.16)$$

From the geometry of the uninflated canopy it is evident that there is a lower limit for the angle ϕ below which the corresponding values of x taken from Equation (1.7.16) do not have any physical meaning. This limiting value of ϕ can be either β or some angle $\beta' > \beta$. This limiting value of ϕ determines an upper point above which the Equation (1.7.16) does not hold because even for $\phi = \beta$ the corresponding x is far from being zero.

Assuming that this limiting value of ϕ is $\beta' > \beta$, the upper portion of the cord must be a curve tending asymptotically to the angle β as it approaches the apex following an equation different than Equation (1.7.16). If the pattern of the canopy has any direct relation to the inflated shape, there must be a relation between the arc $r_1\alpha$ and some line in the flat pattern. As an initial assumption let $r_1\alpha = s\xi$ and $r_1 \sin\alpha = x \sin\pi/N$.

Then $$\frac{r_1\alpha}{r_1 \sin\alpha} = \frac{s\xi}{x \sin(\pi/N)}$$

Near the apex, $x = s\cos\beta$; so $$\alpha/\sin\alpha = \frac{\xi}{\sin(\pi/N)\cos\beta}$$

But if the cord tensions are constant, the cords must have a horizontal tangent at the apex, and $\beta = 0$, $ds = dx$. The $\alpha_o/\sin\alpha_o = \xi/\sin(\pi/N)$ in which $\xi <$ (π/N).

Since $\alpha > \sin\alpha$, this leads to anomalies if $\xi < \pi/N$, as of course it is in a conical canopy. There are two possible alternatives: 1) The cord tension is not really constant and the canopy is not flat on top but rather of a conical shape; 2) the cord tension is constant and the inflated canopy shape is independent of the pattern.

The first alternative appears to be the correct one for solid conical canopies, in which the cords are sewed to the cloth or actually consist of a heavy seam from skirt to vent; but the characteristic conical inflated shape near the apex is not seen in photographs of conical ring slot or personnel guide surface canopies. In the latter the cords are sewed to the canopy only at the skirt and at the vent, but in the conical ring slot canopy the cloth rings are continuously sewed to the cords. The cord tension in the personnel guide surface type is necessarily constant except perhaps for the effect of friction, and photographs of both types show a rounded apex. The second alternative is arrived at by the following reasoning. It is certain that the line described by the arc $2s\xi$ in the plane of the flat gore does not coincide with the arc $2r_1\alpha$ in the inflated state. The center of the arc $2r_1\alpha$ must be a distance greater than s from the apex when measured along the centerline of gore if its ends are a distance s (along the cords) from the same point; so the length of such an arc in the flat pattern must be greater than $2s\xi$.

The smallest value $r_1\alpha$ can have if the anomaly at the apex is to be avoided is $s\pi/N$. Since a conical canopy cannot be flat at the apex when inflated without being wrinkled, there can be no real agreement between the uninflated and inflated shapes, and it is necessary to depend on a solution which is independent of the uninflated shape. One such solution is given by Stevens and Johns (Reference 2,

page 7).

While the reason for this disagreement in the personnel guide surface canopy is of necessity the constant tension in the cords over the canopy, the reason is not at all clear in the case of the conical ring slot type. Jaeger, Culver, and Della-Vedowa (Reference 7) state that in a conical ribbon canopy (with horizontal ribbons), "the conical shape is maintained near the top", although no photographs or other evidence are presented in support of the statement. Later on, however, "observations of photographs" are referred to, which suggest that the conical apex was actually observed. Their analysis, like the present one, gives zero tension at the apex. Thus the conical ring slot canopy, which has a rounded apex, and would be expected to fall between the conical and the conical ribbon types, apparently resembles neither in its inflated shape, since both the latter have conical apexes.

It is concluded above that the portion of the cord around the apex for the conical canopy is a straight line which is assumed to start from the apex and end at the lowest point where $\phi = \beta$. It is evident that this straight line is tangent to the lower curved portion for which Equation (1.7.16) holds.

Differentiating Equation (1.7.16) and substituting cot ϕ ds and sec ϕ ds alternatively for dx and integrating the resulting equations, taking also into account boundary conditions, that is for $\phi = \beta$, $z_o = x_o \tan \beta$ and $s_o = x_o \sec \beta$ where x_o is the value of x taken from Equation (1.7.16) for $\phi = \beta$, we obtain respectively:

$$z = \frac{x_m}{\cot\beta\sqrt{\cos(2\pi/N)}}\sqrt{\cos^2(\pi/N)\cot^2\beta + \cos(2\pi/N)}$$

$$- x_m \frac{\cos^2(\pi/N)}{\sqrt{\cos(2\pi/N)}} \frac{\cot\phi}{\sqrt{\cos^2(\pi/N)\cot^2\phi + \cos(2\pi/N)}} \qquad (1.7.17)$$

$$z = \frac{x_m\sqrt{\cos(2\pi/N)}}{\cos\beta} \frac{1}{\sqrt{\cos^2(\pi/N)\cot^2\beta + \cos(2\pi/N)}} \qquad (1.7.18)$$

$$+ x_m \frac{\sqrt{\cos(2\pi/N)}}{\cos(\pi/N)} \int_\beta^\phi \frac{d\phi}{\left[1 - \tan^2(\pi/N)\sin^2\phi\right]^{3/2}}$$

It is to be noted that elimination of parameter ϕ between Equations (1.7.16) and (1.7.17) leads to the equation

$$\frac{(x/x_m)^2}{1} + \frac{(z/x_m - A)^2}{(\sqrt{B})^2} = 1 \qquad (1.7.19)$$

in which $$A = \sec\beta\sqrt{\frac{\cos^2(\pi/N)\cot^2\beta + \cos(2\pi/N)}{\cos(2\pi/N)}} \qquad (1.7.20)$$

and $$B = \frac{\cos^2(\pi/N)}{\cos(2\pi/N)} \frac{\frac{1}{2}\left[1 + \cos(2\pi/N)\right]}{\cos(2\pi/N)} \equiv \frac{1}{2}\left[\sec(2\pi/N) + 1\right] > 1$$

for $n \geq 4$.

Equation (1.7.19) is that of an ellipse with semi-major axis = $\sqrt{B}$

semi-minor axis = 1

and center at $x/x_m = 0$, $z/x_m = A$

Table 1.7.1 gives values of the non-dimensional coordinates x/x_m and z/x_m for various values of the parameter angle ϕ between β and 90°. The same table

gives also values of s/x_m obtained by numerical integration of Equation (1.7.18). The list of constant values used in this table is given below (values of N and β have been chosen as 24 and 30° respectively for this example):

$$\textcircled{1} = \cos(2\pi/N) = .96593$$

$$\textcircled{2} = \cos^2(\pi/N) = .98295$$

$$\textcircled{3} = \sqrt{\cos(2\pi/N)} = .9828$$

$$\textcircled{4} = \cot\beta = 1.73205$$

$$\textcircled{5} = \frac{\sqrt{\cos^2(\pi/N)\cot^2\beta + \cos(2\pi/N)}}{\cot\beta\sqrt{\cos(2\pi/N)}} = 1.16228$$

$$\textcircled{6} = \frac{\cos^2(\pi/N)}{\sqrt{\cos(2\pi/N)}} = 1.00011$$

$$\textcircled{7} = \cos\beta = .86603$$

$$\textcircled{8} = \frac{\sqrt{\cos(2\pi/N)}}{\cos\beta\sqrt{\cos^2(\pi/N)\cot^2\beta + \cos(2\pi/N)}} = .5735$$

$$\textcircled{9} = \frac{\sqrt{\cos(2\pi/N)}}{\cos(\pi/N)} = .99129$$

$$\textcircled{10} = \tan^2(\pi/N) = .01733$$

Table 1.7.1 - Values of x/x_m, z/x_m, s/x_m vs ϕ for a Conical Canopy - First Approximation

(11)	(12)	(13)	(14)	(15)	(16)	(17)
ϕ	cot ϕ			x/x_m	z/x_m	sin ϕ
		$[(2) \cdot (12)^2 + (1)]^{\frac{1}{2}}$	(13) / (12)	(3) / (13)	(5) - [(6) / (14)]	
30°	1.73205	1.9785	1.14229	.49674	.28675	.50000
36°	1.37638	1.6817	1.22183	.58441	.34375	.58779
42°	1.11061	1.4759	1.32891	.66590	.40969	.66913
48°	.90040	1.3277	1.47457	.74023	.48404	.74314
54°	.72654	1.2185	1.67713	.80657	.56596	.80902
60°	.57735	1.1374	1.97004	.86408	.65462	.86603
66°	.44523	1.0775	2.42010	.91211	.74903	.91355
72°	.32492	1.0343	3.18325	.95021	.84810	.95106
78°	.21256	1.0052	4.72902	.97773	.95080	.97815
84°	.10510	.9883	9.40343	.99443	1.06592	.99452
90°	.00000	.9828	∞	1.00000	1.16228	1.00000

* (13) = $\left[\cos(\pi/N)\cot^2\phi + \cos(2\pi/N)\right]^{\frac{1}{2}}$

Table 1.7.1 (Cont)

ø	(18)	(19)	(20)	(21)	(22)	(23)
	$1 - [(10)\ (17)]^2$	$(18)^{-3/2}$	(19) Δ ø	∫(20)	(9) · (21)	e/x_m (8) + (22)
30°	.99567	1.00653	.10553	.00000	.00000	.57358
36	.99401	1.00904	.10581	.10533	.10461	.67819
42	.99224	1.01175	.10609	.21134	.20950	.78308
48	.99043	1.01453	.10639	.31743	.31467	.88825
54	.98864	1.01729	.10667	.42382	.42013	.99371
60	.98700	1.01983	.10692	.53049	.52587	1.09945
66	.98554	1.02210	.10714	.63741	.63186	1.20544
72	.98432	1.02399	.10731	.74455	.73806	1.31164
78	.98342	1.02540	.10743	.85186	.84444	1.41802
84	.98286	1.02627	.10749	.95929	.95093	1.52451
90°	.98267	1.02656		1.06678	1.05749	1.63107

Portion of the Cord below the Maximum Inflated Radius

Assume that the portion of the cord below the MIR follows a curve (of unknown length) symmetrical to that above the MIR, the symmetry being considered with respect to MIR.

Assume also that $l_c/l_s' = .6$.

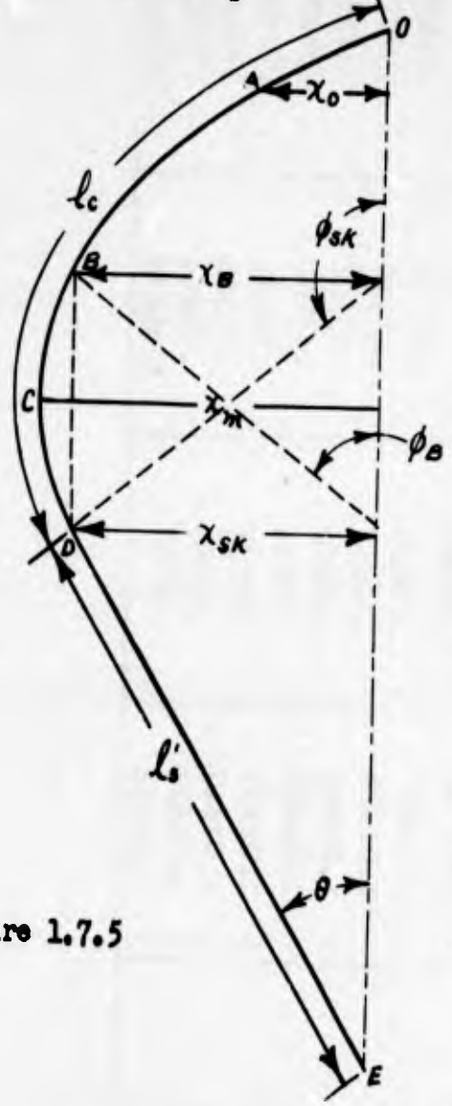

Figure 1.7.5

Arc CD is symmetrical to arc CB about x_m.

B is an unknown point.

$$\theta = \phi_{sk} - 90° \qquad (1.7.21)$$

Due to the symmetry of CB and CD

$$\phi_{sk} = 180° - \phi_B \qquad (1.7.22)$$

Then $\theta = 90° - \phi_B \qquad (1.7.23)$

But $x_{sk} = l_s' \sin\theta = l_s' \cos\phi_B \qquad (1.7.24)$

Also $x_{sk} = x_B$ (due to the symmetry) (1.7.25)

Then Equation (1.7.24) becomes:

$$x_B = l_s' \cos\phi_B \qquad (1.7.26)$$

But $l_c = \widehat{OD} = \widehat{OC} + \widehat{CD} = 2\,\widehat{OC} - \widehat{OB} \qquad (1.7.27)$

Dividing Equations (1.7.27) and (1.7.26) we get

$$l_c/l_s' \cos\phi_B = (2\ \widehat{OC} - \widehat{OB})/x_B$$

or $$.6/\cos\phi_B = (2\ \widehat{OC} - \widehat{OB})/x_B \qquad (1.7.28)$$

Table 1.7.1 provides values for $\widehat{OC}/x_m$ (Column (23) for $\phi = 90°$) as well as for $\widehat{OB}/x_m$ (column (23)). The same table also provides values for x_B/x_m (column (15)

Table 1.7.2 gives values of 0.6 sec ϕ and $(2\ \widehat{OC} - \widehat{OB})/x_m$ vs ϕ.

Figure 1.7.6 represents the graphs of the curves

$$y_1 = 0.6 \sec \phi \quad \text{and} \quad y_2 = (2\,\widehat{OC} - \widehat{OB})/x_m$$

both y_1 and y_2 being plotted against ϕ.

The common point of the curves of Figure 1.7.6 is that which satisfies the equation $y_1 = y_2$ or

$$0.6 \sec \phi = (2\,\widehat{OC} - \widehat{OB})/x_m, \text{ that is Equation (1.7.28)}$$

Consequently the angle ϕ which corresponds to the point of intersection of the above curves is that of the point B.

The graphical solution of Equation (1.7.28) represented in Figure 1.6.6 gives $\phi_B = 72.65°$

Therefore $\phi_{sk} = 180° - 72.65° = 107.35°$ and $\theta = 17.35°$

Figure 1.7.7 gives the complete cord curve from the apex to the skirt.

Table 1.7.2 - Values of $\frac{.6}{\cos \phi}$ and $\frac{2\,\widehat{OC} - \widehat{OB}}{x_B}$ vs ϕ

①	②	③	④	⑤	⑥	⑦	⑧
ϕ	cos ϕ	0.6/cos ϕ	$\widehat{OB}/x_m$	$2\,\widehat{OC}/x_m$	$(2\,\widehat{OC} - \widehat{OB})/x_m$	x_B/x_m	$(2\,\widehat{OC} - \widehat{OB})/x_B$
		0.6/ ②	Column ㉓ of Table 1.7.1	Ref. (see Col. ④ for ϕ = 90°	⑤ - ④	Column ⑮ of Table 1.7.1	⑥ / ⑦
30°	.86603	.69282	.57358	3.26214	2.68856	.49674	5.41241
36	.80902	.74164	.67819		2.58395	.58441	4.42147
42	.74314	.80730	.78308		2.47906	.66590	3.72287
48	.66913	.89669	.88825		2.37389	.74023	3.20696
54	.58779	1.02077	.99371		2.26843	.80657	2.81244
60	.50000	1.20000	1.09945		2.16269	.86408	2.50288
66	.40674	1.47514	1.20544		2.05670	.91211	2.25488
72	.30902	1.94162	1.31164		1.95050	.95021	2.05270
78	.20791	2.88586	1.41802		1.84412	.97773	1.88612
84	.10453	5.73998	1.52451		1.73763	.99443	1.74736
90°	.00000	Infinity	1.63107	3.26214	1.63107	1.00000	1.63107

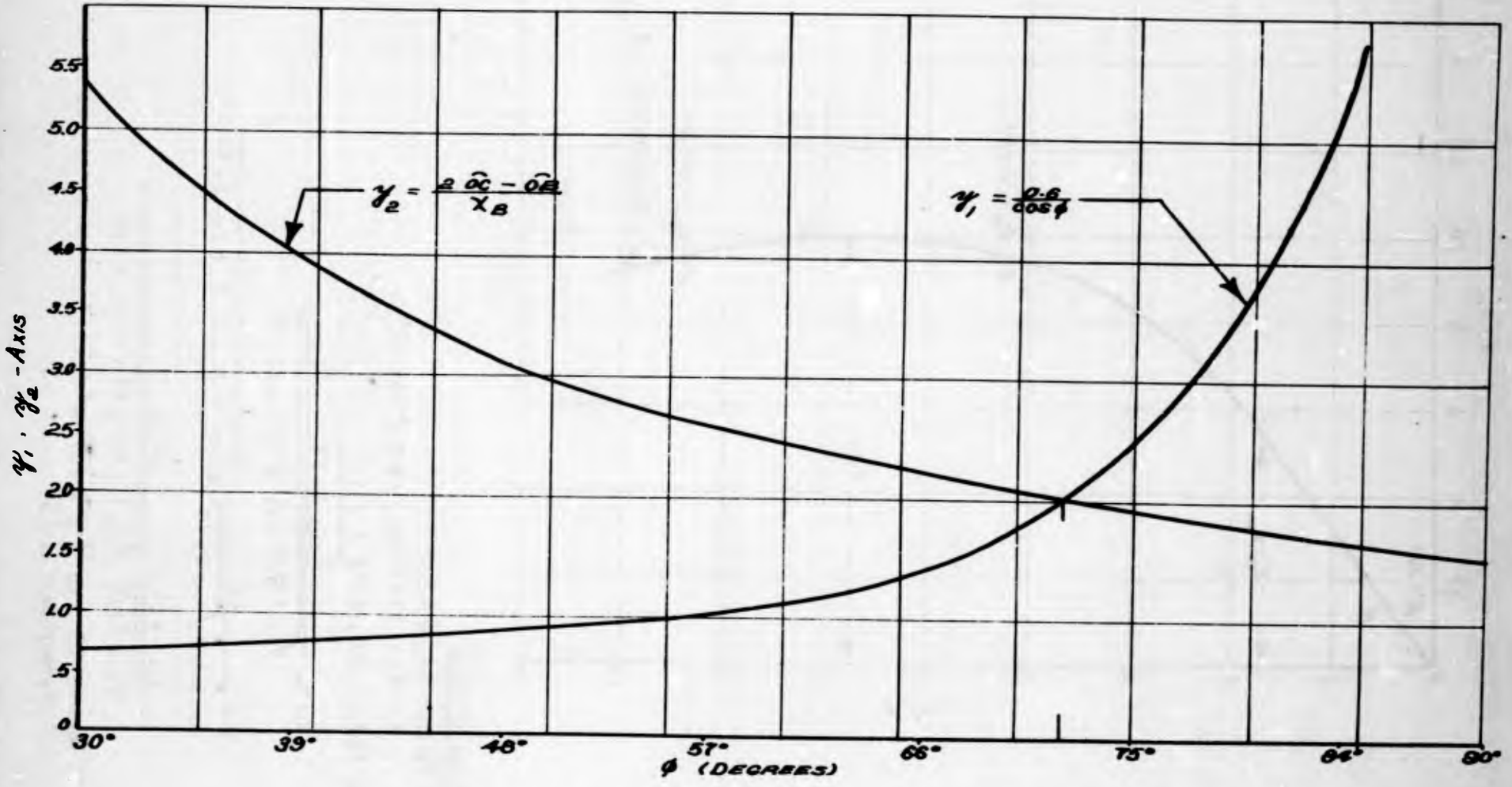

Figure 1.7.6 - Graphical Solution of Equation (1.7.28) - $\phi_B = 72.65°$

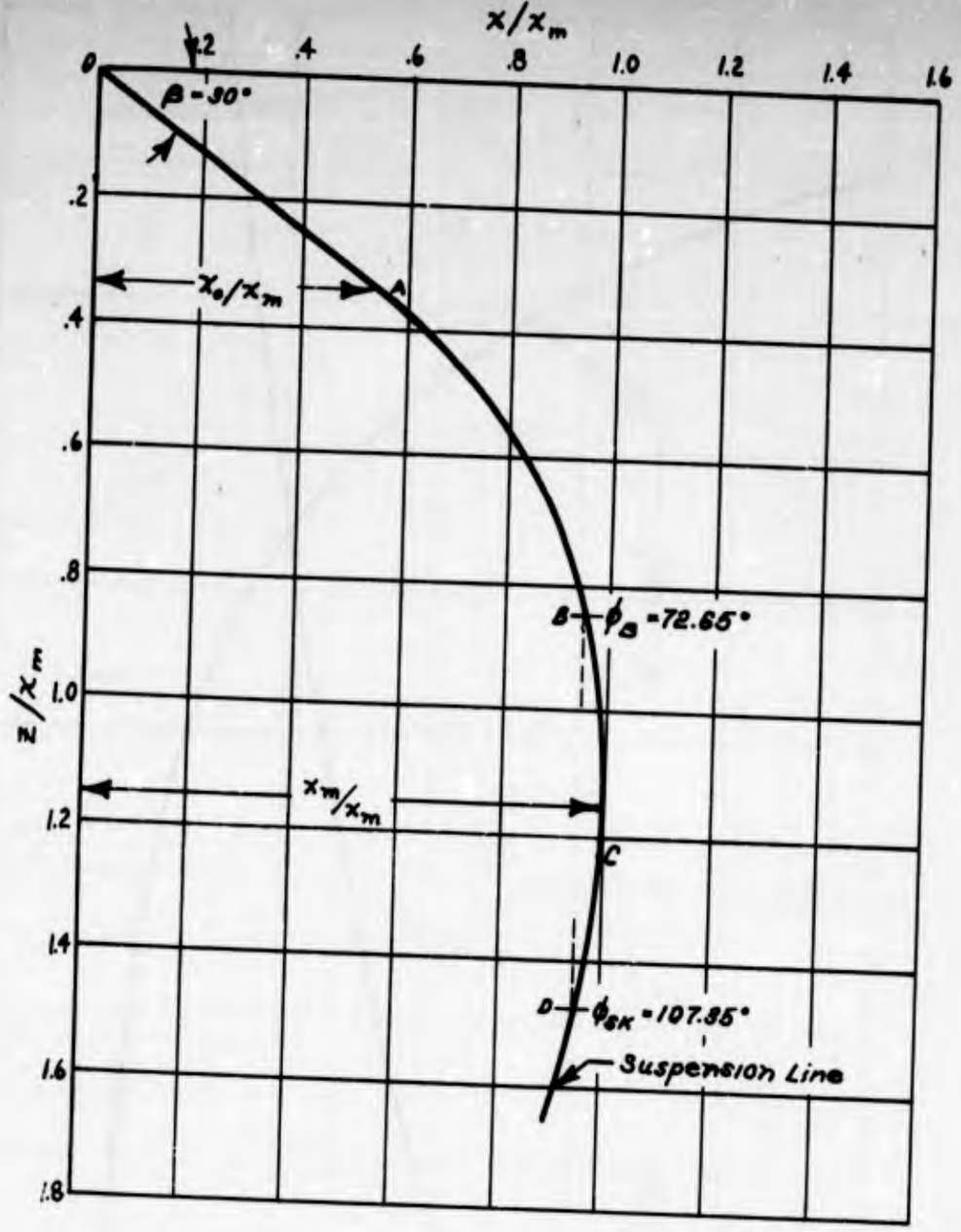

Equations of Cord

1) Portion OA, $\phi = 30°$

$$x_A = x_0 = .49674\, x_m, \quad z = x \tan 30°$$

2) Portion AC, $30° \leq \phi \leq 90°$

$$x = x_m \frac{\sqrt{\cos 2\pi/N}}{\sqrt{\cos^2 \pi/N \cot^2 \phi + \cos 2\pi/N}}$$

$$z = \frac{x_m}{\cot \beta \sqrt{\cos 2\pi/N}} \sqrt{\cos^2 \pi/N \cot^2 \beta + \cos 2\pi/N} - \frac{\cos^2 \pi/N}{\sqrt{\cos 2\pi/N}} \frac{\cot \phi}{\sqrt{\cos^2 \pi/N \cot^2 \phi + \cos 2\pi/N}}$$

3) Portion CD, $90° \leq \phi \leq 107.35°$

Symmetrical of CB

Figure 1.7.7 - Cord Shape of a Conical Canopy. First Approximation
N = 24, $\beta = 30°$, $l_c/l_s = .6$

1.8 Equation of the Cords for the Conical Canopy - Second Approximation

In the previous Section 1.7 the cord shape of a conical canopy has been discussed disregarding fullness in the gores. In the present section the fullness of the canopy between adjacent cords is considered in a manner that simplifies the computations of the cord parametric equations which are derived from the equations of the first approximation.

Because of the complexity of the expressions involved, a numerical solution is given. The particular conical canopy considered whenever numbers are given has these constant parameters: $N = 24$, $\beta = 30°$, $l_c/l_s' = 0.6$

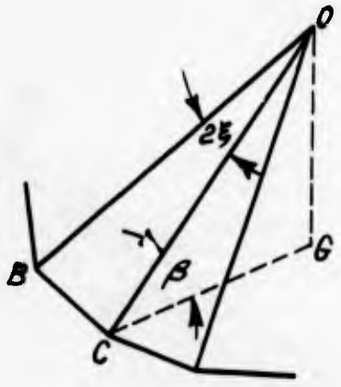

Figure 1.8.1

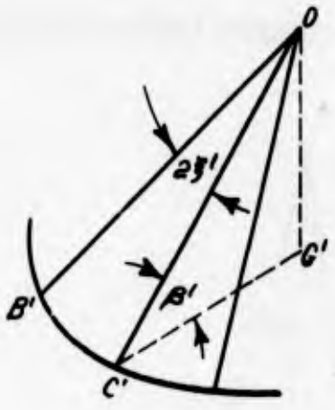

Figure 1.8.2

Figure 1.8.1: Part of the Uninflated Canopy Corresponding to the Uninflated Portion of the Cords (1st Approximation Disregarding Fullness).

$BC/2 = CG \sin(\pi/N) = CO \sin\xi$

$OG/CO \sin(\pi/N) = \sin\xi$

and $\sin\xi = \sin(\pi/N)\cos\beta$ (1.8.1)

Figure 1.8.2: Cone Formed by Cords in Inflated Shape

(Second Approximation Considering Fullness)

$2\pi(C'G') = (OC')\ 2\xi N$

or $\frac{C'G'}{OC'} = \xi N/\pi$, $\cos\beta = \xi N/\pi$ (1.8.2)

and $\cos\beta = \left[\frac{23366.5}{(180)(60^2)}\right] 24 = .865426$

$\beta' = 30°\ 4'\ 8.6''$

Figure 1.8.1 (cont)

$\sin \xi = (.13053)\ (.86603)$

$= .1130429$

$\xi = 6^\circ\ 29'\ 26.5''$

$\cos \xi = .99358895$

Figure 1.8.2 (cont)

$B'C'/2 = C'G' \sin (\pi/N) = OC' \sin \xi'$

$C'G'/OG' \sin (\pi/N) = \sin \xi'$

or $\sin \xi' = \sin (\pi/N) \cos \beta'$ (1.8.3)

$\sin \xi' = (.13053)\ (.865426) = .112964$

$\xi' = 6^\circ\ 29'\ 10.3''$

$\cos \xi' = .99359555$

The equivalence between pyramid and cone is that both have the same central angle when they are developed into flat circular sectors. This is necessary because of the assumed inextensibility of fabric.

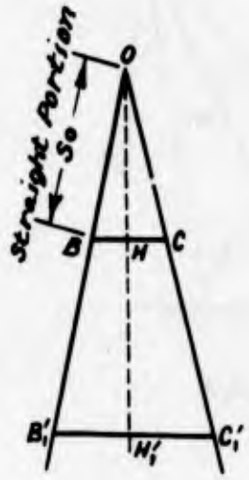

Figure 1.8.3

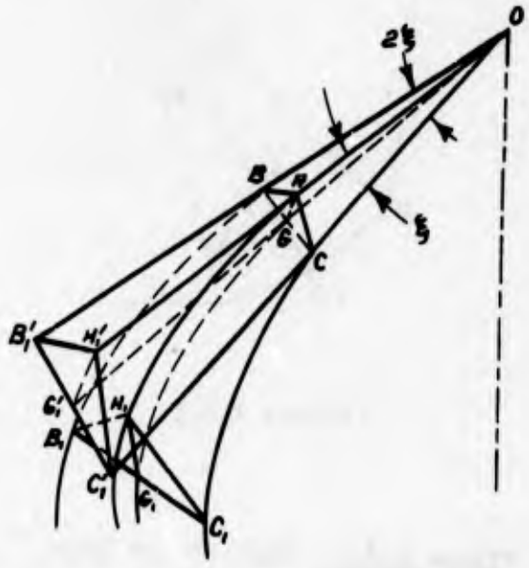

Figure 1.8.4

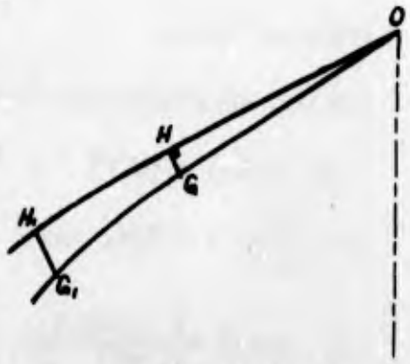

Figure 1.8.5

Consider a plane gore (Figure 1.8.3) and suppose that the angle 2ξ is bisected. Furthermore suppose that the cords, shaped as stated in Section 1.7 (first approximation) approach the vertical axis so that their upper straight portions may form the cone of Figure 1.8.2. In this case the angle included between two adjacent cords is $2\xi' < 2\xi$ and the coordinates of all points of each cord change; namely x's decrease and z's increase. But the variation of the coordinates can be neglected because of the small variation of the angle β.

Now suppose that this plane gore of Figure 1.8.3 is broken along the bisector in such a way that the angle formed by its edges be $2\xi' < 2\xi$. In that case the edges OB and OC of the two-face gore can be brought into coincidence with two adjacent cords of the inflated canopy in the first approximation. This coincidence concerns the straight portions of the cords.

Figure 1.8.4 shows two adjacent cords OBB_1 and OCC_1 of the inflated canopy (in the first approximation) with the broken gore positioned on it. This figure also shows the partial coincidence of the edges of the gore with the straight portions of the cords.

Bringing in coincidence the straight lines CC_1' and BB_1' with the curves CC_1 and BB_1 respectively, the straight line HH_1', (centerline of the gore) follows an assumed curve HH_1, while OG_1' coincides with the centerline OG_1 of the cylindrical gore of the first approximation.

Figure 1.8.5 represents a true view of the curves OGG_1 and OHH_1 lying on the axial plane bisecting the gore.

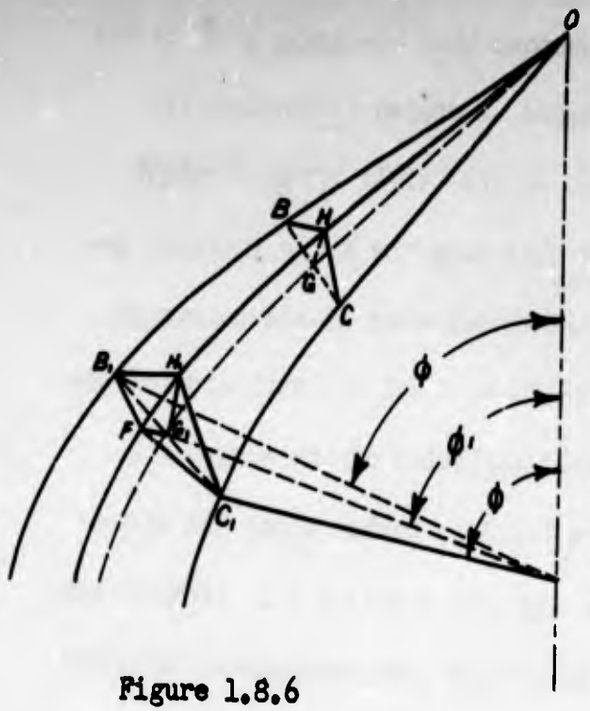

Figure 1.8.6

From Figure 1.8.4 CH ⊥ OH, BH ⊥ OH

Then GH ⊥ OH (GH = Coplanar with CH and BH)

In Figure 1.8.6 suppose that BE ⊥ to the cord OB_1 and C_1E ⊥ to the cord OC_1. The plane B_1C_1E intersects the curve OHH_1 at a point F.

NOTE

The term "limiting case" is used as an abbreviated expression for the case in which the gore of Figure 1.8.3 instead of being bisected, is divided into an infinite number of equal faces, thus forming a conical surface when positioned as described above (see Figure 1.8.4).

Assumptions

1) The intersection B_1FC_1 of the plane B_1C_1E with the two-face gore, as shown in Figure 1.8.6, consists of two straight portions B_1F and FC_1.

2) In the limiting case the lines BHC, $B_1H_1C_1$ and B_1FC_1 keep their lengths.

3) In the limiting case GH, which is normal to OH, keeps its direction. Also G_1H_1 (which comes from $G_1'H_1'$ when the edges of the gore are straight - (see Figure 1.7.4) remains parallel to GH.

4) In the limiting case, the lengthwise invariable line B_1FC_1 is transformed into a circular arc on the gore along which the tensile stress is constant.

5) Since B_1FC_1E defines a plane P_1, the tensile forces from the gore are normal to the cord. The cord tension should therefore be constant. In order to avoid an anomaly at the apex, however, the tension in the straight portion of the cords is

assumed to decrease linearly to zero at the apex. This corresponds approximately to the variation of cord tension in the "first approximation" (see Figure 1.12.1).

Determination of the Direction of GH

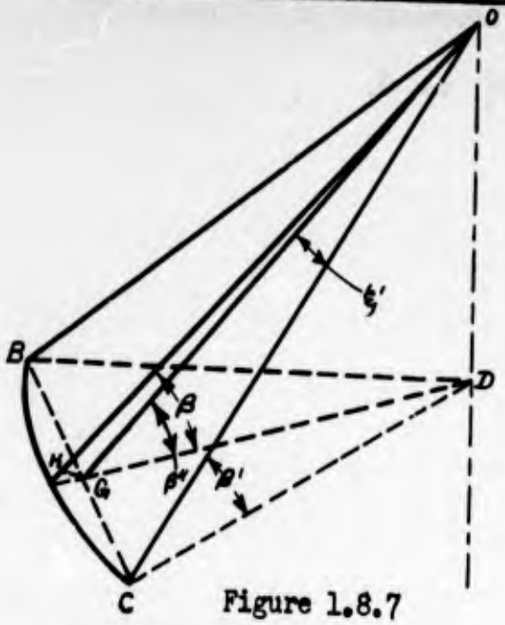

Figure 1.8.7

$BC/2 = CD \tan(\pi/N) = OG \tan \xi'$

Then $\frac{GD}{OG} = \frac{\tan \xi'}{\tan(\pi/N)}$

or $\cos \beta'' = \tan \xi' / \tan(\pi/N) = \frac{.113692}{.13165}$

$= .863593, \quad \beta'' = 30° 16' 40''$

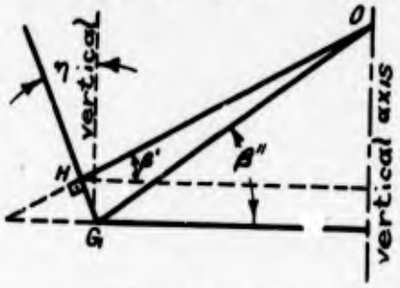

$\eta = \beta''$

$= 30° 4' 8.6''$

Figure 1.8.8

Equation of the Curve OG_1

Representing by x_1 and z_1 the coordinates of G_1 we have:

$$x_1 = x \cos(\pi/N) \tag{1.8.4}$$

$$z_1 = z \tag{1.8.5}$$

where x and z are the coordinates of the corresponding points B_1 or C_1 of the cords. (see Figure 1.8.6).

From the right triangle G_1C_1E: $G_1E = \sqrt{C_1E^2 - G_1C^2}$

But $C_1E = x \csc \phi$ and $G_1C_1 = x \sin(\pi/N)$

Therefore

$$G_1E = \sqrt{x^2/\sin^2 \phi - x^2 \sin^2(\pi/N)} = x \csc \phi \sqrt{1 - \sin^2 \phi \sin^2(\pi/N)} \tag{1.8.6}$$

But $x_1 = G_1E \sin \phi_1$ or $\sin \phi_1 = x_1/G_1E$ (1.8.7)

Taking into account Equation (1.8.4) and (1.8.5), Equation (1.8.7) becomes

$$\sin \phi_1 = \frac{\cos (\pi/N) \sin \phi}{\sqrt{1 - \sin^2 (\pi/N) \sin^2 \phi}} \qquad (1.8.8)$$

The following table gives the values x_1, z_1 of the coordinates of the points of the curve OGG_1 as well as the values of the angle ϕ_1 vs ϕ.

① = $\sin (\pi/N)$ = .13053

② = $\cos (\pi/N)$ = .99144

Table 1.8.1 - Values of x_1, z_1, ϕ_1 (N = 24)

③	④	⑤	⑥	⑦	⑧
ϕ	sin ϕ	x/x_m	$z_1/x_m = z/x_m$	x_1/x_m	cos (π/N) sin ϕ
		See Table 1.7.1	See Table 1.7.1	② · ⑤	② · ④
30°	.50000	.49674	.28675	.49249	.49572
36°	.58779	.58441	.34375	.57941	.58276
42°	.66913	.66590	.40969	.66020	.66340
48°	.74314	.74023	.48404	.73389	.73678
54°	.80902	.80657	.56596	.79967	.80209
60°	.86603	.86408	.65462	.85668	.85862
66°	.91355	.91211	.74903	.90430	.90573
72°	.95106	.95021	.84810	.94208	.94292
78°	.97815	.97773	.95080	.96936	.96978
84°	.99452	.99443	1.06592	.98592	.98601
90°	1.00000	1.00000	1.16228	.99144	.99144
96°	.99452	.99443	1.25864	.98592	.98601
102°	.97815	.97773	1.37376	.96936	.96978
108°	.95106	.95021	1.47646	.94208	.94292

Table 1.8.1 (cont)

(3)	(9)	(10)	(11)	(12)	(13)	(14)
ϕ	$\sin(\pi/N)\sin\phi$	$\sin^2(\pi/N)\sin^2\phi$	$1-\sin^2(\pi/N)\sin^2\phi$		$\sin\phi_1$	ϕ_1
	(1) · (4)	(9) ^{2}	1 − (10)	(11)	(8)/(12)	
30°	.06527	.00426	.99574	.99787	.49678	29° 47'
36°	.07672	.00589	.99411	.99705	.58448	35° 46'
42°	.08734	.00763	.99237	.99618	.66594	41° 45'
48°	.09700	.00941	.99059	.99528	.74027	47° 45'
54°	.10560	.01115	.98885	.99441	.80660	53° 46'
60°	.11304	.01278	.98722	.99359	.86416	59° 47'
66°	.11925	.01422	.98578	.99286	.91224	65° 49'
72°	.12414	.01541	.98459	.99227	.95027	71° 51'
78°	.12768	.01630	.98370	.99182	.97778	77° 54'
84°	.12981	.01685	.98315	.99154	.99442	83° 57'
90°	.13053	.01704	.98296	.99144	1.00000	90° 00'
96°	.12981	.01685	.98315	.99154	.99442	96° 03'
102°	.12768	.01630	.98370	.99182	.97778	102° 06'
108°	.12414	.01541	.98459	.99227	.95027	108° 09'

Parametric Equations of the Curve OHH_1 (see Figures 1.8.6 and 1.8.8)

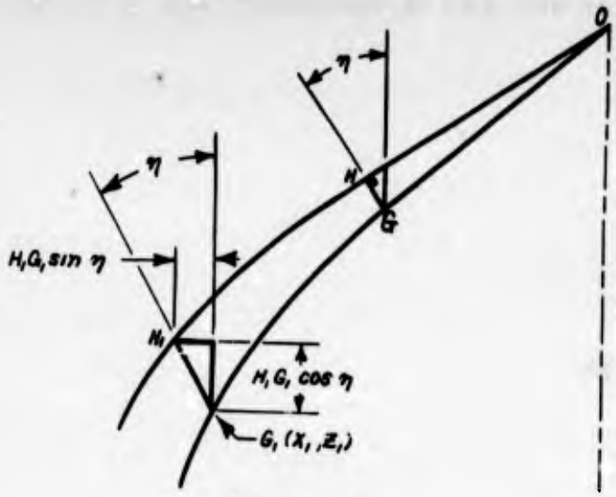

Figure 1.8.9

Representing by x_2 and z_2 the coordinates of H_1 we have:

$$x_2 = x_1 + H_1G_1 \sin \eta \qquad (1.8.9)$$

$$z_2 = z_1 - H_1G_1 \cos \eta \qquad (1.8.10)$$

$G_1H_1 = \sqrt{H_1C_1^2 - G_1C_1^2}$ (see Figure 1.8.6)

or $G_1H_1 = \sqrt{(s \sin \xi)^2 - x^2 \sin^2 (\pi/N)}$

(1.8.11)

The value of G_1H_1 given by Equation (1.8.11) is zero at the end of the straight portion of the cord because the angle included between two adjacent cords is 2ξ for the first approximation and the quantity $s \sin \xi$ is identical to $x \sin (\pi/N)$ for point G.

Taking fullness into account for the part of the canopy corresponding to the straight portion of the cords, the value of GH can be read ily calculated from Figure 1.8.7.

$$GH = GO \sin (\beta'' - \beta')$$ (from right triangle GHO)

But $GO = CO \cos \xi' = S_o \cos \xi'$ ($S_o = .57357\ x_m$ see Section 1.7)

Therefore $GH = S_o \cos \xi' \sin (\beta'' - \beta') = (.57357)(.95359555)\ x_m \sin (12' 31.4)$

or $GH/x_m = (.5699065)\quad (.003643) = .00208$

In order to take into account the fullness of the canopy corresponding to the straight portion of the cords, the quantity G_1H_1 given by Equation (1.8.11) must be increased by the quantity $.00208\ x_m$.

Therefore $$G_1H_1 = s \sin \xi \sqrt{1 - \frac{x^2 \sin^2 (\pi/N)}{s^2 \sin^2 \xi}} + .00208\, x_m \qquad (1.8.12)$$

The following table gives values of G_1H_1 as well as the coordinates x_2, z_2 of the points of the curve OHH_1 vs ϕ.

① = $\sin \xi$ = .1130429

② = $\sin (\pi/N)$ = .13053

③ = $\sin (\pi/N)/\sin \xi$ = 1.15469

④ = $[\sin (\pi/N)/\sin \xi]^2$ = 1.333309

⑤ = $\sin \eta$ = .50105

⑥ = $\cos \eta$ = .86542

Table 1.8.2 - Values of H_1G_1 and Coordinates x_2, z_2 vs ϕ

⑦	⑧	⑨	⑩	⑪	⑫	⑬	⑭	⑮
ϕ	x/x_m	s/x_m	x/s	$(x/s)^2$				$(s/x_m)\sin\xi$
	See Section 1.7		⑧ / ⑨	⑩ ^{2}	④ ⑪	1 - ⑫	$\sqrt{⑬}$	① · ⑨
30°	.46974	.53758	.86603	.75000	1.00000	.000000	.00000	.06484
36°	.58441	.67819	.86172	.74256	.990069	.009931	.09965	.07666
42°	.66590	.78308	.85036	.72311	.964136	.035864	.18938	.08852
48°	.74023	.88825	.83336	.69449	.925977	.074023	.27207	.10041
54°	.80657	.99371	.81168	.65882	.878417	.121583	.34869	.11007
60°	.86408	1.09945	.78592	.61767	.823551	.176449	.42006	.12428
66°	.91211	1.20544	.75666	.57253	.763365	.236635	.48625	.13626
72°	.95021	1.31164	.72444	.52481	.699739	.300261	.54796	.14827
78°	.97773	1.41802	.68950	.47541	.633873	.366127	.60508	.16029
84°	.99443	1.52451	.65229	.42548	.567301	.432699	.65779	.17233
90°	1.00000	1.63107	.61309	.37588	.501168	.498832	.70628	.18438
96°	.99443	1.73763	.57229	.32752	.436689	.563311	.75053	.19642
102°	.97773	1.84412	.53019	.28110	.374796	.625204	.79070	.20846
108°	.95021	1.95050	.48716	.23732	.316423	.683577	.82679	.22048

Table 1.8.2 (cont)

⑦	⑯	⑰	⑱	⑲	⑳	㉑	㉒	㉓
ϕ		$(H_1G_1)/x_m$	$(H_1G_1 \sin \eta)/x_m$	$(H_1G_1 \cos \eta)/x_m$	x_1/x_m	z_1/x_m	x_2/x_m	z_2/x_m
	⑭ · ⑮	.00208 + ⑯	⑤ · ⑰	⑥ · ⑰	See Table 1.8.1	See Table 1.8.1	⑳ + ⑱	㉑ - ⑲
30°	.00000	.00208	.00104	.00180	.49249	.28675	.49353	.28495
36°	.00764	.00972	.00487	.00841	.57941	.34375	.58428	.33534
42°	.01676	.01884	.00944	.01630	.66020	.40969	.66964	.39339
48°	.02732	.02940	.01473	.02544	.73389	.48404	.74862	.45860
54°	.03838	.04046	.02027	.03501	.79967	.56596	.81994	.53095
60°	.05221	.05429	.02720	.04689	.85668	.65462	.88388	.60764
66°	.06626	.06834	.03424	.05914	.90430	.74903	.93854	.68989
72°	.08125	.08333	.04175	.07212	.94208	.84810	.98383	.77598
78°	.09699	.09907	.04964	.08574	.96936	.95080	1.01900	.86506
84°	.11336	.11544	.05784	.09990	.98592	1.06592	1.04376	.96602
90°	.13022	.13230	.06629	.11450	.99144	1.16228	1.05773	1.04778
96°	.14742	.14950	.07491	.12938	.98592	1.25864	1.06083	1.12926
102°	.16423	.16631	.08333	.14393	.96936	1.37376	1.05269	1.22983
108°	.18229	.18437	.09238	.15956	.94208	1.47646	1.03446	1.31690

Determination of the Length FG_1 (see Figure 1.8.6)

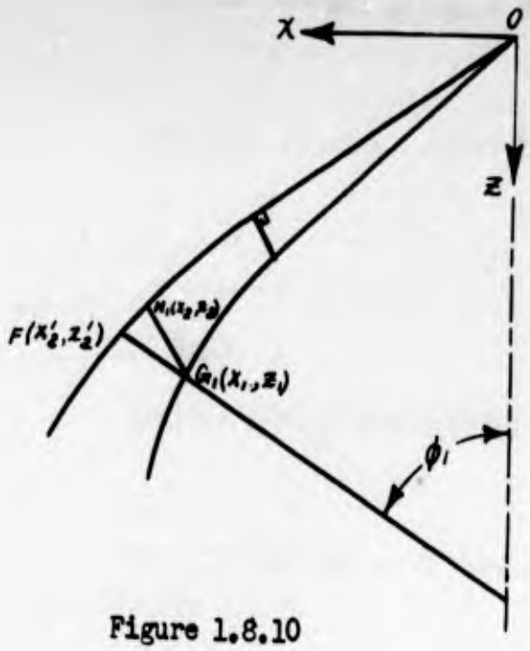

Figure 1.8.10

Equation of straight line FG_1:

$$z - z_1 = \tan(90 + \phi_1)(x - x_1)$$

or $$z - z_1 = -1/\tan\phi\,(x - x_1) \quad (1.8.13)$$

Representing by x_2', z_2' the coordinates of the point F, the length G_1F is given by:

$$G_1F = \sqrt{(x_2' - x_1)^2 + (z_2' - z_1)^2} \quad (1.8.14)$$

To find the coordinates x_2', z_2' of the intersection of the straight line G_1F with the curve OH_1F, a graphical method is used. In Figure 1.8.11 the curve OH_1F is plotted (z against x, the coordinates taken from Columns (22) and (23) of Table 1.8.2); also the straight line of Equation (1.8.13) is plotted for the values ϕ = 30°, 48°. 66°, 84° and 90°.

The intersections of the curve OH_1F with these straight lines represent the points F.

For the above mentioned values of ϕ Equation (1.8.13) becomes respectively:

$$\left.\begin{array}{ll}
\text{For } \phi = 30^\circ & z - .28675 = -1.74727\,(x - .49249) \\
\phi = 48^\circ & z - .48404 = -.90833\,(x - .73389) \\
\phi = 66^\circ & z - .74903 = -.44907\,(x - .90430) \\
\phi = 84^\circ & z - 1.06592 = -.10597\,(x - .98592) \\
\phi = 90^\circ & z - 1.16228 = -.00000\,(x - .99144)
\end{array}\right\} \quad (1.8.15)$$

Values of x_2' and z_2' for intermediate values of ϕ not mentioned in the set of Equations (1.8.15) are taken by interpolation of equal spaced points along the

curve OH_1F for each particular curved portion included between two adjacent straight lines of the set.

Table 1.8.3 gives the values of the coefficient $K = G_1F/x_m$ for the various values of ϕ.

Values of x_2'/x_m and z_2'/x_m in columns ④ and ⑤ of Table 1.8.3 are obtained from the graph of Figure 1.8.11.

From Figure 1.8.6: $FC_1^2 = FG_1^2 + C_1G_1^2$

or $$FC_1^2 = K^2 x_m^2 + x^2 \sin(\pi/N) \qquad (1.8.16)$$

where the coefficient K is given in Column ⑪ of Table 1.8.3 for the various values of ϕ.

Representing by 2α the central angle and by r_1 the radius of the circular arc mentioned in assumption 4 we obtain:

$$\alpha\, r_1 = FC_1 = \sqrt{K^2 x_m^2 + x^2 \sin^2(\pi/N)} \qquad (1.8.17)$$

and $$r_1 \sin\alpha = x \sin(\pi/N) \qquad (1.8.18)$$

Dividing Equation (1.8.17) and (1.8.18) we obtain

$$\alpha/\sin\alpha = \sqrt{1 + \frac{K^2}{(x/x_m)^2}\ \frac{1}{\sin^2(\pi/N)}} \qquad (1.8.19)$$

Table 1.8.4 gives the values of the ratio $\alpha/\sin\alpha$ as well as the values of α vs ϕ.

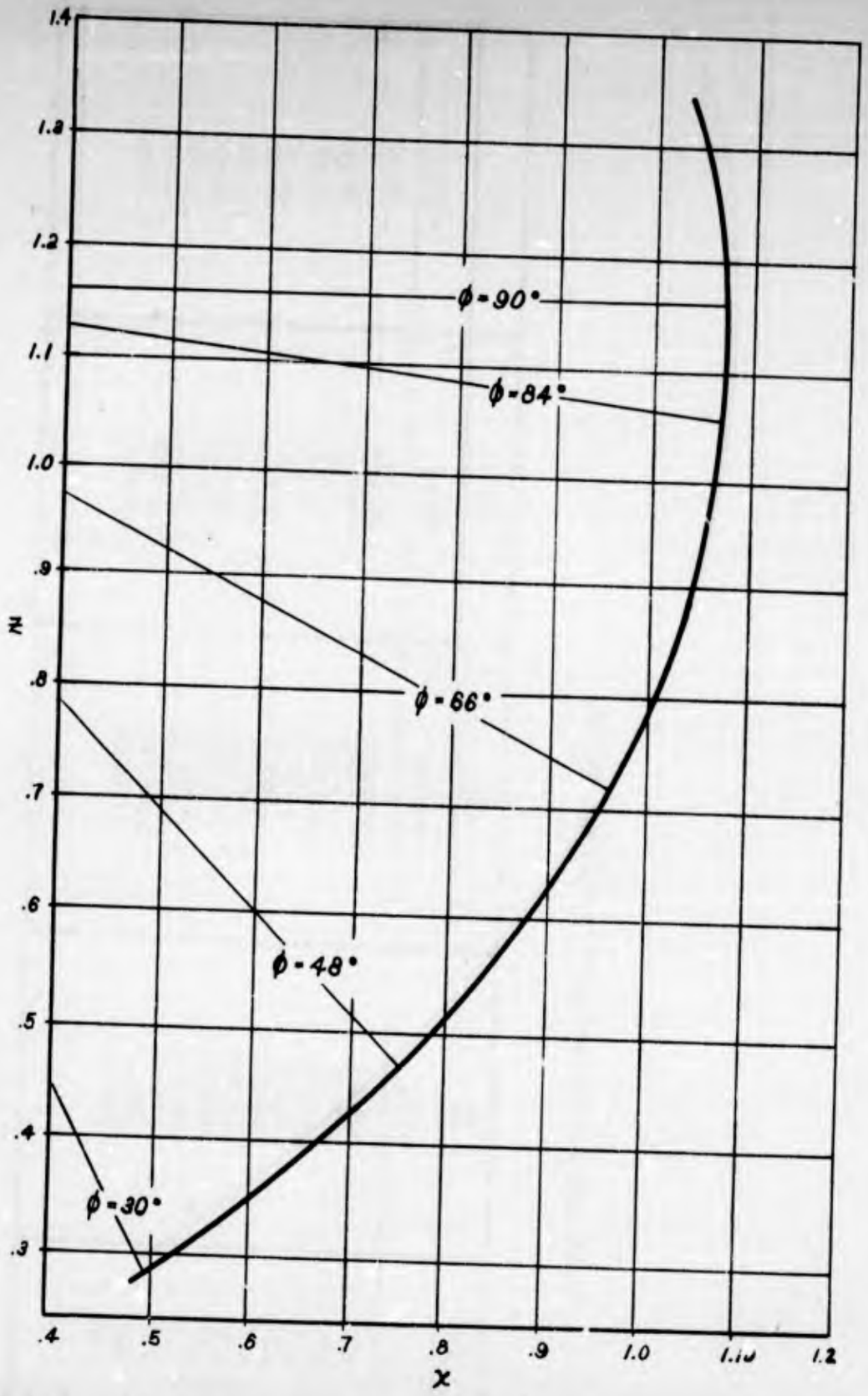

Figure 1.8.11 - Intersection of Curve OH_1F with the Straight Lines (1.8.15)

Table 1.8.3 -- Values of $K = G_1F/x_m$ vs ϕ

①	②	③	④	⑤
ϕ	x_1/x_m	z_1/x_m	x_2^1/x_m	z_2^1/x_m
30°	.49249	.28675	.49400	.28532
36°	.57941	.34375	.58600	.33250
42°	.66020	.40969	.67100	.39600
48°	.73389	.48404	.75550	.46500
54°	.79967	.56536	.83200	.54150
60°	.85668	.65462	.89900	.63000
66°	.90430	.74903	.95900	.72300
72°	.94208	.84810	1.00600	.82800
78°	.96936	.95080	1.03800	.94000
84°	.98592	1.06592	1.05950	1.06300
90°	.99144	1.16228	1.06000	1.16228

Table 1.8.3 (cont)

①	⑥	⑦	⑧	⑨	⑩	⑪
ø	$(x_1 - x_2')/x_m$	$(z_1 - z_2')/x_m$				$K = G_1F/x_m$
	② - ④	③ - ⑤	$⑥^2$	$⑦^2$	⑧ + ⑨	⑩
30	.00151	.00143	.00000228	.00000204	.00000432	.00208
36	.00659	.01125	.000043	.000127	.000170	.01304
42	.01080	.01369	.000117	.000187	.000304	.01743
48	.02161	.01904	.000467	.000363	.000830	.02881
54	.03233	.02446	.001045	.000598	.001643	.04053
60	.04232	.02462	.001791	.000606	.002397	.04896
66	.05470	.02603	.002992	000678	.003670	.06058
72	.06342	.02010	.004086	.000404	.004490	.06701
78	.06864	.01080	.004711	.000117	.004828	.06948
84	.07358	.00292	.005414	.000009	.005423	.07364
90	.06856	.00000	.004700	.000000	.004700	.05856

Table 1.8.4 - Values of α vs ∅

①	②	③	④	⑤	⑥	⑦	⑧	⑨
∅	K	x/x_m	$K/(x/x_m)$	$K/[(x/x_m)\sin(\pi/N)]$			α/sin α	α
Degrees	See Table 1.8.3	See Section 1.7	② / ③	④ /.13053	⑤^2	1 + ⑥	$\sqrt{⑦}$	
30°	.00208	.49674	.004187	.032077	.001029	1.001029	1.00051	3° 10'
36°	.01304	.58441	.022313	.170942	.029221	1.029221	1.01451	16° 50'
42°	.01743	.66590	.026175	.200529	.040212	1.040212	1.01991	19° 40'
48°	.02881	.74023	.038920	.298169	.088905	1.088905	1.04351	28° 50'
54°	.04053	.80657	.050250	.384969	.148201	1.148201	1.07154	36° 38'
60°	.04896	.86408	.056661	.434084	.188429	1.188429	1.09015	40° 53'
66°	.06058	.91211	.066417	.508826	.258904	1.258904	1.12201	47° 04'
72°	.06701	.95021	.070521	.540267	.291888	1.291888	1.13661	49° 35'
78°	.06948	.97773	.071063	.544419	.296392	1.296392	1.13859	49° 54'
84°	.07364	.99443	.074052	.567318	.321850	1.321850	1.14972	51° 42'
90°	.06856	1.00000	.068560	.525243	.275880	1.275880	1.12955	48° 23'

Equation of Cords

Representing by f_1 the constant tension of the fabric along a circular normal section we have:

$$f_1 = p\ r_1 \qquad (1.8.20)$$

The resultant R of the two tensile forces corresponding to two adjacent gores is:

$$R = 2f_1 \cos \chi = 2pr_1 \cos \chi \qquad (1.8.21)$$

where χ is the angle between the direction of f_1 and the normal to the cord.

It can be easily shown that $\sin \phi \sin (\pi/N) = \cos \left[180° - (\alpha + \chi)\right]$ (1.8.22)

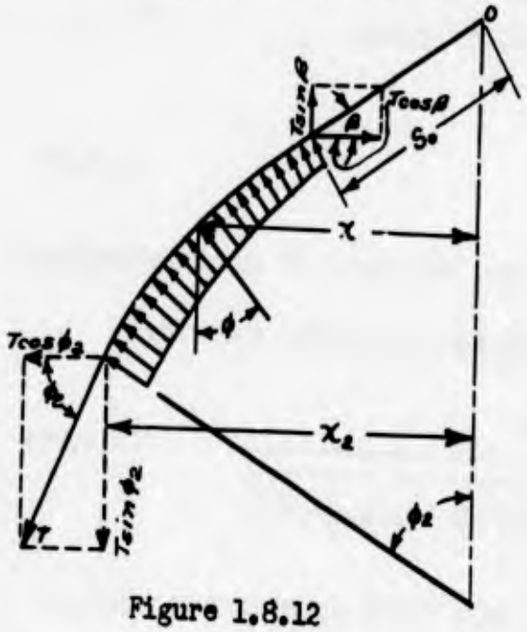

Figure 1.8.12

From Equation (1.8.18)

$$r_1 = x \frac{\sin (\pi/N)}{\sin \alpha}$$

Therefore Equation (1.8.21) becomes

$$R = 2p \cos \chi \frac{x \sin (\pi/N)}{\sin \alpha}$$

Equilibrium of forces on a vertical axis:

$$T (\sin \phi_2 - \sin \beta) = \int R \cos \phi \, ds \qquad (1.8.23)$$

Equilibrium of forces on a horizontal axis:

$$T (\cos \beta - \cos \phi_2) = \int R \sin \phi \, ds \qquad (1.8.24)$$

Dividing Equations (1.8.23), (1.8.24) we obtain:

$$\frac{\sin \phi_2 - \sin \beta}{\cos \beta - \cos \phi_2} = \frac{\int R \cos \phi \, ds}{\int R \sin \phi \, ds} \qquad (1.8.25)$$

But $\sin \phi_2 - \sin \beta = 2 \sin \frac{1}{2} (\phi_2 - \beta) \cos \frac{1}{2} (\phi_2 + \beta)$

$\cos \beta - \cos \phi_2 = 2 \sin \frac{1}{2} (\phi_2 - \beta) \sin \frac{1}{2} (\phi_2 + \beta)$

Therefore Equation (1.8.25) becomes:

$$\cot \tfrac{1}{2} (\phi_2 + \beta) = \frac{\int 2p \cos \chi \frac{x \sin (\pi/N)}{\sin \alpha} ds \cos \phi}{\int 2p \cos \chi \frac{x \sin (\pi/N)}{\sin \alpha} ds \sin \phi} = Q \qquad (1.8.26)$$

The quantity Q is introduced because of the difficulty of obtaining a reasonably simple relation between x and ϕ from Equation 1.8.26.

From $\cot \frac{1}{2}(\phi_2 + \beta) = Q$ we obtain successively:

$$\tan \tfrac{1}{2}(\phi_2 + \beta) = 1/Q, \quad \tan(\phi_2 + \beta) = 2Q/(Q^2 - 1)$$

$$\text{or} \quad \frac{\tan \phi_2 + \tan \beta}{1 - \tan \phi_2 \tan \beta} = \frac{2Q}{Q^2 - 1}, \quad \text{from which finally}$$

$$\tan \phi_2 = \frac{2Q - (Q^2 - 1)\tan \beta}{Q^2 - 1 + 2Q \tan \beta} \tag{1.8.27}$$

On the other hand, reducing Equation (1.8.26) gives

$$Q = \frac{\int (\cos \chi / \sin \alpha) \times \cos \phi \, ds}{\int (\cos \chi / \sin \alpha) \times \sin \phi \, ds} \tag{1.8.28}$$

As the first step (and the only one carried out here) of an iteration procedure, Equation (1.7.16) of the first approximation is assumed to hold:

$$x = \frac{x_m \sqrt{\cos(2\pi/N)}}{\sqrt{\left[\cos^2(\pi/N)/\cos(2\pi/N)\right]\left[\cot^2 \phi + \cos(2\pi/N)\right]}} \tag{1.8.29}$$

The solution of Section 1.7 thus serves as a first approximation much as the Taylor curve was used as a first approximation in analysis of the flat canopy (Section 1.1).

Solving (1.8.29) for tan ϕ yields

$$\tan \phi = \sqrt{\frac{\cos^2(\pi/N)}{\cos(2\pi/N)} \left(\frac{x^2}{x_m^2 - x^2}\right)} \tag{1.8.30}$$

Putting N = 24, $\phi = \phi_2$ and $x = x_2$, one obtains from Equation (1.8.27) and (1.8.30)

$$\sqrt{\frac{1.017623\ x_2^2}{x_m^2 - x_2^2}} = \frac{2Q - (Q_2 - 1)\tan\beta}{Q^2 - 1 + 2Q\tan\beta} \qquad (1.8.31)$$

By making use of the relation

$$dx = ds\cos\phi$$

and using Equation (1.8.29), Equation (1.8.28) can be written as

$$Q = \frac{I_A}{I_B} \qquad (1.8.32)$$

if

$$I_A = \int_\beta^\phi \frac{\cos\chi}{\sin\alpha}\ \frac{\cot\phi}{\sin^2\phi}\left[\cos^2(\pi/N)\cot^2\phi + \cos(2\pi/N)\right]^{-2} d\phi \qquad (1.8.33)$$

$$I_B = \int_\beta^\phi \frac{\cos\chi}{\sin\alpha}\ \frac{1}{\sin^2\alpha}\left[\cos^2(\pi/N)\cot^2\phi + \cos(2\pi/N)\right]^{-2} d\phi \qquad (1.8.34)$$

Equation (1.8.31) solved for x/x_m (where $x = x_2$) becomes:

$$x/x_m = \left(1 + \frac{1.017623}{\left[\frac{2Q - (Q_2 - 1)\tan\beta}{Q_2 - 1 + 2Q\tan\beta}\right]}\right)^{\frac{1}{2}} \qquad (1.8.35)$$

Equation (1.8.35) is evaluated in Table 1.8.5 for $\beta = 30°$ and $N = 24$. Because Equation (1.8.29) does not correspond exactly to Equation (1.8.26) a discrepancy results such that $x/x_m = 1.000$ when $\phi = 81°$ rather than 90°.

This discrepancy could be resolved by extension of the iteration procedure, but to avoid lengthy and laborious calculation, a correction equivalent to an interpolation is applied in Table 1.8.6, Column (1), where

$$\phi' = 30° + \left(\frac{90° - 30°}{81° - 30°}\right)\Delta\phi$$

Determination of z

From $dz = dx\tan\phi'$ integration we obtain:

$$z = \int \tan\phi'\ dx \qquad (1.8.36)$$

Determination of the length of arc s

The length of arc s may be obtained from

$$s = \int dx/\cos \phi' \qquad (1.8.37)$$

Table 1.8.6 shows the variation of z and s with ϕ'.

Table 1.8.5 - Values of I_A, I_B, Q and x/x_m vs. ϕ

①	②	③	④	⑤	⑥	⑦	⑧	⑨	⑩
ϕ	sin ϕ	cos [180° -(α + χ)]	180° -(α + χ)	α	χ	cos χ	sin α	$\sin^2 \phi$	cos χ/sin α
Deg		.13053 ②		See Table 1.8.4				②^2	⑦ / ⑧
30	.50000	.06527	86° 15'	3° 10'	90° 00'	.00000	.05524	.25000	.00000
36	.58779	.07672	85 36	16 50	77 34	.21530	.28959	.34550	.74346
42	.66913	.08734	85 00	19 40	75 20	.25320	.33655	.44773	.75234
48	.74314	.09700	84 26	28 50	66 44	.39501	.48226	.55226	.81908
54	.80902	.10560	83 56	36 38	59 26	.50854	.59669	.65451	.85227
60	.86603	.11304	83 30	40 53	55 37	.56473	.65453	.75000	.86280
66	.91355	.11925	83 09	47 04	49 47	.64568	.73215	.83457	.88190
72	.95106	.12414	82 52	49 35	47 32	.67516	.76135	.90452	.88679
78	.97815	.12768	82 40	49 54	47 26	.67645	.76492	.95678	.88434
81	.98769	.12892	82 36	51 11	46 13	.69193	.77915	.97553	.88806
84	.99452	.12981	82 33	51 42	45 45	.69779	.78478	.98908	.88915
90	1.00000	.13053	82° 30'	48° 23'	49° 07'	.65452	.74761	1.00000	.87543

Table 1.8.5 - (Continued)

①	⑪	⑫	⑬	⑭	⑮	⑯	⑰	⑱
ϕ					I_B	cot ϕ		
Deg	⑩ / ⑨		⑪ · ⑫	⑬$_{Av}$ $\Delta\phi$	$\int$ ⑭		⑬ · ⑯	⑰$_{Av}$ $\Delta\phi$
30	.00000	.06526	.00000		.00000	1.73205	.00000	
				.01780				.02626
36	2.15184	.12503	.26904		.01780	1.37638	.37030	
				.03249				.03996
42	1.68034	.21075	.35413		.05029	1.11061	.39330	
				.04336				.04315
48	1.48314	.31819	.47192		.09365	.90040	.42492	
				.05583				.04505
54	1.30215	.45363	.59069		.14948	.72654	.42916	
				.06689				.02333
60	1.15040	.59751	.68738		.21637	.57735	.39686	
				.07147				.03937
66	1.05671	.74187	.78394		.2[illegible]384	.44523	.34903	
				.08610				.03299
72	.98040	.87380	.85667		.37994	.32492	.27835	
				.09227				.02469
78	.92429	.97948	.90532		.47221	.21256	.19243	
				.04799				.00888
81	.91034	1.01903	.92766		.52020	.15838	.14692	
				.04896				.00644
84	.89897	1.04820	.94230		.56916	.10510	.09904	
				.09863				.00518
90	.87548	1.07186	.93839		.66779	.00000	.00000	

⑪ = $\cos X/(\sin \alpha \sin^2 \phi)$

⑫ = $[\cos^2 (\pi/N) \cot^2 \phi + \cos (2\pi/N)]^{-2}$ (For values of $[\cos^2 (\pi/N) \cot^2 \phi + \cos (2\pi/N)]^{\frac{1}{2}}$ see Table 1.7.1)

Table 1.8.5 - (Continued)

(1)	(19)	(20)	(21)	(22)	(23)	(24)	(25)
ϕ	I_A	Q	Q^2	$Q^2 - 1$	$(Q^2 - 1) \tan \beta$	$2Q \tan \beta$	2Q
Deg	$\int$ (18)	(19) / (15)	(20)^2	(21) - 1	.57735 (23)	1.1547 (20)	2 (20)
30	.00000	1.73205	3.00000	2.00000	1.15470	2.00000	3.46410
36	.02626	1.47528	2.17645	1.17645	.67922	1.70351	2.95056
42	.06622	1.31676	1.73386	.73386	.42369	1.52046	2.63352
48	.10937	1.16786	1.36390	.36390	.21010	1.34853	2.33572
54	.15442	1.03305	1.06719	.06719	.03879	1.19286	2.06610
60	.19775	.91394	.83529	-.16471	-.09510	1.05533	1.82788
66	.23712	.80697	.65120	-.34880	-.20138	.93181	1.61394
72	.27011	.71093	.50542	-.49458	-.28555	.82091	1.42186
78	.29480	.62430	.38975	-.61025	-.35233	.72088	1.24860
81	.30368	.58378	.34080	-.65920	-.38059	.67409	1.16756
84	.31012	.54487	.29688	-.70312	-.40595	.62916	1.08974
90	.31530	.47215	.22293	-.77707	-.44864	.54519	.94430

Table 1.8.5 - (Continued)

(1)	(26)	(27)	(28)	(29)	(30)	(31)	(32)	(33)
β								x/x_a
	(25) - (23)	(22) + (24)	(26) / (27)	$(28)^2$	1.017623/(29)	1 + (30)	$\sqrt{(31)}$	1 / (32)
30	2.30940	4.00000	.57735	.33333	3.05287	4.05287	2.013	.4968
36	2.27134	2.87996	.78867	.62200	1.63605	2.63605	1.624	.6158
42	2.20983	2.25432	.98026	.96091	1.05902	2.05902	1.435	.6969
48	2.12562	1.71243	1.24129	1.54080	.66045	1.66045	1.288	.7764
54	2.02731	1.26005	1.60891	2.58859	.39312	1.39312	1.180	.8475
60	1.92298	.89062	2.15915	4.66193	.21828	1.21828	1.104	.9058
66	1.81532	.58301	3.11370	9.69513	.10496	1.10496	1.051	.9515
72	1.70741	.32633	5.23216	27.37550	.03717	1.03717	1.018	.9823
78	1.60093	.11063	14.47103	209.41071	.00486	1.00486	1.004	.9960
81	1.54815	.01489	103.97246	10810.27	.00009	1.00009	1.000	1.0000

(26) = $2Q - (Q^2 - 1) \tan \beta$

(27) = $(Q^2 - 1) + 2Q \tan \beta$

Table 1.8.6 - Values of s/x_m and s/x_m vs ϕ

	①		②	③	④	⑤	⑥	⑦	⑧	⑨
ϕ	ϕ'		x/x_m	tan ϕ'	cos ϕ'	$\Delta(x/x_m)$	tan $\phi' \Delta(x/x_m)$	s/x_m	$\Delta(x/x_m)/\cos\phi'$	s/x_m
Deg	$30° + (\frac{90-30}{81-30})\Delta\phi$		See Table 1.8.5				③ ⑤	$\int$ ⑥	⑤ / ④	$\int$ ⑧
30	30.00	30° 00'	.4968	.57735	.86603					
36	37.06	37 04	.6158	.75538	.79793	.1190	.0713	.2868	.1388	.5736
42	44.12	44 07	.6969	.96963	.71792	.0811	.0654	.3581	.1042	.7124
48	51.18	51 11	.7764	1.2430	.62683	.0795	.0821	.4235	.1143	.8166
54	58.24	58 14	.8475	1.6149	.52646	.0711	.0927	.5056	.1169	.9309
60	65.30	65 18	.9058	2.1742	.41787	.0683	.1011	.5983	.1167	1.0478
66	72.36	72 22	.9515	3.1460	.30292	.0457	.1081	.6994	.1174	1.1645
72	79.42	79 25	.9823	5.3521	.18367	.0308	.1080	.8075	.1127	1.2819
78	86.48	86 29	.9960	16.272	.06134	.0137	.0840	.9155	.0852	1.3942
81	90.00	90° 00'	1.0000	Inf.	.00000	.0040	.0651	.9995	.0652	1.4794
								1.0646		1.5446

Cord Portion Below the Maximum Inflated Radius.

The shape of the cord below the maximum inflated radius is determined with the equations given in Section 1.3.

In equations $k_{sk} = \dfrac{f(n) + 2k_a}{f(n) + 2n\, k_c/k_s'}$ (1.8.38) (see Equation(1.3.18))

$$k_{sk} = 1 - \frac{\frac{1}{2}\rho_m/x_m}{n^2 - 1} \qquad (1.8.39)$$ (see Equation(1.3.19))

where $f(n) = 2n + (n^2 - 1)\log\dfrac{n+1}{n-1}$ and $n = \dfrac{1}{\sin\theta}$

for this particular canopy we have

$k_a = 1.5446$ (see Table 1.8.6, column (9))

$k_c/k_s' = l_c/l_s' = .6$

$\rho_m/x_m = 1.0574$

The radius of curvature of the cord at MIR is given by the equation

$$\rho = \frac{ds}{d\phi} = \frac{dx}{d\phi}\frac{1}{\cos\phi} \cong \frac{\Delta x}{\Delta\phi}\frac{1}{\cos\phi} = \frac{.0040\, x_m}{.06167}\frac{1}{.06134} = 1.0574\, x_m \qquad (1.8.40)$$

where the numerical values are obtained from Table 1.8.6

The correct value of n satisfying both Equations (1.8.38) and (1.8.39) is n = 3.32

In fact f(n) = 12.8704 and

Equation (1.7.38) gives $k_{sk} = .94691$

Equation (1.7.39) gives $k_{sk} = .94725$

Then $\sin\theta = \dfrac{1}{n} = \dfrac{1}{3.32} = .30120$ $\theta = 17^\circ\ 30'$

From the equation $Z = x_m\sqrt{2\rho_m/x_m}\sqrt{1 - x/x_m}$ (see Equation (1.3.7))

we can compute the coordinates z of several points of the parabolic arc when x's are given arbitrary values between $1.00\, x_m$ and $.94691\, x_m$.

Figure 1.8.13 shows the cord curve of a conical canopy of the first and second ap-

proximation. Both curves have been plotted with the same maximum inflated radius.

Equations of Cord

1) Portion OA, $\phi = \beta = 30°$

$x_A = x_0 = .4968\, x_m$, $z = x \tan 30°$

2) Portion AB, $30° \leq \phi \leq 90°$

$$x = x_m \left[1 + \frac{1.017623}{\left[\frac{2Q - (Q^2-1)\tan\beta}{(Q^2-1) + 2Q\tan\beta} \right]^2} \right]^{-\frac{1}{2}} \quad \text{where } Q = \frac{I_A}{I_B}$$

$$I_A = \int_\beta^\phi \frac{\cos\chi \cot\phi}{\sin\alpha \sin^2\phi} \left[\cos^2 \pi/N \cot^2\phi + \cos 2\pi/N \right]^{-2} d\phi$$

$$I_B = \int_\beta^\phi \frac{\cos\chi}{\sin\alpha \sin^2\phi} \left[\cos^2 \pi/N \cot^2\phi + \cos 2\pi/N \right]^{-2} d\phi$$

$$\sin\phi \sin \pi/N = \cos\left[180 - (\alpha + \chi)\right]$$

3) Portion BC, $\phi \geq 90°$

$x_m \geq x \geq .9469\, x_m$

$z = .10646\, x_m + 1.454\, x_m \sqrt{1 - x/x_m}$

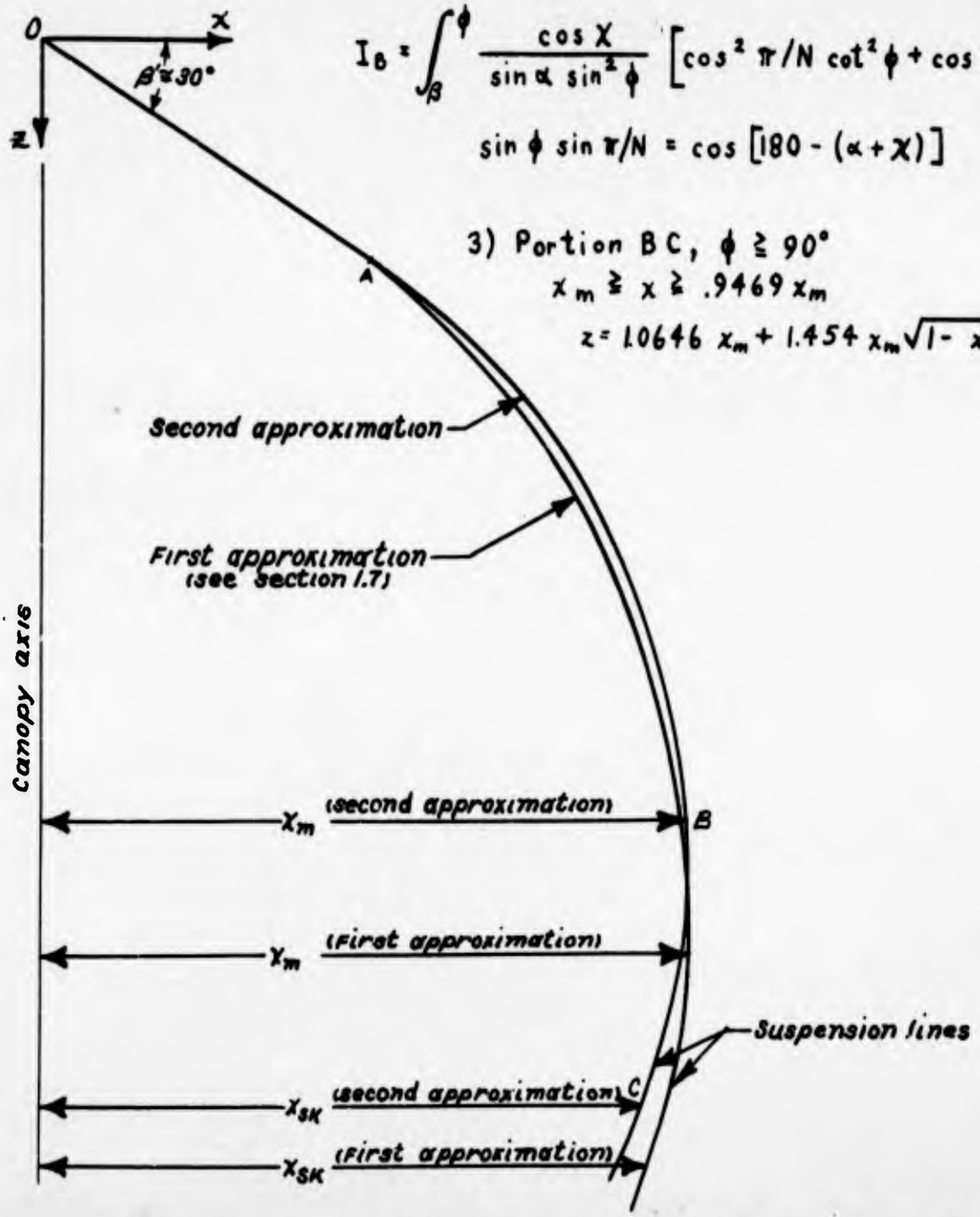

Figure 1.8.13 - Cord Shape of a Conical Canopy - First and Second Approximations (N = 24, $l_c/l_s' = .6$, common x_m)

1.9 Personnel Guide Surface Canopy

The personnel guide surface canopy analyzed here is a conical type having pocket-like extensions fastened to alternate gores. One of the purposes of these extensions is to increase the stability of the canopy.

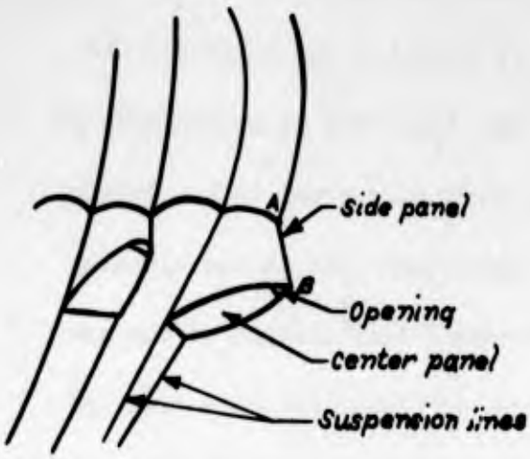

Figure 1.9.1

Figure 1.9.1 is a sketch of these extensions when inflated. A visual examination of Photographs in Reference 9 indicates that the extensions are most efficient when the side panel is fully inflated and the center panel is inflated but rather flat. This means that the side panels exert forces on the canopy and cords but that the forces exerted by the center panels can be neglected. In order to determine the effect of the extension on the shape of the cords and canopy the following assumptions are made:

1. The effect of the extensions is to introduce a force F as in Figure 1.9.2. If this force is assumed to be put into the cord at the skirt instead of at the more correct position (dashed), the cord must undergo a sudden change in slope at that point. Photographs of Reference 9 seem to show such a change of slope. Actually, nevertheless, the force F is probably put into the cords along the entire length of the extension, and the resultant would have to act at a point somewhat

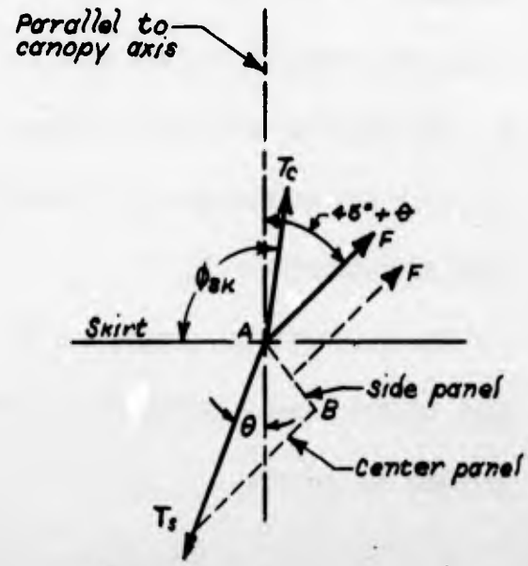

Figure 1.9.2

below the skirt. The error introduced by assuming it to act at the skirt will be disregarded.

2. Circumferential displacements, caused by the existence of the extensions in alternate gores only, are also disregarded for this analysis.

3. The angle that the force F makes with the vertical is $(45° + \theta)$.

4. In order to find the force F it is necessary to determine the projected area normal to the force F. This is done by assuming that this area is rectangular in shape with one side equal to $2r_{sk} \sin \alpha_{sk}$ and the other side equal to the length AB in Figure 1.9.1 and 1.9.2. This neglects the side panel area in the vicinity of the suspension lines, but on the basis of Reference 9 this portion of the extension is rather flat and nearly in an axial plane, and hence the force exerted by the pressure on this part of the side panel may be neglected without introducing a large error. From USAF Dwgs. 52J6026 and 52D6027 the lengths AB and l_c are 21-1/8 in. and 13.857 ft respectively; thus the length $AB = \frac{21.125}{(12)\ (13.857)}\ l_c$ $= .126\ l_c$.

5. The shape of the cords above the maximum inflated radius is the same as that of the flat canopy of Section 1.4, except that x_m is different. This is assumed because, as already discussed in Section 1.7, the personnel guide surface canopy does not exhibit a conical apex when inflated.

6. The shape of the cords between the maximum inflated radius and the skirt is a circular arc of radius ρ and length l_b, and these cords are parallel for the purpose of determining T_c.

7. The differential pressure p in the extensions is equal to that in the main part of the canopy except for the center panel where the differential pressure is assumed to be zero.

8. The number of gores, N, is equal to 24, and ratio l_c/l_s' is equal to 0.42687. This particular ratio comes from an attempt to correlate theory with photographs as discussed in Section 2. Actually, there is only one personnel guide surface parachute design, which seems a good reason for sticking to the design dimensions as closely as possible. For comparison with other types of parachutes, however, a solution with $l_c/l_s' = 0.6$ is worked out in Section 1.11.

9. There is a linear relation between α and ϕ below MIR which can be approximated by $\alpha = 0.64\,\phi + 0.57$. The derivation of this relation is as follows:

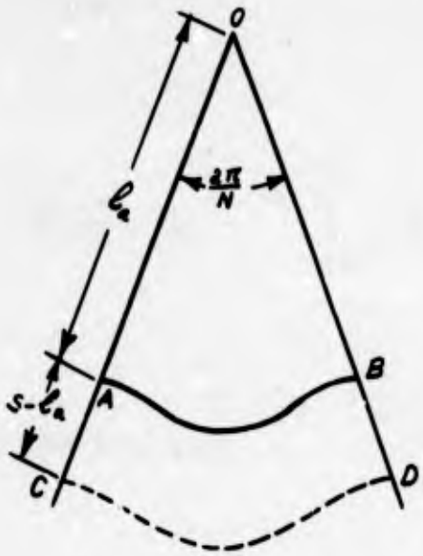

Figure 1.9.3

Figure 1.9.3 shows a flat gore in which the points A and B on the cords OA and OB respectively correspond to MIR.

Assumptions

1) Assume that the sections of one inflated gore cut by planes P_1 below MIR are major circular arcs which give geometrically similar curves when the gore lies flat.

2) Assume that Taylor's equation

$$x = x_m\sqrt{\sin\phi}$$

holds as a first approximation.

The first assumption can be expressed by the following equation:

$$CD = 2r_1\alpha = AB\ s/l_a \qquad (1.9.1)$$

But $AB = xx_m \sin \pi/N$ (see Section 1.1) (1.9.2)

From the second assumption

$$s/l_a = \frac{\int_0^{\phi} d\phi/\sqrt{\sin\phi}}{\int_0^{90^\circ} d\phi/\sqrt{\sin\phi}} \qquad (1.9.3)$$

and $x \sin \pi/N = r_1 \sin \alpha$ or $x_m \sqrt{\sin \phi} \sin \pi/N = r_1 \sin \alpha$ (1.9.4)

Combining Equations (1.9.1) through (1.9.4) we obtain

$$\frac{2x_m \sqrt{\sin \phi} \sin (\pi/N)}{\sin \alpha} \alpha = \pi x_m \sin (\pi/N) \frac{\int_0^{\phi} d\phi / \sqrt{\sin \phi}}{\int_0^{90^\circ} d\phi / \sqrt{\sin \phi}}$$

or

$$\frac{\alpha}{\sin \alpha} = \frac{\pi}{2 \sqrt{\sin \phi}} \frac{\int_0^{\phi} d\phi / \sqrt{\sin \phi}}{\int_0^{90^\circ} d\phi / \sqrt{\sin \phi}} \quad (1.9.5)$$

For $\phi > 90^\circ$, $\int_0^{\phi} d\phi / \sqrt{\sin \phi} = 2 \int_0^{90^\circ} d\phi / \sqrt{\sin \phi} - \int_0^{180^\circ - \phi} d\phi / \sqrt{\sin \phi}$

and since

$$\int_0^{Z} dZ / \sqrt{\sin Z} = \sqrt{2} \left[\int_0^{90^\circ} dt / \sqrt{1 - \tfrac{1}{2} \sin^2 t} - \int_0^{\cos^{-1} (\sqrt{\sin Z})} dt / \sqrt{1 - \tfrac{1}{2} \sin^2 t} \right]$$

the integral $\int_0^{\phi} d\phi / \sqrt{\sin \phi}$ becomes:

$$\int_0^{\phi} d\phi / \sqrt{\sin \phi} = \sqrt{2} \left[\int_0^{90^\circ} dt / \sqrt{1 - \tfrac{1}{2} \sin^2 t} + \int_0^{\cos^{-1} (\sqrt{\sin \phi})} dt / \sqrt{1 - \tfrac{1}{2} \sin^2 t} \right]$$

or $$\int_0^{\phi} dt / \sqrt{\sin \phi} = \sqrt{2} \left(K + u \right) \quad (1.9.6)$$

Where K is the complete elliptic integral of first kind $\int_0^{90^\circ} dt / \sqrt{1 - \tfrac{1}{2} \sin^2 t}$

and u is the elliptic integral of first kind $\int_0^{\cos^{-1}(\sqrt{\sin\phi})} dt/\sqrt{1-\frac{1}{2}\sin^2 t}$

Then Equation (1.9.5) becomes:

$$\alpha/\sin\alpha = (\pi/2)\ \left[1 + u/K\right]\ /\ \sqrt{\sin\phi} \qquad (1.9.7)$$

Table 1.9.1 gives values of α vs ϕ for several values of ϕ. Values of K and u have been taken from Reference 8. K = 1.8541

Figure 1.9.4 represents graphically the variation of the angle α vs ϕ. The graph approximates a straight line whose equation is

$$\alpha = .64\,\phi + .57 \qquad (1.9.8)$$

in which both angles α and ϕ are measured in radians.

Returning to the original analysis, the following definitions apply:

F	is the resultant force on the extension.
T_c and T_s	are the tensions in the cords over the canopy and the suspension lines, respectively. They are not necessarily equal for this analysis.

From the principles of statics, the assumptions, and the geometry a system of 14 simultaneous equations with 14 unknowns is written. These equations are as follows:

Statics

$$F\cos\ \pi/4 - \theta\ + 2T_c \sin(\phi_{sk} - \pi/2) = 2T_s \sin\theta \qquad (1.9.9)$$

$$T_s = W_b/(N\cos\theta) \qquad (1.9.10)$$

$$T_c = \frac{pA_{sk}}{\cos(\phi_{sk} - \pi/2)} \qquad (1.9.11)$$

Table 1.9.1 - Values of α vs ϕ

①	②	③	④	⑤	⑥	⑦	⑧	⑨
ϕ	$\sin \phi$	$\sqrt{\sin \phi}$	$(\pi/2)/\sqrt{\sin \phi}$	$\cos^{-1}\sqrt{\sin \phi}$	u	$1 + u/k$	$\alpha/\sin \alpha$	α
			1.5708/ ③				④ · ⑦	
90°	1.0000	1.0000	1.5708	0° 00'	.0000	1.0000	1.5708	90.00°
93	.9986	.9993	1.5719	2 10	.0378	1.0204	1.5892	91.85
96	.9945	.9973	1.5751	4 13	.0765	1.0413	1.6401	93.70
99	.9877	.9938	1.5806	6 23	.1114	1.0601	1.6755	95.60
102	.9781	.9890	1.5883	8 30	.1485	1.0801	1.7155	97.50
105	.9659	.9828	1.5983	10 38	.1862	1.1004	1.7588	99.45
108	.9511	.9753	1.6106	12 46	.2238	1.1207	1.8050	101.40
111	.9336	.9662	1.6258	14 56	.2520	1.1359	1.8467	103.10
114	.9135	.9558	1.6434	17 06	.3008	1.1622	1.9100	105.50
117	.8910	.9439	1.6642	19 17	.3396	1.1832	1.9690	107.55
120	.8660	.9306	1.6879	21° 28'	.3791	1.2045	2.0330	109.70°

Figure 1.9.4 - Variation of α vs φ

Statics

$$T_c = 2p\rho x_m \sin(\pi/N) \tag{1.9.12}$$

$$W_b = Np\,A_{sk} + (N/2)\,F \sin(\pi/4 - \theta) \tag{1.9.13}$$

$$F = p\,(.126\,l_c)\,2r_{sk} \sin\alpha_{sk} \tag{1.9.14}$$

Geometry

$$A_{sk} = \tfrac{1}{2}x_{sk}^2 \sin(2\pi/N) + r_{sk}^2\alpha_{sk} - \tfrac{1}{2}r_{sk}^2 \sin 2\alpha_{sk} \tag{1.9.15}$$

$$r_{sk} = x_{sk}\,\frac{\sin 2/N}{\sin\alpha_{sk}} \tag{1.9.16}$$

$$\rho = \frac{x_m - x_{sk}}{1 - \cos(\phi_{sk} - \pi/2)} \tag{1.9.17}$$

$$\rho = \frac{l_b}{(\phi_{sk} - \pi/2)} \tag{1.9.18}$$

$$x_{sk} = l_s' \sin\theta \tag{1.9.19}$$

Assumptions

$$\alpha_{sk} = .64\,\phi_{sk} + .57 \tag{1.9.20}$$

$$l_c = .42687\,l_s' \tag{1.9.21}$$

$$l_c = 1.3409\,x_m + l_b \tag{1.9.22}$$

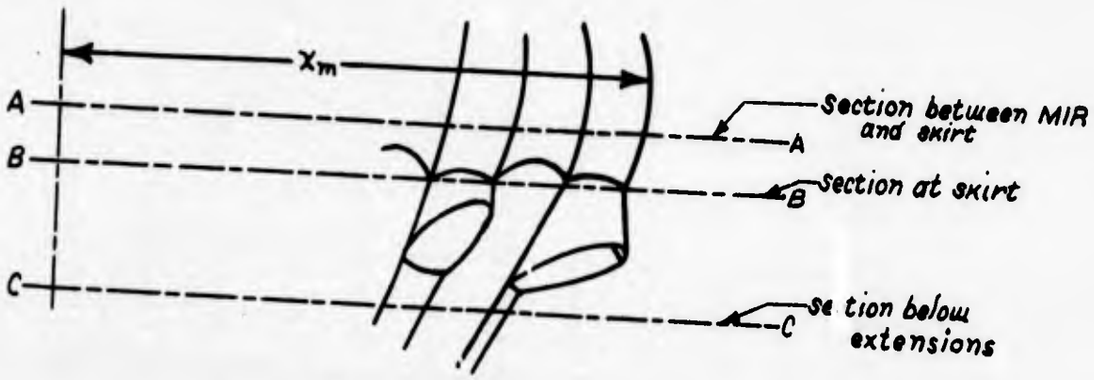

Figure 1.9.5

Equation (1.9.9) is derived from the summation of the horizontal components of the forces in Figure 1.9.2 using F/2 in place of F since the extensions are on alternate gores only. Equation (1.9.10) is derived by a summation of vertical

forces for a free body below section C-c. Equation (1.9.11) is derived by a vertical summation of forces for free body just above B-B. Equation (1.9.12) is derived from the hoop tension formula yielding a force acting upon an infinitesimal length of cord at A-A. Equation (1.9.13) is derived by a vertical summation of forces acting on a free body just below section B-B when this section is just above the skirt. Equation (1.9.14) is simply the force F due to pressure acting on the rectangular area of step 4 above.

The 14 equations when solved simultaneously yield two transcendental equations containing the unknowns θ and ϕ_{sk}. These two equations are:

$$\tan\theta \quad \frac{-\cot\phi_{sk} + \sqrt{\cot^2\phi_{sk} - 4c\,(c-1)}}{2c} \tag{1.9.23}$$

$$.26106\,\frac{d - 1.3409}{\phi_{sk} - \pi/2} - 5.4879\,\frac{bd^2\,\sin^2\theta}{\cos\,(\phi_{sk} - \pi/2)} = 0 \tag{1.9.24}$$

in which

$$a = .64\,\phi_{sk} + .57 \tag{1.9.25}$$

$$b = .12941 + .01704\,\frac{a - \sin a\cos a}{\sin^2 a} \tag{1.9.26}$$

$$c = 1 - \frac{.00496}{b} \tag{1.9.27}$$

$$d = \frac{1.3409\,\left[1 - \cos\,(\phi_{sk} - \pi/2)\right] + \phi_{sk} - \pi/2}{1 - \cos\,(\phi_{sk} - \pi/2) + 2.345\,(\phi_{sk} - \pi/2)\,\sin\theta} \tag{1.9.28}$$

The solution of Equations (1.10.23) and (1.10.24) is effected by trial and error as follows: First assume ϕ_{sk} and calculate "a", use "a" to calculate "b", use "b" to calculate "c". The values of "c" and ϕ_{sk} are used to determine θ from Equation (1.10.23). This value of θ is then used together with ϕ_{sk} to cal-

culate "d". Finally the values of "b", "d", θ, and ϕ_{sk} are used in Equation (1.10.24) to see if this equation is satisfied. Usually four trials are required to yield a solution. With the conditiors given here the solution is $\phi_{sk} = 100^\circ\ 50'$ and $\theta = 16^\circ\ 50'$. With these values of ϕ_{sk} and θ the MIR and the radius of the circular portion of the cord may be determined as shown below.

Let $l_s' = k_s' x_m$ or $x_{sk}/\sin\theta = k_s' x_m$ or $x_{sk} = k_s' \sin\theta\ x_m$ (1.9.29)

Equation (1.9.29) combined with Equations (1.9.17), (1.9.18), (1.9.21) and (1.9.22) gives:

$$\frac{x_m - k_s' \sin\theta\ x_m}{1 - \cos(\phi_{sk} - \pi/2)} = \frac{.42687\ k_s' x_m - 1.3409\ x_m}{\phi_{sk} - \pi/2}$$

or

$$\frac{1 - k_s' \sin\theta}{1 - \cos(\phi_{sk} - \pi/2)} = \frac{.42687\ k_s' - 1.3409}{\phi_{sk} - \pi/2}$$

For $\phi_{sk} = 100^\circ\ 50'$ and $\theta = 16^\circ\ 50'$ the above equation gives

$$\frac{1 - .28959\ k_s'}{.01782} = \frac{.42687\ k_s' - 1.3409}{.18907} \quad \text{from which } k_s' = 3.41500$$

Then $l_c = (.42687)(3.41500) x_m = 1.45776\ x_m$

The central angle of the assumed circular arc for the portion of the cord below the MIR is $\phi_{sk} - \pi/2 = 100^\circ\ 50' - 90^\circ = 10^\circ\ 50'$ and the radius of curvature is

$$\rho = \frac{l_b}{\phi_{sk} - \pi/2} = \frac{(1.45776 - 1.34090)\ x_m}{.18907} = .61807\ x_m$$

But the true value of l_c is 13.857 ft.

Then $x_m = l_c/1.45776 = 13.857/1.45776 = 9.506$ ft

$x_{ak} = k_g' \sin\theta\, x_m = (3.46500)\ (.28959)\ (9.506) = 9.40$ ft

$\rho = (.61807)\ (9.506) = 5.875$ ft

The resulting shape is shown in Figure 2.4.3.

1.10 Conical Ring Slot Canopy

As has been discussed already in Section 1.7, the conical ring slot canopy does not exhibit the pointed apex characteristic of the conical canopy for cone angles in the neighborhood of 30°. For this reason a modification of the flat canopy theory is used for the conical ring slot.

The modification is based on the assumption that the shapes of the flat canopy of Section 1.1 and the conical ring slot canopy are geometrically similar above the MIR, the only difference being that due to a reduction in differential pressure for the ring slot canopy. The reduced differential pressure p' assumed to act on a ring slot canopy is determined by the ratio of actual cloth area to cloth area plus area of slots. The method of analysis is illustrated by an example using an actual canopy.

Figure 1.10.1 shows one gore of the conical ring slot canopy. The calculation of the reduced pressure p' is shown below.

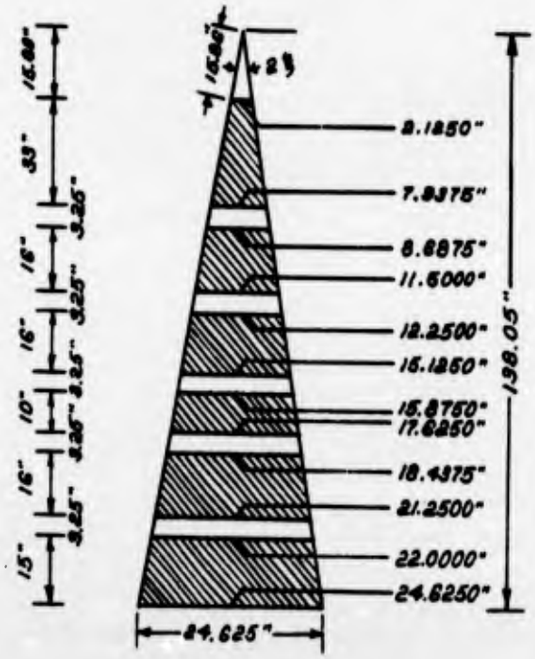

Figure 1.10.1

Area of slots:

$\frac{1}{2} \times 3.25 \times (7.9375 + 8.6875) = (1.625)\ (16.6250)\ \text{in.}^2$

$\frac{1}{2} \times 3.25 \times (11.5000 + 12.2500) = (1.625)\ (23.7500)\ \text{in.}^2$

$\frac{1}{2} \times 3.25 \times (15.1250 + 15.8750) = (1.625)\ (31.0000)\ \text{in.}^2$

$\frac{1}{2} \times 3.25 \times (17.6250 + 18.4375) = (1.625)\ (36.0625)\ \text{in.}^2$

$\frac{1}{2} \times 3.25 \times (21.2500 + 22.0000) = \frac{(1.625)}{(1.625)}\ \frac{(43.2500)}{(150.688)}\ \text{in.}^2$

$= 244.87\ \text{in.}^2$

Area of vent corresponding to one gore

$\frac{1}{2}\ (15.80)\ (2.125) = 16.79\ \text{in.}^2$

Total $261.66\ \text{in.}^2$

Total gore area $= (\frac{1}{2})\ (24.625)\ (138.05) = 1699.74\ \text{in.}^2$

Percentage of slot area:

$$\frac{261.66}{1699.74}\ (100) = 15.39\%$$

The reduced pressure is $p' = \frac{100 - 15.39}{100}\ p$ or $p' = .8461\ p$

A ring slot canopy whose diameter is the same as that of a solid canopy would carry a smaller suspended load. If the ring slot canopy were to carry the same load it would have to be larger. Here, the shape of the ring slot canopy is determined in connection with the shape of a solid flat canopy carrying the same load.

Using primes in the case of the ring slot canopy to distinguish the same quantities from those of a flat one, we proceed as follows:

For a given suspended weight W_b ommon for both flat and ring slot canopies having equal number of gores N and equal l_c and l_c/l_s', the equations of equilibrium

of the lower free bodies, assuming the canopies cut by planes passing through the skirt, are respectively

$$W_b = MA_{sk}p \tag{1.10.1}$$

$$W_b = MA'_{sk}p' \tag{1.10.2}$$

Equating right hand members we obtain $A_{sk}\ p = A'_{sk}\,p'$ (1.10.3)

Taking equation $p' = .8461$ into account, Equation (1.10.3) becomes

$$A_{sk} = .8461\ A'_{sk} \tag{1.10.4}$$

Assuming that the areas A_{sk} and A'_{sk} correspond to geometrically similar figures, Equation (1.10.4) yields $x'_{sk} = 1.09\ x_{sk}$ (1.10.5)

The equation for the portion of the cord from MIR to skirt is assumed to be a parabolic arc having the equation

$$Z' = c'\sqrt{X'} \tag{1.10.6}$$

where Z''s are measured from MIR downward and $X' = x'_m - x'$

Differentiating Equation (1.10.6) results in

$$dZ'/dX' = c'/2\sqrt{X'} \tag{1.10.7}$$

In Equation (1.10.7) for $x' = x'_{sk}$, $dZ'/dX' = \cot\theta' = \sqrt{n'^2 - 1}$

$$\text{hence} \quad \sqrt{n'^2 - 1} = \frac{c'}{2\sqrt{x'_m - x'_{sk}}} \tag{1.10.8}$$

The length of the parabolic arc is given by the expression $\frac{1 - k'_{sk}}{2} f(n')\ x'_m$

or $\frac{x'_m - x_{sk}}{2}\ f(n')$ (see Section 1.3)

Then $l_c - 1.3409\ x'_m = \frac{x'_m - x'_{sk}}{2}\ f(n')$ (1.10.9)

Finally from the right triangle formed by l'_s, x'_{sk} and the canopy axis we obtain

$$\sin\theta' = 1/n' = x'_{sk}/l'_s \tag{1.10.10}$$

The coordinate x_{sk} of the flat canopy can be determined from Equations (1.3.18) and (1.3.19) of Section 1.3. The x'_{sk} is found from Equation (1.10.5). Equation (1.10.10) gives the value of n' from which $f(n') = 2n' + (n'^2 - 1) \log \frac{n' + 1}{n' - 1}$ is calculated. Then from Equation (1.10.9) x'_m is determined. Finally from equation (1.10.8) we determine the value of the parameter c' and the equation of the parabolic arc becomes:

$$z' = .6816\, x'_m + c' \sqrt{x_m - x'} \qquad (1.10.11)$$

where z's are measured from the apex.

Discussion

From Equation (1.10.9) it is evident that $l_c - 1.3409\, x'_m > 0$ or $x'_m < \frac{l_c}{1.3409}$ (1.10.12)

Since x'_{sk} is less than x'_m, Equation (1.10.12) yields

$$x'_{sk} < l_c/1.3409 \qquad (1.10.13)$$

Combining Equation (1.10.5) and (1.10.13) results in $1.09\, x_{sk} < l_c/1.3409$ or $1.09\, (l'_s/n) < l_c/1.3409$ from which $l_c/l'_s > 1.4616/n$ (1.10.14)

Taking Equation (1.10.14) into account, the equation

$$k_{sk} = \frac{f(n) + (2)\,(1.340)}{f(n) + 2n\ l_c/l'_s} = 1 - \frac{.25}{n^2 - 1}$$ (see Section 1.3, in this calculation

$l_s/x_m = 1.3409$ and $\rho_m/x_m = \frac{1}{2}$) becomes

$$\frac{f(n) + 2.6818}{f(n) + 2n\ 1.4616/n} > 1 - \frac{.25}{n^2 - 1} \equiv \frac{n^2 - 1.25}{n^2 - 1}$$

Substituting $4.240n - 1.184$ for $f(n)$ (see Section 1.3 Equation (1.3.20)) in the above inequality and simplifying we obtain $n^2 - 4.391n - 2.801 < 0$ which is satisfied for values of $n < 4.956$ (since $n > 0$). This inequality, which assumes values of n involving values of the ratio l_c/l'_s greater than .295 (see Equation (1.10.14)),

i.e., angles θ greater than 11° 40', gives the necessary and sufficient condition for the problem to have a real solution.

In Section 1.11, the shape of the conical ring slot canopy is worked out for N = 24, and $l_c/l_s' = .6$. The result is plotted in Figure 1.11.1.

1.11 Comparison of Cord Shapes of Five Different Canopies in the Fully Inflated Equilibrium Condition Holding the Parameters l_c, l_s' and N Constant

In the present section, shapes of the theoretical cord curves of five canopy types are compared, holding N = 24, $l_c/l_s' = 0.6$, and $l_c = 10$ feet for all types to make them as nearly equivalent as possible.

The five types to be compared are a) a flat canopy; b) an extended skirt canopy, with an extension e assumed to be 10%; c) a conical canopy with an angle β assumed to be 30°; d) a conical ring slot canopy; and e) a personnel guide surface canopy. For the personnel guide surface canopy the pocket area will be assumed a function of the canopy parameters identical to the one given in Section 2.4.

Relative coordinates x/x_m and z/x_m for the cord portion from the apex to MIR are taken from Table 1.4.1 for all canopy types but the conical canopy.

a) Flat Canopy

The parabolic cord portion from MIR to skirt is determined by using equations

$$k_{sk} = \frac{f(n) + 2k_a}{f(n) + 2n\,(l_c/l_s')} = \frac{f(n) + 2.6818}{f(n) + 1.2n} \qquad (1.11.1)$$

$$k_{sk} = 1 - \frac{\frac{1}{2}(\rho_m/x_m)}{n^2 - 1} = 1 - \frac{.25}{n^2 - 1} \qquad (1.11.2)$$

where $f(n) = 2n + (n^2 - 1)\log\frac{n+1}{n-1}$, $n = 1/\sin\theta$ (see Section 1.3)

The correct value of n satisfying both Equations (1.11.1) and (1.11.2) is n = 2.686.

$$f(n) = 10.23294, \quad k_{sk} = .95977, \quad \theta = 21°\ 51'$$

The absolute value of x_m is found by the equation $x_m \frac{l_c}{n\,k_{sk}\,(l_c/l_s')}$ to be equal to 6.465 ft.

The equation of the parabolic arc is $z/x_m = .6816 + \sqrt{1 - x/x_m}$ (1.11.3)

where $x_m \geq x \geq .95977\ x_m$

b) Extended Skirt Canopy

Solving Equation (1.6.5) for x_m results in

$$x_m = \frac{l_c}{1.3409\left(1 + \frac{2e}{\cos(\pi/N)}\right)} = \frac{10}{1.3409\left(1 + \frac{.2}{.99144}\right)} = 6.206 \text{ ft}$$

The value of n which satisfies the equation

$$f(n) = \frac{4e}{\frac{\cos(\pi/N)}{1.3409} - (1/n)(\cos \pi/N + 2e)\frac{k_s'}{k_c}} = \frac{.4}{\frac{.99144}{1.3409} - (1/n)(.99144 + .2)(1/.6)}$$

(see Section 1.6, Equation (1.6.7)) is n = 2.82698.

Then k_{sk} can be found from equation

$$k_{sk} = \frac{1.3409}{n}\left(1 + \frac{2e}{\cos(\pi/N)}\right)(k_s'/k_c) = .95000$$

The equation of the parabolic arc is

$$z/x_m = .6816 + 2\sqrt{(n^2 - 1)(1 - k_{sk})}\sqrt{1 - x/x_m}$$ (see Equation (1.6.11))

where z's are measured from the apex downward.

Substituting the numerical values for n and k_{sk} in the above equation we get

$$z/x_m = .6816 + 1.18252\sqrt{1 - x/x_m}$$

where $x_m \geq x \geq .95000\ x_m$

c) Conical Canopy

In the discussion of the conical canopy in Section 1.8 for which $l_c/l_s' = .6$ and N = 24 it has been found that n = 3.32, k_{sk} = .94691, θ = 17° 30', $\rho_m = 1.0574\ x_m$.

Then $l_c = (.6)\ (3.32)\ (.94691)\ x_m = 1.88624\ x_m$, $x_m = \dfrac{l_c}{1.88624} = 5.302$ ft.

The equation of the parabolic arc for the cord portion between MIR and Skirt is

$$z/x_m = 1.0646 + 1.454\ \sqrt{1 - x/x_m} \qquad (1.11.4)$$

where $x_m \geq x \geq .94691\ x_m$; z's are measured from the apex downward (See Table 1.8.6 for the value of z at $\phi' = 90°$, and Equation (1.3.7).)

d) Ring Slot Canopy (see Section 1.10)

$x_{sk} = (.95977)\ (6.465) = 6.205$ ft

$x'_{sk} = (1.09)\ (6.205) = 6.763$ ft (see Equation (1.10.5))

$\sin \theta = 1/n' = x'_{sk}/l'_s = \dfrac{6.763}{10/.6} = .40578$ (see Equation 1.10.10))

$n' = 1/.40578 = 2.4644 \qquad \theta' = 23° 56'$

From Equation (1.10.9) the MIR is determined;

$$10 - 1.3409\ x'_m = \frac{x'_m - 6.763}{2}\ (9.2973);\ \text{from which } x'_m = 6.919 \text{ ft}$$

The constant c' of the parabolic arc is determined from Equation (1.10.8)

$$c' = 2\ \sqrt{2.4644^2 - 1}\ \sqrt{6.919 - 6.763} = 1.77924 = .676\ \sqrt{x'_m}$$

Therefore the equation of the parabolic arc is

$$z/x_m = .6816 + .676\ \sqrt{1 - x/x_m} \qquad (1.11.5)$$

where $x'_m \geq x \geq \dfrac{6.763}{6.919}\ x'_m = .9775\ x'_m$

e) Personnel Guide Surface Canopy

Equations (1.9.9) to (1.9.20) and Equation (1.9.22) of Section 1.9 are also applied here; Equation (1.9.21) is replaced here by

$$l_c = .6\ l'_s \qquad (1.11.6)$$

These 14 equations yield two transcendental equations containing the unknowns θ and ϕ_{sk}. These two equations are

$$\tan\theta = \frac{-\cot\phi_{sk} + \sqrt{\cot^2\phi_{sk} - 4c\,(c-1)}}{2c} \qquad (1.11.7)$$

$$.26106\,\frac{d - 1.3409}{\phi_{sk} - \pi/2} - 2.7778\,\frac{b\,d^2\sin^2\theta}{\cos\,(\phi_{sk} - \pi/2)} = 0 \qquad (1.11.8)$$

where $a = .64\,\phi_{sk} + .57$ (1.11.9)

$$b = .12941 + .01704\,\frac{a - \sin a\cos a}{\sin^2 a} \qquad (1.11.10)$$

$$c = 1 - \frac{.00698}{b} \qquad (1.11.11)$$

$$d = \frac{1.3409\,\left[1 - \cos\,(\phi_{sk} - \pi/2)\right] + \phi_{sk} - \pi/2}{1 - \cos\,(\phi_{sk} - \pi/2) + 1.6667\,(\phi_{sk} - \pi/2)\,\sin\theta} \qquad (1.11.12)$$

True value of ϕ_{sk} satisfying the above equations is $\phi_{sk} = 106°\ 30'$

Then $a = 1.75962$ radians $= 100°\ 49'$, $b = .16374$, $c = .95737$, $\tan\theta = .41635$, $\theta = 22°\ 36'$, $\sin\theta = .38430$, $d = 1.5211$, and the left hand member of Equation (1.11.8) becomes .00128 ($\cong 0$).

From Equation (1.9.19) $x_{sk} = l_s'\ \sin\theta = (10/.6)\,(.38430) = 6.406$ ft

Combining Equations (1.9.17), (1.9.18) and (1.9.22) we obtain

$$\frac{x_m - x_{sk}}{1 - \cos\,(\phi_{sk} - \pi/2)} = \frac{l_c - 1.3409\,x_m}{\phi_{sk} - \pi/2}$$

or $$\frac{x_m - 6.406}{.04118} = \frac{10 - 1.3409\,x_m}{.28798}$$ from which $x_m = 6.575$ ft

The radius ρ of the circular arc below MIR is from Equation (1.9.17)

$$\rho = \frac{x_m - x_{sk}}{1 - \cos\,(\phi_{sk} - \pi/2)} = \frac{6.575 - 6.406}{.04118} = \frac{.169}{.04118} = 4.104\ \text{ft}$$

The following tables give the non-dimensional and absolute coordinates of several points of the cords for the five canopy types.

Table 1.11.1 - Coordinates of Several Points of the Parabolic Arc. Z's are Measured from MIR Downward

Flat Canopy				Extended Skirt Canopy				
(1)	(2)	(3)	(4)	(5)	(6)	(7)	(8)	(9)
x/x_m	$1 - x/x_m$	Z/x_m	z/x_m	x/x_m	$1 - x/x_m$		Z/x_m	z/x_m
		$\sqrt{(2)}$	.6816 + (3)			$\sqrt{(6)}$	1.1825 (7)	.6816 + (8)
1.0000	.00000	.00000	.6816	1.0000	.00000	.0000	.00000	.6816
.99196	.00804	.08967	.7713	.99000	.01000	.1000	.11825	.7999
.98392	.01608	.12681	.8084	.98000	.02000	.14142	.16723	.8488
.97588	.02412	.15531	.8369	.97000	.03000	.17321	.20482	.8864
.96784	.03216	.17933	.8609	.96000	.04000	.20000	.23650	.9181
.95977	.04023	.20058	.8822	.95000	.05000	.22361	.26442	.9460

Conical Canopy					Conical Ring Slot Canopy				
(10)	(11)	(12)	(13)	(14)	(15)	(16)	(17)	(18)	(19)
x/x_m	$1 - x/x_m$		Z/x_m	z/x_m	x/x_m'	$1 - x/x_m'$		Z/x_m'	z/x_m'
		$\sqrt{(11)}$	1.454 (12)	1.0646 + (13)			$\sqrt{(16)}$	.676 (17)	.6816 + (18)
1.00000	.00000	.0000	.0000	1.0646	1.0000	.0000	.0000	.0000	.6816
.98673	.01327	.1152	.1675	1.2321	.9955	.0045	.0671	.0454	.7270
.97346	.02654	.1628	.2367	1.3013	.9910	.0090	.0949	.0642	.7458
.96019	.03981	.1995	.2901	1.3547	.9865	.0135	.1162	.0786	.7602
.94691	.05309	.2304	.3350	1.3996	.9820	.0180	.1342	.0907	.7723
					.9775	.0225	.1500	.1014	.7830

Table 1.11.2 - Coordinates of Several Points of the Cord of a Conical Canopy with 24 Gores, $l_c/l_s' = .6$ and $l_c = 10$ ft

①	②	③	④	⑤	⑥	⑦	⑧	⑨	⑩
ø	x/x_m	z/x_m	x	z	ø	x/x_m	z/x_m	x	z
			5.302 ②	5.302 ③				5.302 ⑦	5.302 ⑧
30° 00'	.4968	.2868	2.634	1.520	79° 25'	.9823	.9155	5.208	4.854
37 04	.6158	.3581	3.265	1.899	86 29	.9960	.9995	5.280	5.299
44 07	.6969	.4235	3.695	2.245	90° 00'	1.0000	1.0646	5.302	5.644
57 11	.7764	.5056	4.116	2.680		.9867	1.2321	5.231	6.532
58 14	.8475	.5983	4.493	3.172	Parabolic Arc	.9735	1.3013	5.161	6.899
65 18	.9058	.6994	4.802	3.708		.9602	1.3547	5.091	7.182
72° 22'	.9515	.8075	5.044	4.281		.9469	1.3996	5.020	7.420

Table 1.11.3 – Coordinates of Several Points of the Cords of Flat, Extended Skirt, Ring Slot, and Personnel Guide Surface Canopies Having N = 24, $l_c/l_s' = .6$, and $l_c = 10$ ft.

①	②	③	Flat. Canopy		Extended Skirt		Conical Ring Slot		Personnel Guide Surface	
ø	x/x_m	z/x_m	x (ft)	z (ft)	x (ft)	z (ft)	x (ft)	z (ft)	x (ft)	z (ft)
Deg			6.465 ②	6.465 ③	6.206 ②	6.206 ③	6.919 ②	6.919 ③	6.575 ②	6.575 ③
0	.0000	.0000	.000	.000	.000	.000	.000	.000	.000	.000
4	.1115	.0038	.721	.025	.692	.024	.771	.026	.733	.025
10	.2647	.0227	1.711	.147	1.643	.141	1.831	.157	1.740	.149
20	.4723	.0779	3.053	.504	2.931	.483	3.268	.539	3.105	.512
30	.6405	.1561	4.141	1.009	3.975	.969	4.432	1.080	4.211	1.026
40	.7802	.2541	5.046	1.643	4.842	1.579	5.398	1.758	5.130	1.671
45	.8409	.3095	5.436	2.001	5.219	1.921	5.818	2.141	5.529	2.035
50	.8752	.3470	5.658	2.243	5.431	2.153	6.056	2.401	5.754	2.282
60	.9306	.4262	6.018	2.755	5.775	2.645	6.439	2.949	6.119	2.802
70	.9694	.5093	6.267	3.293	6.016	3.161	6.707	3.524	6.374	3.349
80	.9924	.5948	6.416	3.845	6.159	3.691	6.866	4.115	6.725	3.911
90	1.0000	.6816	6.465	4.407	6.206	4.230	6.919	4.716	6.575	4.482
Parabolic Arc			6.413	4.986	6.144	4.964	6.888	5.030	Circular Arc	
			6.361	5.226	6.082	5.268	6.857	5.160		
			6.309	5.411	6.020	5.501	6.826	5.260		
			6.257	5.566	5.958	5.698	6.794	5.344		
			6.205	5.703	5.896	5.871	6.763	5.418		

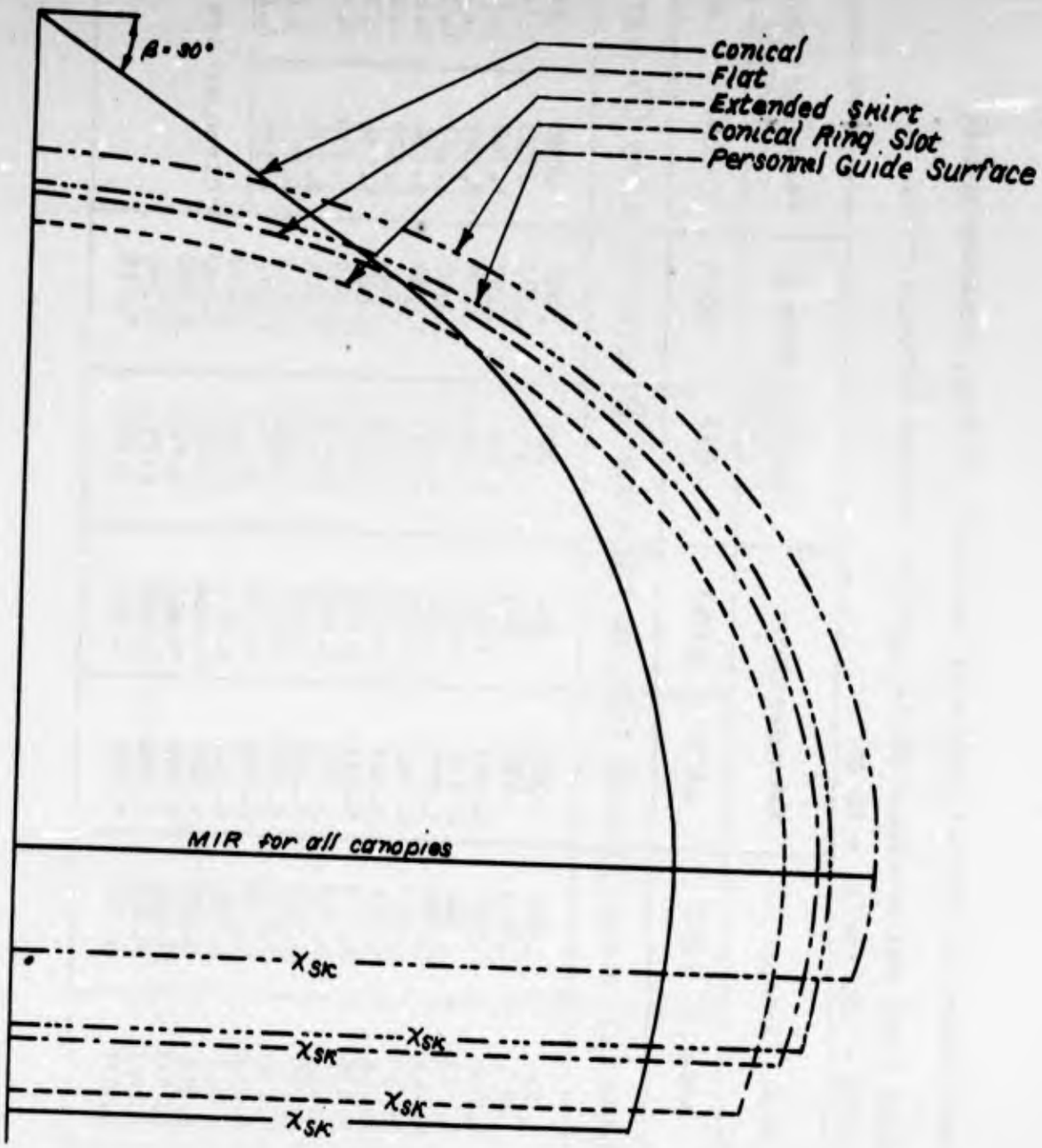

Figure 1.11.1 - Comparison of Theoretical Cord Shapes of Five Different Canopy Types in Fully Inflated Equilibrium Condition with Constant l_c, l_s' and N. (N = 24, l_c/l_s' = .6 for all five types)

1.12 Calculated Cord Tensions in Five Canopy Types with Common l_c, l'_{sa} N and Differential Pressure p

Assuming a horizontal section of the canopy passing through the MIR the equation of equilibrium of the upper free body is

$$T = A\ p \tag{1.12.1}$$

where A is the horizontal projection of the part of one gore corresponding to the upper free body. Disregarding the effect of the gore fullness on the area A, the following equation results:

$$A = (1/N)\ \pi\ x_m^2 \tag{1.12.2}$$

Hence $$T = (1/N)\ \pi\ x_m^2\ p \tag{1.12.3}$$

Equation (1.12.3) is used for all except the "first approximation" to the conical canopy.

a) Flat Canopy

For x_m = 6.465 ft (see Table 1.11.3)

$$T = (1/24)\,\pi\,(6.465)^2\ p = 5.47p \text{ or } T/p = 5.47 \text{ ft}^2 \tag{1.12.4}$$

b) Extended Skirt Canopy

For x_m = 6.206 ft (see Table 1.11.3)

$$T = (1/24)\,\pi\,(6.206)^2\ p = 5.04\ p \quad \text{or } T/p = 5.04 \tag{1.12.5}$$

c) Conical Canopy - First Approximation

The following equations are taken from Section 1.7

$$dT = 2\ f_1\ ds\ \cos\lambda\ \sin\lambda \tag{1.12.6}$$

where

$$ds = x_m\ \cos^2 \pi/N \left[\cos^2 \pi/N\ \cos^2 \phi + \cos\,(2\pi/N)\ \sin^2 \phi\right]^{-3/2} \sqrt{\cos\,(2\pi/N)}\ d\phi \tag{1.12.7}$$

$$\cos\lambda = \sqrt{1 - \sin^2 \pi/N\ \cos^2 \phi}\,. \tag{1.12.8}$$

$$\sin \lambda = \sin (\pi/N) \cos \phi \qquad (1.12.9)$$

$$f_1 = \frac{xp \cos \lambda}{2 \cos (\pi/N) \sin \phi} \qquad (1.12.10)$$

$$x = x_m \frac{\sqrt{\cos (2\pi/N)}}{\sqrt{\cos^2 (\pi/N) \cot^2 \phi + \cos (2\pi/N)}} \qquad (1.12.11)$$

Replacing the parameters in the right-hand member of Equation (1.12.6) by their values from the above equation we obtain

$$dT = \frac{px_m^2 \sin (4\pi/N)}{4} \frac{\cos \phi}{\sin^4 \phi} \left[1 - \sin^2 (\pi/N) \cos^2 \phi\right] \left[\cos^2 (\pi/N) \cot^2 \phi + \cos (2\pi/N)\right]^{-2} d\phi$$

Integrating:

$$T - T\phi_o = \frac{px_m^2 \sin (4\pi/N)}{4} \int_{\phi_o}^{\phi} \frac{\left[1 - \sin^2 (\pi/N) \cos^2 \phi\right] \cos \phi \, d\phi}{\sin^4 \phi \left[\cos^2 (\pi/N) \cot^2 \phi + \cos (2\pi/N)\right]^2}$$

For $N = 24$ and $\phi_o = 30°$ the above equation becomes:

$$T - T(30) = \frac{px_m^2}{8} \int_{30}^{\phi} \frac{\left[1 - \sin^2 (\pi/N) \cos^2 \phi\right] \cos \phi \, d\phi}{\sin^4 \phi \left[\cos^2 (\pi/N) \cot^2 \phi + \cos (2\pi/N)\right]^2} \qquad (1.12.12)$$

Setting $$k\phi = \int_{30}^{\phi} \frac{\left[1 - \sin^2 (\pi/N) \cos^2 \phi\right] \cos \phi \, d\phi}{\sin^4 \phi \left[\cos^2 (\pi/N) \cot^2 \phi + \cos (2\pi/N)\right]^2} \qquad (1.12.13)$$

Equation (1.12.12) can be written $$T - T_{(30)} = k\phi \frac{px_m^2}{8} \qquad (1.12.14)$$

But for $\phi = 90°$, $T = \frac{1}{2} x_m^2 p \sin(2\pi/N) = .12941\, x_m^2 p$ with $N = 24$ and $k_{90} = .52426$ (see Table 1.12.1 Column (13))

Then Equation (1.12.14) gives: $.12941\, x_m^2 p - T_{(30)} = .52426\, p x_m^2/8$

or $T_{(30)} = .06388\, p x_m^2$

Therefore Equation (1.12.14) becomes:

$$T = (.06388 + k\phi/8)\, p x_m^2 \qquad (1.12.15)$$

Equation $0.6/\cos \phi_B = \dfrac{2\,\widehat{OC} - \widehat{OB}}{x_B}$ (1.12.16)

(See Section 1.7) when solved by trial and error gives $\phi_B = 72.65°$ and $x_B = .95349\, x_m$ (See Table 1.7.2)

Then $l_c = \dfrac{0.6\, x_B}{\cos \phi_B} = \dfrac{(.6)\,(.95349)}{.29821}\, x_m = 1.9184\, x_m$

For $l_c = 10$ ft, $x_m = \dfrac{10}{1.9184} = 5.213$ ft

Substituting 5.213 for x_m in Equation (1.12.15) results in

$$T = (.06388 + k\phi/8)\,(5.213)^2\, p \qquad (1.12.17)$$

Table 1.12.1 provides values of the ratio T/p for a conical canopy in the first approximation.

c') Conical Canopy - Second Approximation

For $x_m = 5.302$ ft (see Table 1.11.3)

$$T/p = (1/24)\,\pi\,(5.302)^2 = 3.680 \text{ ft}^2 \qquad (1.12.18)$$

d) Ring Slot Canopy

For $x_m = 6.919$ ft (see Table 1.11.3)

$T = (1/24)\,\pi\,(6.919)^2\, p' = (1/24)\,\pi\,(6.919)^2\,(.8461)\, p$ or $T/p = 5.302$ ft^2

(1.12.19)

Table 1.12.1 - Values of T/p vs s for a Conical Canopy in the 1st Approximation

①	②	③	④	⑤	⑥	⑦	⑧	⑨
ϕ	s/π_m	$\cos\phi$	$\sin\phi$	$\sin^4\phi$	*	*		*
							⑥ / ⑦	.01704 ③^2
30	.57358	.86603	.50000	.06250	13.85648	15.32300	.90429	.01278
36	.67819	.80902	.58779	.11937	6.77741	7.99821	.84737	.01115
42	.78308	.74314	.66913	.20046	3.70717	4.74490	.78130	.00941
48	.88825	.66913	.74314	.30499	2.19394	3.10743	.70603	.00763
54	.99371	.58779	.80902	.42839	1.37209	2.20445	.62242	.00589
60	1.09945	.50000	.86603	.56250	.88889	1.67361	.53112	.00426
66	1.20544	.40674	.91355	.69651	.58397	1.34794	.43323	.00282
72	1.31164	.30902	.95106	.81815	.37771	1.14442	.33004	.00163
78	1.41802	.20791	.97815	.91542	.22712	1.02096	.22246	.00073
84	1.52451	.10453	.99452	.97826	.10685	.95401	.11200	.00019
90	1.63107	.00000	1.00000	1.00000	.00000	.93295	.00000	.00000

* ⑥ = $\cos\phi/\sin^4\phi$

⑦ = $\left[\cos^2 \pi/N \cot^2\phi + \cos(2\pi/N)\right]^2$ ⑨ = $\cos^2\phi \sin^2 \pi/N$

①	⑩	⑪	⑫	⑬	⑭	⑮	⑯
ϕ				k_ϕ	.06388 + k_ϕ	T/p	s
	1 - ⑨	⑧ · ⑩	⑪$_{Av}$ $\Delta\phi$	$\int$ ⑫		$(5.213)^2$ ⑭	5.213 ②
30	.98722	.89273		.00000	.06388	1.736	2.99
36	.98885	.83792	.09068	.09068	.07522	2.044	3.54
42	.99059	.77395	.08446	.17514	.08577	2.330	4.08
48	.99237	.70064	.07726	.25240	.09543	2.593	4.63
54	.99411	.61875	.06913	.32153	.10407	2.828	5.18
60	.99574	.52886	.06014	.38167	.11159	3.032	5.73
66	.99718	.43201	.05036	.43203	.11788	3.203	6.28
72	.99837	.32950	.03992	.47195	.12287	3.339	6.84
78	.99927	.22230	.02892	.50087	.12649	3.437	7.39
84	.99981	.11198	.01752	.51839	.12868	3.496	7.95
90	1.00000	.00000	.00587	.52426	.12941	3.516	8.50

e) Personnel Guide Surface Canopy

For $x_m = 6.575$ ft (see Table 1.11.3). Then Equation (1.12.3) gives

$$T/p = (1/24)\,\pi\,(6.575)^2 = 5.659 \text{ ft}^2$$

Figure 1.12.1 gives the graphs of variation of T/p vs s for the five canopy shapes as found above.

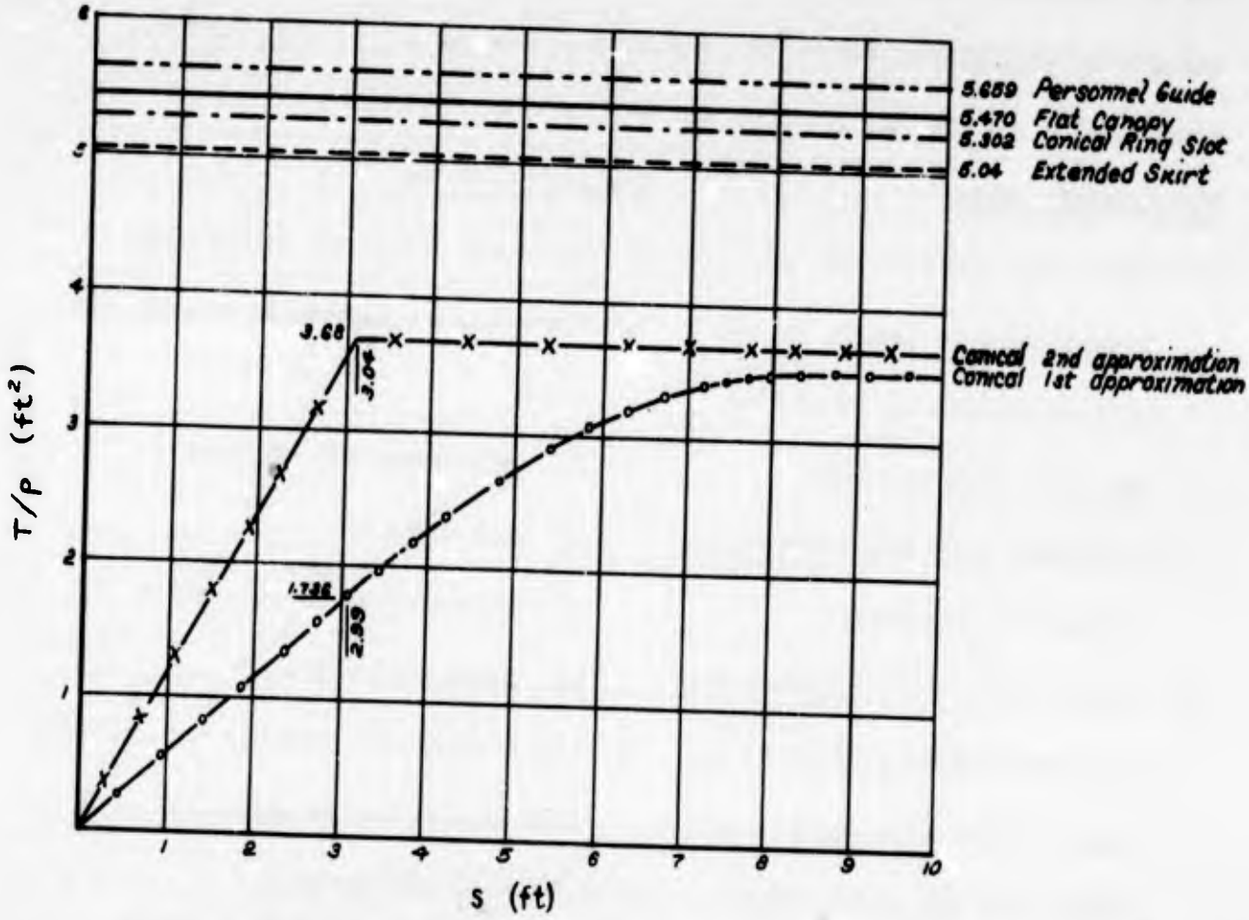

Figure 1.12.1 - Cord Tensions in Five Canopy Types Having Common $l_c = 10$ ft, $l_s' = 10/6$ ft, N = 24 and Differential Pressure p.

SECTION 2 - COMPARISON OF THEORETICAL WITH PHOTOGRAPHICALLY DETERMINED CANOPY SHAPES

INTRODUCTION

Several photographs of parachutes in steady descent were studied and five were used for purposes of comparison. The scale of a photograph may be determined if the magnitude of some length is known absolutely and if this length can be observed in its true perspective. Disagreement between photographical and theoretical shapes should not necessarily condemn the theory, however. Sources of error and disagreement may be listed as follows:

Photographic Shape

1) Suspension lines do not meet in common point so lengths had to be corrected to l_s'; this also may cause some parallax.
2) Camera-eye axis may be slightly oblique to canopy axis
3) Camera perspective angle is such that true canopy profile is not seen. Perspective angle is not known; so θ and canopy shape cannot be corrected.
4) Canopy may be pulsing, or not at constant rate of descent; or swaying with consequent asymmetry.
5) Cords over canopy cannot be seen.

Theoretical Shape

1) Lines and cloth are extensible.
2) There may be inaccurate assumptions about
   a) gore shape and fullness
   b) cord tensions
   c) mathematical relationships
   d) shape near skirt
3) The pressure is probably not constant over the entire canopy.
4) The cloth may wrinkle.
5) The vent area is neglected.

The influence of some of the factors listed would be difficult to estimate. The most important, however, are probably items (1) and (5) under photographic shape, and (2) and (4) under theoretical shape. The effect of camera angles and perspective would be to make the angle θ between the axis of the canopy and a suspension line appear larger than it really is. Since in most cases, it was found that the theoretical angle was slightly smaller than the corresponding photograph indicated for all but one canopy, it appears that this factor was not important except perhaps for the conical canopy. The influence of the extensibility of the lines is shown in Section 3.4 to be small because the tensions in the steady descent are small — less, in fact, than the manufacturing pre-tensions.

Sections 2.1 to 2.5 compare the theoretical with the photographically determined shapes of a flat canopy (type T-7), extended skirt canopy (T-10), conical canopy, personnel guide surface canopy (type C-11), and a conical ring slot canopy respectively. The final comparison in each case consists of one page showing both the theoretical and photographic gore centerline shapes together with the equations of the theoretical cord and gore centerline. Section 2.6 gives cord coordinates for a Taylor curve with the same parameters as in a flat canopy. The portion of the cord below the MIR is assumed to be on the one hand symmetrical with the Taylor curve and on the other hand to be parabolic as is done in the flat canopy. The curves of Section 2.6 are shown in Section 2.1.

Reference 10 develops the intrinsic equation of equilibrium for heavy cords. Section 2.7 shows that the intrinsic equation may be used in conjunction with experimental data.

2.1 Comparison of the Theoretical with the Photographically Determined Shape of a Fully Inflated Flat Canopy (Type T-7, D_o = 28 ft, N = 28, l_c = 14 ft, l_s = 22 ft 10 in.)

Photographic Shape

The parachute has dimensions in accordance with USAF Dwg. 50E6877. Thus the nominal diameter is 28 ft which is 2 l_c for all practical purposes. The length of suspension lines l_s = 22 ft 10 in. This latter length is used to determine the scale of the photograph reproduced as Figure 2.1.4.

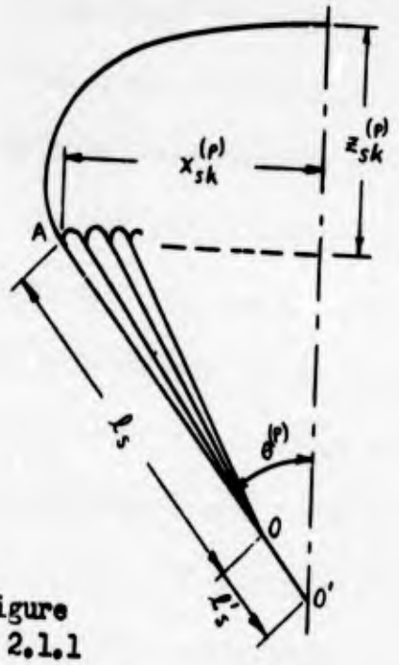

Figure 2.1.1

Figure 2.1.1 shows a sketch of the outline of a flat canopy as obtained from the photograph. The lengths A0 and A0' are scaled using a scale of 1/40. By measuring the photograph

$$A0 = \frac{137.0}{(40)\ (12)} = .2854 \text{ ft}$$

$$A0' = \frac{150.0}{(40)\ (12)} = .3125 \text{ ft}$$

(Note: the quantity 137.0 is actually 137.0 $\pm$ .5)

The true length A0 is l_s = 22 ft 10 in. as obtained from the drawing. Therefore the scale of the photograph is 22.83/.2854 = 80 to 1. The true length A0' = l_s' = (.3125) (80) = 25.00 ft.

Other quantities are:

$$l_c/l_s' = 14/25 = .56$$

$$x_{sk}^{(p)} = \frac{(52.0)\ (80)}{(40)\ (12)} = 8.67 \text{ ft}$$

$$z_{sk}^{(P)} = \frac{(48.0)(80)}{(40)(12)} = 8.00 \text{ ft}$$

$$\sin \theta^{(P)} = 8.67/25 = .3467, \quad \theta = 20° 17'$$

Coordinates of several points of the gore centerline are plotted in Figure 2.1.5 together with those obtained by theoretical means.

Theoretical Cord Coordinates

For the flat canopy the coordinates of the cord above the MIR are given in non-dimensional units in Table 1.4.1. It is only necessary to determine the absolute value of x_m, the coordinates of the parabolic portion, and the angle θ of the suspension lines. These are calculated by first solving Equation (2.1.1) and (2.1.2) for n.

$$k_{sk} = \frac{f(n) + 2.6818}{f(n) + 2(.56)n} = \frac{f(n) + 2.6818}{f(n) + 1.12n} \qquad (2.1.1)$$

and

$$k_{sk} = 1 - \frac{.25}{n^2 - 1} \qquad (2.1.2)$$

in which the factor (.56) in Equation (2.1.1) is the ratio l_c/l_s' which is a characteristic of this particular parachute. The correct value 2.8385 of n gives

$$f(n) = 2n + (n^2 - 1) \log \frac{n+1}{n-1} = 10.8724$$

$$k_{sk} = \frac{f(n) + 2.6818}{f(n) + 1.12n} = .96460$$

$$k_{sk} = 1 - \frac{.25}{n^2 - 1} = .94658$$

$$\theta = \theta^{(T)} = \csc^{-1} 2.8385 = 20° 38' \text{ (compares with } \theta^{(P)} = 20°17') \qquad (2.1.4)$$

Since $l_s' = k_{sk} x_m \csc \theta = n k_{sk} x_m$ (see Equations (1.3.12) and (1.3.13)) then

$$x_m = l_s'/nk_{sk} = \frac{25.00}{(2.8385)(.96460)} = 9.13 \text{ ft} \qquad (2.1.5)$$

and $x_{sk} = x_{sk}^{(T)} = k_{sk}\, x_m = (.9646)(9.13) = 8.81$ ft (2.1.6)

(compares with $x_{sk}^{(P)} = 8.67$ ft)

The coordinates of the parabolic portion are given by Equation (1.4.10).

$$z = z_m + Z = z_m + x_m \sqrt{1 - x/x_m} \qquad (2.1.7)$$

Table 2.1.1 gives non-dimensional coordinates of the parabolic portion while Table 2.1.2 gives the non-dimensional coordinates of the portion above the MIR from Table 1.4.1 together with the absolute cord coordinates from apex to skirt.

Table 2.1.1 - Coordinates of Several Points of the Parabolic Portion

x/x_m	$1 - x/x_m$	$\dfrac{z/x_m}{\sqrt{1 - x/x_m}}$
1.0000	.0000	.0000
.9929	.0071	.0843
.9858	.0142	.1192
.9787	.0213	.1460
.9716	.0284	.1685
.9646	.0354	.1881

Table 2.1.2 - Non-Dimensional and Absolute Coordinates of Several Points on the Cord from Apex to Skirt

① ø	② x/x_m	③ z/x_m	④ x 9.13 ②	⑤ z 9.13 ③	⑥ ø	⑦ x/x_m	⑧ z/x_m	⑨ x 9.13 ⑦	⑩ z 9.13 ⑧
0°	.0000	.0000	.0000	0	50°	.8752	.3470	7.991	3.168
4°	.1115	.0038	1.018	.035	60°	.9306	.4262	8.496	3.891
10°	.2647	.0227	2.417	.207	70°	.9694	.5093	8.851	4.650
20°	.4723	.0779	4.312	.711	80°	.9924	.5948	9.061	5.431
30°	.6405	.1561	5.848	1.425	90°	1.0000	.6816	9.130	6.223
40°	.7802	.2541	7.123	2.320	Parabolic Arc	.9929	.7659	9.065	6.993
45°	.8409	.3095	7.677	2.826		.9858	.8008	9.000	7.311
						.9787	.8276	8.936	7.556
						.9716	.8501	8.871	7.761
						.9646	.8697	8.807	7.940

Theoretical Gore Centerline

It is impossible to get a true view of a cord in a canopy from a photograph, but it is possible to get a nearly true view of the centerline of the gore. In order to compare a theoretical with a photographic shape it is necessary to be able to compute the shape of the gore centerline from the cord shape. This is done with the help of several assumptions.

In Sections 1.1 and 1.4 a cylindrical shape was postulated for the gore shape for $0 \leq \phi \leq 45°$. With this assumption it is possible to determine the coordinates of the gore centerline from the coordinates of the cord. In Figure 2.1.2(a) the outer curve is that of the gore centerline, the next curve is that formed by the intersection of an axial plane with the surface of revolution generated by a cord curve. Figure 2.1.2(b) shows a horizontal section through one gore.

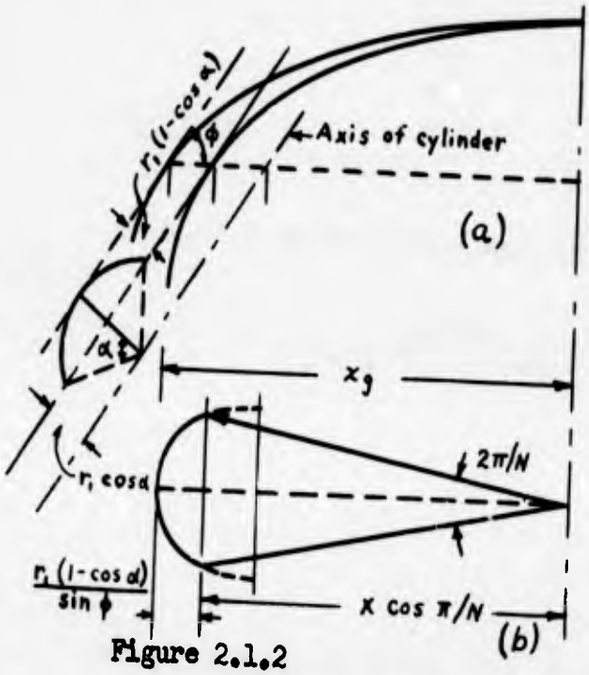

Figure 2.1.2

From Figure 2.1.2

$$x_g = x\cos\pi/N + r_1(1-\cos\alpha)\csc\phi$$

but $r_1 = x_m \sin\pi/N$ and $\sin\alpha = \sqrt{\sin\phi}$

Then $$x_g = x_m\cos\pi/N\left[x/x_m + \tan(\pi/N)\frac{1-\sqrt{1-\sin\phi}}{\sin\phi}\right] \quad (2.1.8)$$

Let z be the ordinate measured from the apex downward and common to both the cord and the gore centerline. Then

$$dz = \tan\phi\, dx \text{ or } dz/dx_g = \tan\phi\ dx/dx_g$$

$$dz/dx_g = \tan\phi\,(dx/d\phi)\,(d\phi/dx_g) \quad (2.1.9)$$

But from Equation (1.4.1)

$$x = .5036\, x_m \frac{.8409}{.7564} \log \left[5.85 \frac{.351 + \sin \phi}{2.083 - \sin \phi} \right] \qquad (2.1.10)$$

then

$$dx/d\phi = .5036 \frac{2.434 \cos \phi}{(.351 + \sin \phi)(2.083 - \sin \phi)} \frac{.8409}{.7564} x_m \qquad (2.1.11)$$

At $\phi = 45°$

$$dx/d\phi \Big|_{\phi = 45°} = .6594\, x_m \qquad (2.1.12)$$

Differentiation of Equation (2.1.8) gives

$$dx_g/d\phi = x_m \cos \pi/N \left[(1/x_m)(dx/d\phi) + \tan \pi/N \frac{\frac{\cos \phi \sin \phi}{2\sqrt{1 - \sin \phi}} - \cos \phi \left[1 - \sqrt{1 - \sin \phi} \right]}{\sin^2 \phi} \right] \qquad (2.1.13)$$

At $\phi = 45°$, $N = 28$

$$dx_g/d\phi \Big|_{\phi = 45°} = .6861\, x_m \qquad (2.1.14)$$

Therefore from Equation (2.1.9) the slope of the gore centerline at $\phi = 45°$ is

$$dz/dx_g \Big|_{\phi = 45°} = \tan 45° \; dx/d\phi \Big|_{\phi = 45°} \; d\phi/dx_g \Big|_{\phi = 45°}$$

$$= \frac{.6594\, x_m}{.6861\, x_m} = .96108$$

or $\phi_g \Big|_{\phi = 45°} = \tan^{-1} .96108 = 43° 52'.$

Knowing the coordinates z and x_g and the angle ϕ_g at $\phi = 45°$ it is possible to determine the coordinates of the gore centerline for $45° \leq \phi \leq 90°$. This is done by assuming the gore centerline to follow a Taylor curve for $45° \leq \phi \leq 90°$. In some cases it may be possible for the gore centerline to have a "maximum inflated

radius" of its own in which case a parabolic portion may be determined as by Equations (2.1.1) to (2.1.7). The Taylor equation for the gore centerline for $43° 52' \leq \phi_g \leq 90°$ is

$$x_g = x_{mg} \sqrt{\sin \phi_g} \qquad (2.1.15)$$

The constant x_{mg} is determined by letting

$$x_g \Big|_{\phi = 45°} = x_{mg} \sqrt{\sin 43° 52'} \qquad (2.1.16)$$

From Equations (2.1.8) and (2.1.10)

$$x_g \Big|_{\phi = 45°} = .9083\, x_m$$

or $$x_{mg} = \frac{.9083}{\sqrt{\sin 43° 52'}} \quad x_m = 1.0872 \quad x_m \qquad (2.1.17)$$

Equation (2.1.15) becomes:

$$x_g = 1.0872\, x_m \sqrt{\sin \phi_g} \qquad (2.1.18)$$

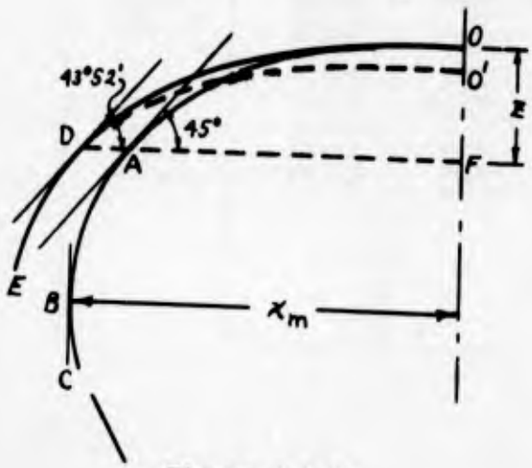

Figure 2.1.3

The z_g coordinates are given by Equation (1.2.4), with an added constant needed to correct the origin from O' to O (see Figure 2.1.3) for these coordinates, multiplied by 1.0872. Therefore

$$z_g = 1.0872\, (x_m/\sqrt{2}) \left\{ 2 \left[E - E(u) \right] - \left[K - u \right] \right\} + C \qquad (2.1.19)$$

The constant C is determined by equating z_g from Equation (2.1.19) to z_g at $\phi = 45°$ for the gore centerline curve OD, (see Figure 2.1.3). Using the notation of Jahnke-Emde (Reference 8)

$$u = F\left(45°, \cos^{-1} \sqrt{\sin 43° 52'}\right) = F(45°, 33° 39') = .6043$$

$K = 1.8541$, $E(u) = E(45°, 33° 39')$ = .5712, $E = 1.3506$

$$z_g\Big|_{\phi = 45°} = .3095\, x_m = 1.0872\,(x_m/\sqrt{2}) \quad (2)\left[(.7784) - 1.2498\right] + C$$

or $C = .0719\, x_m$

Then $$z_g = 1.0872\,(x_m/\sqrt{2})\left\{2\left[E - E(u)\right] - \left[K - u\right]\right\} + .0719\, x_m \qquad (2.1.20)$$

Tables 2.1.3 and 2.1.4 give the coordinates of the complete gore centerline.

Table 2.1.3 - Coordinates of Gore Centerline for $0 \leq \phi \leq 45°$

①	②	③	④	⑤	⑥	⑦	Abeolute Coordinates	
ϕ	x/x_m	z/x_m	*			x_g/x_m	x_g (ft)	z_g (ft)
	*	*		④ tan π/N	② + ⑤	⑥ cos π/N	9.13 ⑦	9.13 ③
0	0	0	.5000	.0564	.0564	.0560	.511	.000
4	.1115	.0038	.5090	.0574	.1689	.1678	1.532	.035
10	.2647	.0227	.5238	.0591	.3238	.3218	2.938	.207
20	.4723	.0779	.5521	.0623	.5346	.5312	4.850	.711
30	.6405	.1561	.5858	.0661	.7066	.7021	6.410	1.425
40	.7802	.2541	.6259	.0706	.8508	.8454	7.719	2.320
45	.8409	.3095	.6488	.0732	.9141	.9083	8.293	2.826

* For ② and ③ see Table 2.1.2.

④ = $\dfrac{1 - \sqrt{1 - \sin\phi}}{\sin\phi}$

The absolute coordinates from Tables 2.1.2, 2.1.3, and 2.1.4 are plotted in Figure 2.1.5. The portion of the gore centerline beyond $\phi_g = 90°$, i.e. below MIR, is of negligible length. This was shown to be true by a graphical integration of the length of the gore centerline that showed that the length from $\phi = 0$ to $\phi_g = 90°$ was very close to $l_c \cos \pi/N$, the actual length of the gore centerline.

Table 2.1.4 - Coordinates of Gore Centerline for $43° 52' \leq \phi_g \leq 90°$

① ϕ	② ϕ_g	③ x_g/x_{mg} *	④ *	⑤ $\frac{z_g - c}{x_m}$ 1.0872 ④	⑥ z_g/x_m ⑤ + c/x_m	⑦ x_g/x_m 1.0872 ③	Absolute Coordinates x_g (ft) 9.13 ⑦	Absolute Coordinates z_g (ft) 9.13 ⑥
45°	43° 52'	.9083 / 1.0872	.2185	.2275	.3095	.9083	8.293	2.825
	50	.8752	.2644	.2874	.3593	.9515	8.687	3.280
	60	.9306	.3436	.3735	.4454	1.0117	9.237	4.067
	70	.9694	.4267	.4639	.5358	1.0539	9.622	4.892
	80	.9924	.5122	.5568	.6287	1.0789	9.858	5.740
	90	1.0000	.5990	.6512	.7231	1.0872	9.926	6.602

* For ③ and ④ see Table 1.2.1

$$④ = \frac{z_g - c}{1.0872\, x_m}$$

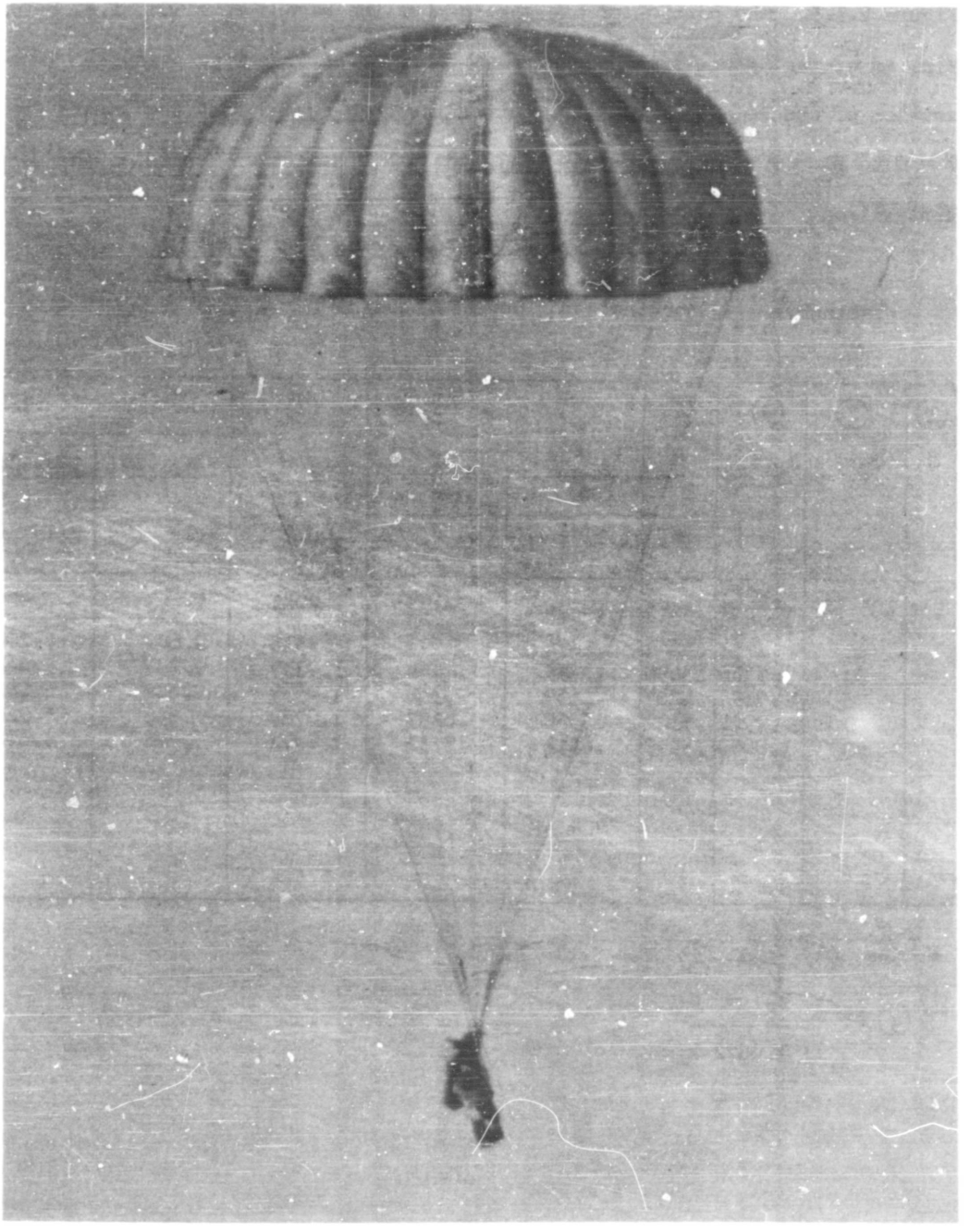

Figure 2.1.4 - Representative Photograph of a Fully Inflated Flat Canopy (T-7)

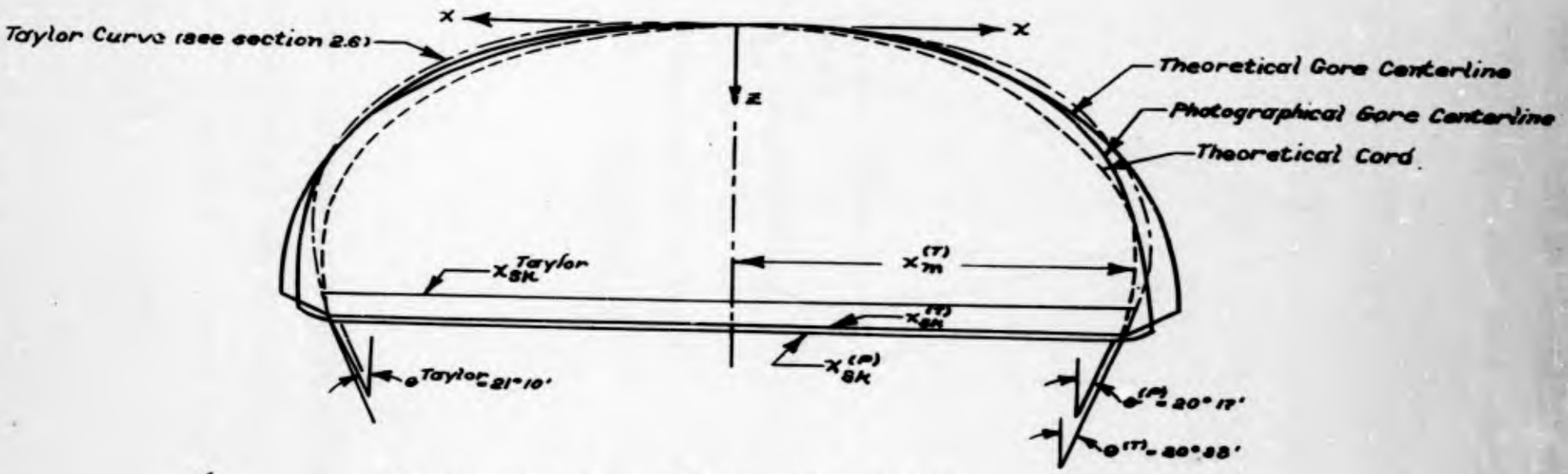

Equations of the cord

$0° \leq \phi \leq 45°$

$$x = 1.1117\,(.5036\,x_m)\log\left(5.85\,\frac{.361 + \sin\phi}{2.083 - \sin\phi}\right)$$

$$z = 1.1117\,(.5036\,x_m)\left[2.28\tan^{-1}\frac{2.083\tan\frac{\phi}{2} - 1}{1.827} - .375\log\frac{.361\tan\frac{\phi}{2} + .064}{.361\tan\frac{\phi}{2} + 1.836} - .138\right]$$

$45° \leq \phi \leq 90°$

$$x = x_m\sqrt{\sin\phi}$$

$$z = \frac{x_m}{\sqrt{2}}\left[2(E - E(u)) - (K - u)\right] + .0686\,x_m$$

where u and $E(u)$ are the elliptic integrals of 1st and 2nd kind respectively with modular angle 45°

$\phi \geq 90°$

$$z = z_m + x_m\sqrt{1 - x/x_m} \quad ; \quad (x_{SK} = .9646\,x_m)$$

Equations of gore centerline

$0° \leq \phi \leq 45°$

$$x_g = x_m \cos\frac{\pi}{N}\left[\frac{x}{x_m} + \tan\frac{\pi}{N}\,\frac{1 - \sqrt{1 - \sin\phi}}{\sin\phi}\right], \quad z_g = z$$

$45° \leq \phi \leq 90°$

$$z_g = 1.0872\,\frac{x_m}{\sqrt{2}}\left[2(E - E(u)) - (K - u)\right] + .0719\,x_m, \quad x_g = 1.0872\,x_m\sqrt{\sin\phi_g}, \quad \phi_g \geq 43°52'$$

Figure 2.1.5 - Comparison of Theoretical with Photographically Determined Shape of a Fully Inflated Flat Canopy. (Type T-7; D_o = 28 ft, N = 28, l_c = 14 ft, l_s = 22 ft 10 in)

2.2 Comparison of the Theoretical with the Photographically Determined Shape of a Fully Inflated Extended Skirt Canopy. (Type T-10, D_o = 35 ft, N = 30, l_c = 17.90 ft, l_s = 25.5 ft)

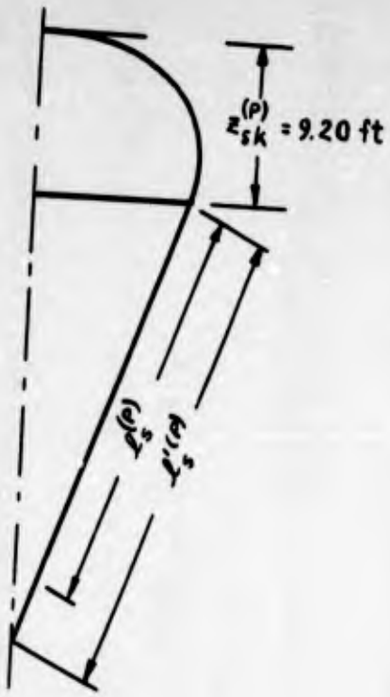

Figure 2.2.1

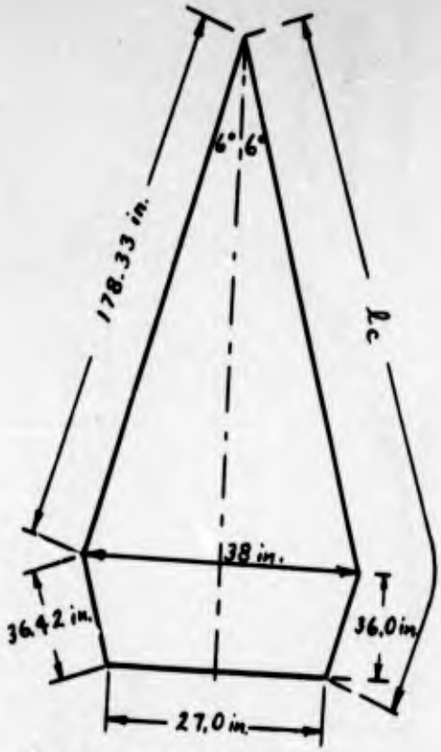

l_s = 25.50 ft (not shown)

Figure 2.2.2

Photographic Shape

The outline shown in Figure 2.2.1 is taken from Figure 2.2.4 which is a reproduction of an actual photograph. Figure 2.2.2 shows one gore and its dimensions as obtained from USAF Dwg. 49H7142. On a scale of 1:50 the distances $l_s^{(P)}$ = 105.5 units and $l_s'^{(P)}$ = 114.2 units. Therefore $l_s'^{(P)} = \left(\frac{114.2}{105.5}\right)(25.50) = 27.60 \therefore l_s'$.

$$l_c = \frac{178.33 + 36.42}{12} = 17.90 \text{ ft}$$

Using the above measurements to determine the scale of the photograph, the angle $\theta^{(P)}$ is found to be 21° 51' and the coordinates of the gore centerline are plotted in Figure 2.2.5 .

Theoretical Cord Coordinates

The coordinates of the cord above MIR are known once x_m is determined since these coordinates can be obtained from Section 1.6. From Figure 2.2.2 and Section 1.6,

$$l_a = \frac{178.33}{12} = 1.3409 \; x_m \qquad (2.2.1)$$

or $x_m = 11.08$ ft

The cord coordinates from apex to MIR are given in Table 2.2.1.

Table 2.2.1 - Cord Coordinates from Apex to MIR

①	②	③	Absolute Coordinates	
ø	x/x_m	z/x_i	x	z
	See Table 1.4.1		11.08 ②	11.08 ③
0	0	0	0	0
4	.1115	.0038	1.24	.04
10	.2647	.0227	2.93	.25
20	.4723	.0779	5.23	.86
30	.6405	.1561	7.10	1.73
40	.7802	.2541	8.64	2.82
45	.8409	.3095	9.32	3.43
50	.8752	.3470	9.70	3.84
60	.9306	.4262	10.31	4.72
70	.9694	.5093	10.74	5.64
80	.9924	.5948	11.00	6.59
90	1.0000	.6816	11.08	7.55

The portion below the MIR is assumed to be a parabolic arc determined as outlined in Section 1.6. In order to determine the parameters of the parabolic portion it is necessary to solve Equations (1.6.7) and (1.6.12) after which the equation of the parabolic portion is given by Equation (1.8.11). Those equations are given below

$$f(n) = 2n + (n^2 - 1) \log \frac{n+1}{n-1} = \frac{4e}{\frac{\cos \pi/N}{1.3409} - (1/n)(\cos \pi/N + 2e)(k_s'/k_c)} \qquad (2.2.2)$$

$$k_{sk} = \frac{1.3409}{n} \left(\frac{\cos \pi/N + 2e}{\cos \pi/N} \right) (k_s'/k_c) \qquad (2.3.3)$$

$$z = z_m + Z = .6816\, x_m + 2\, x_m \sqrt{(n^2 - 1)(1 - k_{sk})(1 - x/x_m)} \qquad (2.2.4)$$

The data to be used are:

$$N = 30,\ l_c/l_s' = k_c/k_s' = \frac{17.90}{26.60} = .6486,\ e = \frac{36}{2\,(178.33)} \cong .1$$

These give $n = 2.625$

$\theta = \csc^{-1} 2.625 = 22^\circ\ 24'$ compares with $\theta^{(P)} = 21^\circ\ 51'$

$k_{sk} = .94596$

Equation (2.2.4) then becomes

$$z/x_m = .6816 + 1.1284 \sqrt{1 - x/x_m} \qquad (2.2.5)$$

The coordinates of several points of the parabolic portion are given in Table 2.2.2.

Table 2.2.2 - Coordinates of Several Points of the Parabolic Portion

x/x_m	z/x_m	x (ft)	z (ft)
1.00000	.6816	11.08	7.55
.98000	.8412	10.86	9.32
.96000	.9073	10.64	10.05
.94596	.9440	10.48	10.46

The value for z_{sk} = 10.46 ft compares with $z_{sk}^{(p)}$ = 9.20 ft.

Theoretical Gore Centerline

The gore centerline is determined in the same manner as in the case of the flat canopy, Section 2.1. In Figure 2.2.3 the curve OAB is the cord curve from apex to MIR, OD is the gore centerline curve as obtained by a modification of the curve OA, and DE is a Taylor curve extension of the curve OA to form the gore centerline curve. The non-dimensional equation of the curve OD is the same as that of the flat canopy, Equation (2.1.8).

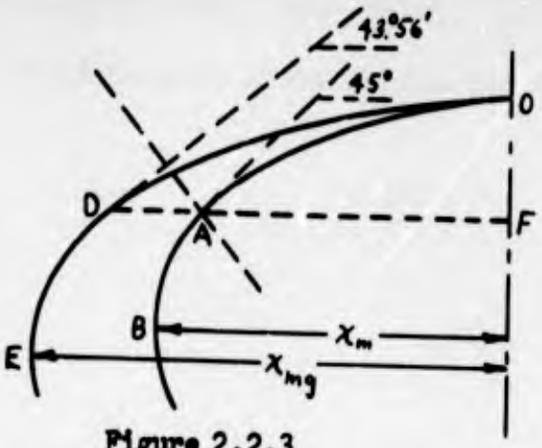

Figure 2.2.3

$$x_g/x_m = \left[(x/x_m) + \tan(\pi/N) \left(\frac{1 - \sqrt{1 - \sin\phi}}{\sin\phi} \right) \right] \cos \pi/N \qquad (2.2.6)$$

$$dz/dx_g = \tan\phi \, (dx/d\phi) \, (d\phi/dx_g) \qquad (2.2.7)$$

$$dx/d\phi \Big|_{\phi = 45°} = .6594 \, x_m \quad \text{(as before)} \qquad (2.2.8)$$

$$dx_g/d\phi \Big|_{\phi = 45°} = .6845 \, x_m \qquad (2.2.9)$$

Therefore

$$dz/dx_g \Big|_{\phi = 45°} = \frac{.6594 \, x_m}{.6845 \, x_m} = .96333 \qquad (2.2.10)$$

or $\phi_g \Big|_{\phi = 45°} = \tan^{-1} .96333 = 43° \, 56'$. The gore centerline equation is

$$x_g = x_{mg} \sqrt{\sin \phi_g}, \quad 43° \, 56' \leq \phi_g \leq 90° \qquad (2.2.11)$$

$$x_{mg} = \frac{x_g}{\sqrt{\sin \phi_g}} \Bigg|_{\phi_g = 43° \, 56'} = \frac{.90412 \, x_m}{\sqrt{\sin 43° \, 56'}} = 1.0854 \, x_m \qquad (2.2.12)$$

Hence $x_g = 1.0854\, x_m \sqrt{\sin \phi_g}$, $43^\circ\ 56' \leq \phi_g \leq 90^\circ$ (2.2.13)

The z coordinate is given by

$$z_g = 1.0854\, (x_m/\sqrt{2}) \left\{ 2 \left[E - E(u) \right] - \left[K - u \right] \right\} + .0717\, x_m \qquad (2.2.14)$$

The coordinates x_g and z_g are given in Tables 2.2.3 and 2.2.4. These coordinates together with those of the cord, (Tables 2.2.1 and 2.2.2), are plotted in Figure 2.2.5.

Table 2.2.3 - Coordinates of Gore Centerline for $0 \leq \phi \leq 45°$

①	②	③	④	⑤	⑥	⑦	Absolute Coordinates	
ϕ	x/x_m	z/x_m	$\frac{1-\sqrt{1-\sin\phi}}{\sin\phi}$			x_g/x_m	x_g(ft)	z_g (ft)
	See Table 2.1.2	See Table 2.1.2		④ tan π/N	② + ⑤	⑥ cos π/N	11.08 ⑦	11.08 ③
0	.0000	.0000	.5000	.05255	.05255	.05226	.529	0
4	.1115	.0038	.5090	.05350	.16500	.16410	1.818	.042
10	.2647	.0227	.5238	.05503	.31973	.31798	3.523	.252
20	.4723	.0779	.5521	.05805	.53035	.52744	5.844	.863
30	.6405	.1561	.5858	.06157	.70207	.69822	7.736	1.730
40	.7802	.2541	.6259	.06578	.84598	.84134	9.322	2.815
45	.8409	.3095	.6488	.06819	.90909	.90411	10.018	3.429

Table 2.2.4 - Coordinates of Gore Centerline for $43° 56' \leq \phi_g \leq 90°$

①	②	③	④	⑤	⑥	⑦	Absolute Coordinates	
ϕ	ϕ_g	x_g/x_{mg}	$\frac{z_g - .0717\, x_m}{1.0854\, x_m}$	$\frac{z_g - .0717\, x_m}{x_m}$	z_g/x_m	x_g/x_m	x_g (ft)	z_g(ft)
		See Table 2.1.2	See Table 1.2.1	1.0854 ④	⑤ + .0717	1.0854 ③	11.08 ⑦	11.08 ⑥
45°	43° 56'	.90412/1.0854	.2191	.2378	.3095	.9041	10.017	3.429
	50	.8752	.2644	.2870	.3587	.9499	10.525	3.974
	60	.9306	.3436	.3729	.4446	1.0101	11.192	4.926
	70	.9694	.4267	.4631	.5348	1.0522	11.658	5.926
	80	.9924	.5122	.5559	.6276	1.0772	11.935	6.954
	90	1.0000	.5990	.6502	.7219	1.0854	12.026	7.999

Figure 2.2.4 - Representative Photograph of a Fully Inflated Extended Skirt Canopy (T-10)

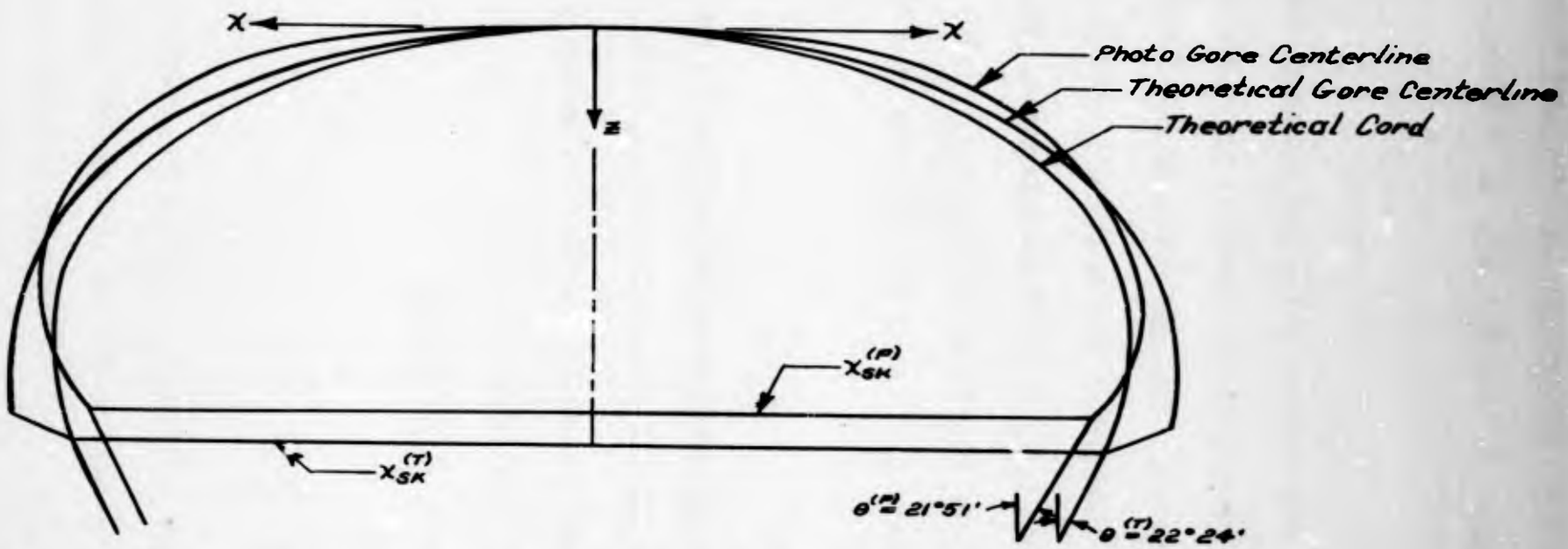

Equations of cord

$0 \leq \phi \leq 45°$

$$x = 1.1117\,(.5036\,x_m)\log\left(5.85\,\frac{.351+\sin\phi}{2.083-\sin\phi}\right)$$

$$z = 1.1117\,(.5036\,x_m)\left[2.28\tan^{-1}\frac{2.083\tan\frac{\phi}{2}-1}{1.827} - .375\log\frac{.351\tan\frac{\phi}{2}+.064}{.351\tan\frac{\phi}{2}+1.936} - .138\right]$$

$45 \leq \phi \leq 90$

$$x = x_m\sqrt{\sin\phi}$$

$$z = \frac{x_m}{\sqrt{2}}\left[2\,(E-E(\omega))-(K-\omega)\right] + .0826\,x_m$$

{where u and E(u) are the elliptic integrals of 1st and 2nd kind respectively with modular angle 45°

$\phi \geq 90°$

$$z/x_m = .6816 + 1.1284\sqrt{1 - x/x_m}\,, \text{ where } .94596\,x_m \leq x \leq x_m \quad (x_m = 11.08 \text{ ft.})$$

Equations of gore centerline

$0 \leq \phi \leq 45°$

$$x_g = x_m\cos\left(\frac{\pi}{N}\right)\left[\frac{x}{x_m} + \tan\frac{\pi}{N}\,\frac{1-\sqrt{1-\sin\phi}}{\sin\phi}\right], \quad z_g = z$$

$45 \leq \phi \leq 90°$

$$x_g = 1.0864\,x_m\sqrt{\sin\phi_g}\,, \quad z_g = 1.0864\,\frac{x_m}{\sqrt{2}}\left[2\,(E-E(u))-(K-u)\right] + .0717\,x_m\,, \quad \phi_g \geq 43°56'$$

Figure 2.2.5 - Comparison of Theoretical with Photographically Determined Shape of a Full Inflated Extended Skirt Canopy. (Type T-10, D_o = 35 ft, N = 30, l_c = 17.90 ft, l_s = 25.5 ft)

2.3 Comparison of the Theoretical with the Photographically Determined Shape of a Fully Inflated Conical Canopy. ($N = 24$, $\beta = 30°$, $l_c = 14$ ft, $l_s = 22$ ft 10 in.)

Photographic Shape

The gores and suspension lines are the same as those of the flat canopy of Section 2.1. The conical shape is achieved by leaving out four gores and suspension lines from the 28-gored flat canopy of Section 2.1. Thus $\cos \beta = 24/28$ and $\beta \cong 30°$ By measuring the lengths l_s and l_s' and knowing that $l_c = 14$ ft and $l_s = 22$ ft 10 in. the scale of the photograph and the ratio $l_c/l_s' = .5339$ was determined. The angle θ was determined from x_{sk} and l_s' and found to be 17° 30'. Figure 2.3.3 shows a plot of the photographic shape of this conical canopy taken from the reproduction shown in Figure 2.3.2.

Theoretical Cord Coordinates

The non-dimensional coordinates of the cord from apex to MIR are given in Table 1.8.6. These values together with the absolute coordinates are given in Table 2.3.1. In order to determine the parabolic portion below MIR it is necessary to solve Equations (1.3.18) and (1.3.19). These are:

$$k_{sk} = \frac{f(n) + k_a}{f(n) + 2n\,(k_c/k_s')} = \frac{f(n) + 3.08920}{f(n) + 1.0678n} \qquad (2.3.1)$$

and

$$k_{sk} = 1 - \frac{\frac{1}{2}\,(\rho_m/x_m)}{n^2 - 1} = 1 - \frac{.5287}{n^2 - 1} \qquad (2.3.2)$$

in which the values $k_a = 1.5446$ and $\rho_m = 1.0574\, x_m$ are obtained from Section 1.8. The values $k_c/k_s' = l_c/l_s' = .5339$ is explained above. The solution of Equations (2.3.1) and (2.3.2) is $n = 3.62$, $\theta = \csc^{-1} 3.62 = 16°\ 02'$ which compares with 17° 30'. This value of n gives $k_{sk} = .95681$. The equation of the parabolic portion

is given by Equation (1.3.7)

$$z = z_m + Z = z_m + x_m \sqrt{2\rho_m/x_m}\sqrt{1 - x/x_m} \qquad \text{or}$$

$$z/x_m = 1.0646 + 1.454\sqrt{1 - x/x_m} \tag{2.3.3}$$

The MIR x_m is determined from $l_c = .5339\, l_s' = .5339\, n\, x_{sk} = .5339\, n\, k_{sk}\, x_m$, therefore

$$x_m = \frac{l_c}{.5339\, n\, k_{sk}} = \frac{14}{(.5339)\,(3.62)\,(.95681)} = 7.5707 \text{ ft}$$

The non-dimensional and absolute coordinates are given in Table 2.3.1

Table 2.3.1 - Cord Coordinates for a Conical Canopy

FROM APEX TO MIR					BELOW MIR			
ϕ'	x/x_m	z/x_m	x	z	x/x_m	z/x_m	x	z
30°	.4968	.2868	3.761	2.171	1.0000	1.0646	7.571	8.060
37° 04'	.6158	.3581	.4662	2.711	.99136	1.19975	7.505	9.083
44° 07'	.6969	.4235	5.276	3.206	.98272	1.25573	7.440	9.507
51° 11'	.7764	.5056	5.878	3.828	.97408	1.29868	7.374	9.832
58° 14'	.8475	.5983	6.416	4.530	.96544	1.33490	7.309	10.106
65° 18'	.9058	.6994	6.858	5.295	.95681	1.36677	7.244	10.347
72° 22'	.9515	.8075	7.204	6.113				
79° 25'	.9823	.9155	7.437	6.931				
86° 29'	.9960	.9995	7.540	7.567				
90°	1.0000	1.0646	7.571	8.060				

Theoretical Gore Centerline

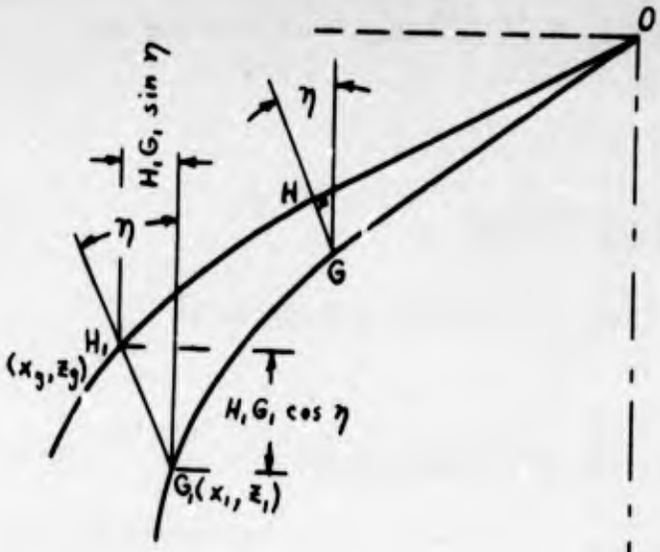

Figure 2.3.1

The curve OGG_1 in Figure 2.3.1 is the gore centerline of the first approximation and the curve OHH_1 is the gore centerline for the second approximation. The coordinates x_1, z_1 are calculated from the coordinates x, z of the cord in the second approximation, while the coordinates x_g, z_g are determined by the length $H_1 G_1$, where values are taken from Table 1.8.2 by interpolation.

Table 2.3.2 gives coordinates x, z, coordinates x_1, z_1 and x_g, z_g.

In Figure 2.3.3 are plotted the theoretical cord curve and the theoretical gore centerline of the second approximation together with the photographic gore centerline as obtained from the photograph.

Table 2.3.2 - Coordinates of the Theoretical Gore Centerline

①	②	③	④	⑤	⑥	⑦	⑧	⑨	⑩
ϕ	x/x_m	$z/x_m = z_1/x_m$	x_1/x_m	$\frac{H_1 G_1 \sin\eta}{x_m}$	$\frac{H_1 G_1 \cos\eta}{x_m}$	x_g/x_m	z_g/x_m	x_g	z_g
		See Table 1.8.6	.99144 ②			④ + ⑤	③ - ⑥	7.5707 ⑦	7.5707 ⑧
30°	.4968	.2868	.4925	.00104	.00180	.4935	.2850	3.736	2.158
37 04	.6158	.3581	.6105	.00564	.00975	.6161	.3484	4.664	2.638
44 07	.6969	.4235	.6909	.01125	.01943	.7022	.4041	5.316	3.059
51 11	.7764	.5056	.7698	.01779	.03072	.7876	.4749	5.963	3.595
58 14	.8475	.5983	.8402	.02524	.04359	.8654	.5547	6.552	4.199
65 18	.9058	.6994	.8980	.03337	.05763	.9314	.6418	7.051	4.859
72 22	.9515	.8075	.9434	.04222	.07293	.9856	.7346	7.462	5.561
79 25	.9823	.9155	.9739	.05156	.08906	1.0255	.8264	7.764	6.256
86 29	.9960	.9995	.9875	.06131	.10590	1.0488	.8936	7.940	6.765
90	1.0000	1.0646	.9914	.06629	.11450	1.0577	.9501	8.008	7.193

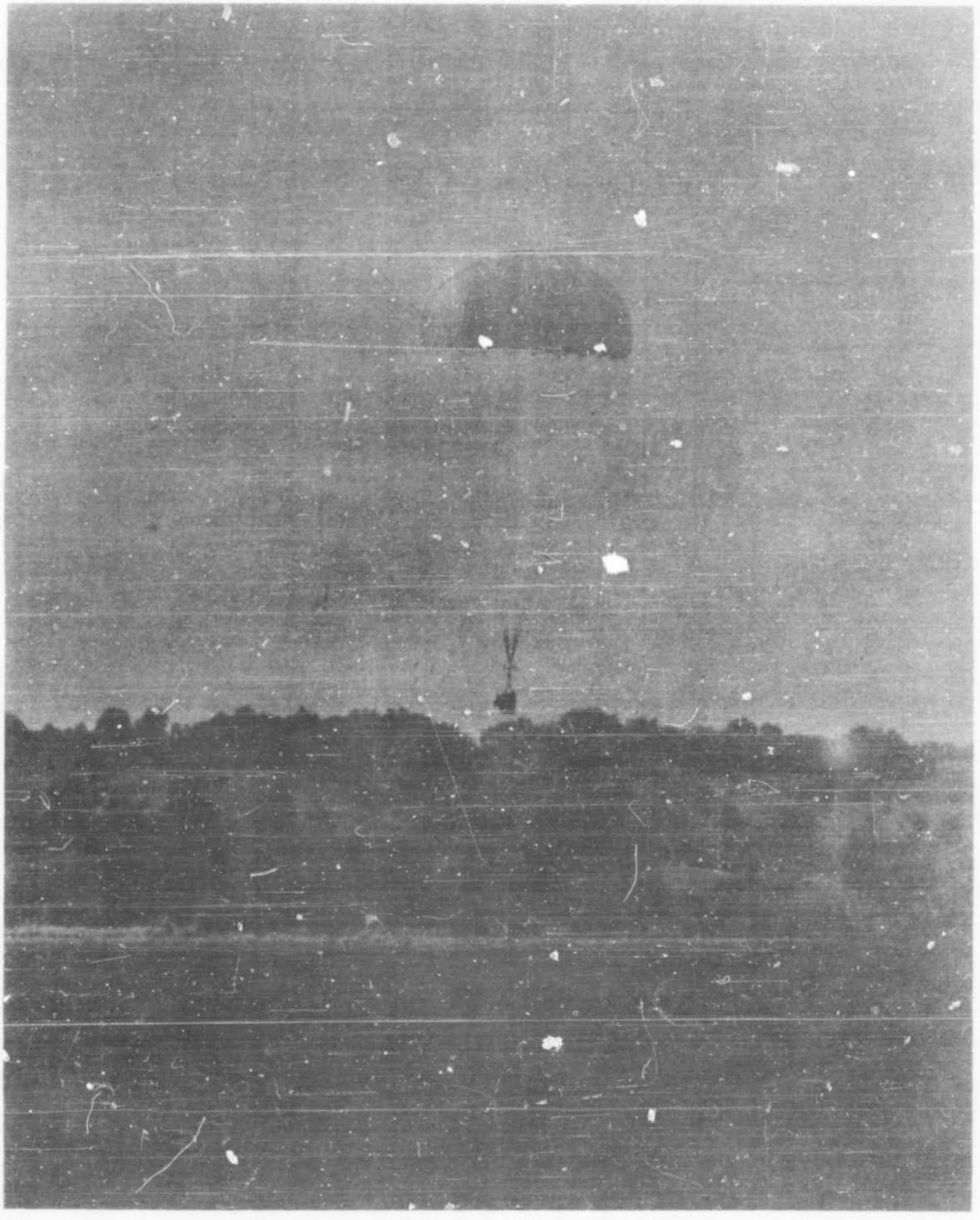

Figure 2.3.2 - Representative Photograph of a Fully Inflated Conical Canopy

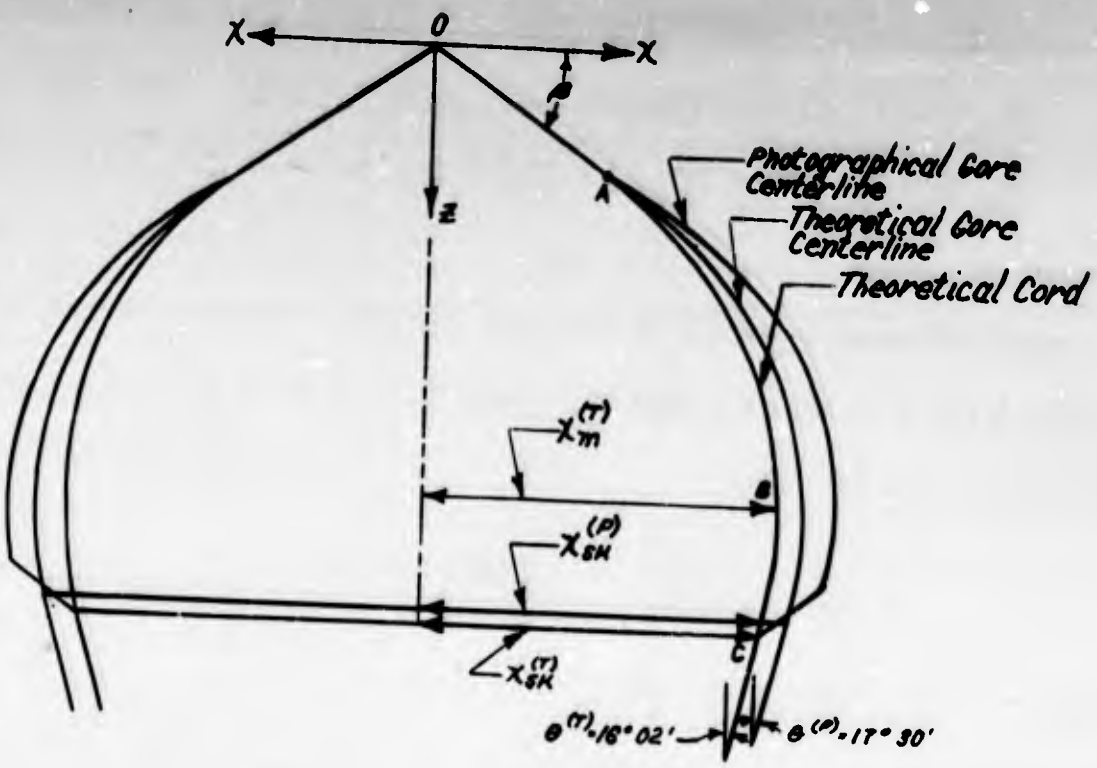

Equations of cord

(1) Portion OA
$\phi = \beta = 30°$
$X_A = X_o = .4968 X_m$

$$Z = (\tan 30°)\, X$$

(2) Portion AB
$30 \leq \phi \leq 90$

$$X = X_m \left[1 + \frac{1.017623}{\left[\frac{2Q - (Q^2-1)\tan\beta}{Q^2 - 1 + 2Q\tan\beta} \right]} \right]^{-\frac{1}{2}}$$

where $Q = \frac{I_A}{I_B}$

$$I_A = \int_\beta^\phi \frac{\cos\chi \cot\phi}{\sin\alpha \sin^2\phi} \left[\cos^2(\pi/N)\cot^2\phi + \cos(2\pi/N) \right]^{-2} d\phi$$

$$I_B = \int_\beta^\phi \frac{\cos\chi}{\sin\alpha \sin\phi} \left[\cos^2(\pi/N)\cot^2\phi + \cos(2\pi/N) \right]^{-2} d\phi$$

$$\sin\phi \sin(\pi/N) = \cos\left[180 - (\alpha + \chi) \right]$$

(3) Portion BC
$\phi \geq 90$
Parabolic arc
$(\theta = 16° 02')$

$$Z = \left[1.0846 + 1.454 \sqrt{1 - X/X_m} \right] X_m$$

Coordinates of Theoretical Gore Centerline: See Table 2.3.2

Figure 2.3.3 - Comparison of Theoretical with Photographically Determined Shape of a Fully Inflated Conical Canopy (N = 24. β = 30°, l_c = 14 ft, l_s = 22 ft 10 in.)

2.4 Comparison of the Theoretical with the Photographically Determined Shape of a Fully Inflated Personnel Guide Surface Canopy. (Type C-11, D_o = 30 ft, N = 24, β = 30°, l_c = 13.857 ft, l_s = 30 ft)

Photographic Shape

The canopy was made according to USAF Dwg. 52J6026. From the drawing, l_c = 13 ft 5 in. + ½ (14-9/16 in.) = 13.857 ft. Using l_s = 30 ft to scale the drawing, l_s' = 32.462 ft which gives

$$\frac{l_s}{l_s'} = \frac{13.857}{32.462} = .42687 \qquad (2.4.1)$$

also $\theta(P) = 16° 43'$

The photographic shape was determined from the photograph shown in Figure 2.4.3.

Theoretical Cord Cordinates

The portion of the cord above MIR is assumed to be that of the flat canopy but with a different x_m. The portion below MIR is assumed to be a circular arc. The determination of x_m and the length and radius of the circular arc are accomplished by the solution of 14 simultaneous equations given in Section 1.9. For this canopy these equations have already been solved in Section 1.9.

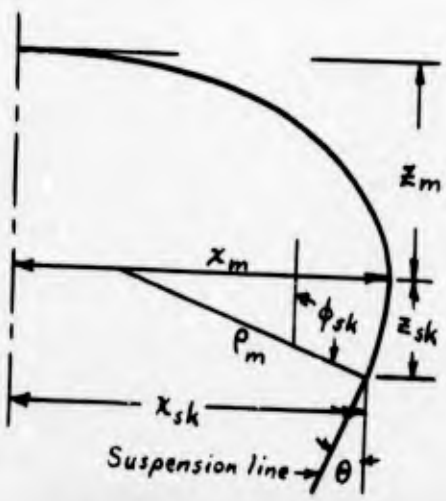

Figure 2.4.1

From Section 1.9 the values in Figure 2.4.1 are:

ϕ_{sk} = 100° 50'

θ = 16° 51' (compares with 16° 43')

x_m = 9.506 ft

ρ_m = 5.875 ft

The non-dimensional coordinates of the portion of the cord above MIR are obtained from the flat canopy, Section 1.4, and are given in Table 2.4.1 together with the absolute coordinates using x_m = 9.506 ft.

The coordinates of the skirt are

$$x_{sk} = x_m - \rho \left[1 - \cos (\phi_{sk} - 90)\right] \qquad (2.4.2)$$

$$= 9.506 - 5.875 (1 - \cos 10° 50') = 9.401 \text{ ft}$$

and $$z_{sk} = z_m + Z_{sk} = z_m + \rho \sin (\phi_{sk} - 90) \qquad (2.4.3)$$

$$= 6.479 + 5.875 \sin 10° 50' = 7.533 \text{ ft}$$

Table 2.4.1 - Cord Coordinates for a Personnel Guide Surface Canopy

①	②	③	④	⑤	⑥	⑦	⑧	⑨	⑩
ϕ	x/x_m	z/x_m	x (ft) 9.506 ②	z (ft) 9.506 ③	ϕ	x/x_m	z/x_m	x (ft) 9.506 ⑦	z (ft) 9.506 ⑧
0°	0	0	0	0	45°	.8409	.3095	7.994	2.942
4°	.1115	.0038	1.060	.036	50°	.8752	.3470	8.320	3.298
10°	.2647	.0227	2.516	.215	60°	.9306	.4262	8.846	4.051
20°	.4723	.0779	4.490	.740	70°	.9694	.5093	9.215	4.841
30°	.6405	.1561	6.089	1.484	80°	.9924	.5948	9.434	5.654
40°	.7802	.2541	7.417	2.415	90°	1.0000	.6816	9.506	6.479

Theoretical Gore Centerline

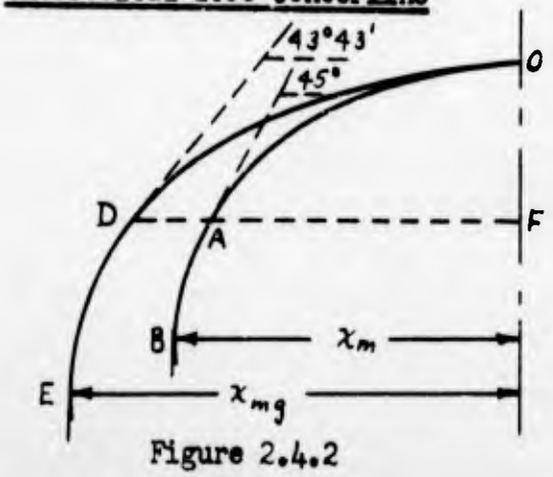

Figure 2.4.2

The gore centerline is determined as in the case of the flat and extended skirt canopies, Sections 2.1 and 2.2 respectively. The actual values are slightly different because of N. The preliminary calculations follow:

$$\left.dx/d\phi\right|_{\phi = 45^\circ} = .6594\ x_m \quad \text{(as before)} \tag{2.4.4}$$

$$\left.dx_g/d\phi\right|_{\phi = 45^\circ} = .6896\ x_m \tag{2.4.5}$$

$$\left.dz/dx_g\right|_{\phi = 45^\circ} = \frac{.6594\ x_m}{.6896\ x_m} = .95621 \tag{2.4.6}$$

$$\phi_g = \tan^{-1} .95621 = 43^\circ\ 43'$$

The gore centerline equation is

$$x_g = 1.1047\ x_m \sqrt{\sin \phi_g} \qquad 43^\circ\ 43' \leq \phi_g \leq 90^\circ \tag{2.4.7}$$

The z-coordinate is given by

$$z_g = 1.1047\ (x_m/\sqrt{2}) \left\{2\ \left[E - E\ (u)\right] - \left[K - u\right]\right\} + .0692\ x_m \tag{2.4.8}$$

These coordinates x_g and z_g are given in Table 2.4.2 and 2.4.3 and plotted in Figure 2.4.4 together with the coordinates of the theoretical cord.

Table 2.4.2 - Coordinates for Gore Centerline for $0 \leq \phi \leq 45°$

①	②	③	④	⑤	⑥	⑦	Absolute Coordinates	
ϕ	x/x_m	z/x_m	$\frac{1-\sqrt{1-\sin\phi}}{\sin\phi}$			x_g/x_m	x_g (ft)	z_g (ft)
	See Table 2.1.2			④ tan π/N	② + ⑤	⑥ cos π/N	9.506 ⑦	9.506 ③
0	0	0	.5000	.0658	.0658	.0652	.620	0
4	.1115	.0038	.5090	.0670	.1785	.1770	1.683	.036
10	.2647	.0227	.5238	.0689	.3336	.3307	3.144	.216
20	.4723	.0779	.5521	.0727	.5450	.5403	5.136	.741
30	.6405	.1561	.5858	.0771	.7176	.7115	6.764	1.484
40	.7802	.2541	.6259	.0824	.8626	.8552	8.130	2.415
45	.8409	.3095	.6488	.0854	.9263	.9184	8.730	2.942

Table 2.4.3 - Coordinates of Gore Centerline for 43° 43' $\leq \phi_g \leq$ 90°

①	②	③	④	⑤	⑥	⑦	Absolute Coordinates	
ϕ	ϕ_g	x_g/x_{mg}	$\frac{z_g - .0692\, x_m}{1.1047\, x_m}$	$\frac{z_g - .0692\, x_m}{x_m}$	z_g/x_m	x_g/x_m	x_g (ft)	z_g (ft)
		See Table 2.1.2	See Table 1.2.1	1.1047 ④	⑤ + .0692	1.1047 ③	9.506 ⑦	9.506 ⑥
45	43° 43'	.9184/1.1047	.2175	.2403	.3095	.9184	8.730	2.942
	50	.8752	.2644	.2921	.3613	.9668	9.190	3.435
	60	.9306	.3436	.3796	.4488	1.0280	9.772	4.266
	70	.9694	.4267	.4714	.5406	1.0709	10.180	5.139
	80	.9924	.5122	.5658	.6350	1.0963	10.421	6.036
	90	1.0000	.5990	.6617	.7309	1.1047	10.501	6.948

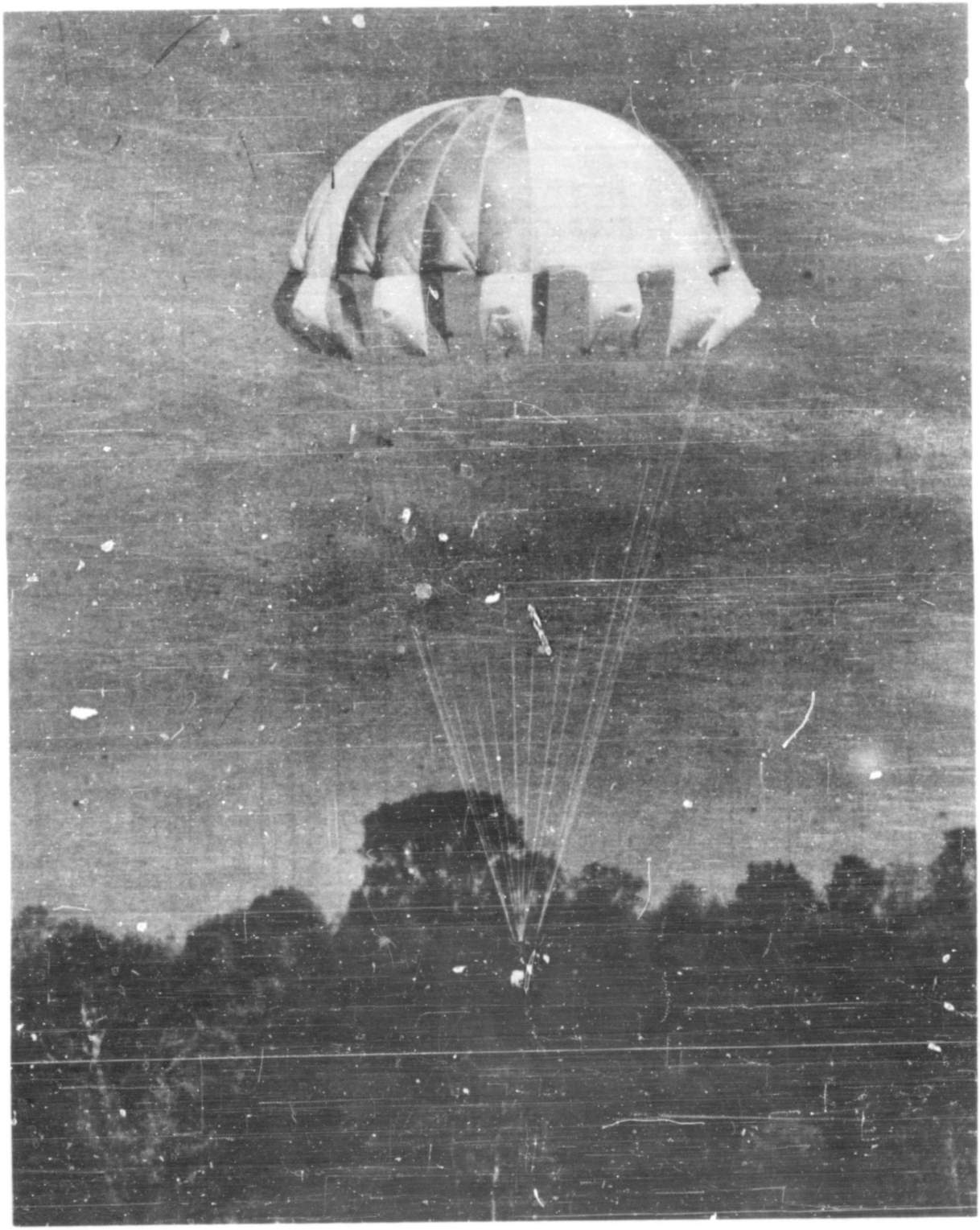

Figure 2.4.3 - Representative Photograph of a Fully Inflated Personnel Guide Surface Canopy (C-11)

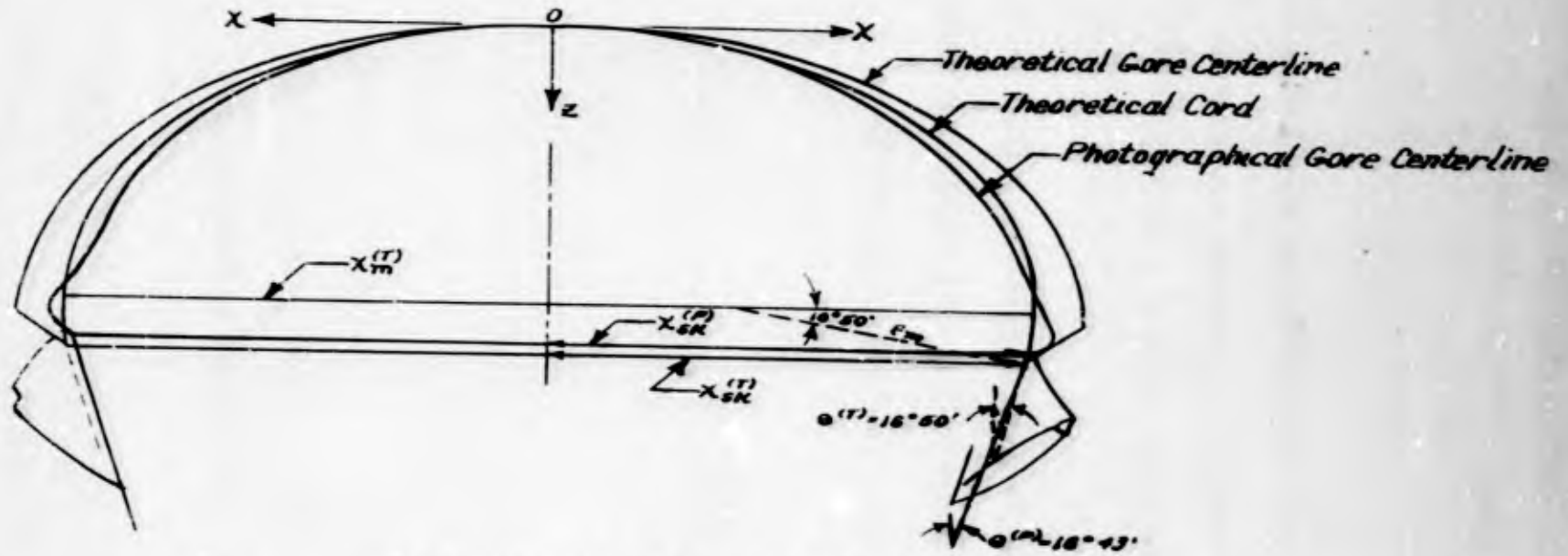

Equations of cord (X_m = 9.506')

$0 \le \phi \le 45°$:

$$X = 1.1117(.5036\,X_m)\log\left(5.85\,\frac{.351+\sin\phi}{2.083-\sin\phi}\right)$$

$$Z = 1.1117(.5036\,X_m)\left[2.28\tan^{-1}\frac{2.083\tan\frac{\phi}{2}-1}{1.827} - .375\log\frac{.351\tan\frac{\phi}{2}+.064}{.351\tan\frac{\phi}{2}+1.836} - .138\right]$$

$45 \le \phi \le 90°$:

$$X = X_m\sqrt{\sin\phi}$$

$$Z = \frac{X_m}{\sqrt{2}}\left[2\,(E-E(u))-(K-U)\right] + .0628\,X_m$$

where u and E(u) are the elliptic integrals of 1st and 2nd kind respectively with modular angle 45°

$\phi > 90°$ circular arc with radius ρ_m = 5.875 and central angle 10°50' (X_{SK} = 9.401', Z_{SK} = 2.683')

Equations of core centerline

$0° \le \phi \le 45°$: $X_g = X_m \cos\frac{\pi}{N}\left[\frac{X}{X_m} + \tan\frac{\pi}{N}\,\frac{1-\sqrt{1-\sin\phi}}{\sin\phi}\right]$, $Z_g = Z$

$45° \le \phi \le 90°$: $Z_g = 1.1047\,\frac{X_m}{\sqrt{2}}\left[2\,(E-E(u))-(K-U)\right] + .0628\,X_m$

Figure 2.4.4 - Comparison of Theoretical with Photographically Determined Shape of a Fully Inflated Personnel Guide Surface Canopy (Type C-11, D_o = 30 ft, N = 24, β = 30°, l_c = 13.857 ft, l_s = 30 ft)

2.5 Comparison of the Theoretical with the Photographically Determined Shape of a Fully Inflated Conical Ring Slot Canopy. ($N = 32$, $\beta = 25°$, $l_c = 11.55$ ft, $l_s = 22$ ft)

Photographic Shape

The photograph used for comparison was taken when the parachute was close to the ground, as represented in Figure 2.5.1. By scaling the photograph and using dimensions from USAF Dwgs. X53J7080E and EL-53-H-73 the length $l_s' = 25.04$ ft.

Theoretical Cord Coordinates

In order to determine the cord shape it is necessary to calculate x_{sk} using Equations (1.3.18) and (1.3.19) as if the canopy were flat. The data used in these equations are obtained from Section 1.10 and the procedure outlined therein is followed to obtain the cord shape.

$$k_{sk} = \frac{f(n) + 2\,(1.3409)}{f(n) + 2\,(.46)\,n} = \frac{f(n) + 2.6818}{f(n) + .92\,n} \qquad (2.5.1)$$

$$k_{sk} = 1 - \frac{.25}{n^2 - 1} \qquad (2.5.2)$$

These equations give $n = 3.35$, $k_{sk} = .97510$ and

$$x_{sk} = l_s \sin\theta = l_s'/n = 25.04/3.35 = 7.475 \text{ ft} \qquad (2.5.3)$$

$$x_m = x_{sk}/k_{sk} = 7.475/.97510 = 7.666 \text{ ft} \qquad (2.5.4)$$

These are the skirt and MIR values for a flat solid canopy and must be modified to give the values for the conical ring slot. Using primes to denote the ring slot quantities (see Section 1.10)

$$x_{sk}' = 1.09\, x_{sk} = 8.148 \text{ ft} \qquad (2.5.5)$$

$$\sin\theta' = x_{sk}'/l_s' = 8.148/25.04 = .3254 = 1/n' \qquad (2.5.6)$$

$$n' = 3.073 \quad (\theta' = 18° 02')$$

$$f(n') = 2n' + (n'^2 - 1)\,\log\frac{n' + 1}{n' - 1} = 11.848$$

Solving Equation (1.10.9) for x_m' yields

$$x_m' = \frac{2\,l_0 + x_{sk}'\,f(n')}{2.6818 + f(n')} \qquad (2.5.7)$$

$$= \frac{(2)\,(11.5)+(8.148)\,(11.848)}{2.6818 + 11.848} = 8.234 \text{ ft}$$

$$k_{sk}' = 8.148/8.234 = .9896 \qquad (2.5.8)$$

Knowing x_m' and k_{sk}' the coordinates are determined using the non-dimensional coordinates of the flat canopy. Table 2.5.1 gives the cord coordinates.

Table 2.5.1 - Cord Coordinates for a Conical Ring Slot Canopy

ø	x/x_m	z/x_m	x	z
0	0	0	0	0
4	.1115	.0038	.918	.031
10	.2647	.0227	2.180	.187
20	.4723	.0779	3.889	.641
30	.6405	.1561	5.274	1.285
40	.7802	.2541	6.424	2.092
45	.8409	.3095	6.924	2.548
50	.8752	.3470	7.206	2.857
60	.9306	.4262	7.663	3.509
70	.9694	.5093	7.982	4.194
80	.9924	.5948	8.171	4.858
90	1.0000	.6816	8.234	5.612
	.9946	.7251	8.190	5.970
	.9896	.7420	8.148	6.110

Note: Equation of the parabolic portion

$$z'/x_m' = .6816 + 2\sqrt{(n'^2 - 1)\,(1 - x_{sk}'/x_m')}\,\sqrt{1 - x'/x_m'}$$

(see Equations (1.10.11) and (1.10.8))

or $$z'/x_m' = .6816 + .5926\,\sqrt{1 - x'/x_m'}$$

Theoretical Gore Centerline

Using the method of Section 2.1, the equations of the gore centerline are as given below.

$$x_g = x_m \cos(\pi/N) \left[x/x_m + \tan(\pi/N) \frac{1 - \sqrt{1 - \sin\phi}}{\sin\phi} \right] \qquad (2.5.9)$$

z_g = same as for cord at x. (2.5.10)

$$x = .5599\, x_m \log\left(5.85 \frac{.351 + \sin\phi}{2.081 - \sin\phi}\right) \qquad (2.5.11)$$

Equations (2.5.9), (2.5.10) and (2.5.11) hold for $0 \leq \phi \leq 45°$. For $\phi > 45°$ the equations are:

$$x_g = 1.0803 \quad x_m \sqrt{\sin\phi_g} \qquad (2.5.12)$$

$$z_g = 1.0803\, (x_m/\sqrt{2}) \left\{ 2\left[E - E(u)\right] - \left[K - u\right] \right\} + .0723\, x_m \qquad (2.5.13)$$

which hold for $44° \leq \phi_g \leq 90°$. The lower value of ϕ_g is calculated as follows:

$$44° = \tan^{-1} \frac{dx}{d\phi} \frac{d\phi}{dx_g}\bigg|_{\phi = 45°} = \tan^{-1} \frac{.6594\, x_m}{.6830\, x_m} \qquad (2.5.14)$$

The constant 1.0803 is determined by

$$\frac{x_g\big|_{\phi = 45°}}{\sqrt{\sin 44°}} = \frac{.9004}{.83346} = 1.0803$$

The constant $.0723\, x_m$ is the distance OO' of Figure 2.1.3. The coordinates are given in Tables 2.5.2 and 2.5.3.

A comparison of the theoretical and photographically determined shape is shown in Figure 2.5.2.

Table 2.5.2 - Coordinates for Gore Centerline for $0 \leq \phi \leq 45°$

①	②	③	④	⑤	⑥	⑦	Absolute Coordinates	
ϕ	x/x_m	z/x_m	$\frac{1-\sqrt{1-\sin\phi}}{\sin\phi}$			x_g/x_m	x_g (ft)	z_g (ft)
	See Table 2.1.2			④ tan π/N	② + ⑤	⑥ cos π/N	8.234 ⑦	8.234 ③
0	0	0	.5000	.0493	.0493	.0491	.404	0
4	.1115	.0038	.5090	.0501	.1616	.1608	1.324	.031
10	.2647	.0227	.5238	.0516	.3163	.3148	2.592	.187
20	.4723	.0779	.5521	.0544	.5267	.5242	4.316	.641
30	.6405	.1561	.5858	.0577	.6982	.6948	5.721	1.285
40	.7802	.2541	.6259	.0616	.8418	.8377	6.898	2.092
45	.8409	.3095	.6488	.0639	.9048	.9004	7.414	2.548

Table 2.5.3 - Coordinates for Gore Centerline for $44° \leq \phi_g \leq 90°$

①	②	③	④	⑤	⑥	⑦	Absolute Coordinates	
ϕ	ϕ_g	x_g/x_{mg}	$\frac{z_g - .0723\,x_m}{1.0803\,x_m}$	$\frac{z_g - .0723\,x_m}{x_m}$	z_g/x_m	x_g/x_m	x_g (ft)	z_g (ft)
		See Table 2.1.2	See Table 1.2.1	1.0803 ④	⑤ + .0723	1.0803 ③	8.234 ⑦	8.234 ⑥
45	44	.9004/1.0803	.2196	.2372	.3095	.9004	7.414	2.548
	50	.8752	.2644	.2856	.3579	.9455	7.785	2.947
	60	.9306	.3436	.3712	.4435	1.0053	8.278	3.652
	70	.9694	.4267	.4610	.5333	1.0472	8.623	4.391
	80	.9924	.5122	.5533	.6256	1.0721	8.828	5.151
	90	1.0000	.5990	.6471	.7194	1.0803	8.895	5.924

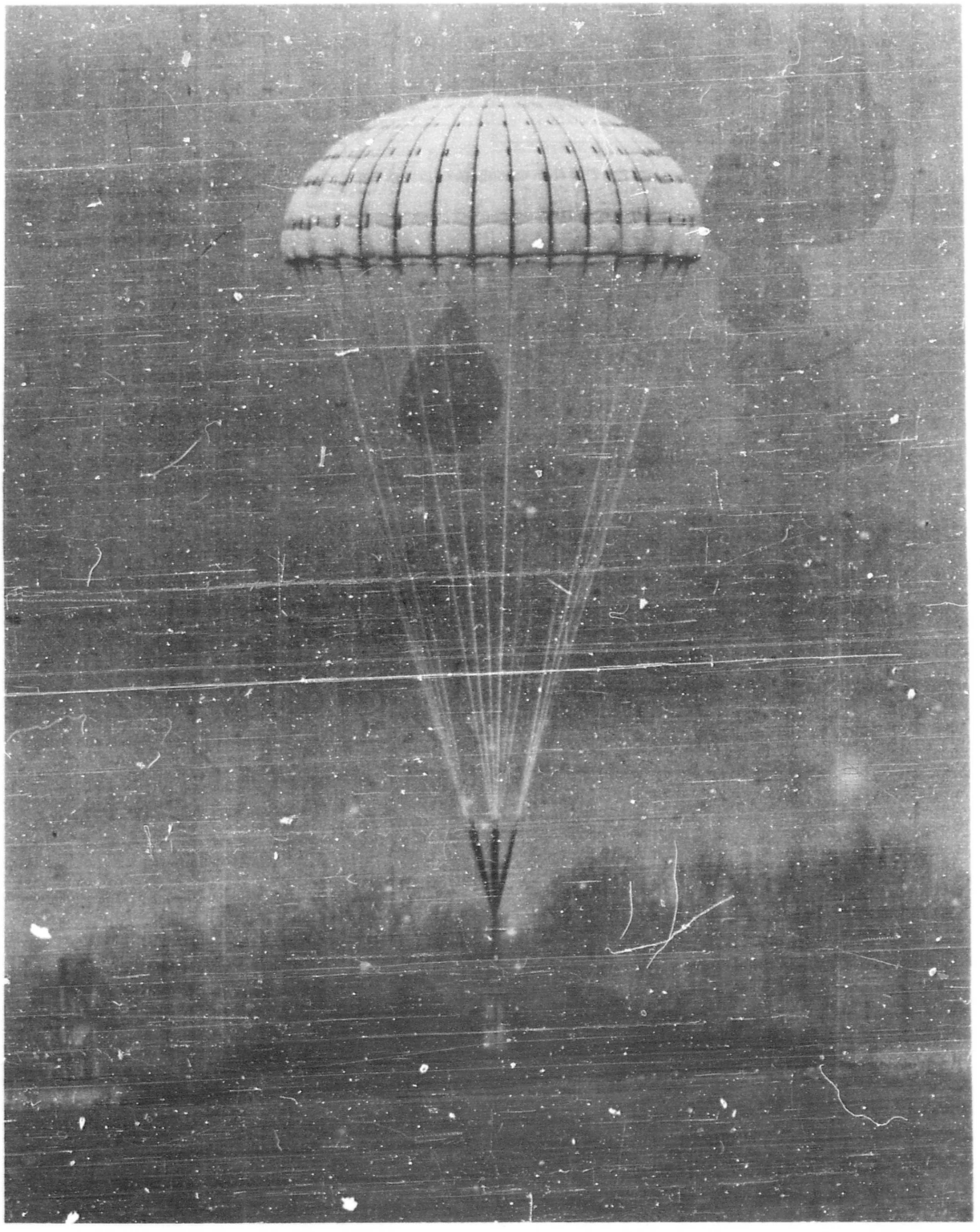

Figure 2.5.1 - Representative Photograph of a Fully Inflated Conical Ring Slot Canopy

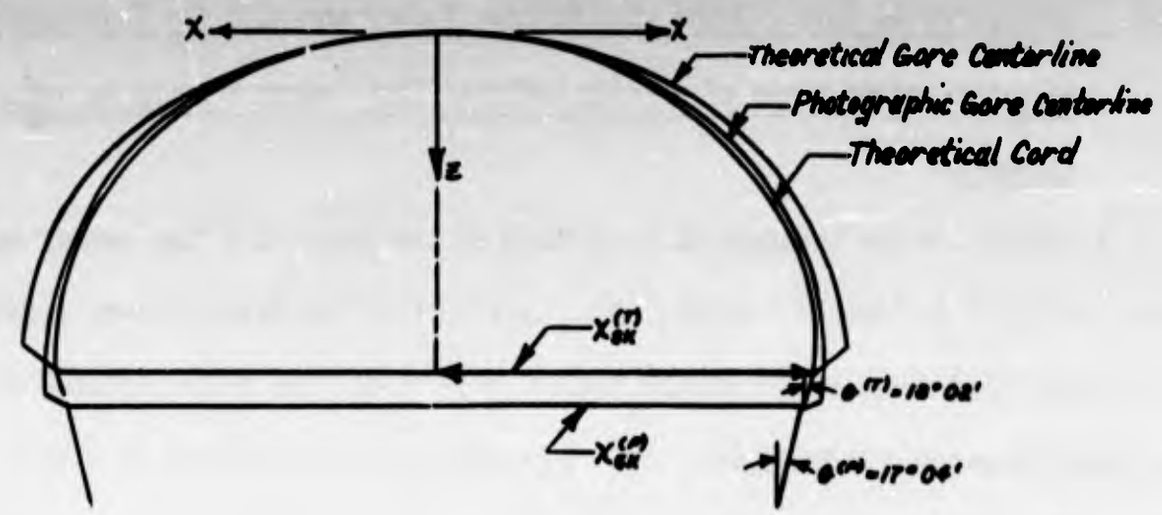

Equations of the cord

$$0 \le \phi \le 45° \begin{cases} X = 1.1117(.5036\,X_m)\log\left(5.85\,\frac{.351+\sin\phi}{2.083-\sin\phi}\right) \\ Z = 1.1117(.5036\,X_m)\left[2.28\tan^{-1}\frac{2.083\tan\frac{\phi}{2}-1}{1.827} - \right. \\ \left. -.375\log\frac{.351\tan\frac{\phi}{2}+.064}{.351\tan\frac{\phi}{2}+1.936} - .138\right] \end{cases}$$

$$45° \le \phi \le 90° \begin{cases} X = X_m\sqrt{\sin\phi} \\ Z = \frac{X_m}{\sqrt{2}}\left[2(E-E(u))-(K-u)\right] + .0826\,X_m \end{cases}$$

Where u and $E(u)$ are the elliptic integrals of 1st and 2nd kind respectively with modular angle 45°

$$\phi \ge 90° \qquad \frac{Z}{X_m} = .6816 + .5928\sqrt{1-\frac{X}{X_m}} \quad \text{where } .9838\,X_m \le X \le X_m = 8.234\text{ ft}$$

Equations of gore Centerline

$$0 \le \phi \le 45° \qquad X_g = X_m\cos\left(\frac{\pi}{N}\right)\left[\frac{X}{X_m} + \tan\left(\frac{\pi}{N}\right)\frac{1-\sqrt{1-\sin\phi}}{\sin\phi}\right], \quad Z_g = Z$$

$$45° \le \phi \le 90° \begin{cases} X_g = 1.0803\,X_m\sqrt{\sin\phi_g}, & \phi_g \ge 44° \\ Z_g = 1.0803\frac{X_m}{\sqrt{2}}\left[2\left(E-E(u)\right)-(K-u)\right] + .0728\,X_m \end{cases}$$

Figure 2.5.2 - Comparison of Theoretical with Photographically Determined Shape of a Fully Inflated Conical Ring Slot Canopy (N = 32, β = 25°, l_c = 11.55 ft, l_s = 22 ft)

2.6 Comparison of Taylor Shape with Present Theory and with the Photographically Determined Shape of a Fully Inflated Flat Canopy Holding l_c and l_s' Constant

A method for the theoretical prediction of the shape of a flat canopy has been developed in Section 1 which, being derived from the Taylor curve, purports to predict more accurately than the Taylor curve itself the fully inflated shape in steady descent. Particularly since this solution has been used as a basis for predicting the shapes of several other canopy types, it is of interest to evaluate the new theory against the original Taylor curve, which has the advantage to begin with of being much simpler to obtain.

The coordinates of the Taylor shape are given in Section 1.2. If it is assumed that the portion of the cord below MIR is also a Taylor curve symmetrical with that above MIR, it is necessary to find the length of the portion below MIR. For a flat canopy l_c = 14 ft and l_s' = 25 ft. In Figure 2.6.1 the curve OB is a complete Taylor curve while BC is symmetrical with BA. At point C the angular parameter is ϕ_{sk} i.e. point C is at the skirt. Because of the symmetry of points A and C the angular parameter is 180° - ϕ_{sk}. The line CD is the length l_s' and is tangent to the cord at C; therefore the angle θ = ϕ_{sk} - 90°. The length OB = l_a and BC = BA = l_b. The following equation can be written using the equations of Section 1.2:

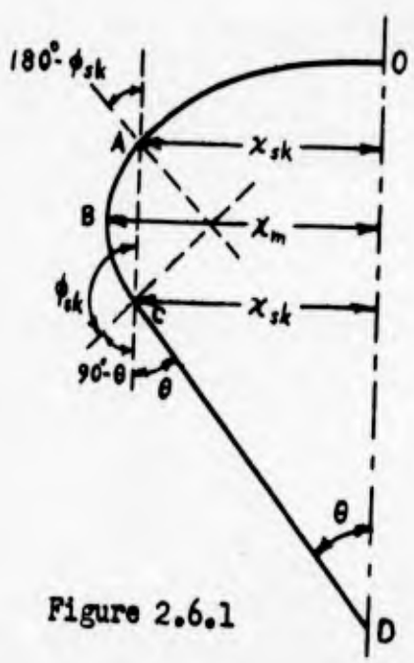

Figure 2.6.1

$$l_a = 1.3111\ x_m \tag{2.6.1}$$

$$l_b = \frac{x_m}{\sqrt{2}} \int_0^{\cos^{-1}\sqrt{\sin(180 - \phi_{sk})}} \frac{d\psi}{\sqrt{1 - \tfrac{1}{2}\sin^2\psi}} \tag{2.6.2}$$

$$l_a + l_b = l_c = 14 \text{ ft} \tag{2.6.3}$$

$$x_{sk} = l_s' \sin\theta = x_m \sqrt{\sin(180 - \phi_{sk})} \tag{2.6.4}$$

$$l_s' = 25 \text{ ft} \tag{2.6.5}$$

Using $\phi_{sk} - 90° = \theta$ and $180° - \phi_{sk} = 90° - \theta$ Equations (2.6.1) through (2.6.5) may be solved to yield

$$x_m = \frac{14}{1.3111 + (1/\sqrt{2}) \int_0^{\cos^{-1}\sqrt{\cos\theta}} \frac{d\psi}{\sqrt{1 - \tfrac{1}{2}\sin^2\psi}}} \tag{2.6.6}$$

and $$x_m = (25 \sin\theta)/\sqrt{\cos\theta} \tag{2.6.7}$$

These last two equations may be solved by trial and error using a table of elliptic integrals of the first kind. If tables of elliptic functions are available, the equations may be solved by eliminating x_m and transforming the resulting equation with

$$\text{cn}u = \sqrt{\cos\theta} \tag{2.6.8}$$

to get:

$$u = \sqrt{2}\left[(14/25)\frac{\text{cn}\,u}{\text{sn}\,u\sqrt{1 + \text{cn}^2 u}} = 1.3111\right] \tag{2.6.9}$$

which may also be solved by trial and error. The solution of Equations (2.6.6) and (2.6.7) is ϕ_{sk} = 111° 10' or θ = 21° 10' from which x_m = 9.348 ft.

An interesting variation of the Taylor shape is to assume that the portion below the MIR is parabolic and is determined by the method of Section 1.3. In the equations

$$k_{sk} = \frac{f(n) + 2\,k_a}{f(n) + 2n\,(k_c/k_s')} \tag{2.6.10}$$

$$k_{sk} = \frac{\frac{1}{2}\,(\rho_m/x_m)}{n^2 - 1} \tag{2.6.11}$$

k_a = 1.3111, $\rho_m = \frac{1}{2}\,x_m$ and k_c/k_s' = .56 thus the solution is n = 2.794 or $\theta = \csc^{-1} n$ = 20° 58' which is virtually the same as the value above. The value of k_{sk} is .96324 and

$$x_m = l_s'/nk_{sk} = 25/(2.794)\,(.96324) = 9.29 \text{ ft}$$

The coordinates of these two Taylor curves are given in Table 2.6.1 together with the cord coordinates for the flat canopy. The two Taylor curves are so close together that only one is plotted. Cord shapes are plotted in Figure 2.1.4 for the Taylor curve and the new theory, together with photographic shapes, using a common apex.

Examination of Figure 2.1.4 indicates that the new theory developed in Section 1 comparesmore favorably than the Taylor shape with the photographic shapes. Although no photographic cord curve is available, it must, of course, fall inside the curve for centerline of gore and be collinear with the suspension line at the skirt. While both theories predict the angle θ between suspension lines and the

axis of the canopy within a degree, the skirt level of the Taylor shape is too high and consequently its cords bulge to the sides too much. The Taylor curve remains a useful first approximation, however.

Table 2.6.1 - Cord Coordinates for Taylor Curves and Flat Canopy with Common l_c and l'_s

	Taylor Curve above & Below MIR		Taylor Curve with Parabola		Theoretical Flat Canopy Cord Curve (See Table 2.1.2)	
ϕ	x'	z'	x'	z'	x'	z'
0	0	0	0	0	0	0
2	1.75	.03	1.74	.03	.49	.01
4	2.47	.06	2.45	.06	1.02	.04
6	3.02	.11	3.00	.11	1.51	.08
8	3.49	.17	3.47	.17	1.98	.14
10	3.90	.22	3.87	.22	2.42	.21
20	5.47	.63	5.43	.63	4.31	.71
30	6.61	1.17	6.57	1.16	5.85	1.43
40	7.49	1.79	7.45	1.77	7.12	2.32
45	7.86	2.12	7.81	2.11	7.68	2.83
50	8.18	2.47	8.13	2.46	7.99	3.17
60	8.70	3.21	8.65	3.19	8.50	3.89
70	9.06	3.99	9.01	3.96	8.85	4.65
80	9.28	4.79	9.22	4.76	9.06	5.43
90	9.35	5.60	9.29	5.56	9.13	6.22
100	9.28	6.41	9.16	6.67	9.00	7.31
11°10'	9.03	7.30	8.95	7.35	8.81	7.94

2.7 Analysis of the Tension and Loading in the Cord of the Flat Canopy Using the Intrinsic Equation of Equilibrium for Heavy Cords

In Sections 1.1 and 1.4 a study has been made for the determination of the shape of the cord for the inflated flat canopy. A basic assumption of this study was that the tension of the cord remains constant along its entire length from the apex to the hypothetical point of concurrence of the suspension lines. This assumption simplified the problem by confining it chiefly to geometrical considerations. However, the tension of the cord perhaps should not be considered as constant along its entire length, since the flat canopy is a special case of a conical one and the cord tension at the apex for the conical can be shown from considerations of statics to be zero.

The present section deals with the determination of the cord tension T and the exterior forces R_1 per unit length applied on the cord as functions of the variable angle ϕ. The intrinsic equation is very important because it can be applied to any flexible cord with any kind of load. In its original form the equation is a vectorial differential equation and hence it leads to two equations in Cartesian coordinates for plane curves. These two equations contain three unknowns $\overline{T}$, $\overline{R}_1$ and the angle ζ included between the vectors of $\overline{R}_1$ and the normal $\overline{n}$ to the curve at any point. Therefore the system of two simultaneous equations with three unknowns has an infinite number of solutions. However, the physical problem has one and only one solution which can be obtained if one unknown is replaced by a properly chosen function of ϕ, and boundary conditions for the three variables are established to fit satisfactorily the physical problem.

As an example, suppose $\overline{T} = 0$ at the apex and $\overline{R}_1$ = maximum at the skirt are reasonable boundary conditions, and let the angle ζ be given by an arbitrary

function of ϕ satisfying other boundary conditions. With these assumptions the solution of the two simultaneous equations is obtained.

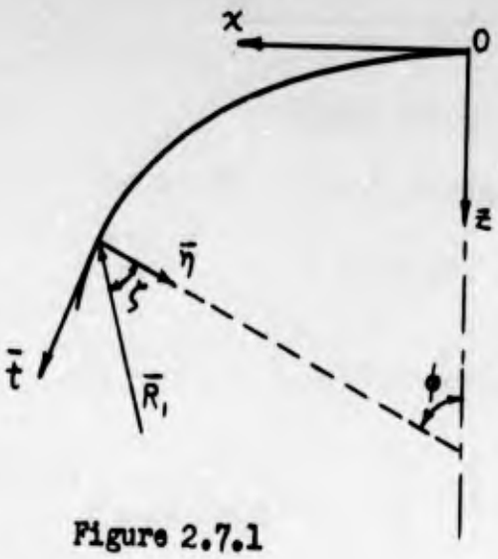

Figure 2.7.1

The intrinsic equation of equilibrium, using vector notation,

$$\overline{R_1} + \frac{d(T \cdot \bar{t})}{ds} = 0$$

(Reference 10, page 266)

or, in Cartesian coordinates,

$$\overline{R_1} \cdot \bar{t} + \frac{dT}{ds} = 0 \qquad (2.7.1)$$

$$\overline{R_1} \cdot \bar{n} + \frac{T}{\rho} = 0 \qquad (2.7.2)$$

where $\overline{R_1}$ is the exterior force per unit length of the curve

$T = |\bar{T}|$ is the magnitude of the cord tension (scalar tension)

ρ is the radius of curvature of the curve

ds is the differential arc length

$\bar{t}$ is the unit vector along the tangent of the cord

$\bar{n}$ is the unit vector along the normal to the cord

ζ is the angle included between $\bar{n}$ and $-\overline{R_1}$

$\overline{R_1} \cdot \bar{t} = -R_1 \sin\zeta$, $\overline{R_1} \cdot \bar{n} = -R_1 \cos\zeta$, where $R_1 = |R_1|$

Then Equations (2.7.1) and (2.7.2) become respectively

$$R_1 \sin\zeta = dT/ds$$

$$R_1 \cos\zeta = T/\rho$$

Dividing these two equations and taking equation $ds = \rho d\phi$ into acount we obtain

$$dT/T = \tan \zeta \, d\phi$$

Integrating $T = ce^{\int \tan \zeta \, d\phi}$ (2.7.3)

Assumed Boundary Conditions

$T = 0$ at $\phi = 0$ (apex)

$T =$ maximum at $\phi = \pi/2 + \theta$ (skirt)

The second boundary condition gives $dT/d\phi = 0$ at $\pi/2 + \theta$

or $ce^{\int \tan\zeta d\phi} \tan \zeta = 0$ which is true for $\tan \zeta = 0$ when $\phi = \pi/2 + \theta$.

This can be accomplished by assuming that $\tan \zeta = \frac{1}{\phi^2} - \frac{1}{(\theta + \pi/2)^2}$ (2.7.4)

In fact $\int \tan\zeta d\phi = \int \left[\frac{1}{\phi^2} - \frac{1}{(\theta + \pi/2)^2}\right] d\phi = -\frac{1}{\phi} - \frac{\phi}{(\theta + \pi/2)^2}$ and Equation (2.7.3) becomes

$$T = ce^{\left[-\frac{1}{\phi} - \frac{\phi}{(\theta + \pi/2)^2}\right]} \quad (2.7.5)$$

Equation (2.7.5) satisfies both boundary conditions; that is, for $\phi = 0$

$T = ce^{-\infty} = 0$ and for $\phi = \theta + \pi/2$, $dT/d\phi = ce^{\left[-\frac{2}{\theta + \pi/2}\right]} \left[\frac{1}{(\theta + \pi/2)^2} - \frac{1}{(\theta + \pi/2)^2}\right] = 0$

hence T is maximum when $\phi = \theta + \pi/2$

Determination of the Constant of Integration c in Equation (2.7.5)

For $\phi = \pi/2$, $T = T_m$

Therefore $T_m = ce^{\left[-(2/\pi) - \frac{\pi}{2(\theta + \pi/2)^2}\right]}$; and $c = T_m e^{\left[2/\pi + \frac{\pi}{2(\theta + \pi/2)^2}\right]}$

Then Equation (2.7.5) becomes

$$T = aT_m e^{-\left[\frac{1}{\phi} + \frac{\phi}{(\theta + \pi/2)^2}\right]} \tag{2.7.6}$$

where $a = e^{\left[2/\pi + \frac{\pi}{2(\theta + \pi/2)^2}\right]}$ (2.7.7)

and finally, solving Equation (2.7.2) for R_1 results in

$$R_1 = \frac{T}{\rho \cos \zeta} = \frac{aTm}{\rho\, e^{\left[\frac{1}{\phi} + \frac{\phi}{(\theta + \pi/2)^2}\right]} \cos\left[\tan^{-1}\left\{\frac{1}{\phi^2} - \frac{1}{(\theta + \pi/2)^2}\right\}\right]} \tag{2.7.8}$$

Starting with any assumed cord shape whatsoever the cord tension T and loading R_1 can be calculated as functions of ϕ from Equations (2.7.6) and (2.7.8) respectively.

It can be easily shown that Equations (2.7.1) and (2.7.2) yield the Taylor curve for the same assumptions for which this curve was derived. Thus for $\zeta = 0$ Equation (2.7.1) gives T = constant, and for $R_1 = (2x\,\pi/N)p$ Equation (2.7.2) gives $2x(\pi/N)p = T/\rho$ or $\rho = ds/d\phi = \frac{dx}{d\phi \cos \phi} = (NT/2\pi px)\, d\phi$. Integrating this last equation results in $x^2 = (NT/p\pi)\sin \phi$ or $x^2 = x_m^2 \sin \phi$ where $x_m^2 = NT/p\pi$ (compare Reference 2).

This approach to the determination of the variation of canopy cord tensions between skirt and apex could be very helpful in the analysis of experimental data. If, for example, the shape of the cords could be seen, as it cannot in existing photographs, and if the direction of the resultant forces on the cord could be determined from the observed strain patterns, the cord tension at any point could

be found using as boundary conditions (1) the known tension at the skirt, and (2) $dT/d\phi = 0$ at the skirt. In the absence of data of this sort, too many assumptions which cannot be easily justified are necessary for the approach to be very useful.

SECTION 3 - EFFECTS OF VARIOUS PARAMETERS ON CANOPY SHAPES AND STRESSES

INTRODUCTION

Section 3.1 gives the effect of suspension line length on the cord shape of the flat canopy. This effect is shown by means of cord curves from apex to MIR for l_c/l_s' ratios varying from 0.2 to 2.0 while l_c, N, and p are held constant. The suspension line angles are also given.

The effect of cone angle on the canopy shape and stresses in conical canopies is given in Section 3.2. Approximations are used to simplify the calculations.

Sections3.3 and 3.4 show the effect on the canopy shapes and stresses of such design practices as increasing fullness and pre-tensioning of the cord lines. At the vent, seams are reinforced with nylon webbing; extra folds of cloth are used at all seams. The cord over the vent is purposely shortened. All these design practices are discussed in Section 3.5.

Section 3.6 gives the effect of N upon the canopy shape of a flat canopy. Since the number of gores does not occur explicitly in the equations of Section 1.4 for the cord shape of the flat canopy, a modified Taylor cord shape that does depend upon N is developed. This is done by taking into account the fullness of the gores in horizontal cross-sections.

3.1 Effect of Suspension Line Length on the Cord Shape of a Flat Canopy

For different values of l_c/l_s', the values of k_{sk} and x_m are found by the following equations

$$k_{sk} = \frac{f(n) + 2.6818}{f(n) + 2n\,(l_c/l_s')} \quad \text{where } f(n) = 2n + (n^2 - 1)\log\left(\frac{n+1}{n-1}\right)$$

$$k_{sk} = 1 - \frac{.25}{n^2 - 1} \quad \text{and} \quad n = \csc\theta$$

(see Equations (1.4.5) (1.4.6))

$$\text{Also} \quad x_m = \frac{l_c}{n\,k_{sk}\,(l_c/l_s')}$$

Table 3.1.1 - Values of θ and x_m vs l_c/l_s' of a Flat Canopy with l_c = 10 ft

l_c/l_s'	k_{sk}	n	θ	x_m (ft)
.2	.99495	7.1	8° 6'	7.07799
.4	.98108	3.77	15° 23'	6.75917
.5	.97138	3.12	18° 42'	6.59913
.6	.95992	2.69	21° 49'	6.45448
.8	.93180	2.16	27° 35'	6.2106
1.0	.89928	1.866	32° 24'	5.93926
2.0	.71580	1.371	46° 50'	5.09497

Using the values of l_c/l_s' from Table 3.1.1 the cord length l_c is assumed constant and equal to 10 ft. Tables 3.1.2 and 3.1.3 contain the x and z coordinates of the cord from apex to skirt for the various ratios of l_c/l_s' and l_c = 10 ft. These values are plotted in Figure 3.1.1.

Table 3.1.2 - Coordinates of Points of Cord on a Parabolic Arc for Different Values of l_c/l_s' for a Flat Canopy

$l_c/l_s' = .2$				$l_c/l_s' = .4$				$l_c/l_s' = .5$			
①	②	③	④	①	②	③	④	①	②	③	④
1.00000	.00000	.00000	.68160	1.00000	.00000	.00000	.68160	1.00000	.00000	.00000	.68160
.99899	.00101	.03178	.71338	.99622	.00378	.06148	.74328	.99428	.00572	.07563	.75743
.99798	.00202	.04495	.72655	.99244	.00756	.08695	.76875	.98856	.01144	.10696	.78876
.99697	.00303	.05505	.73665	.98866	.01134	.10649	.78829	.98284	.01716	.13100	.81280
.99596	.00404	.06357	.74517	.98488	.01512	.12296	.80476	.97712	.02288	.15126	.83306
.99495	.00505	.07107	.75267	.98108	.01892	.13755	.81935	.97138	.02862	.16917	.85097

$l_c/l_s' = .6$				$l_c/l_s' = .8$				$l_c/l_s' = 1.0$			
①	②	③	④	①	②	③	④	①	②	③	④
1.00000	.00000	.00000	.68160	1.00000	.00000	.00000	.68160	1.00000	.00000	.00000	.68160
.99199	.00801	.08950	.77130	.98636	.01364	.11679	.79859	.97986	.02014	.14192	.82372
.98398	.01602	.12657	.80837	.97272	.02728	.16517	.84697	.95972	.04028	.20070	.88250
.97597	.02403	.15502	.83682	.95908	.04092	.20229	.88409	.93958	.06042	.24580	.92760
.96796	.03204	.17900	.86080	.94544	.05456	.23358	.91538	.91944	.08056	.28383	.96563
.95992	.04008	.20020	.88200	.93180	.06820	.26115	.94295	.89928	.10072	.31736	.99916

$l_c/l_s' = 2.0$			
①	②	③	④
1.00000	.00000	.00000	.68160
.94316	.05684	.23841	.92021
.88632	.11363	.33716	1.01896
.82948	.17052	.41294	1.09474
.77264	.22736	.47682	1.15862
.71580	.28420	.53311	1.21491

① = x/x_m

② = $1 - x/x_m$

③ = $Z/x_m = \sqrt{②}$

④ = Modified z/x_m = .6816 + ③

Table 3.1.3 - Actual Values of Coordinates of the Cord with Different Values of l_c/l_s'

①	②	③	$l_c/l_s' = .2$		$l_c/l_s' = .4$	
ø	x/x_m	z/x_m	x (ft)	z (ft)	x (ft)	z (ft)
			7.07799 ②	7.07799 ③	6.75917 ②	6.75917 ③
0	.0000	.0000	.0000	.0000	.0000	.0000
4	.1115	.0038	.789	.027	.754	.026
10	.2647	.0227	1.874	.161	1.789	.153
20	.4723	.0779	3.343	.551	3.192	.527
30	.6405	.1561	4.533	1.105	4.329	1.055
40	.7802	.2541	5.522	1.799	5.274	1.718
45	.8409	.3095	5.952	2.191	5.684	2.092
50	.8752	.3470	6.195	2.456	5.916	2.345
60	.9306	.4262	6.587	3.017	6.290	2.881
70	.9694	.5093	6.861	3.605	6.552	3.442
80	.9924	.5948	7.024	4.210	6.708	4.020
90	1.000	.6816	7.078	4.824	6.759	4.607
Parabolic Arc Modified x/x_m & z/x_m for various values of l_c/l_s' from Table 3.1.2			7.071	5.049	6.734	5.024
			7.064	5.143	6.708	5.196
			7.057	5.214	6.683	5.328
			7.049	5.274	6.657	5.440
			7.042	5.327	6.631	5.538

①	②	③	$l_c/l_s' = .5$		$l_c/l_s' = .6$	
ø	x/x_m	z/x_m	x (ft)	z (ft)	x (ft)	z (ft)
			6.59913 ②	6.59913 ③	6.45448 ②	6.45448 ③
0	.0000	.0000	.0000	.0000	.0000	.0000
4	.1115	.0038	.736	.025	.720	.025
10	.2647	.0227	1.747	.150	1.709	.147
20	.4723	.0779	3.117	.514	3.048	.503
30	.6405	.1561	4.227	1.030	4.134	1.008
40	.7802	.2541	5.149	1.677	5.036	1.640
45	.8109	.3095	5.549	2.042	5.428	1.998
50	.8752	.3470	5.776	2.290	5.649	2.240
60	.9306	.4262	6.141	2.813	6.007	2.751
70	.9694	.5093	6.327	3.361	6.257	3.287
80	.9924	.5948	6.549	3.925	6.405	3.839
90	1.000	.6816	6.599	4.498	6.454	4.399
Parabolic Arc Modified x/x_m & z/x_m for various values of l_c/l_s' from Table 3.1.2			6.561	4.998	6.402	4.978
			6.524	5.205	6.351	5.218
			6.486	5.364	6.299	5.401
			6.448	5.497	6.248	5.556
			6.410	5.616	6.196	5.693

Table 3.1.3 (cont)

①	②	③	$l_c/l_s' = .8$		$l_c/l_s' = 1.0$	
ø	x/x_m	z/x_m	x (ft)	z (ft)	x (ft)	z (ft)
			6.21060 ②	6.21060 ③	5.95926 ②	5.95926 ③
0	.0000	.0000	.0000	.0000	.0000	.0000
4	.1115	.0038	.692	.024	.664	.023
10	.2647	.0227	1.644	.141	1.577	.135
20	.4723	.0779	2.933	.484	2.815	.464
30	.6405	.1561	3.978	.959	3.817	.930
40	.7802	.2541	4.846	1.578	4.649	1.514
45	.8409	.3095	5.222	1.922	5.011	1.844
50	.8752	.3470	5.436	2.155	5.216	2.068
60	.9306	.4262	5.780	2.647	5.546	2.540
70	.9694	.5093	6.021	3.163	5.777	3.035
80	.9924	.5948	6.163	3.694	5.914	3.545
90	1.0000	.6816	6.211	4.233	5.959	4.062
Parabolic Arc Modified x/x_m & z/x_m values of l_c/l_s from Table 3.1.2			6.126	4.960	5.839	4.909
			6.041	5.260	5.719	5.259
			5.956	5.491	5.599	5.528
			5.872	5.685	5.479	5.754
			5.787	5.856	5.359	5.954

①	②	③	$l_c/l_s' = 2.0$	
ø	x/x_m	z/x_m	x (ft)	z (ft)
			5.09497 ②	5.09497 ③
0	.0000	.0000	.0000	.0000
4	.1115	.0038	.568	.019
10	.2647	.0227	1.349	.116
20	.4723	.0779	2.406	.397
30	.6405	.1561	3.263	.795
40	.7802	.2541	3.975	1.295
45	.8409	.3095	4.284	1.577
50	.8752	.3470	4.459	1.768
60	.9306	.4262	4.741	2.171
70	.9694	.5093	4.939	2.595
80	.9924	.5948	5.056	3.030
90	1.0000	.6816	5.095	3.473
Parabolic Arc Modified x/x_m & z/x_m values of l_c/l_s from Table 3.1.2			4.805	4.688
			4.516	5.192
			4.226	5.578
			3.937	5.903
			3.647	6.190

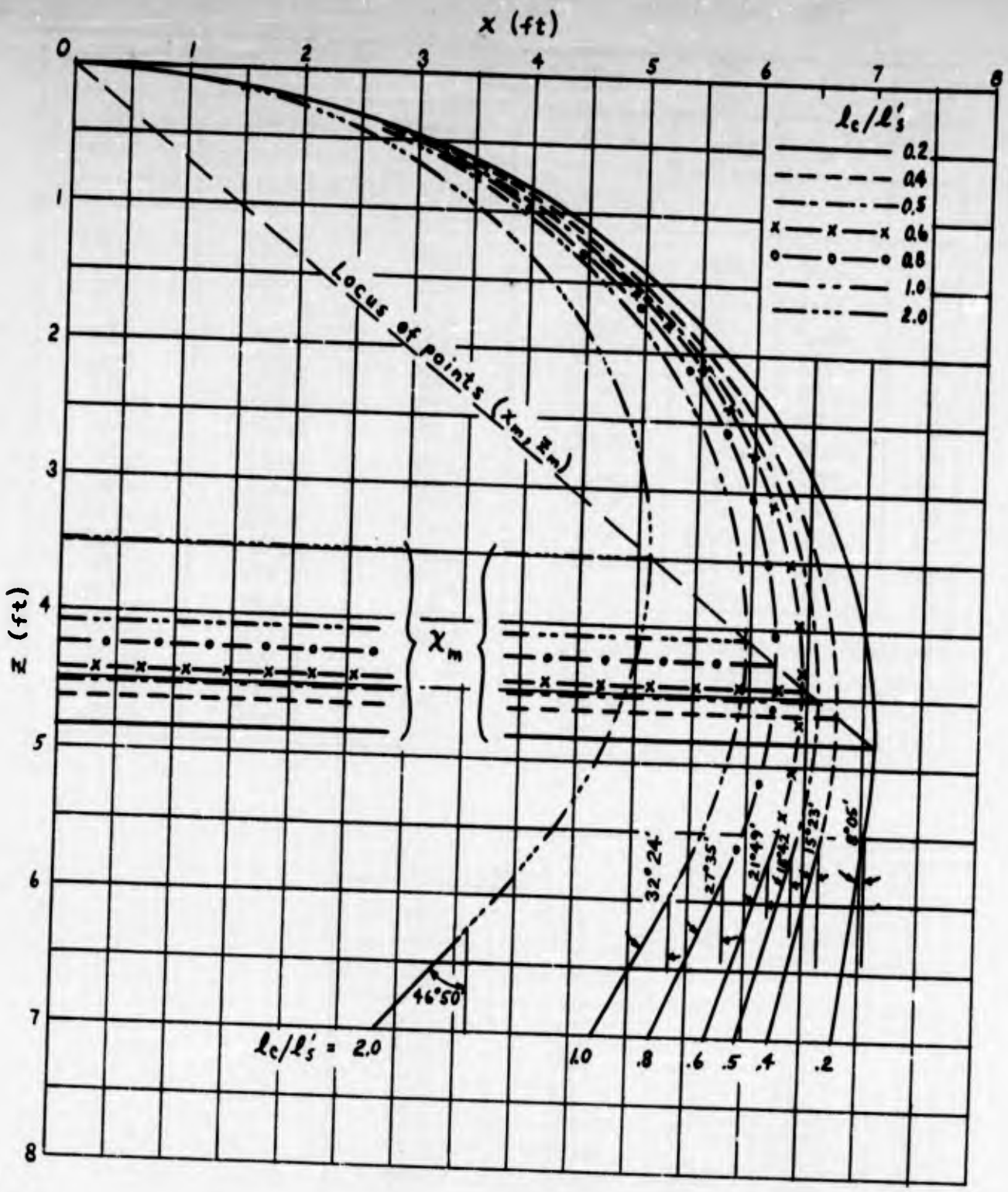

Figure 3.1.1 - Cord Shapes of a Flat Canopy with Different Ratios l_c/l'_s but with the same l_c

3.2 Effect of Cone Angle Variation on the Canopy Shape and Stresses of a Conical Canopy

In this study the equations of the first approximation (see Section 1.7) are used because an undue amount of labor would be required if the equations of the second approximation were used. Also the cord curves of the two approximations are rather close together (Figure 1.8.13). Computations for the cord shape and canopy stresses are made for cone angles of β = 10°, 15°, 20°, 25° and 30°. These computations show that the cord curves for small β are above those for larger β, and that the cord tension and cloth stresses decrease as β increases, if the cords have common apex and length over the canopy.

The calculations are based in part on approximate equations derived from those of Section 1.7 by letting $\cos \pi/N \cong \cos 2\pi/N \cong 1$ and $\tan \pi/N \cong 0$.

From Article 1.7 the parametric equations of the cords are:

$$x/x_m = \sqrt{\frac{\cos 2\pi/N}{\cos^2 \pi/N \cot^2 \phi + \cos 2\pi/N}} \qquad (3.2.1)$$

$$z/x_m = \tan\beta \sqrt{\frac{\cos^2 \pi/N \cot^2 \beta + \cos 2\pi/N}{\cos 2\pi/N}} - \frac{\cos^2 \pi/N \cot \phi}{\sqrt{\cos 2\pi/N (\cos^2 \pi/N \cot^2 \phi + \cos 2\pi/N)}} \qquad (3.2.2)$$

Since β appears only in the first term of Equation 3.2.2, Table 1.7.1 can be modified to include the several values of β. This is done in Table 3.2.1. In Figure 3.2.1 the cord curves for β = 10°, 20° and 30° are plotted.

The equations for the tension in the cord and the stresses in the canopy are given by:

Table 3.2.1 - Coordinates of Cord for Various Cone Angles β

⑦	⑧	⑨	⑩	⑪	⑫
ϕ	tan ϕ	cot ϕ			x/x_m
			$\sqrt{② \cdot ⑨^2 + ①}$	⑩ / ⑨	
10	.17633	5.6713	5.7081	1.0065	.17218
15	.26795	3.7321	3.8286	1.0259	.25670
20	.36397	2.7475	2.8959	1.0540	.33938
25	.46631	2.1445	2.3423	1.0922	.41959
30	.57735	1.7321	1.9785	1.1423	.49674
42	.90040	1.11061	1.4759	1.3289	.66590
54	1.37638	.72654	1.2185	1.6771	.80657
66	2.24604	.44523	1.0775	2.4201	.91211
78	4.70463	.21256	1.0052	4.7290	.97773
90	∞	0	.9828	∞	1.0000

⑦		z/x_m				
ϕ		⑤ - ⑥ / ⑪				
	⑥ / ⑪	β = 10°	β = 15°	β = 20°	β = 25°	β = 30°
10	.99365	.0305				
15	.97486	.0492	.0689			
20	.94887	.0752	.0949	.1236		
25	.91568	.1084	.1281	.1568	.1957	
30	.87553	.1486	.1683	.1970	.2359	.2868
42	.75259	.2715	.2912	.3199	.3588	.4097
54	.59632	.4278	.4475	.4762	.5151	.5660
66	.41325	.6109	.6306	.6593	.6982	.7490
78	.21148	.8126	.8323	.8610	.8999	.9508
90	0	1.0241	1.0438	1.0725	1.1114	1.1623

① = .96593
② = .98295
③ = .9828
④ = cot β
⑥ = 1.00011

See list of constants just before Table 1.7.1

$$⑤ = \frac{\sqrt{② \cdot ④^2 + ①}}{④ \cdot ③} = \frac{\tan \beta}{⑫ \ (\phi = \beta)} =$$

1.0241 for β = 10°
1.0438 for β = 15°
1.0725 for β = 20°
1.1114 for β = 25
1.1623 for β = 30°

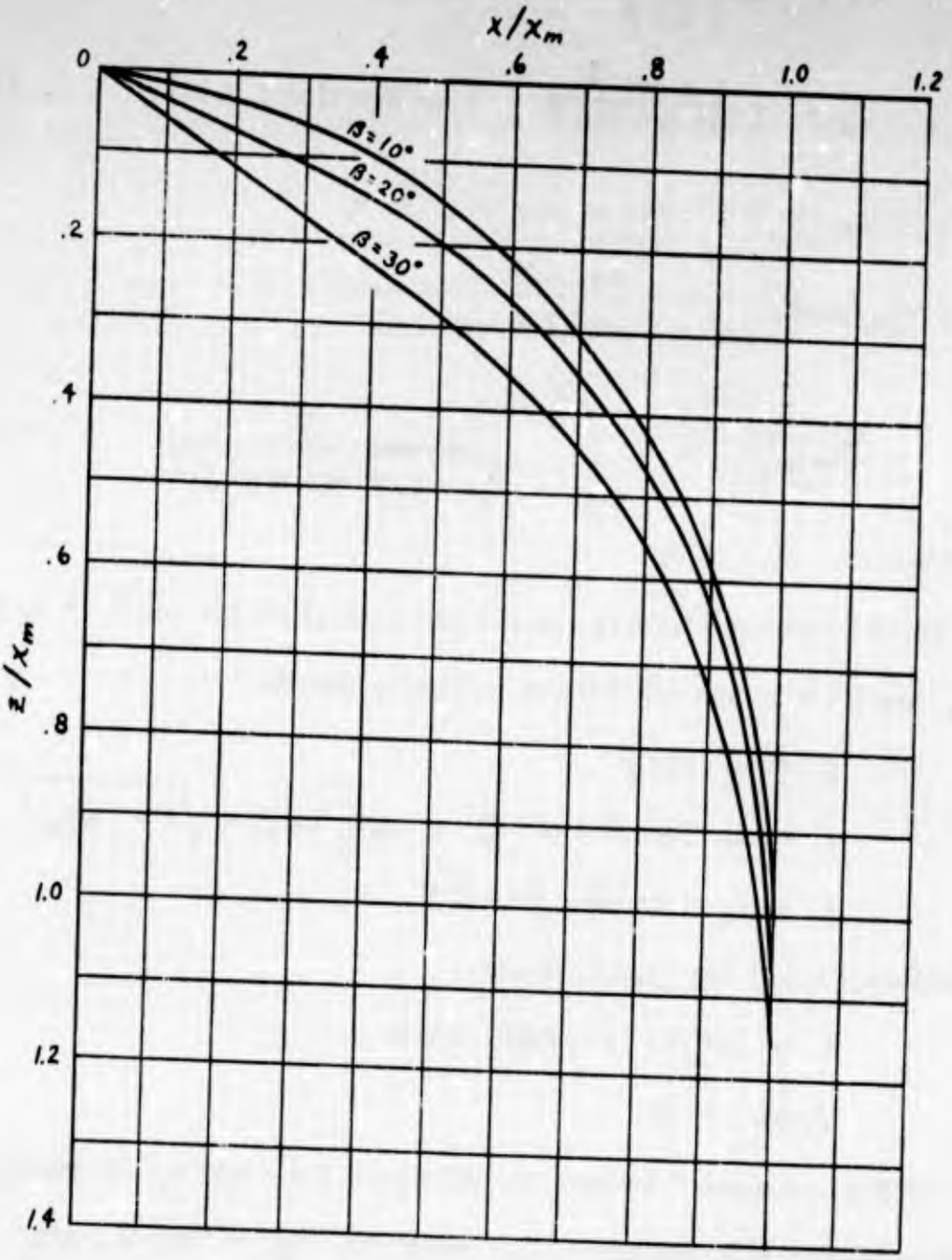

Figure 3.2.1 = Cord Curves for Various Cone Angles β

$$T = \frac{p\,x^2 \sin 2\pi/N}{2 \sin \phi} \qquad \text{(see Equation 1.7.1)} \qquad (3.2.3)$$

$$f_1 = \frac{p\,x \cos \lambda}{2 \cos \pi/N \sin \phi} \qquad \text{(see Equation 1.7.11)} \qquad (3.2.4)$$

The equation for the length of arc is given by

$$s = (x_m/\cos\beta)\sqrt{\frac{\cos 2\pi/N}{\cos^2 \pi/N \cot^2 \beta + \cos 2\pi/N}}$$

$$+ \frac{x_m \sqrt{\cos 2\pi/N}}{\cos \pi/N} \int_{\beta}^{\phi} \frac{d\phi}{\sqrt{(1 - \tan^2 \pi/N \sin^2 \phi)^3}} \qquad (3.2.5)$$

(see Equation (1.7.18)).

If in Equations (3.2.1), (3.2.2) and (3.2.5) we let $\cos \lambda = 1$, $\cos 2\pi/N = 1$, $\cos \pi/N = 1$, $\tan \pi/N = 0$ the following result:

$$x = x_m \sin \phi$$

$$z = x_m (\sec \beta - \cos \phi) = x_m \left[\sec \beta - \sqrt{1 - (x/x_m)^2} \right]$$

$$s = x_m (\tan \beta + \phi - \beta)$$

Equations (3.2.3) and (3.2.4) become

$$T = (p x_m^2/2) \sin 2\pi/N \sin \phi$$

$$f_1/p x_m = \tfrac{1}{2}$$

If ϕ is eliminated between the equations for x and z, the equation of a circle results with radius = 1, center at $z/x_m = \sec \beta$, $x/x_m = 0$:

$$(x/x_m)^2 + (z/x_m - \sec \beta)^2 = 1 \qquad (3.2.6)$$

The portion of the curve below the maximum inflated radius is symmetrical with a part above MIR. In order to determine the x coordinate of the part below MIR the following equation must be solved:

$$\frac{2\,\widehat{OC} - \widehat{OB}}{x_B} = m/\cos \phi_B \qquad \text{(see Equation 1.7.27)} \qquad (3.2.7)$$

where $\widehat{OC}$ = Length of cord to MIR

$\widehat{OB}$ = Length of cord to x_B

x_B = Coordinate of end of portion below MIR ($= x_{sk}$)

ϕ_B = ϕ at x_B above MIR

$m = l_c/l_s'$

Using $\widehat{OB} = x_m (\tan\beta - \beta + \phi_B)$

$x_B = x_m \sin \phi_B$

Equation (3.2.7) becomes:

$$m \tan \phi_B + \phi_B = k + \beta - \tan \beta \qquad (3.2.8)$$

where $k = 2\,\widehat{OC}/x_m$.

The following table gives values of s/x_m vs ϕ by using the approximate equation $s = x_m (\tan \beta + \phi - \beta)$.

For the solution of Equation (3.2.8) values of k are taken from Table 3.2.2 .

Thus $m \tan \phi_B + \phi - k (\tan \beta - \beta) =$

$2\,(1.57260) - .00180 = 3.14340$ for $\phi = 10°$

$2\,(1.57695) - .00615 = 3.14775$ for $\phi = 15°$

$2\,(1.53570) - .01490 = 3.15650$ for $\phi = 20°$

$2\,(1.60078) - .02998 = 3.17158$ for $\phi = 25°$

$2\,(1.62455) - .05375 = 3.19535$ for $\phi = 30°$

Assuming $m = 0.6$ and solving the above equation by trial and error we obtain respectively:

Table 3.2.2 - Values of s/x_m vs ϕ for Several Cone Angles

(1)	(2)	$s/x_m = \tan\beta + \phi - \beta$ (*)				
ϕ	ϕ	$\beta = 10°$	$\beta = 15°$	$\beta = 20°$	$\beta = 25°$	$\beta = 30°$
Degrees	Radians	(2) + .00180	(2) + .00615	(2) + .01490	(2) + .02998	(2) + .05375
10	.17453	.17633	-	-	-	-
15	.26180	.26360	.26795	-	-	-
20	.34907	.35087	.35522	.36397	-	-
25	.43633	.43813	.44218	.45123	.46631	-
30	.52360	.52540	.52975	.53850	.55358	.57735
36	.62832	.63012	.63447	.64322	.65830	.68207
42	.73304	.73484	.73919	.74794	.76302	.78679
48	.83776	.83956	.84391	.85266	.86774	.89151
54	.94248	.94428	.94863	.95738	.97246	.99623
60	1.04720	1.0490	1.05335	1.06210	1.07718	1.10095
66	1.15192	1.15372	1.15807	1.16682	1.18190	1.20567
72	1.25664	1.25844	1.26279	1.27154	1.28662	1.31039
78	1.36136	1.36316	1.36751	1.37626	1.39134	1.41511
84	1.46608	1.46788	1.47223	1.48098	1.49606	1.51983
90	1.57080	1.57260	1.57695	1.58570	1.60078	1.62455

(*) For $\beta = 10°$, $\tan\beta - \beta = .00180$
$\beta = 15°$, $= .00615$
$\beta = 20°$, $= .01490$
$\beta = 25°$, $= .02998$
$\beta = 30°$, $= .05375$

ϕ_B = 72° 19' For β = 10°

= 72° 21' = 15°

= 72° 25' = 20°

= 72° 31' = 25°

= 72° 42' = 30°

From Equation (1.7.27) $l_c = 2\,\widehat{OC} - \widehat{OB}$ or $l_c/x_m = 2k\ s_{\phi_B}/x_m$

where $s\phi_B$ is the cord length from the apex to the point B (see Figure 1.7.5). Values of x_m for all values of β and for l_c = 14 ft can be found by using the above values of ϕ_B.

Thus for β = 10; $l_c/x_m = 2\,(1.57260) - \left[1.25844 + (1.30316 - 1.25844)\,(.317/6)\right]$

$= 3.14520 - (1.25844 + .00553) = 1.88123$

Then $x_m = l_c/1.88123 = 14/1.88123 = 7.44194$ ft

For β = 15°, $l_c/x_m = 2\,(1.57695) - \left[1.26279 + (1.36751 - 1.26279)\,(.35/6)\right]$

$= 1.88500$

$x_m = 14/1.88500 = 7.42706$ ft

For β = 20°, $l_c/x_m = 2\,(1.58570) - \left[1.27154 + (1.37626 - 1.27154)\,(.417/6)\right]$

$= 1.89258$

$x_m = 14/1.89258 = 7.39731$ ft

For β = 25°, $l_c/x_m = 2\,(1.60078) - \left[1.28662 + (1.39134 - 1.28662)\,(.517/6)\right]$

$= 1.90592$

$x_m = 14/1.90592 = 7.34533$ ft

For β = 30°, $l_c/x_m = 2\,(1.62455) - \left[1.31039 + (1.41511 - 1.31039)\,(.7/6)\right]$

$= 1.92649$

$x_m = 14/1.92649 = 7.26710$ ft

Given x_m, x and z can now be found by using the equations for x/x_m and z/x_m given in Article 1.7 (Equations 1.7.16 and 1.7.17). T/p and f_1/p can then be computed from Equations 1.7.1 and 1.7.11 respectively. All these values are given in Table 3.2.3.

Because these latter factors vary so slightly with β, no curves are drawn, though Figures 1.7.15, 1.12.1, and 4.1.2 in which $\beta = 30°$, may be referred to. Variation of cone angle has little effect, therefore, on cord tensions and cloth stresses for $\phi > \beta$, where the maximums occur, and both approach zero toward the apex.

Table 3.2.3 - Values of T and f_1 vs ϕ and Absolute Coordinates x and z of a Conical Canopy for Several Cone Angles β . N = 24, l_c = 14 ft, l_c/l_s' = .6

ϕ	x/x_m	T/px_m^2	f_1/px_m	β = 10°, x_m = 7.44194 ft				
				z/x_m	x(ft)	z (ft)	T/p	f_1/p
10°	.17218	.02209	.49589	.0305	1.2814	.2270	1.2234	3.6904
15	.25670	.03295	.49619	.0492	1.9103	.3661	1.8249	3.6926
20	.33938	.04358	.49664	.0752	2.5256	.5596	2.4136	3.6960
25	.41959	.05391	.49718	.1084	3.1226	.8067	2.9857	3.7000
30	.49674	.06386	.49781	.1486	3.6967	1.1059	3.5367	3.7047
36	.58441	.07519	.49861	.2056	4.3491	1.5301	4.1642	3.7106
42	.66590	.08576	.49950	.2715	4.9556	2.0205	4.7496	3.7172
48	.74023	.09542	.50042	.3459	5.5087	2.5742	5.2846	3.7241
54	.80657	.10406	.50129	.4278	6.0024	3.1837	5.7631	3.7306
60	.86408	.11157	.50209	.5164	6.4304	3.8430	6.1790	3.7365
66	.91211	.11785	.50281	.6109	6.7879	4.5463	6.5268	3.7419
72	.95021	.12286	.50345	.7099	7.0714	5.2830	6.8043	3.7466
78	.97773	.12647	.50393	.8126	7.2762	6.0473	7.0042	3.7502
84	.99443	.12868	.50421	.9177	7.4005	6.8295	7.1266	3.7523
90	1.0000	.12941	.50431	1.0241	7.4419	7.6213	7.1670	3.7530

Table 3.2.3 (cont)

ø	β = 15°, x_m = 7.42706 ft					β = 20°, x_m = 7.39731 ft				
	z/x_m	x (ft)	z (ft)	T/p	f_1/p	z/x_m	x (ft)	z (ft)	T/p	f_1/p
10	–	–	–	–	–	–	–	–	–	–
15	.0689	1.9065	.5117	1.8176	3.6852	–	–	–	–	–
20	.0949	2.5206	.7048	2.4039	3.6886	–	–	–	–	–
25	.1281	3.1163	.9514	2.9737	3.6926	.1236	2.5105	.9143	2.3847	3.6738
30	.1683	3.6893	1.2500	3.5226	3.6973	.1568	3.1038	1.1599	2.9500	3.6778
36	.2253	4.3404	1.6733	4.1476	3.7032	.1970	3.6745	1.4573	3.4944	3.6825
42	.2912	4.9457	2.1628	4.7306	3.7098	.2540	4.3231	1.8789	4.1144	3.6884
48	.3656	5.4977	2.7153	5.2635	3.7166	.3199	4.9259	2.3664	4.6928	3.6950
54	.4475	5.9904	3.3236	5.7401	3.7231	.3943	5.4757	2.9168	5.2214	3.7018
60	.5361	6.4176	3.9816	6.1543	3.7291	.4762	5.9664	3.5226	5.6942	3.7082
66	.6306	6.7743	4.6835	6.5007	3.7344	.5648	6.3919	4.1780	6.1051	3.7141
72	.7296	7.0573	5.4188	6.7771	3.7392	.6593	6.7472	4.8770	6.4488	3.7194
78	.8323	7.2617	6.1815	6.9762	3.7427	.7583	7.0290	5.6094	6.7229	3.7242
84	.9374	7.3857	6.9621	7.0981	3.7447	.8610	7.2326	6.3691	6.9205	3.7277
90	1.0438	7.4271	7.7524	7.1384	3.7455	.9661	7.3561	7.1465	7.0414	3.7298
						1.0725	7.3973	7.9336	7.0813	3.7305

Table 3.2.3 (cont)

ø	$\beta = 25°$, $x_m = 7.34553$ ft					$\beta = 30°$, $x_m = 7.26710$ ft				
	z/x_m	x (ft)	z (ft)	T/p	f_1/p	z/x_m	x (ft)	z (ft)	T/p	f_1/p
10	-	-	-	-	-	-	-	-	-	-
15	-	-	-	-	-	-	-	-	-	-
20	-	-	-	-	-	-	-	-	-	-
25	.1957	3.0821	1.4375	2.9088	3.6521	-	-	-	-	-
30	.2359	3.6488	1.7328	3.4457	3.6567	.2868	3.6099	2.0842	3.3725	3.6176
36	.2929	4.2928	2.1515	4.0570	3.6626	.3437	4.2470	2.4977	3.9708	3.6234
42	.3588	4.8914	2.6356	4.6273	3.6691	.4097	4.8292	2.9773	4.5290	3.6299
48	.4332	5.4374	3.1821	5.1486	3.6759	.4840	5.3793	3.5173	5.0392	3.6366
54	.5151	5.9247	3.7837	5.6147	3.6822	.5660	5.8614	4.1132	5.4955	3.6429
60	.6037	6.3471	4.4345	6.0200	3.6881	.6546	6.2794	4.7570	5.8921	3.6487
66	.6982	6.6999	5.1286	6.3588	3.6934	.7490	6.6284	5.4431	6.2237	3.6540
72	.7972	6.9798	5.8559	6.6291	3.6981	.8481	6.9053	6.1632	6.4883	3.6586
78	.8999	7.1819	6.6102	6.8239	3.7016	.9508	7.1053	6.9096	6.6790	3.6621
84	1.0050	7.3046	7.3823	6.9432	3.7037	1.0559	7.2266	7.6733	6.7957	3.6641
90	1.1114	7.3455	8.1638	6.9826	3.7044	1.1623	7.2671	8.4466	6.8342	3.6649

3.3 Effect on Canopy Shapes & Stresses of Cloth Fullness at the Vent of Six Different Canopies

In recently designed canopies the gores are made 10% fuller at the vent reinforcement, than the uninflated cone geometry indicates. This fullness is tapered to zero at the skirt. If the vent reinforcement is allowed to increase by 10% the result would be a gore D"E"CB instead of the original DECB.

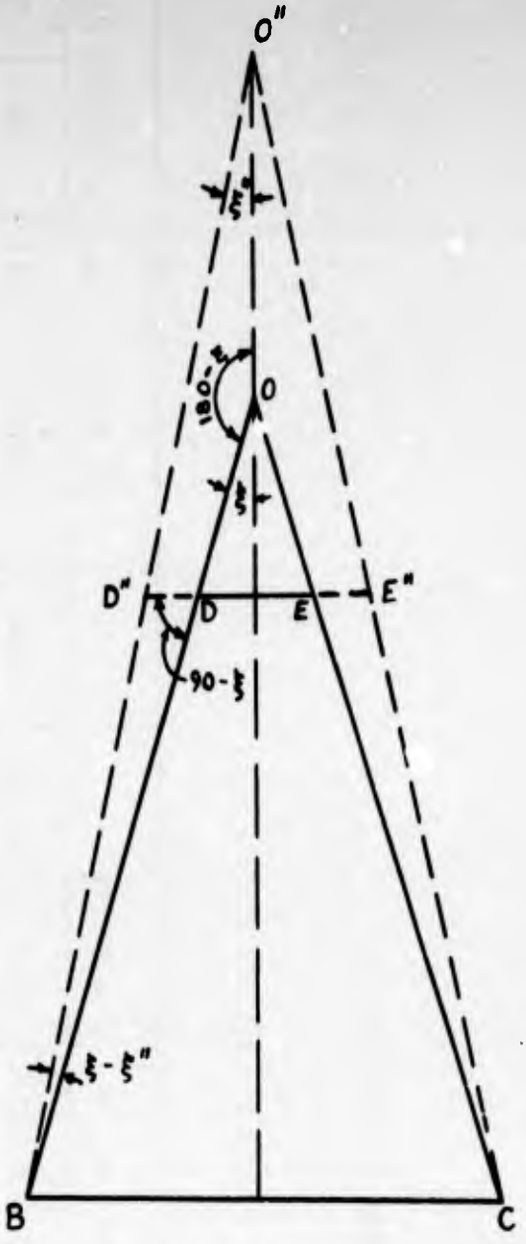

Figure 3.3.1

The new gore shape may be found by determining angle ξ'' in Figure 3.3.1.

Let 2ξ = gore angle when flat

$2\xi''$ = gore angle when flat but with an increase at the vent of "a", where "a" is defined by

$D''E'' = (1 + a)\, DE$

Let OB, OD, and ξ be the given quantities in addition to "a" above.

Then $\sin \xi'' = \frac{D''E''}{2\, O''D''} = \frac{(1 + a)\, DE}{2\, O''D''}$

$= (1 + a) \sin \xi \frac{OD}{O''D''}$

But $O''D'' = O''B - D''B$

In Δ OBO" $O''B/\sin(180 - \xi) = OB/\sin \xi''$ or $O''B = (\sin \xi / \sin \xi'')\, OB$

In Δ BD"D, $D''D/\sin(\xi - \xi'') = D''B/\sin(90 - \xi)$ or $D''B \cos \xi / \sin(\xi - \xi'')\, D''D$

But $2D''D + DE = D''E'' = (1 + a)\,DE$

Then $D''D = \frac{1}{2}\,a\,DE$

$$D''B = \frac{\cos \xi}{\sin (\xi - \xi'')} \cdot \frac{1}{2}\,a\,DE$$

$$O''D'' = OB \sin \xi / \sin \xi'' - \frac{\cos \xi}{\sin (\xi - \xi'')} \cdot \frac{1}{2}\,a\,DE$$

$$\sin \xi'' = \frac{(1 + a) \sin \xi\ OD}{\frac{\sin \xi}{\sin \xi''} - \frac{\cos \xi}{\sin (\xi - \xi'')} \cdot \frac{1}{2}\,a\,DE}$$

After some simplification the above becomes

$$\tan \xi'' = \frac{u \sin \xi}{1 + u \cos \xi}$$

where $u = (2/a\,DE)\left[BD - a\,OD\right] \tan \xi$. If $DE = 2\,OD \sin \xi$ is substituted into the above the following results

$$\tan \xi'' = \tan \xi \left[1 - a\,OD/BD\right] \qquad (3.3.1)$$

Table 3.3.1 - The Angle ξ''

Type of Canopy	USAF Dwg.	N	OD (ft)	OB (ft)	ξ	a (OD/OB)	$\tan \xi''$	ξ''
Flat	50E6877	28	.75	14	5° 25'	.005357	.11186	6° 23'
Extended Skirt	49J7141	30	.8333	14.86	6 00	.005608	.10451	5 58
Personnel Guide Surface	52J6026	24	.607	13.857	6 30	.004380	.11344	6 28
Conical Ring Slot	X53J7080E	32	.8125	12.11	5 06	.006709	.08865	5 04
Flat Ring Slot	EL-H-785	48	1.5938	23.0	3 45	.006929	.06509	3 43
Flat Ring Slot	X53J7080	20	.625	7.8	9 00	.008012	.15711	8 56

Since ξ'' differs from ξ by only 2' to 4', it is evident that geometrical changes are negligible.

Since the geometrical changes in the canopy are negligible they can be neglected when considering the effect of the extra fullness on the stresses. As has been stated in Section 1.7, the smallest value that $r_1\alpha$ can have is $s\pi/N$. In the vicinity of the vent, the curvature of the vent is slight and because of the assumed inextensibility of the fabric the equation

$$r_1\alpha = s\pi/N \tag{3.3.2}$$

can be considered to be a good approximation. The geometrical equation

$$r_1 \sin\alpha = x \sin \pi/N \tag{3.3.3}$$

is true for all values of ϕ. With an increase in fullness at the vent Equation (3.3.2) would change but Equation (3.3.3) would not. In fact at the vent

$$r_{1v}\,\alpha_v = (1 + a)\; s_v\pi/N \tag{3.3.4}$$

because of 100a% extra fullness. Solving Equations (3.3.3) and (3.3.4) simultaneously yields

$$\frac{\sin\alpha_v}{\alpha_v} = \frac{x_v \sin \pi/N}{(1 + a)\; s_v\; \pi/N} \tag{3.3.5}$$

Using the first two terms of the sine series in Equation (3.3.5) yields

$$1 - \frac{\alpha_v^2}{6} = \frac{x_v}{(1 + a)\; s_v} \left(1 - \frac{\pi^2}{6^2}\right) \cong \frac{x_v}{(1 + a)\; s_v} \tag{3.3.6}$$

Solving Equations (3.3.4) and (3.3.6)

$$r_{1v} = \frac{s_v\pi}{N} \sqrt{\frac{(1 + a)^3}{6\,(1 + a - x_v/s_v)}} \tag{3.3.7}$$

Since $f_1 = pr_1$, Equation 3.3.7 gives the fabric stresses when p is known.

In the vicinity of the vent $s_v \cong x_v$. With this approximation and with $a = 0.1$ Equation (3.3.7) becomes

$$r_{1v} = 4.68\; s_v/N \tag{3.3.8}$$

Table 3.3.2 gives values of r_{1v} and r_1 using s_v = OD from Table 3.3.1 for three parachutes. This table shows that the 10% extra fullness at the vent decreases the stresses to 1/8 of their value without extra fullness.

Table 3.3.2 - Values of r_{1v} and r_1 for Three Canopies

Type of Canopy	N	s_v(ft)	r_{1v}(ft)	r_1(ft)
Flat, T-7	28	.750	.125	1.137
Extended Skirt, T-10	30	.833	.130	1.287
Personnel Guide Surface, C-11	24	.607	.118	1.379

Equation (3.3.7) can be used to determine the fabric stresses anywhere along the cord if the extra fullness "a" is known. If in Equation (3.3.1) the lengths O"D and OD are allowed to vary, it can be seen that this equation gives the value "a" anywhere along the cord. Solving this equation for "a" yields

$$a = \frac{OB - OD}{OD}\left[1 - (\tan \xi''/\tan \xi)\right] = (l_c/s - 1)\left[1 - (\tan \xi''/\tan \xi)\right] \quad (3.3.9)$$

For a flat canopy l_c = 14 ft, s_v = 0.75 ft, and the extra fullness at the vent is 10%.

$$a = 0.00566\,(l_c/s - 1) \quad (3.3.10)$$

and from Equation (3.3.7)

$$r_1 = .04581\, s \sqrt{(1 + a)^3/(1 + a - x/s)} \quad (3.3.11)$$

Table 3.3.3 shows values of r_1 as determined by Equations (3.3.10) and (3.3.11) and using values of x and s for a flat canopy.

Table 3.3.3 - r_1 for a Flat Canopy, Type T-7

ø	s/x_m	x/x_m	x/s	14/s	a	r_1(ft)	s (ft)
20°	.4858	.4723	.9722	3.1565	.01221	1.04	4.44
30	.6711	.6405	.9544	2.2850	.00727	1.23	6.13
40	.8417	.7803	.9271	1.8218	.00465	1.27	7.68
45	.9254	.8409	.9087	1.6570	.00372	1.26	8.45

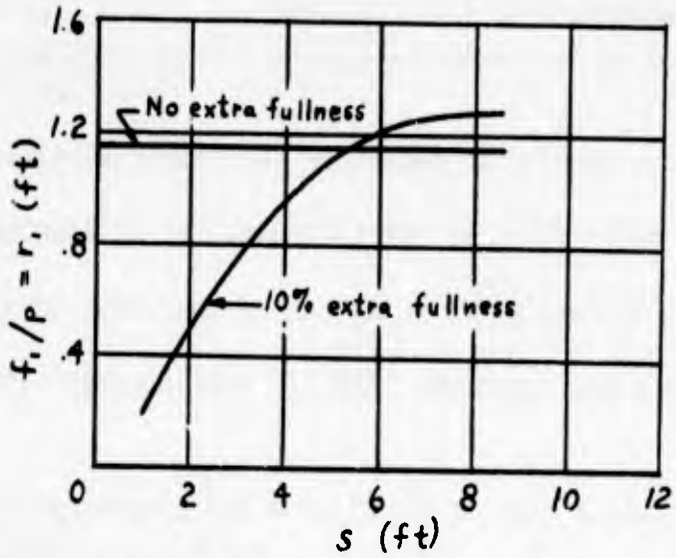

Figure 3.3.2 - Effect of 10% Extra Fullness on Cloth Stress

Figure 3.3.2 suggests that although stresses are relieved locally in the upper part, the maximum cloth stress in a flat canopy is higher, rather than lower, as a result of adding extra fullness at the vent. This may be of little significance if stresses during the opening process tend to concentrate at the vent. If, however, in the infinite mass case, the maximum stresses occur in the fully inflated condition, some reconsideration of design rules may be called for in drag parachute applications.

3.4 Effect of Shortness of Cords on Cord Shape and Fabric Stresses of a Flat Canopy

In a personnel parachute the lines over the canopy are shorter than the corresponding cloth length from apex to skirt by the amount that the cord stretches under a 20 lb load.

In a typical example of a nylon cord (Reference 11, page 23) stretched under an ultimate load of 550 lbs, the elongation at break was found to be 35%. Extrapolation of the proper curve of page 23 in Reference 11 indicates an elongation of 5.5% for a 20 lb load. Since the cord is shorter by 5.5% relative to the canopy, the latter wrinkles radially in the uninflated state.

Assuming that the carried load is 200 lbs and the angle θ is 20° in the steady state, the cord tension is $T = 200/(24 \cos \theta) = 8.9$ lbs for a 24-gore canopy. Therefore in the steady state the canopy wrinkles can be assumed as if the cord were pre-stretched by a load of 20 minus 8.9, that is 11.1 lbs. Assuming that the cord elongation is proportional to the applied load for magnitudes in the vicinity of the above loads, the shortness of the cord, that is, the fabric excess along the cord relative to the cord, in the steady state is $5.5\ (11.1/20) \cong 3\%$.

Differentiating the equation $x \sin(\pi/N) = r_1 \sin \alpha$ (see Section 1.1 - Step 8) results in

$$\sin(\pi/N)\, dx = r_1 \cos \alpha\, d\alpha + \sin \alpha\, dr_1$$

$$\sin \pi/N \cos \phi = r_1 \cos \alpha\, (d\alpha/ds) + \sin \alpha\, (dr_1/ds)$$

If r_1 is constant, which according to Figure 4.1.9 is very nearly true for a flat canopy, this becomes

$$\sin \pi/N \cos \phi = r_1 \cos \alpha\, (d\alpha/ds)$$

If r_1 is independent of ϕ, then according to Section 1.1, Step 8,

$$\sin \alpha = \sqrt{\sin \phi}$$

whence $$\cos \alpha = \sqrt{1 - \sin \phi}$$

so $$d\alpha/ds = \sin \pi/N \frac{\cos \phi}{r_1 \sqrt{1 - \sin \phi}}$$

When $\phi = \pi/2$, the application of L'Hospital's rule gives

$$(d\alpha/ds)_{\phi = \pi/2} = \frac{\sqrt{2}}{r_1} \sin \pi/N$$

Then, if $\Delta \alpha_m / \Delta s_m = (d\alpha/ds)_{\phi = \pi/2}$

$$\Delta \alpha_m = (\sqrt{2}/r_1) \Delta s_m \sin \pi/N .$$

Assuming the relations $r_1 = x_m \sin \pi/N$ and $s_m = 1.4896\, x_m$ (see Equation 1.1.16)) still hold, and $\Delta s/s = .03$, this yields

$$\Delta \alpha_m \frac{.03 \cdot (1.4896) x_m \sqrt{2}}{x_m} = .06320 = 3^\circ\ 37'$$

Then $\alpha_m = 90^\circ + 3^\circ\ 37' = 93^\circ\ 37'$

From equations of Section 1.5 it can be easily seen that variation of $\sin \alpha_m$ by 0.1 involves variation of the coordinates and the arc length by approximately 4%. If a linear proportionality is assumed for values of α_m exceeding 90° and in the vicinity of 90°, the variation of coordinates of the cord for $\alpha_m = 93^\circ\ 37'$ ($\sin \alpha_m = .998$) is approximately 4 (.002/.1) = .08%; therefore for all practical purposes this variation is insignificant. Since the radius r_1 has been assumed constant the canopy stresses are also invariable.

3.5 Effect of Rib, Skirt, and Vent Reinforcement and Shortness of Vent Lines on Canopy Shape and Stresses

Two types of vent reinforcement are shown in Figures 3.5.2 and 3.5.3. Figure 3.5.2 shows one in which the cord is continuous from riser to apex while Figure 3.5.3 shows one in which the cord from riser to apex consists of a nylon cord suspension line from riser to skirt, nylon webbing in the canopy, and nylon cord over the vent.

In Section 3.3 the effect of extra fullness at the vent was determined. The shortness of vent line over the vent gives an analogous effect which can be added to that due to extra fullness. This is illustrated with Figure 3.5.1 and the subsequent discussion.

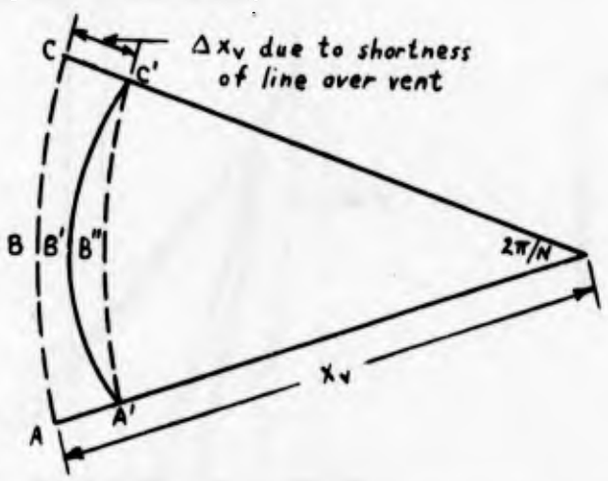

Figure 3.5.1 - Section Normal to Parachute Axis (One Gore)

Let OA = x_v = x = coordinate of point on cord at vent reinforcement.

ABC = Length of canopy vent reinforcement without extra fullness and without considering shortness of vent lines.

A'B'C' = ABC = Length of canopy vent reinforcement without extra fullness but assumed fastened at A' and C' to consider shortness of vent lines.

A'B"C' = Circular arc of radius OA'.

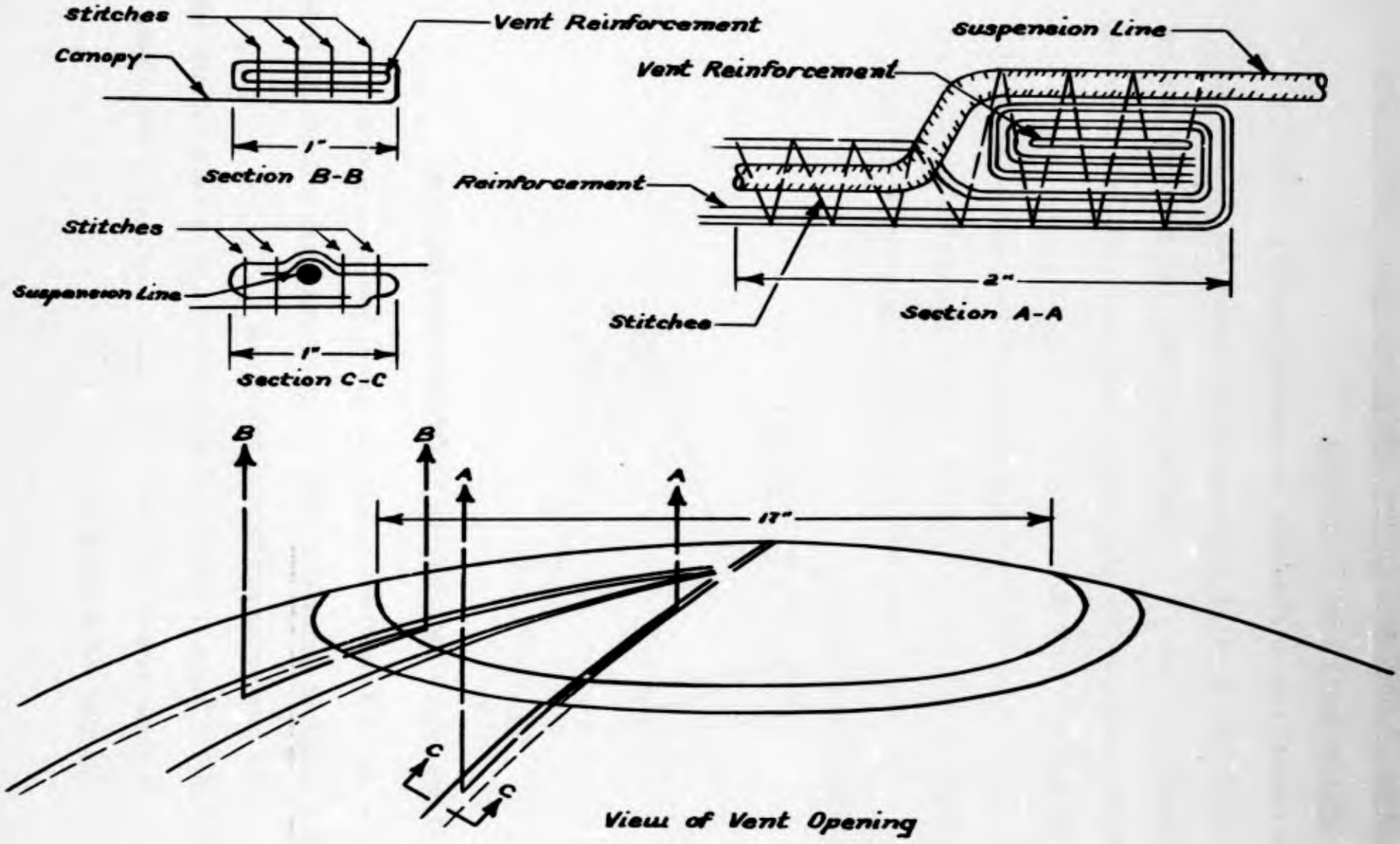

Figure 3.5.2 -- Sketches of Vent Reinforcements for a 28-Foot Flat Canopy

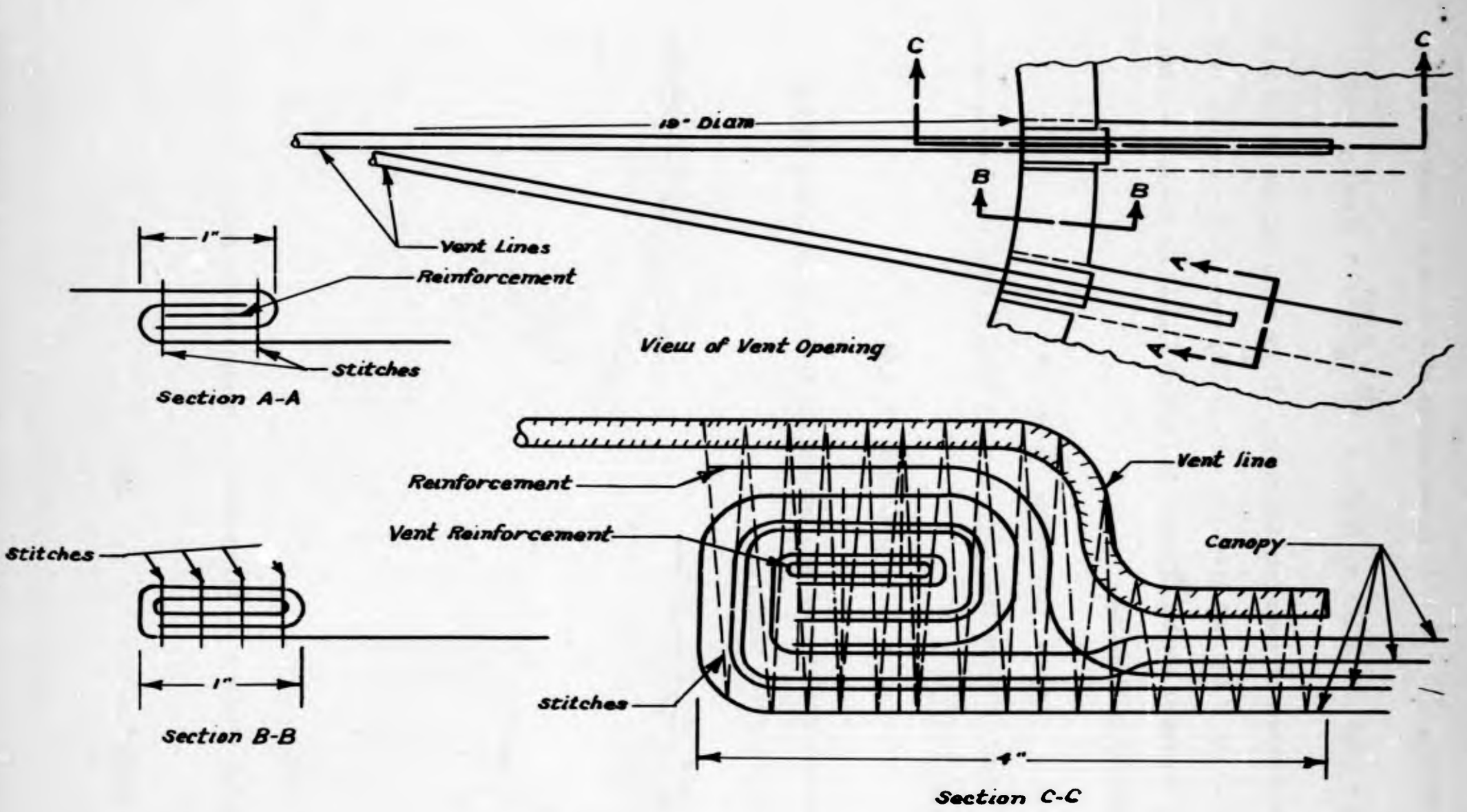

Figure 3.5.3 - Sketches of Vent Reinforcements for a 35-Ft Extended Skirt Canopy

In general, if $C = \pi D$ = the circumferences of a circle of diameter D, then

$\Delta C = \pi \Delta D$ and $\Delta C/C = \Delta D/D = \frac{ABC - A'B'C'}{ABC} = \Delta x_v/x_v$; thus

$\Delta C/C$ = shortness of cords over the canopy. If the extra fullness is 10% as in Article 3.3 and if the vent lines are short by 10%, then $\Delta C/C = 1 - (.9)(.9) = .19$ is the sum of the two effects. In Equation (3.3.6) the factor $1 + \alpha$ can be replaced by 1/.81 giving

$$\alpha_v = 1.06 \text{ radians} \cong 60° 10'$$

For the canopy of Figure 3.5.2 , $x_v = s_v = 9.0\ (.9) = 8.1$ in., N = 28, and from Equation (3.3.7)

$$r_v = 123\ s_v\ \pi / 28\ \alpha_v = 1.05 \text{ in.}$$

The stresses at the vent reinforcement can be determined in part by the equations of the hoop tension.

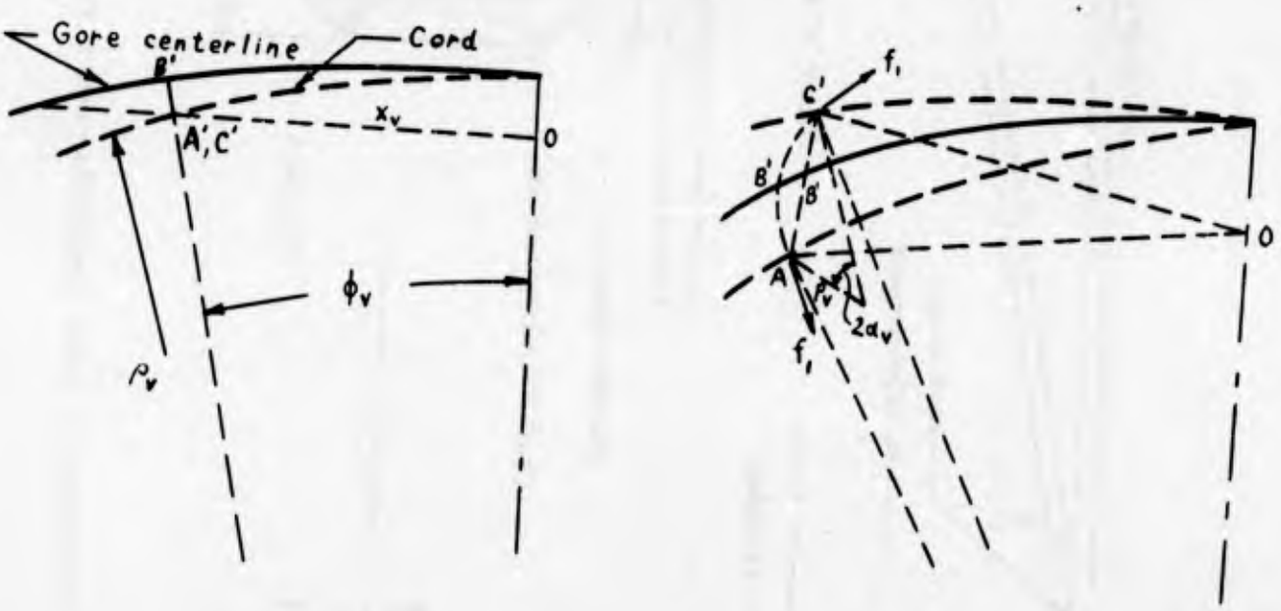

Figure 3.5.4 -Fullness and Circumferential Stresses at the Vent

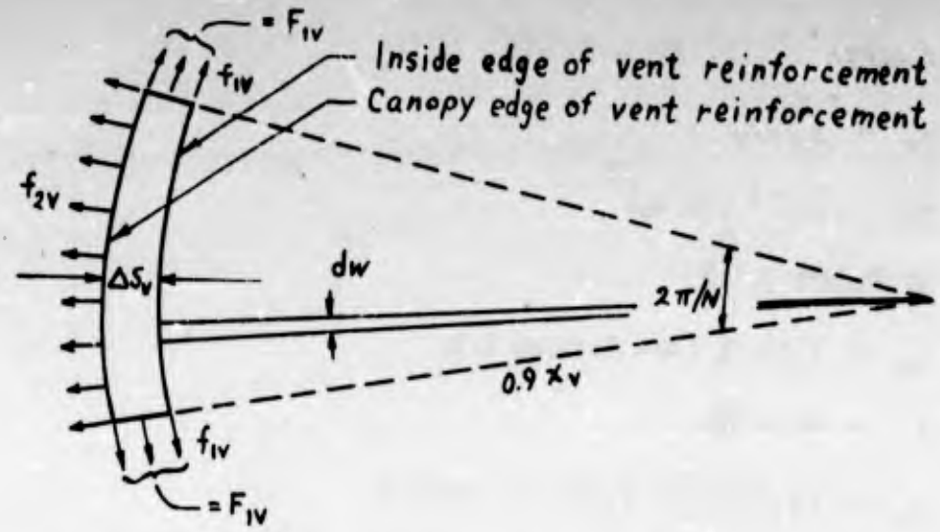

Figure 3.5.5 - Sketch Showing Stresses Acting on a Strip of Vent Reinforcement Between two Adjacent Cords. (Air Pressure is not shown)

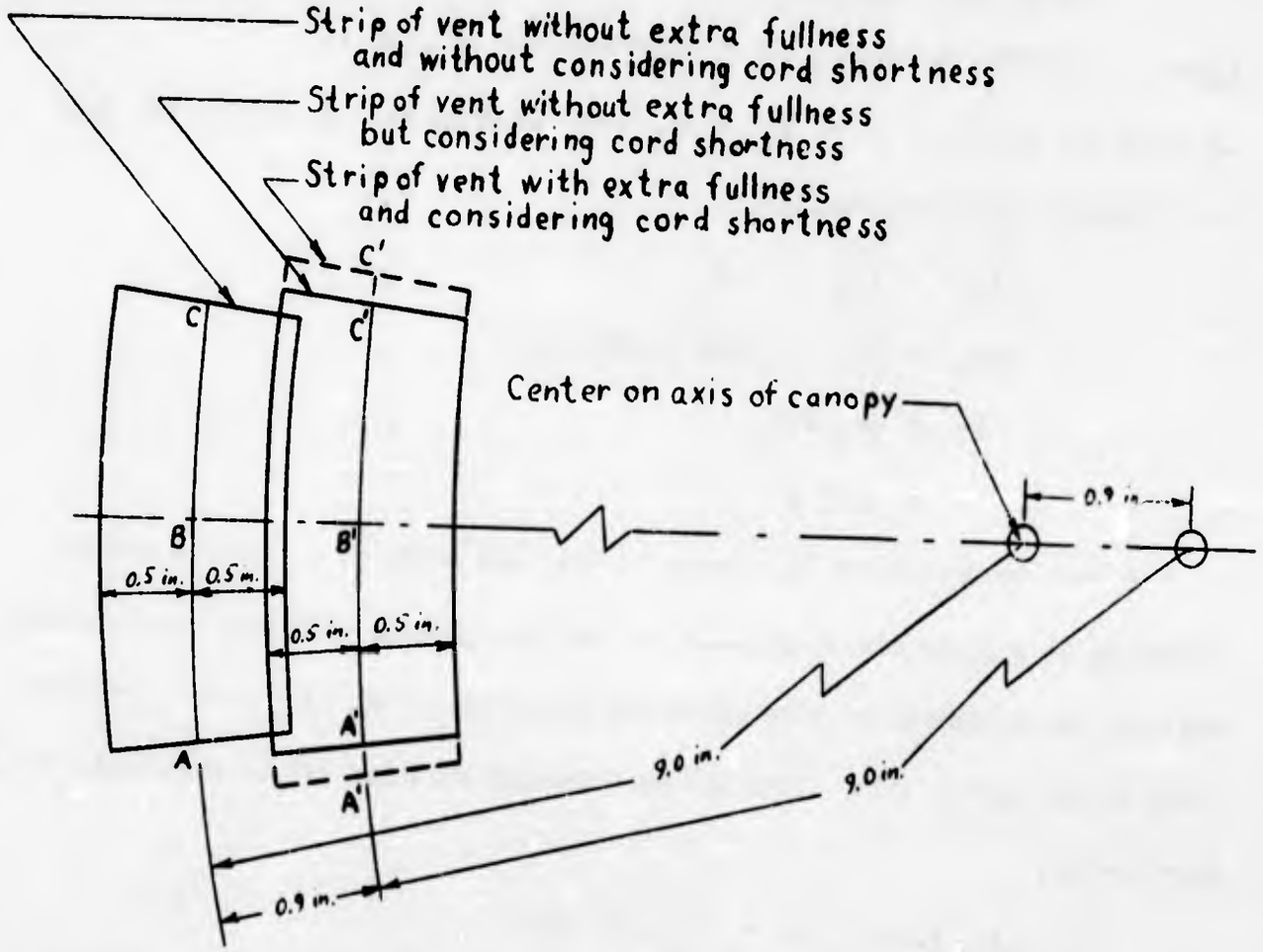

Figures 3.5.6 - Sketch of Vent Strip of Figure 3.5.5 above with and without Fullness and Cord Shortness

Using the Taylor curve

$$\rho_v = x_m^2/2x_v$$

$$\phi_v = \sin^{-1} (x_v/x_m)^2$$

For the canopy of Figure 3.5.2

x_m = 9.13 ft (see Section 2.1)

x_v = 9/12 ft

$\rho_v = (9.13)^2/(2)\ (.75)$ = 55.6 ft

$\phi_v = (.75/9.13)^2$ = .0056 radians = 0.32°

$(A'B'C')_f = ABC/.9 = 2x_v \pi/.9N = 2\ (9)\ \pi/\ .9\ (28)$ = 2.84 in.

$(A'B'C')_f$ includes 10% extra fullness

Also $A'B'C' = 2r_v \alpha_v = 2\ (1.05)\ (1.06)$ = 2.23 in.

Applying the equation $f_1 = f_1' = pr_1$ (hoop tension) at the edge of the vent the following equations result:

$$f_{1v} = f'_{1v} = pr_1$$

Δs_v = 1" (see Figure 3.5.2)

$$F_v = pr_v \Delta s_v$$

$$= 1.05\ p$$

The vent reinforcement is assumed to take the shape of a circular arc of radius r_v in a plane almos. parallel to the canopy axis. The vent reinforcement may also be considered to have curvature of radius $0.9\ x_v$ in a plane perpendicular to the canopy axis. Thus the hoop tension equation can be used again as is shown below:

$$f_{2v}\ (.9\ x_v)\ dw = 2F_v \sin\ dw/2$$

$$f2_v = F_v/(0.9\ x_v) = 1.05\ p/8.1 = .130\ p \quad \text{lb/in.}$$

The vent reinforcement consists of three layers of cloth and a tubular nylon webbing. The force $F_v = 1.05\ p$ is distributed among these five items and hence the stresses are very small. The stresses $f_2 = .130\ p$ lb/in. are also negligible, because in the steady state $p < .1$ lb/in^2.

After the cord emerges from the vent reinforcement into the open vent space, the only forces acting on it are those due to the drag of the cord in the air stream. This drag can be estimated by using the equation for the drag of a stranded cable in air. This equation is:

$$D = .00031\ V^2\ d$$

where D = drag in lbs/ft of length

V = air speed, in miles/hr

d = cable diameter in inches

Let $V = 20$ miles/hr

$d = 3/16$ in. (scaled from USAF dwg. 50E6877)

Then $D = .00031\ (400)(3/16) = .02325$ lb/ft.

If the cord is assumed to take the shape of a circular arc of radius $\rho_v = 55.6$ ft then using

$$F = (\rho_v)\ (\text{drag})\ \ (\text{hoop tension})$$

$$= (55.6)\ (.02325) = 1.29 \text{ lbs}$$

This load also gives negligible stresses in the cord and vent reinforcement.

The stresses in the skirt and rib reinforcements are of the same order of magnitude as those in the vent reinforcement and hence are negligible also.

3.6 Effect of Number of Gores on Canopy Shape

The equations of the cords of the flat canopy obtained in Section 1.1 and of the Taylor canopy which is combined with it in Section 1.4, do not contain the number of gores explicitly. Both shapes depend upon the canopy having a large number of gores. In order to determine the effect of N, the number of gores, two cord shapes dependent upon N are derived herein. One of these cord shapes is (except for a function of N) a Taylor curve; the other is not a Taylor curve but is derived in a manner similar to that of Section 1.1.

The effect of N on the cord shape may be considered to be due to the effect of N on the gore fullness. The Taylor curve neglects fullness entirely while the equations of Section 1.1 do not neglect fullness but they do neglect to consider the effect of N on the gore fullness explicitly.

Figure 3.6.1 shows a horizontal section through any one gore. AEB is a circular arc of radius x, x being a cord coordinate for any given ϕ. The arc ACB is the one formed by the intersection of a horizontal plane and the gore material.

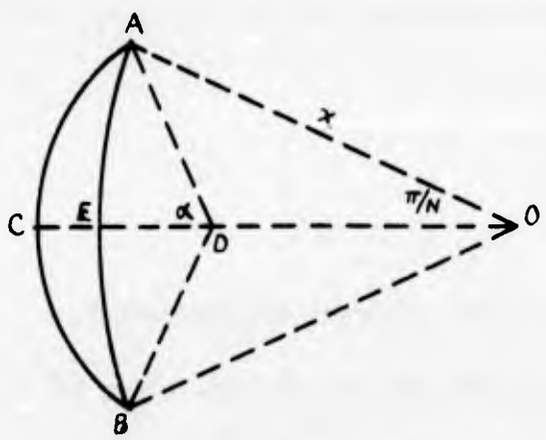

Figure 3.6.1

The difference between these two arcs is the fullness. In Section 1.1 the arc ACB was assumed to be part of an ellipse. Here this arc is assumed to be (1) an epicycloid formed by rolling a circle of radius x/N on the circular arc AEB, or (2) a circular arc of radius r_1. The area OACB is found by integration to be

$$A^{(E)} = \frac{\pi (N + 1) (N + 2)}{N^3} x^2 \qquad (3.6.1)$$

when the arc ACB is an epicycloid and

$$A^{(C)} = \tfrac{1}{2}\left[(2\alpha - \sin 2\alpha)\, r_1^2 + x^2 \sin 2\pi/N\right] \qquad (3.6.2)$$

when the arc ACB is a circular arc. If the tension in the cord is constant

$$T \sin \phi = A_p$$

where $T = A_m p$

A_m being the area A at $\phi = 90°$. For a Taylor curve

$$A_m = (\pi/N)(x_m^T)^2$$

x_m^T being the MIR of a Taylor curve. For the epicycloid and circular arcs

$$A_m^E = \frac{\pi (N + 1)(N + 2)}{N^3} (x_m^E)^2 \qquad (3.6.3)$$

$$A_m^C = \alpha_m r_{1m}^2 + \tfrac{1}{2}\left[(x_m^C)^2 \sin (2\pi/N) - r_1^2 \sin 2\alpha_m\right] \qquad (3.6.4)$$

Equations (3.6.1) and (3.6.4) contain the variables r_1, r_{1m}, α, and α_m. These may be determined from $r_1 \sin \alpha = x \sin \pi/N$ and by assuming that r_1 is constant and that $\sin \alpha = \sqrt{\sin \phi}$. With these relations and assumptions

$$r_1 = r_{1m} = x_m^C \sin \pi/N$$

$$\alpha = \sin^{-1} \sqrt{\sin \phi}, \qquad \alpha_m = \pi/2$$

$$A_m^C = \tfrac{1}{2} (x_m^C)^2 (\pi \sin^2 \pi/N + \sin 2\pi/N)$$

If the tension T in the case of the epicycloid and circular arcs are assumed equal to each other and equal to that in a Taylor curve, then the canopies will support practically the same loads. The equations of the cords are

$$x^E = \frac{N}{\sqrt{(N + 1)(N + 2)}}\, x^T \qquad (3.6.5)$$

and

$$x^C = \sqrt{\frac{2\pi}{N \sin 2\pi/N}\left[1 - \frac{2\alpha - \sin 2\alpha}{\sin^2 \alpha\, (\pi + 2 \cot \pi/N)}\right]}\, x^T \qquad (3.6.6)$$

in the cases of the epicycloid and circular arcs respectively. In the latter equations $x^T = x_m^T \sqrt{\sin \phi}$ = x coordinate of the Taylor curve. It is evident that Equation (3.6.5) is a Taylor curve but that Equation (3.6.6) is not. Because of the extreme difficulty of calculating the z-coordinates corresponding to Equation (3.6.6) and because the z-coordinates of the Taylor curve have already been calculated, it is better to use Equation (3.6.5) to discuss the effect of N on the cord shape.

Figure 3.6.2 shows the cord curve above MIR for a flat canopy and for a Taylor curve with the same T/p. With N = 24,

$$x^E = .944\, x^T \qquad (3.6.7)$$

is the equation of the cord curve when the gores have epicycloid sections. As N increases, the cord curve approaches more closely the Taylor curve. At N = 100, $x^E = .985\, x^T$. The variation of MIR with N is shown in Figure 3.6.3, which may be of help in the application of model data to prototype parachutes.

As a consequence of affecting MIR, N also affects the angle of the suspension lines. Referring to Figure 3.6.2 it can be seen that $\theta^E < \theta^T$ because the length ABC = AB'C' and l' is common to both. Therefore the angle of the suspension lines increases with N. This may help to explain the discrepancy between the theoretically and photographically determined x_m's and suspension line angles observed in Section 2, since the photographic values are somewhat less than the theory predicts for all but the conical canopy.

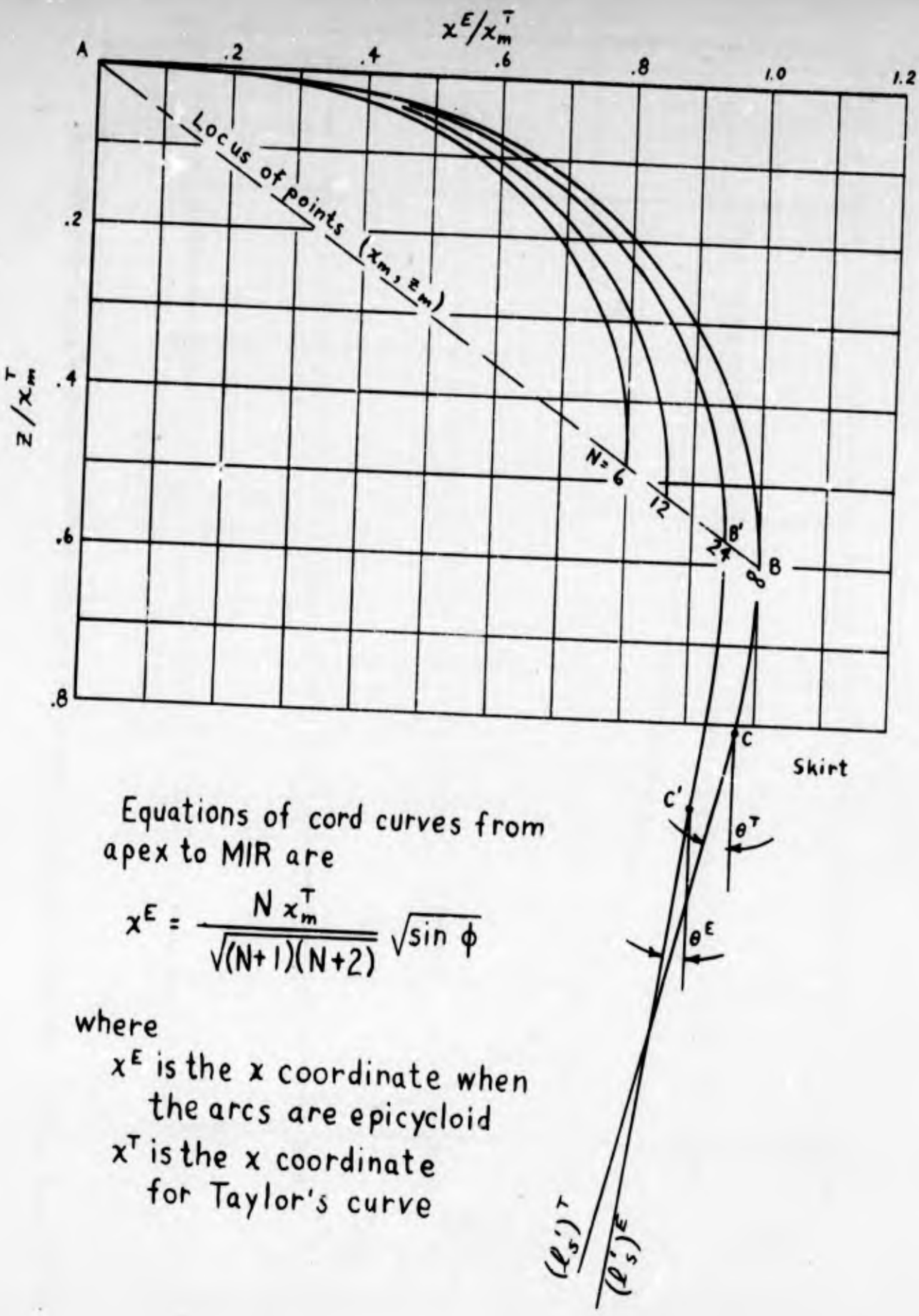

Equations of cord curves from apex to MIR are

$$x^E = \frac{N x_m^T}{\sqrt{(N+1)(N+2)}} \sqrt{\sin \phi}$$

where

x^E is the x coordinate when the arcs are epicycloid

x^T is the x coordinate for Taylor's curve

Figure 3.6.2 - Comparison of Cord Shape for Flat Canopies with same T/p and Showing the Effect of the Number of Gores on Cord Shape and Angle of Suspension Lines

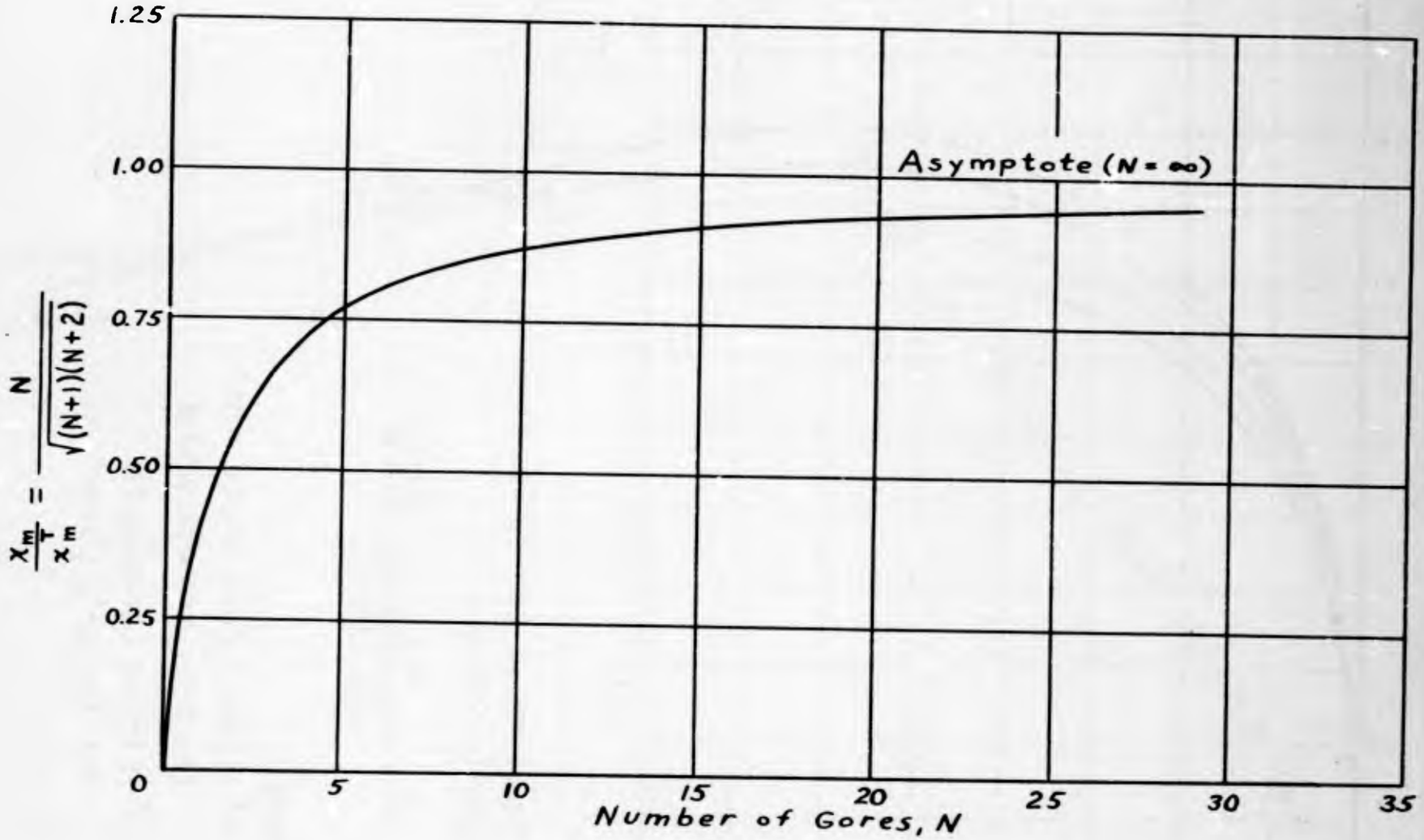

Figure 3.6.3 - Effect of Number of Gores on Maximum Inflated Radius in a Flat Canopy

SECTION 4 - CLOTH STRESSES

INTRODUCTION

Section 4.1 gives the cloth stresses immediately adjacent to the cords for the five canopy shapes studied. The stresses are given in terms of the ratio f_1/ρ from apex to skirt.

Using principles based on the statics and geometry of stresses and strains that occur in cloth subjected to shear, the effect on cloth stress of straight and biased gores is given in Section 4.2. Both meridional and circumferential stresses over a gore as well as those stresses adjacent to a cord are discussed. A need for biaxial strength data is brought out.

Section 4.3 discusses some experimental data on the stress-strain relationships in parachute cloth and airplane and airship fabrics. Inherent inaccuracies in strain measurements of cloth and fabrics are considered, and the kind of data needed for analytical purposes is pointed out.

The effect of cloth stresses on porosity is given in Section 4.4. Changes in geometric porosity due to thread shear and thread extension are calculated. Porosity data from other sources are examined and the stresses that occur during porosity measurements are calculated.

4.1 Variation of Cloth Stresses with Distance from the Apex for Five Canopy Shapes

Cloth stresses are calculated for the following canopy shapes: 1) Flat (T-7); 2) Extended Skirt (T-10); 3) Conical; 4) Conical Ring Slot; and 5) Personnel Guide Surface (C-11) canopies. For the conical canopy the cloth stress has been determined for both of the shapes given in Section 1.7 (1st approximation) and 1.8 (2nd approximation). The shape of each of the above canopies has been discussed in previous sections and available data from those sections, concerning the geometry of inflated or uninflated canopies, have been used in the present section.

The determination of the cloth stress f_1 is reduced to the determination of the radius r_1, since the formula $f_1 = pr_1$ holds for all cases except for the case of the conical canopy in the first approximation, where the formula is

$$f_1 = \frac{x\ p\ \cos\lambda}{2\cos\pi/N\ \sin\phi}$$

(see Equation (1.7.11)).

a) Flat Canopy (T-7, N = 28, l_c = 14 ft, l_s = 22.83 ft, l_c/l_s' = .56)

See Sections 1.4 and 2.1

For $0 = \phi = 45°$ the radius r_1 is constant and equals $x_{mm} \sin \pi/N$

where $x_{mm} = 1.117\ x_m = 1.117\ (9.13) = 10.15$ because of the magnification described in Section 2.1.

$$r_1 = 10.15 \sin(\pi/28) = 1.137 \text{ ft}$$

For $45° < \phi \leq 90°$, assume that the intersection of the gore by a plane P_1 is a circular arc (Figure 4.1.1).

From geometry

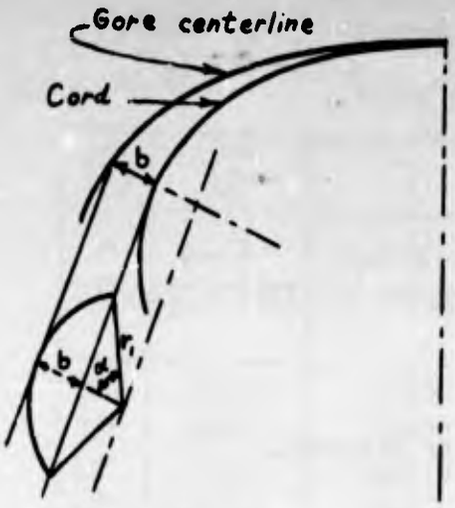

Figure 4.1.1

$$r_1 \sin \alpha = x \sin \pi/N \qquad (4.1.1)$$

$$b = r_1 (1 - \cos \alpha) \qquad (4.1.2)$$

where b is the length indicated in Figure 4.1.1, perpendicular to the cord and which can be measured from Figure 2.1.4.

Dividing Equations (4.1.1) and (4.1.2) results in

$$\frac{\sin \alpha}{1 - \cos \alpha} = \frac{x \sin \pi/N}{b} \quad \text{or} \quad \tan (\alpha/2) = \frac{b}{x \sin \pi/N} \qquad (4.1.3)$$

The angle α is determined from Equation (4.1.3) and then Equation (4.1.1) gives the values of r_1.

The following table gives values of r_1 for several values of ϕ.

Table 4.1.1 - Values of r_1 vs ϕ ($45° \leq \phi \leq 90°$) for a Flat Canopy (T-7)

①	②	③	④	⑤	⑥	⑦	⑧
ϕ	b (Ft)	x (Ft)	x sin π/N	tan $\alpha/2$	α	sin α	r_1 (Ft)
	Measured from Figure 2.1.4	See Table 2.1.2	.11205 ③	② / ④			④ / ⑦
45°	.4438	7.677	.8602	.5159	54° 34'	.8148	1.056
50	.4818	7.991	.8954	.5381	56° 34'	.8345	1.073
60	.5579	8.496	.9520	.5860	60° 44'	.8723	1.091
70	.6213	8.851	.9918	.6264	64° 08'	.8998	1.102
80	.6847	9.061	1.0153	.6744	68° 00'	.9272	1.095
90°	.7608	9.130	1.0230	.7437	73° 16'	.9577	1.068

b) Extended Skirt Canopy (T-10, N = 30, l_c = 17.9 ft, l_s = 25.5 ft, l_c/l_s' = 17.9/27.6 = .6486) (see Section 2.2).

x_m = 11.08 ft.

For $0 \leqq \phi \leqq 45°$ r_1 = constant = $x_{mm} \sin \pi/N$ = (11.08) (1.1117) (.10453) = 1.287 ft.

For $45° < \phi \leqq 90°$ the procedure of the flat type is followed.

Table 4.1.2 - Values of r_1 vs ϕ ($45° \leqq \phi \leqq 90°$) for an Extended Skirt Canopy (T-10)

①	②	③	④	⑤	⑥	⑦	⑧
ϕ	b (Ft)	x (Ft)	x sin π/N	tan $\alpha/2$	α	sin α	r_1 (Ft)
	Measured from Figure 3.2.4	See Table 3.2.1	.10453 ③	② / ④			④ / ⑦
45°	.2646	9.32	.9742	.2716	30° 24'	.5060	1.925
50°	.2886	9.70	1.0139	.2846	31° 46'	.5265	1.926
60°	.3367	10.31	1.0777	.3124	34° 42'	.5693	1.893
70°	.4040	10.74	1.1227	.3598	39° 34'	.6370	1.762
80°	.4762	11.00	1.1498	.4142	45° 00'	.7071	1.626
90°	.5195	11.08	1.1582	.4486	48° 20'	.7470	1.550

c) Conical Canopy - First Approximation

N = 24, β = 30, l_c = 14 ft, l_s = 22.83 ft, l_c/l_s' = .5339

Equation (1.7.28), in replacing 0.6 by .5339 becomes:

$$\frac{.5339}{\cos \phi_B} = \frac{2\,\widehat{OC} - \widehat{OB}}{x_B} \qquad (4.1.4)$$

Table 4.1.3 - Values of f_1/p and s vs ϕ for a Conical Canopy in the First Approximation

①	②	③	④	⑤	⑥	⑦
ϕ	cos ϕ	sin ϕ	sin λ	cos λ	x/x_m	s/x_m
			.13053 ②		See Table	1.7.1
30°	.86603	.50000	.11304	.99359	.49674	.57357
36°	.80902	.58779	.10560	.99440	.58441	.67819
42°	.74314	.66913	.09700	.99528	.66590	.78308
48°	.66913	.74314	.08734	.99617	.74023	.88825
54°	.58779	.80902	.07672	.99705	.80657	.99371
60°	.50000	.86603	.06527	.99786	.86408	1.09945
66°	.40674	.91355	.05309	.99858	.91211	1.20544
72°	.30902	.95106	.04034	.99918	.95021	1.31164
78°	.20791	.97815	.02714	.99963	.97773	1.41802
84°	.10453	.99452	.01364	.99991	.99443	1.52451
90°	.00000	1.00000	.00000	1.00000	1.00000	1.63107

①	⑧	⑨	⑩	⑪	⑫
ϕ	(x/x_m) cos λ	2 cos (π/N) sin ϕ	f_1/px_m	f_1/p (Ft)	s (Ft)
	⑤ · ⑥	1.98288 · ③	⑧ / ⑨	7.4024 ⑩	7.4024 ⑦
30°	.49356	.99144	.49782	3.6940	4.2562
36°	.58114	1.1655	.49862	3.7000	5.0324
42°	.66276	1.3268	.49952	3.7066	5.8108
48°	.73740	1.4736	.50041	3.7132	6.5912
54°	.80419	1.6042	.50130	3.7198	7.3737
60°	.86223	1.7172	.50211	3.7259	8.1584
66°	.91081	1.8115	.50279	3.7309	8.9448
72°	.94943	1.8858	.50346	3.7359	9.7329
78°	.97737	1.9396	.50390	3.7391	10.522
84°	.99434	1.9720	.50423	3.7416	11.312
90°	1.00000	1.9829	.50431	3.7422	12.103

This equation solved in a manner similar to that stated in Section 1.7 gives $\phi_B = 74° 15'$; then from Table 1.7.1 x_B can be found by interpolation

$$x_B = .96155\, x_m = x_{sk}.$$

Hence $l_c = \frac{.5339}{\cos \phi_B} x_B = \frac{(.5339)(.96155)}{.27144} x_m = 1.89129\, x_m$

Then $x_m = l_c/1.89129 = 14/1.89129 = 7.4024$ ft

The force f_1 per unit length acting between the fabric and the cord in the direction of BC (see Figure 1.7.1) is from Equation (1.7.11).

$$f_1 = \frac{xp \cos \lambda}{2 \cos \pi/N \sin \phi} \qquad (4.1.5)$$

where $\sin \lambda = \sin \pi/N \cos \phi$ (see Equation(1.7.4))

Table 4.1.3 gives values of f_1/p and s vs ϕ

c) Conical Canopy - Second Approximation

N = 24, $\beta = 30°$, $l_c = 14$ ft, $l_s = 22.83$ ft, $l_c/l_s' = .5339$

$l_c = .5339\, l_s' = .5339\, nx_{sk} = (.5339)(3.62)(.95681)\, x_m = 1.84924\, x_m$ (see Section 2.3);

then $x_m = l_c/1.84924 = 14/1.84924 = 7.5707$ ft

$$r_1 = \frac{x \sin (\pi/N)}{\sin \alpha}$$

Table 4.1.4 - Values of s and r_1 vs ϕ for a Conical Canopy

①	②	③	④	⑤	⑥	⑦	⑧	⑨
ϕ	α (*)	sin α	x/x_m	sin (π/N)/sin α	s/x_m	r_1/x_m	s (Ft)	r_1 (Ft)
	See Table 1.8.4		See Table 1.8.6	.13053/ ③	See Table 1.8.6	④ · ⑤	7.5707 ⑥	7.5707 ⑦
30°	3° 10'	.05524	.4968	2.36296	.5736	1.1739	4.343	8.887
37.06	17 14	.29626	.6158	.44059	.7124	.2713	5.393	2.054
44.12	22 44	.38644	.6969	.33778	.8166	.2354	6.182	1.782
51.18	33 09	.54683	.7764	.23870	.9309	.1853	7.048	1.403
58.24	39 21	.63406	.8475	.20586	1.0478	.1745	7.933	1.321
65.30	46 48	.72897	.9058	.17906	1.1645	.1622	8.816	1.228
72.36	49 33	.76097	.9515	.17153	1.2819	.1632	9.705	1.236
79.42	50 30	.77162	.9823	.16916	1.3942	.1662	10.56	1.258
86.48	50 24	.77051	.9960	.16941	1.4794	.1687	11.20	1.277
90°	48° 23'	.74760	1.0000	.17460	1.5446	.1746	11.69	1.322

(*) Values of α are taken from Table 1.8.4 by linear interpolation.

d) Conical Ring Slot Canopy (N = 32, β = 25°, l_c = 12.11 ft, l_s = 22 ft, l_c/l_s' = .48363) (see Section 2.5)

x_m = 8.03 ft

For 0° ≤ ϕ ≤ 45° r_1 = constant = $x_m \sin \pi/N$ = (8.03) (.09802) = .8750 ft

For 45° ≤ ϕ ≤ 90° the procedure of the flat type is followed.

Table 4.1.5 - Values of r_1 vs ϕ (45° ≤ ϕ ≤ 90°) for a Conical Ring Slot Canopy

①	②	③	④	⑤	⑥	⑦	⑧
ϕ	b (Ft)	x (Ft)	x sin π/N	tan $\alpha/2$	α	sin α	r_1 (Ft)
	Measured from Figure 2.5.1	See Table 2.5.1	.09802 ③	② / ④			④ / ⑦
45°	.3704	6.924	.6787	.5458	57° 15'	.8410	.7869
50	.4080	7.206	.7063	.5776	60° 02'	.8663	.7952
60	.4574	7.663	.7511	.6090	62° 41'	.8885	.8244
70	.5272	7.982	.7824	.6738	67° 57'	.9269	.8231
80	.6143	8.171	.8009	.7670	74° 58'	.9658	.8088
90°	.6579	8.234	.8071	.8151	78° 22'	.9795	.8036

e) Personnel Guide Surface Canopy (N = 24, β = 30°, l_c = 13.857 ft, l_s = 30 ft, l_c/l_s' = .42687) (see Section 2.4).

x_m = 9.506 ft

For 0 ≤ ϕ ≤ 45° r_1 = constant = $x_m \sin \pi/N$ = (9.506) (.13053) (1.117) = 1.3794 ft

For 45° ≤ ϕ ≤ 90° the procedure of the flat type is followed.

Table 4.1.6 - Values of r_1 vs ϕ ($45° \leq \phi \leq 90°$) for a Personnel Guide Surface Canopy

①	②	③	④	⑤	⑥	⑦	⑧
ϕ	b (Ft)	x (Ft)	x sin π/N	tan $\alpha/2$	α	sin α	r_1 (Ft)
	Measured from Figure 3.4.3	See Table 3.4.1	.13053 ③	② / ④			④ / ⑦
45°	.4278	7.994	1.0435	.4100	44° 36'	.7022	1.4860
50	.4754	8.320	1.0860	.4378	47 18	.7349	1.4778
60	.6338	8.846	1.1547	.5489	57 32	.8437	1.3686
70	.7606	9.215	1.2028	.6324	64 37	.9035	1.3313
80	.8715	9.434	1.2314	.7077	70 34	.9430	1.3058
90°	.9349	9.506	1.2408	.7535	74° 00'	.9613	1.2908

The arc length of Taylor's curve from $\phi = 45°$ to $\phi > 45°$ is given by the expression $\int_{45}^{\phi} ds$ which is equivalent to

$$\frac{x_m}{\sqrt{2}} \left[\int_0^{\cos^{-1}\sqrt{.7071}} \frac{dt}{\sqrt{1 - \frac{1}{2}\sin^2 t}} - \int_0^{\cos^{-1}\sqrt{\sin\phi}} \frac{dt}{\sqrt{1 - \frac{1}{2}\sin^2 t}} \right]$$

The arc length of the cords for the flat, extended skirt, ring slot and personnel guide surface canopies from the apex to $\phi = 45°$ is (.8324 x_m) (1.1117) or .9254 x_m (see first term of right hand member of Equation (1.5.7)).

Therefore the length s of the cord curves for the above four canopies is

$$s = x_m \left[.9254 + \frac{1}{\sqrt{2}} \int_0^{\cos^{-1}(\sqrt{.7071})} \frac{dt}{\sqrt{1 - \frac{1}{2}\sin^2 t}} - \frac{1}{\sqrt{2}} \int_0^{\cos^{-1}(\sqrt{\sin \phi})} \frac{dt}{\sqrt{1 - \frac{1}{2}\sin^2 t}} \right] \qquad (4.1.6)$$

But $\frac{1}{\sqrt{2}} \int_0^{\cos^{-1}\sqrt{.7071}} \frac{dt}{\sqrt{1 - \frac{1}{2}\sin^2 t}} = .4155$ (elliptic integral of first kind); then

Equation (4.1.6) becomes:

$$s = x_m \left[1.3409 - \frac{1}{\sqrt{2}} \int_0^{\cos^{-1}\sqrt{\sin \phi}} \frac{dt}{\sqrt{1 - \frac{1}{2}\sin^2 t}} \right] \qquad (4.1.7)$$

Table 4.1.7 gives the values of s for the above four canopy types for several values of ϕ.

Figure 4.1.2 shows the variation of cloth stresses vs s for five canopy types. For the conical canopy, curves are plotted for both approximations.

Figure 4.1.2 shows that cloth stresses are very nearly constant for all except the conical canopy and the extended skirt canopy. The cusp indicated by the second approximation seems improbable, and results from the assumed variation of cord tension (see Section 1.8 and Figure 1.12.1). The first approximation probably gives a better indication of the actual variation of both cord tension and cloth stress. The sudden change of stress in the extended skirt canopy is at $\phi = 45°$, and suggests that this is not a good choice of transition point (Section 1.4) for this canopy, or that α_m should have been assumed to be less than $\pi/2$ for this canopy in calculating the shape of the upper portion (Section 1.5).

Table 4.1.7 - Values of s vs ϕ for T-7, T-10, Ring Slot, and Personnel Guide Surface Canopies

①	②	③	④	⑤	⑥	⑦
ϕ	$\sin\phi$	$\sqrt{\sin\phi}$	$\cos^{-1}\sqrt{\sin\phi}$	$\int_0^{\cos^{-1}\sqrt{\sin\phi}} \frac{dt}{\sqrt{1-\frac{1}{2}\sin^2 t}}$	⑤ $/\sqrt{2}$	1.3409 - ⑥
45°	.7071	.8409	32.767°	.5876	.4155	.9254
50	.76604	.8752	28.930°	.5158	.3647	.9762
60	.86603	.9306	21.470°	.3792	.2681	1.0728
70	.93969	.9694	14.214°	.2495	.1764	1.1645
80	.98481	.9924	7.055°	.1233	.0872	1.2537
90°	1.0000	1.0000	.000°	.0000	.0000	1.3409

	$s = x_m$ ⑦ (Ft)			
ϕ	T-7	T-10	Ring Slot	Personnel Guide Surface
	9.13 ⑦	11.08 ⑦	8.23 ⑦	9.506 ⑦
45°	8.449	10.253	7.616	8.797
50	8.913	10.816	8.034	9.280
60	9.795	11.887	8.829	10.198
70	10.632	12.903	9.584	11.070
80	11.446	13.891	10.318	11.918
90°	12.242	14.857	11.036	12.747

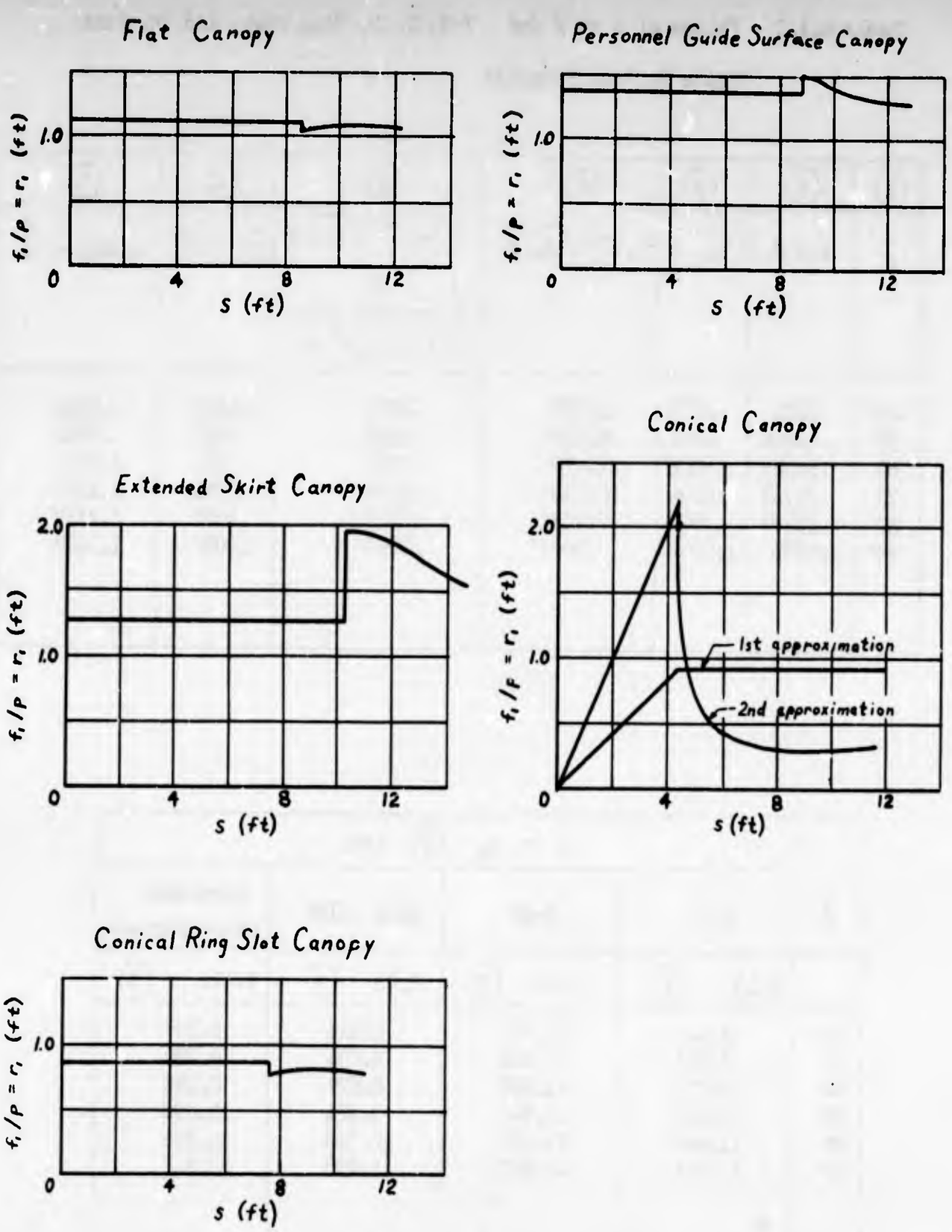

Figure 4.1.2 - Variation of Cloth Stresses with Distance from the Apex for Five Canopy Shapes

4.2 Effect of Cloth Stress in Straight and Bias Gores

In Figure 4.2.1 values of the ratio σ_1/σ_2 as given by Haas' equation (Reference 13, pages 156 - 158):

$$\tan \alpha \tan \beta = \sigma_1/\sigma_2 \qquad (4.2.1)$$

are given as functions of α for various values of β. (Here, β and α are defined in Figure 4.2.1). Haas' equation is a relationship between the shear rotation of the warp and fill threads and the directions and magnitudes of the principal stresses. This relationship satisfies both statics and the assumption of pure tension in the threads. Of particular interest are the curves $\beta/\alpha = \infty$ and $\beta/\alpha = 1$, corresponding in a parachute canopy approximately to straight and bias gore construction, respectively. The first corresponds to $\alpha = 0$, so that the warp threads are parallel to σ_2, the minimum principal stress, and the fill threads are parallel to σ_1 (assuming a one-piece gore). Figure 4.2.1 shows that $\sigma_2 = 0$, so that the fill threads take all the stress. When $\alpha = \beta$, on the other hand, σ_1/σ_2 may have any value, depending on β. If the elongation of the cord lines and threads is neglected, there can be no shearing deformation, so $\alpha = \beta = \pi/4$, since θ, the original bias angle, is 45°. (Note: In practical canopies, θ may be π/N in straight gores and $\pi/4 \pm \pi/N$ in bias gores for economy reasons.)

For this case, it is seen from Figure 4.2.1 that, $\sigma_1/\sigma_2 = 1$; i.e., there are equal stresses in all directions, and

$$\sigma_w = \sigma_f = \sigma_1 = \sigma_2 \qquad (4.2.2)$$

If σ_1 is the same for both the straight and bias gores, there is no difference in the maximum stresses for the two types of construction.

If, however, some deformation does take place, α and β remain equal but decrease, so that σ_1/σ_2 decreases, which means σ_2 increases if σ_1 remains constant. If the state of stress were uniaxial, as in the straight gore case, it can be seen that $\sigma_1/\sigma_2 \to \infty$ and $\alpha = \beta \to \pi/2$; i.e., the warp and fill threads tend to become parallel. In this situation the bias construction would have twice the strength of straight construction, assuming equal strengths in warp and fill. Of course, this does not happen, and would be prevented by thread jamming in any case; but it suggests that the true state of stress and strain is between the two conditions described. If β could be determined by experimental means, the true values of σ_1, σ_2, σ_w' and σ_f' could be found readily.

As an example, suppose β is 50° (apparently $\theta - \beta$ is small). Then $\sigma_1/\sigma_2 = (1.1918)^2 = 1.422$. From Haas' relations, it can be shown that

$$\sigma_f' = \sigma_1 \cos\beta / \sin\alpha = 2 \sin\beta / \cos\alpha \qquad (4.2.3)$$

$$\sigma_w' = \sigma_1 \cos\alpha / \sin\beta = 2 \sin\alpha / \cos\beta$$

where σ_f' and σ_w' are the fill and warp stresses after the threads have rotated.

When $\alpha = \beta$, these reduce to

$$\sigma_f' = \sigma_w' = \sigma_1 \cot\alpha = \sigma_2 \tan\alpha \qquad (4.2.4)$$

Then with $\beta = 50° = \alpha$,

$$\sigma_f' = \sigma_w' = .839\ \sigma_1 \qquad (4.2.5)$$

so that the stress is decreased 16% if this amount of deformation takes place. More important than this, however, are energy considerations. Parachute failures occur during opening, when the loading is unquestionably dynamic. Now, the energy

absorption capacity of a material is a function not only of its strength but of the volume of the stressed material. In a bias-construction, assuming the same cloth is used, approximately $2/\sqrt{2} = 1.41$ times as many threads are loaded in each gore as in the corresponding straight gore (disregarding conditions near the skirt). Furthermore, the length of each thread, even if the gore angle is small enough to be disregarded, is about 41% longer than the circumferential threads in a straight gore, making the total stressed volume at least twice as great as in the straight gore. Examination of a typical unit area leads to the same conclusion. Even with no shearing deformation, therefore, the bias gore can absorb twice the energy which the straight gore can, since

$$U = \frac{\sigma^2}{2E} \cdot (\text{volume}) \qquad (4.2.6)$$

If actual bias gores are not observed to be twice as strong as straight gores, this may possibly be explained by (1) stress concentrations at seams (stress concentrations are particularly important under dynamic loading), (2) what Coplan and Singer (Reference 14) have called "yarn angulation", i.e., the angle, θ_y, which a set of threads (e.g., warp) must make with the plane of the cloth in order to pass over and under the transverse set (e.g., fill). This latter disappears when the transverse set of threads is slack, but is always present in biaxially stressed cloth, and tends to increase the thread tension in proportion to $\sec \theta_y$. However, θ_y would have to be about 30° to reduce U by 25%. This requires a thread spacing of roughly 1.5 thread diameters, which would be a tight weave for parachute cloth.

Returning to consideration of the first item, the question which needs to be answered is whether stitched seams along the bias are relatively weaker in some

way than seams parallel to one set of threads. This question remains to be investigated.

No tests to investigate the influence of the biaxial stress ratio on the strength of parachute cloth seem to have been made. LaVier (Reference 21) carried his tests to failure, but the results have not been organized and it is not even clear whether failure occurred in the warp or in the fill. Biaxial tests on rubberized airship fabrics indicate that static strength is independent of the biaxial stress ratio (Reference 15); however, the presence of the rubber raises doubts about the applicability of these results to parachute cloth.

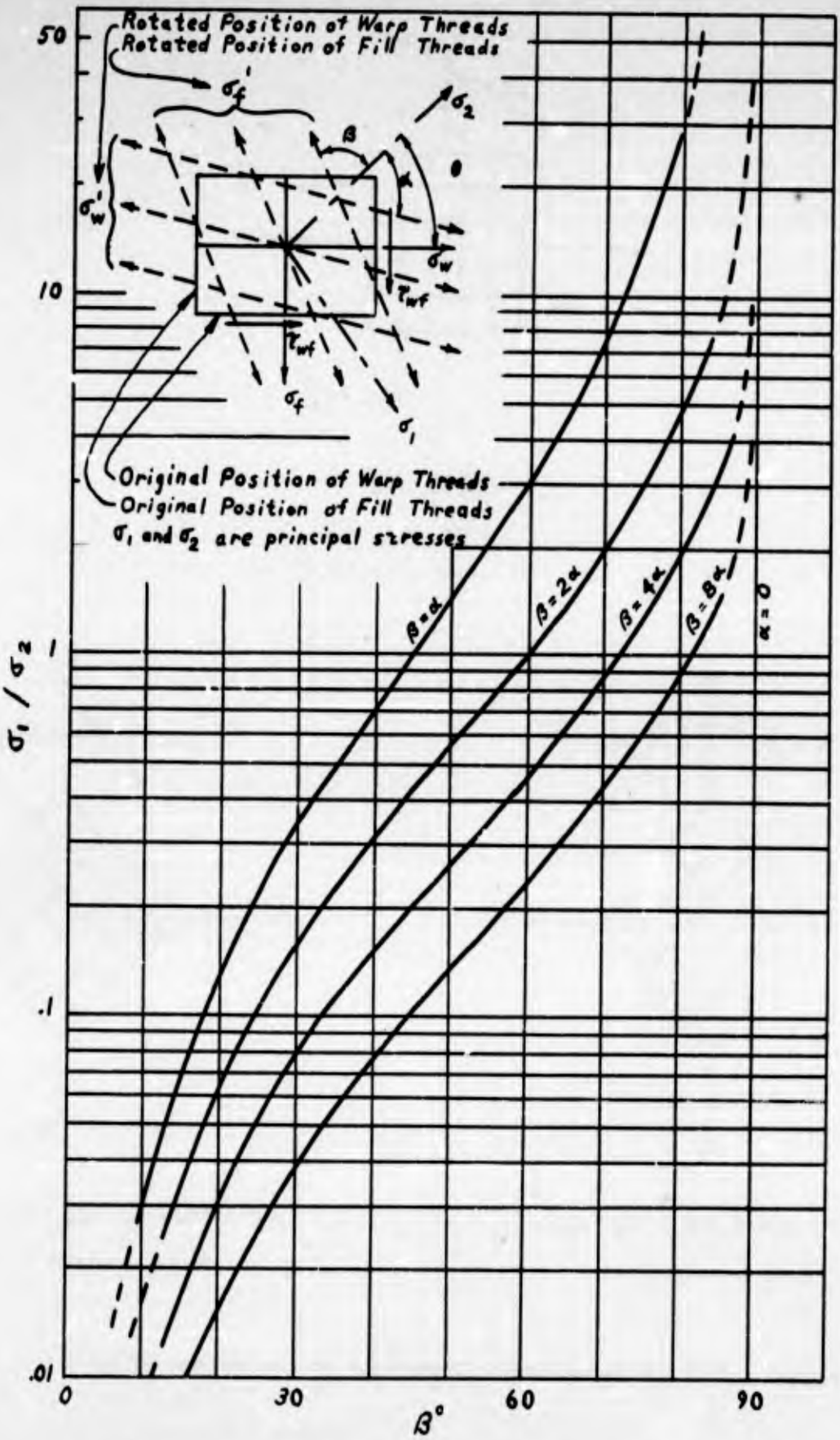

Figure 4.2.1 – Plots of tan α tan β = σ_1 / σ_2

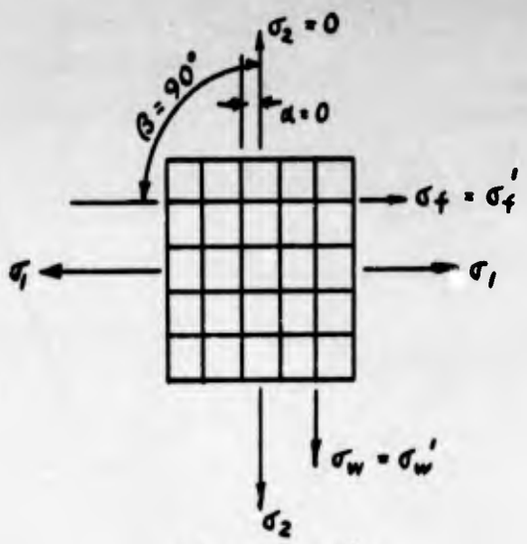

$\sigma_1 = \sigma_f = \sigma_f'$

$\sigma_2 = \sigma_w = \sigma_w' = 0$

Straight Construction

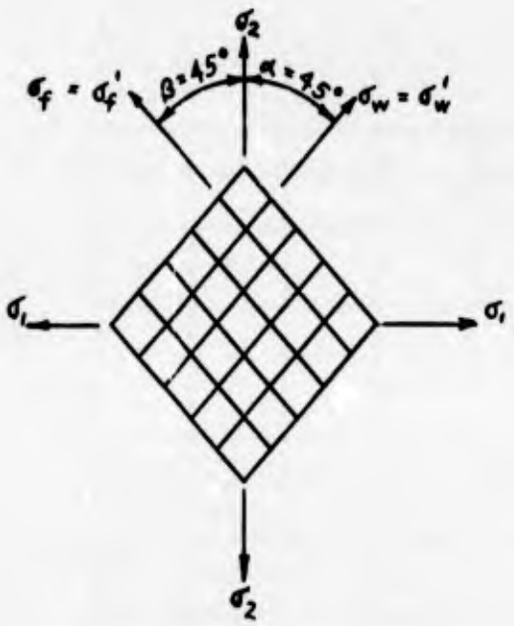

$\sigma_1 = \sigma_2 = \sigma_w = \sigma_w' = \sigma_f = \sigma_f'$

Bias Construction

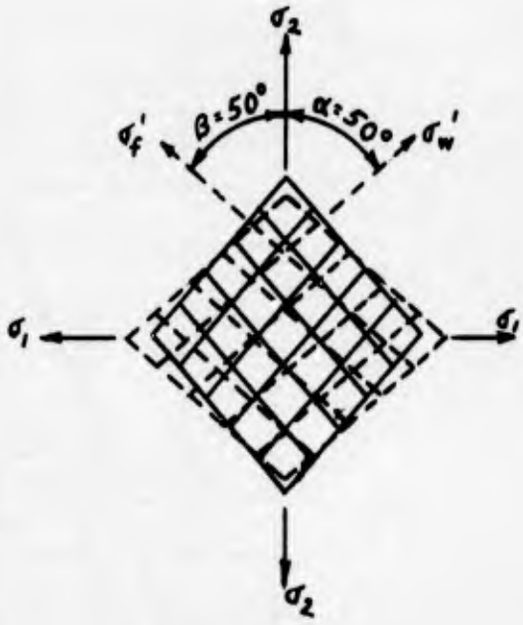

$\sigma = 1.422\,\sigma_2$; $\sigma_w' = \sigma_f' = .839\,\sigma_1$

Bias Construction

Figure 4.2.2 - Stress-Strain Conditions at Centerline of Gore

4.3 Experimental Determination of Stress-Strain Relations in Cloth and Fabric

While the present investigation is an analytical study, all physical theory ultimately must be based on experimental observations from which are formulated, more or less approximately, physical "laws". In stress analysis, one such fundamental and indispensable law is the relation between stress and strain, of which Hooke's law is the most important example. But until specific elastic constants are known, Hooke's law is merely a qualitative relationship. In this section, a few exploratory experiments are discussed.

Preliminary experiments on two specimens of a rip-stop nylon parachute cloth, in which the cloth was subjected to biaxial stress on the small tester shown in Figures 4.3.1 and 4.3.2, yielded the families of curves called normal characteristics by Haas (Reference 13), shown in Figures 4.3.4 and 4.3.5. Strains were measured with the U-shaped gage of Figure 4.3.3. The tests were carried only to about 50% of the quick-break strip-tensile strength of the cloth, but in this range, it is found that, in general, the test results fall within a narrow band which seems to be no wider than the scatter band of the test points for any one stress ratio. An exception to this may be indicated for the warp direction in Figure 4.3.4 where there seem to be two main branches: one for the three highest fill stress values and one for the three lowest. If data at higher warp stresses were available, however, it is quite possible that this feature of the curves would turn out to be merely an accident of scatter, since the corresponding curve of Figure 4.3.5 does not exhibit this duality. It is noticeable, however, that there is more difference in the warp curves than in the fill curves for both specimens.

These curves are, in one important respect, unlike other normal characteristics for fabric which have so far been published. Figure 4.3.6 shows the normal characteristics for an airship envelope fabric, which is similar to existing published data for airship fabrics and doped airplane fabrics. An elastic isotropic material would give a family of curves similar to Figure 4.3.6 but straight, parallel, and equally spaced for equal increments of the "fill" stress. The spacing would be proportional to the Poisson's ratio of the material. If, then, the spacing between curves is small as in Figures 4.3.4 and 4.3.5 the effective Poisson's ratio for the cloth in question is small, and in fact can perhaps be taken as zero for practical purposes (except perhaps for uniaxial states of stress). This is a very significant thing from the point of view of the stress analyst, and will need some verification.

There are four possible theoretical reasons why the results differ in this respect from airship and airplane fabrics. First, the airship fabric has a bias ply — one at 45° with the other plies (though there may be some question as to its effectiveness in biaxial test using cruciform specimens such as were used here); secondly, it has a coating of neoprene (or dope in the case of airplane fabric); thirdly, the parachute cloth is a relatively loose and open weave; fourthly, the parachute cloth is nylon rather than cotton or linen. Since linen airplane fabric having no bias ply gives curves similar to Figure 4.3.6 (Reference 16), neither the first nor the fourth factor appear to be the significant ones. To investigate the third factor, a strong, tightly woven nylon-tow-target fabric was tested, with, however, inconclusive results (Figure 4.3.4 and 4.3.5), inasmuch as the capacity of the tester was only great enough that the specimen could be stressed to about one-tenth of its ultimate strength. The scatter at low

stresses is believed to be greater that at high stresses.

On the other hand, the peculiar results may be a result of experimental inaccuracy. Parachute cloths are much lighter than airship fabrics, and methods of strain measurement which are satisfactory for the latter may be completely unsatisfactory for the former. Most strain gages, including that of Figure 4.3.3 (which incidentally is similar in principle to that described by LaVier in Reference 21), remove some load from the tested material in order to produce a small elastic deformation which is measured either electrically, as in the present case, or by some mechanical means. If, in a pin-type gage, the force which deflects the gage is appreciable compared with the total carried by a strip of material of a certain width (difficult to estimate) between the points of the gage, the gage affects the deformation of the material in the vicinity of the gage. The gage reading then does not indicate the state of strain in the undisturbed material.

To investigate the accuracy of the pin-type gage, strains in uniaxially-loaded, four-inch wide strips were measured by three methods: (1) the pin-type gage; (2) calipers; and (3) a roller-type elongation indicator (Figures 4.3.9 and 4.3.10). A six-inch gage length was used with methods (2) and (3). The results are shown in Figures 4.3.11 through 4.3.13 and revealed that the pin-type gage used is unsuitable for parachute cloth, although comparatively accurate for airship fabrics. While longer legs and thinner metal in the U (.010 in. was used in this instance) would improve accuracy, no such gage should be used without checking its accuracy with the lightest material to be tested.

The curves of Figures 4.3.4 and 4.3.5, in the light of these facts, cannot be accepted at their face value, and the question of biaxial stress-strain relations in parachute cloth must await development of better experimental techniques.

In this connection, it perhaps needs to be pointed out that when strains are applied at the jaws of the testing machine in an arbitrarily fixed ratio, as done by LaVier (Reference 21) and by Woo and Montgomery (Reference 22), the relations which are obtained apply only for a single stress ratio which is not controlled and probably is not even constant during the test, so that the results have little value for analytical purposes. In Reference 21, strain gages are used so that even the strain ratio presumably is neither controlled nor constant. What is needed is data which can be plotted to obtain diagrams like those given by Haas (Reference 13) or alternatively, those suggested by Everling (Reference 23).

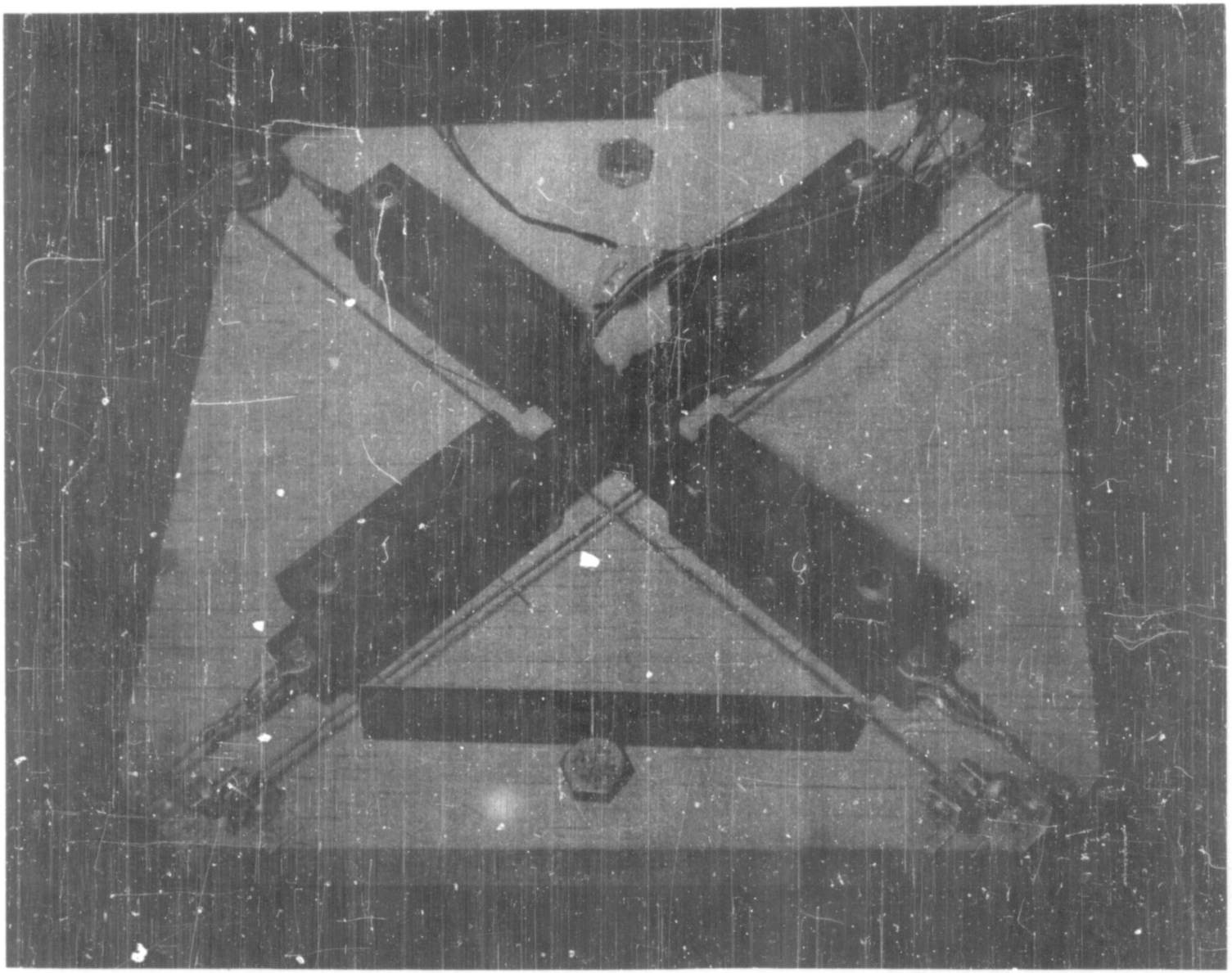

Figure 4.3.1 - Close up of GAC Small Biaxial Tester Used for Testing of Nylon Parachute Cloth

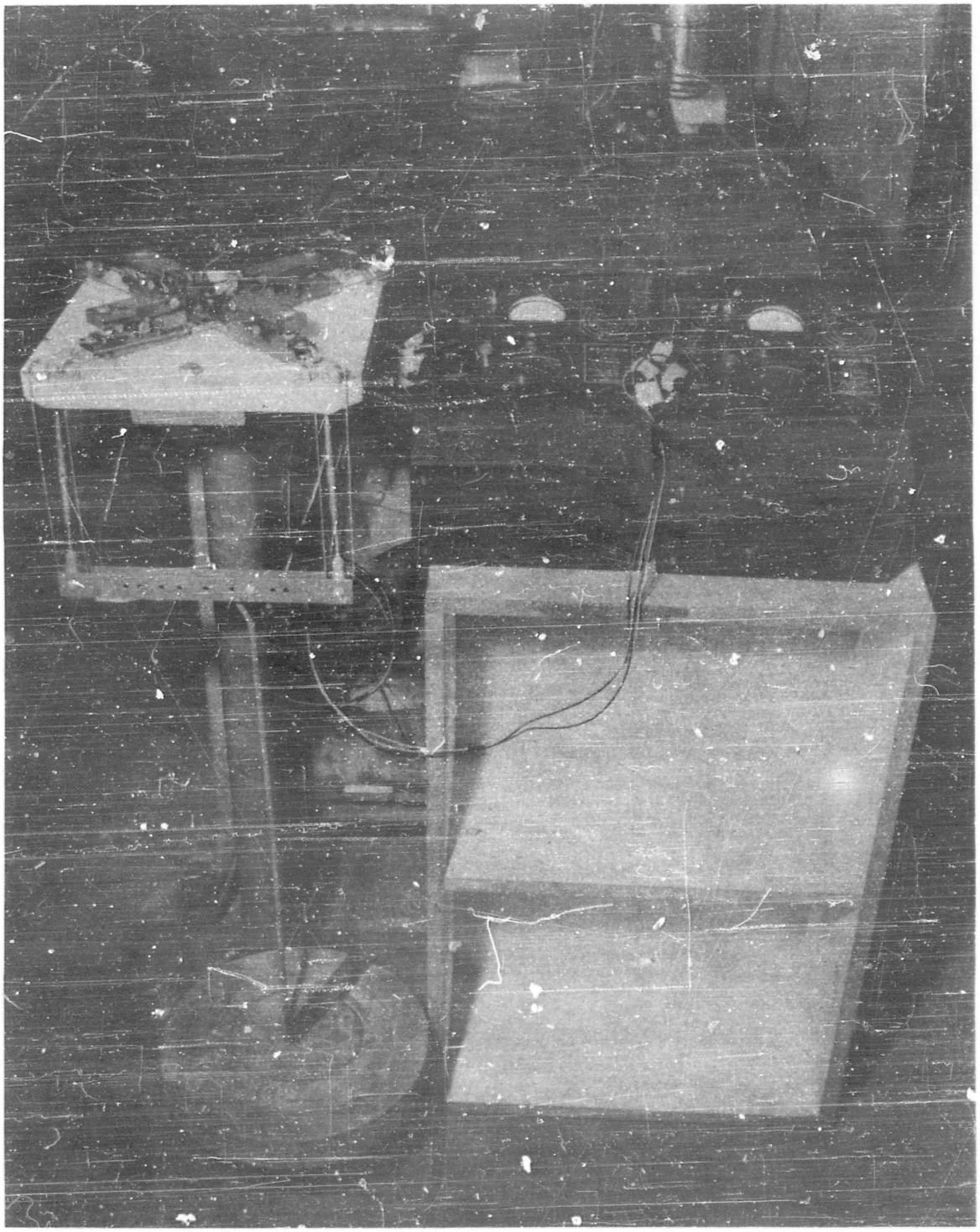

Figure 4.3.2 - GAC Small Biaxial Tester for Fabric and Its Allied Instrumentation

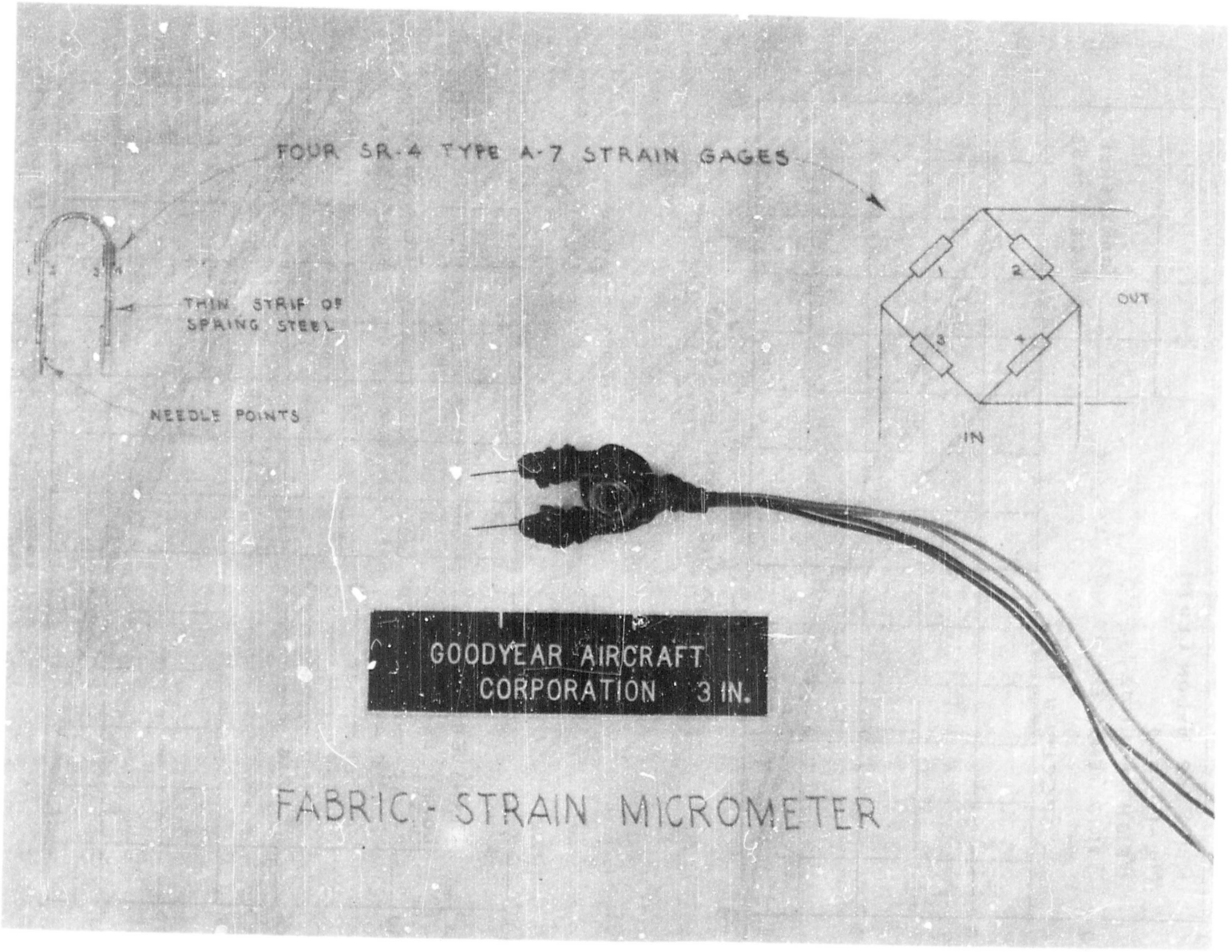

Figure 4.3.3 - GAC Fabric Strain Micrometer with Sketch Showing Construction and Operating Principles

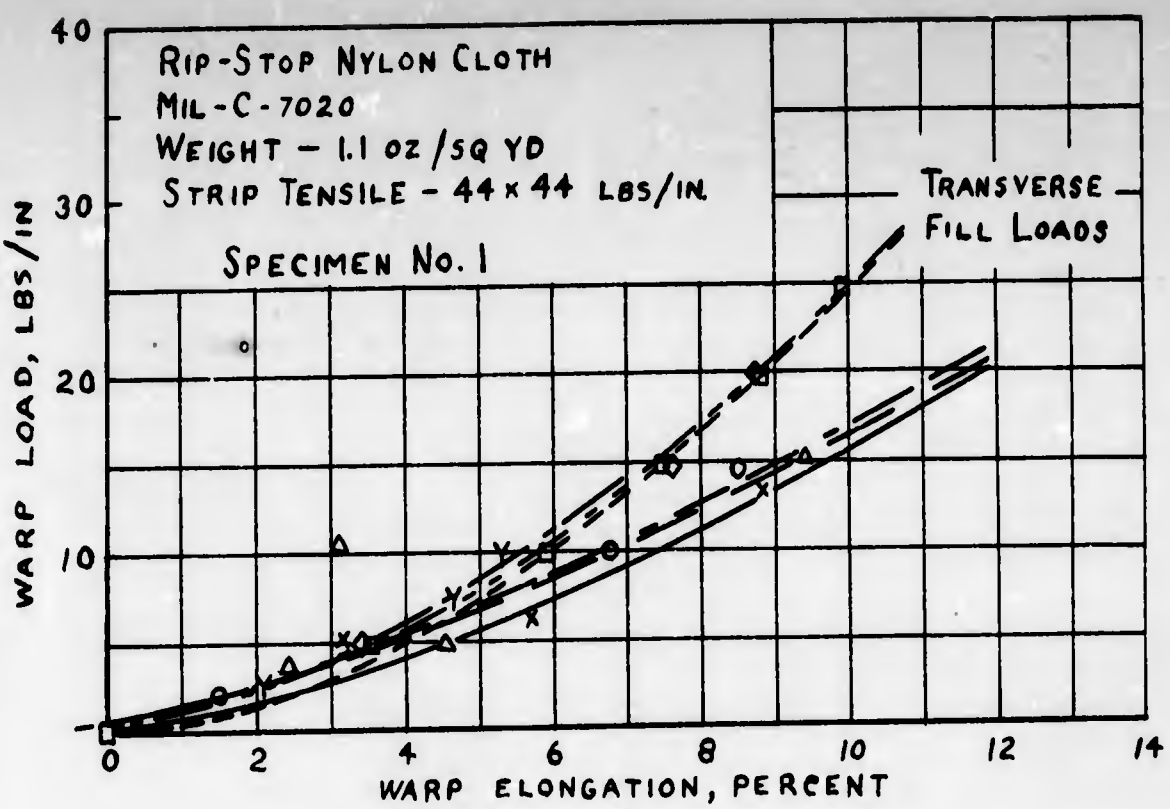

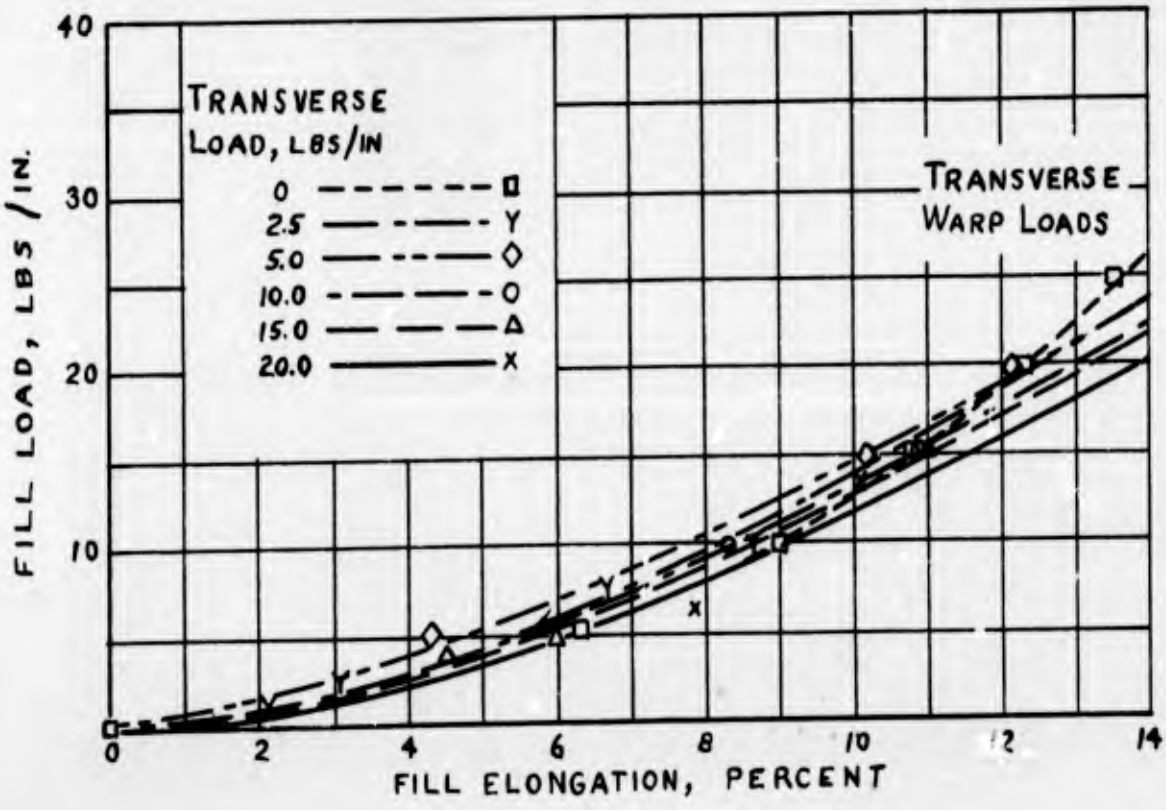

Figure 4.3.4 - Normal Characteristics of Rip-Stop Nylon Cloth

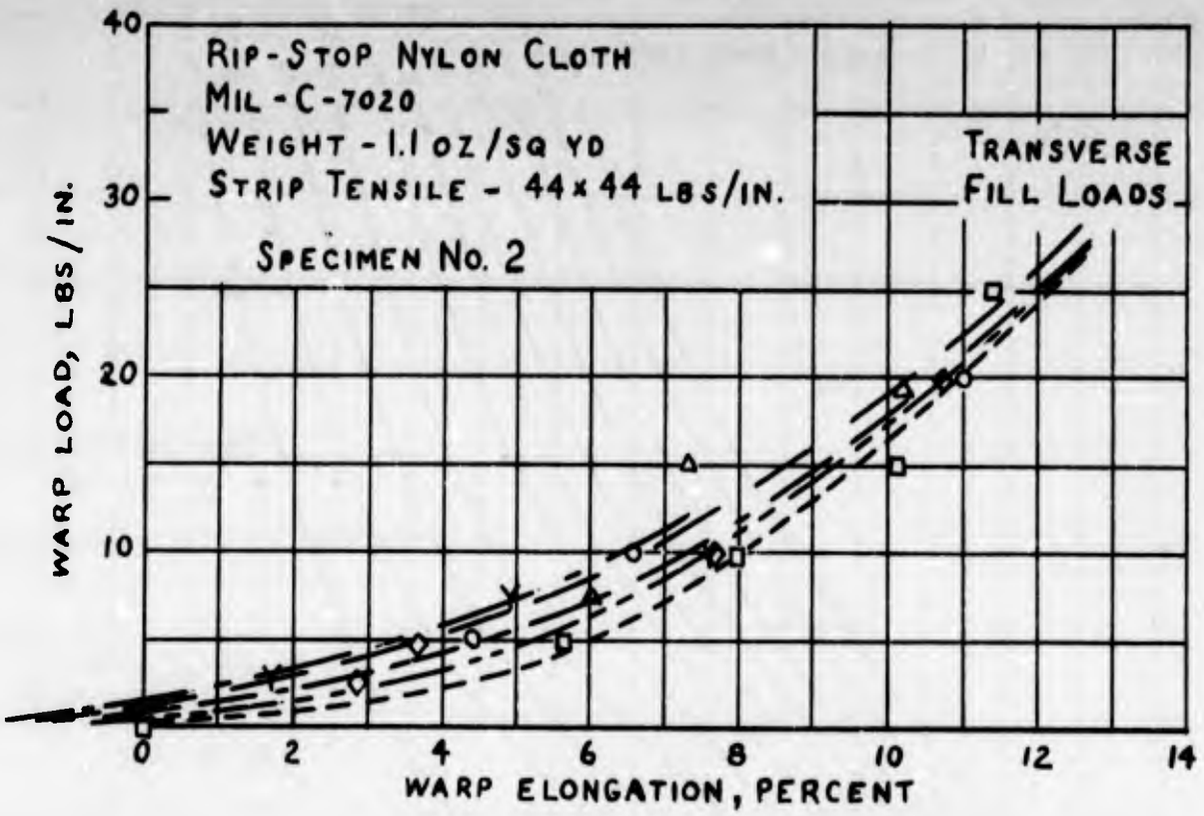

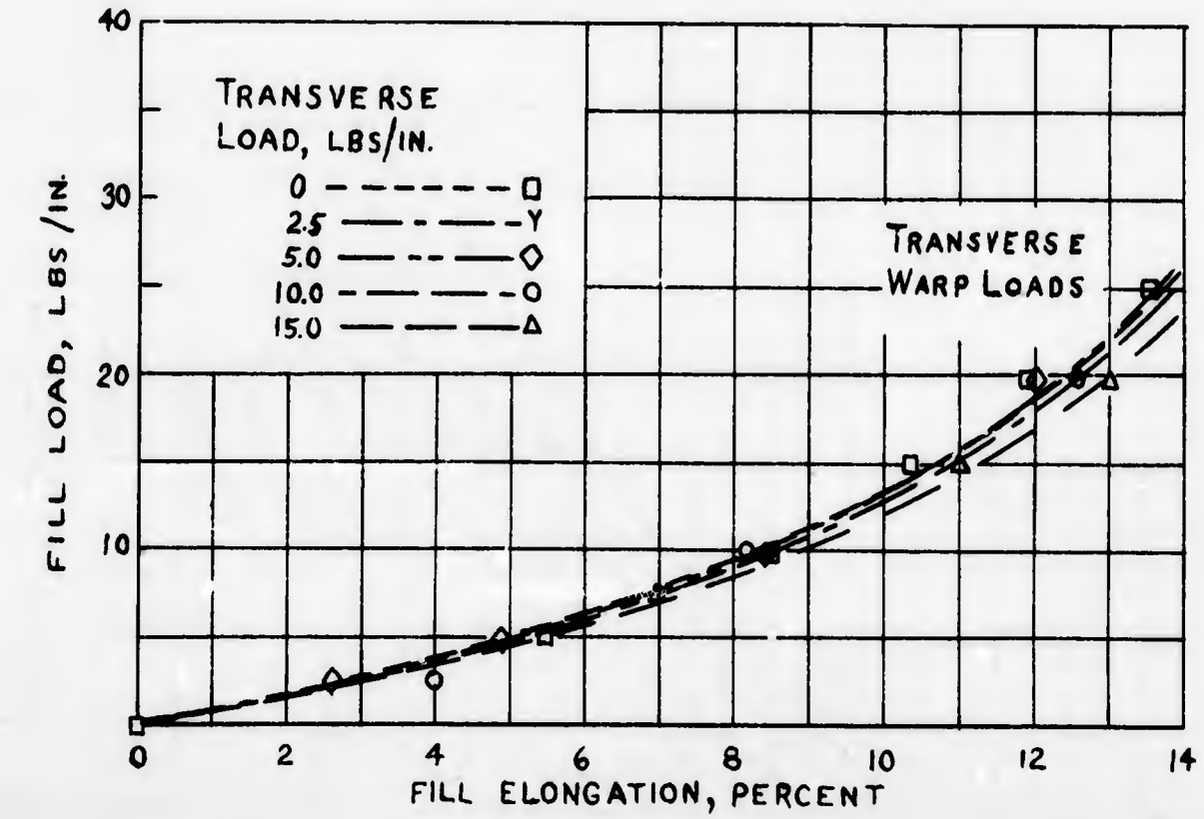

Figure 4.3.5 - Normal Characteristics of Rip-Stop Nylon Cloth

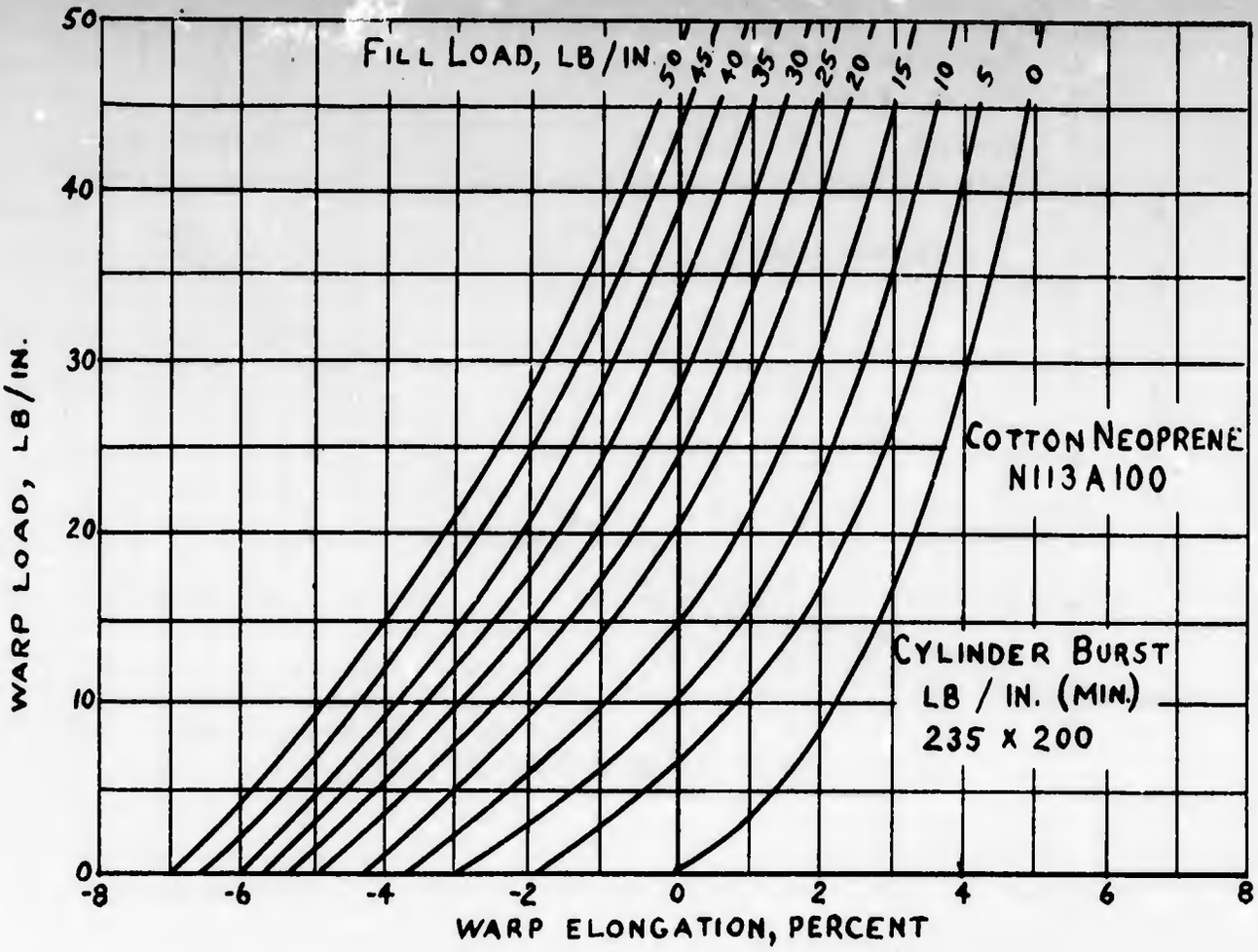

Figure 4.3.6 - Normal Characteristics of Cotton-Neoprene

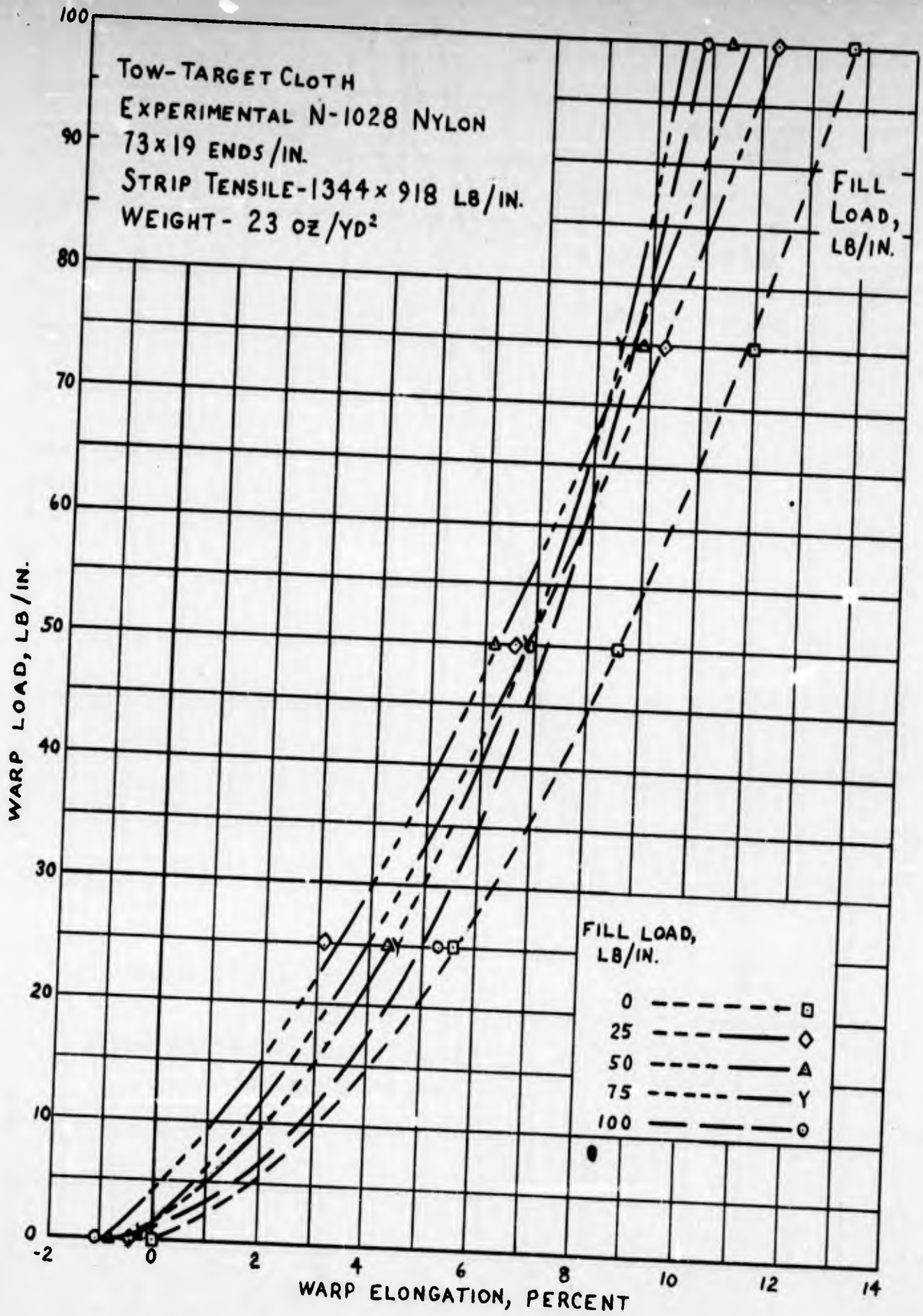

Figure 4.3.7 - Normal Characteristics of Tow-Target Cloth

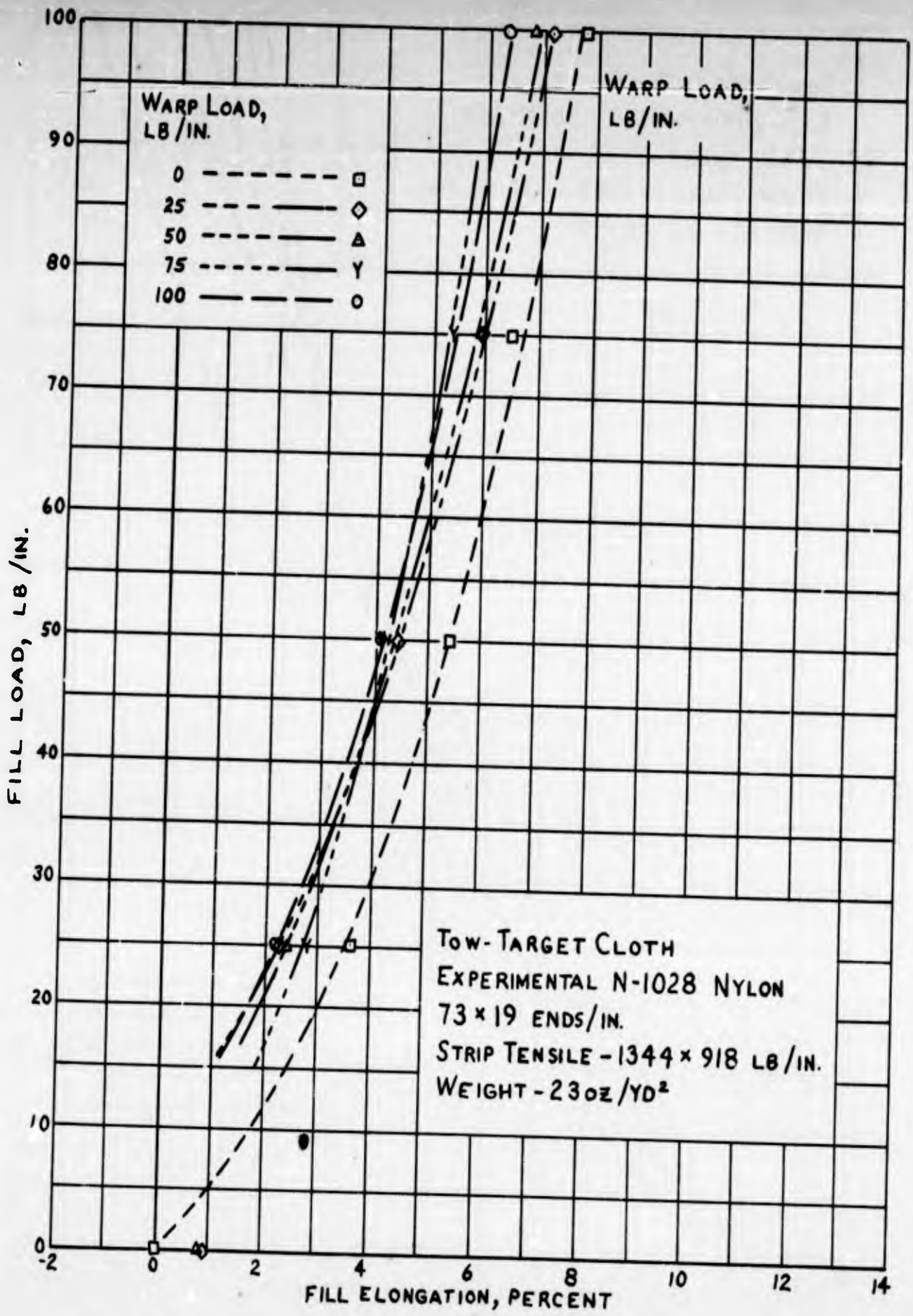

Figure 4.3.8 - Normal Characteristics of Tow-Target Cloth

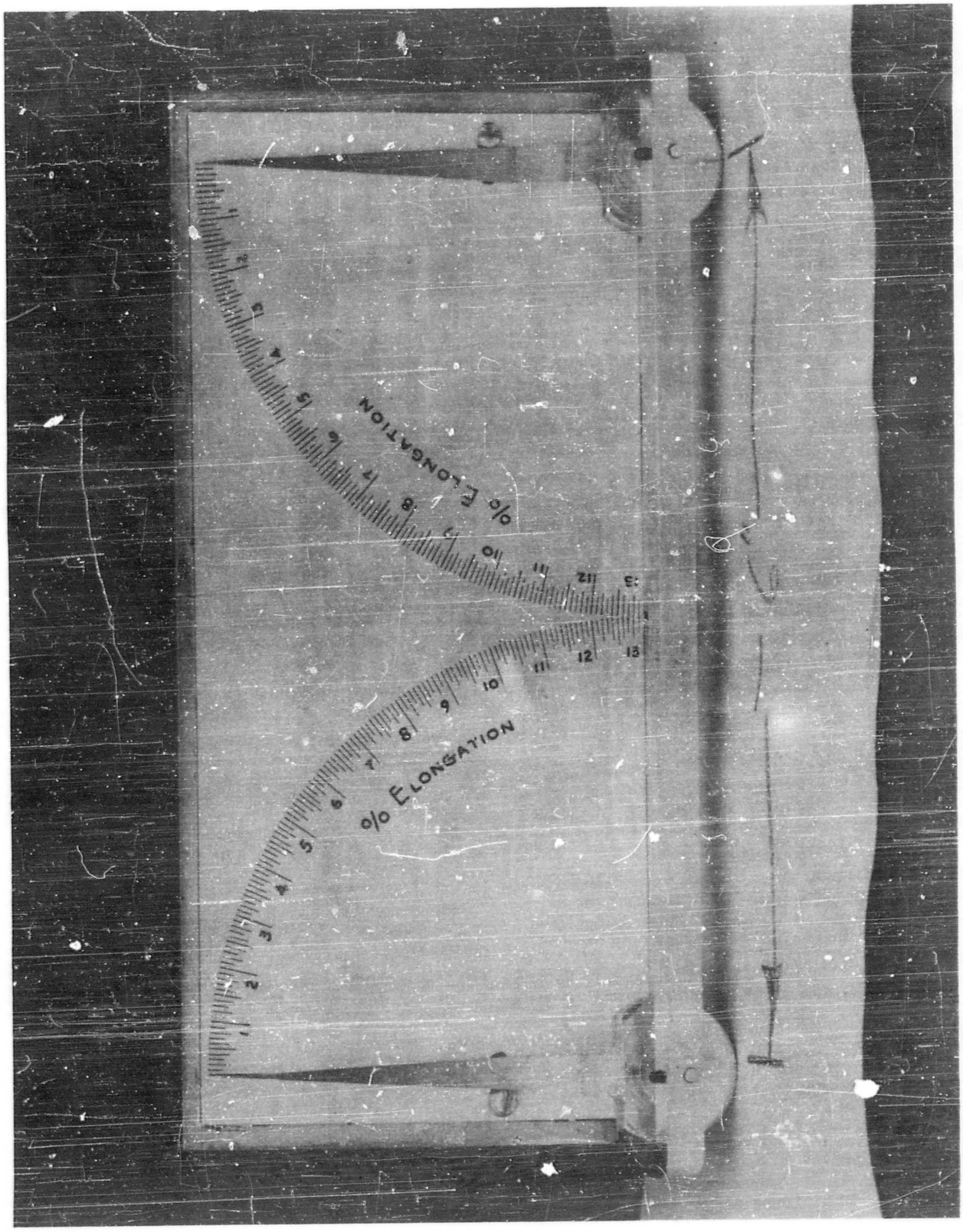

Figure 4.3.9 - Roller Type Elongation Indicator (RTEI)

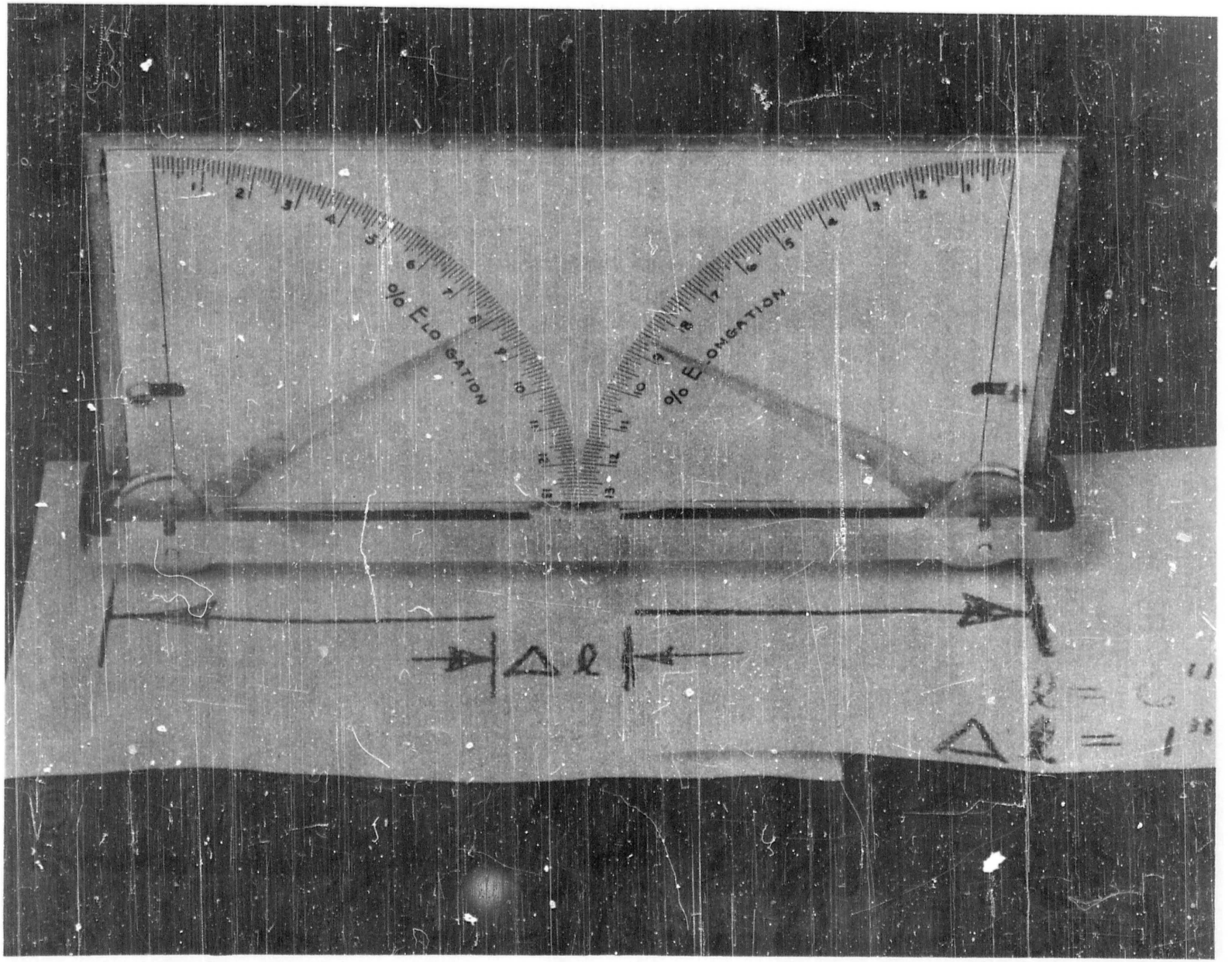

Figure 4.3.10 - Roller Type Elongation Indicator, Deflected

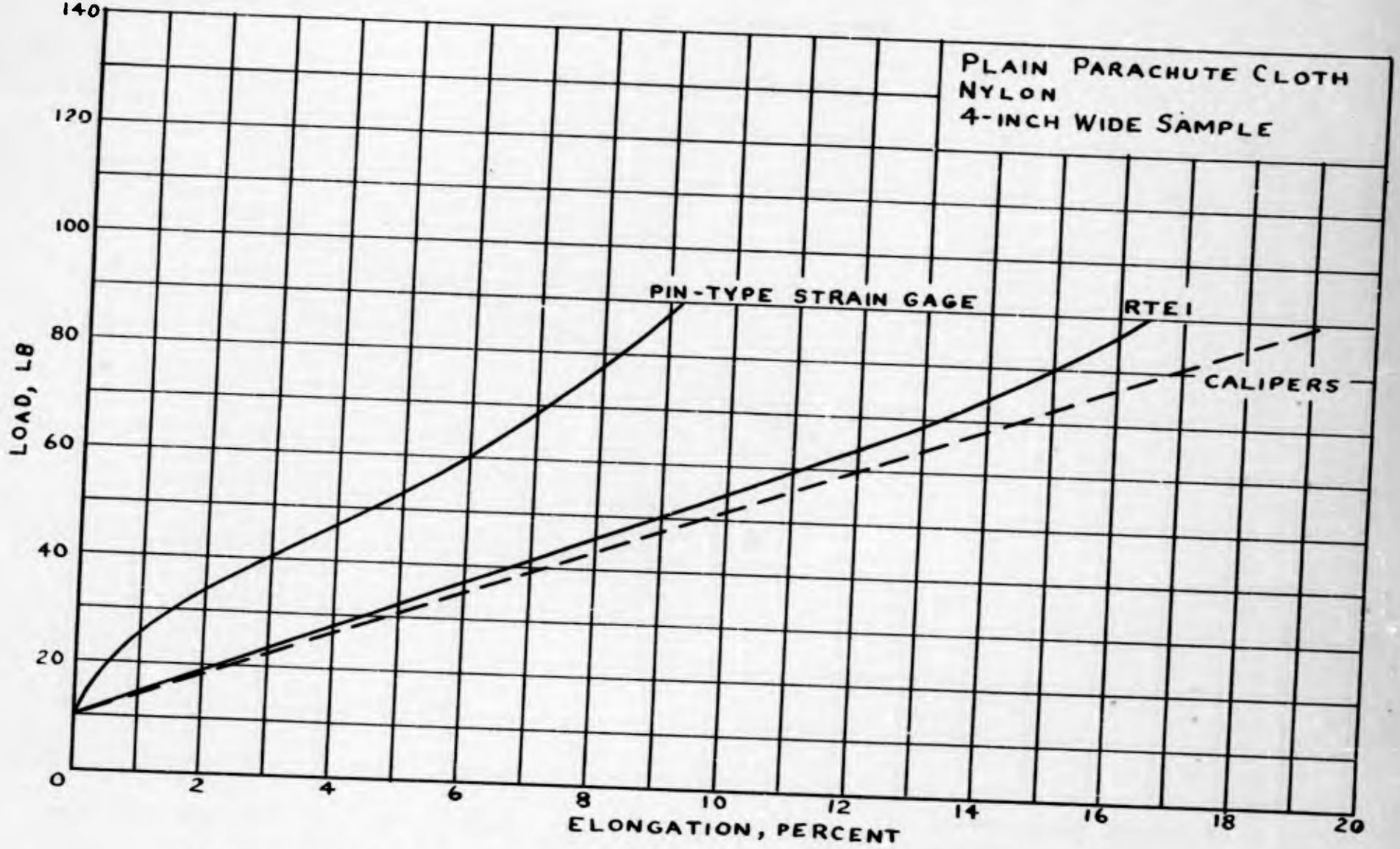

Figure 4.3.11 - Strain Measurements in Parachute Cloth

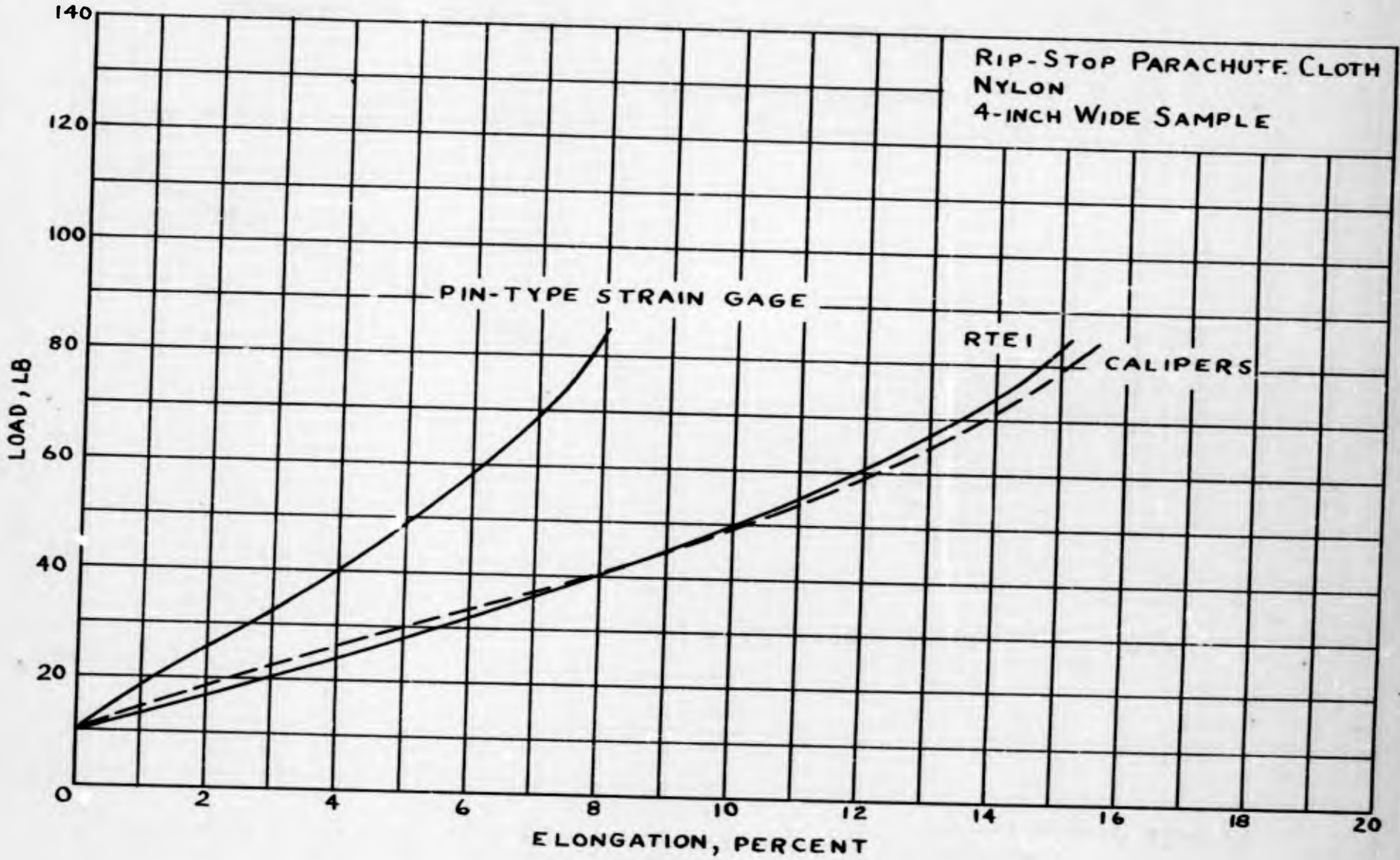

Figure 4.3.12 - Strain Measurements in Parachute Cloth

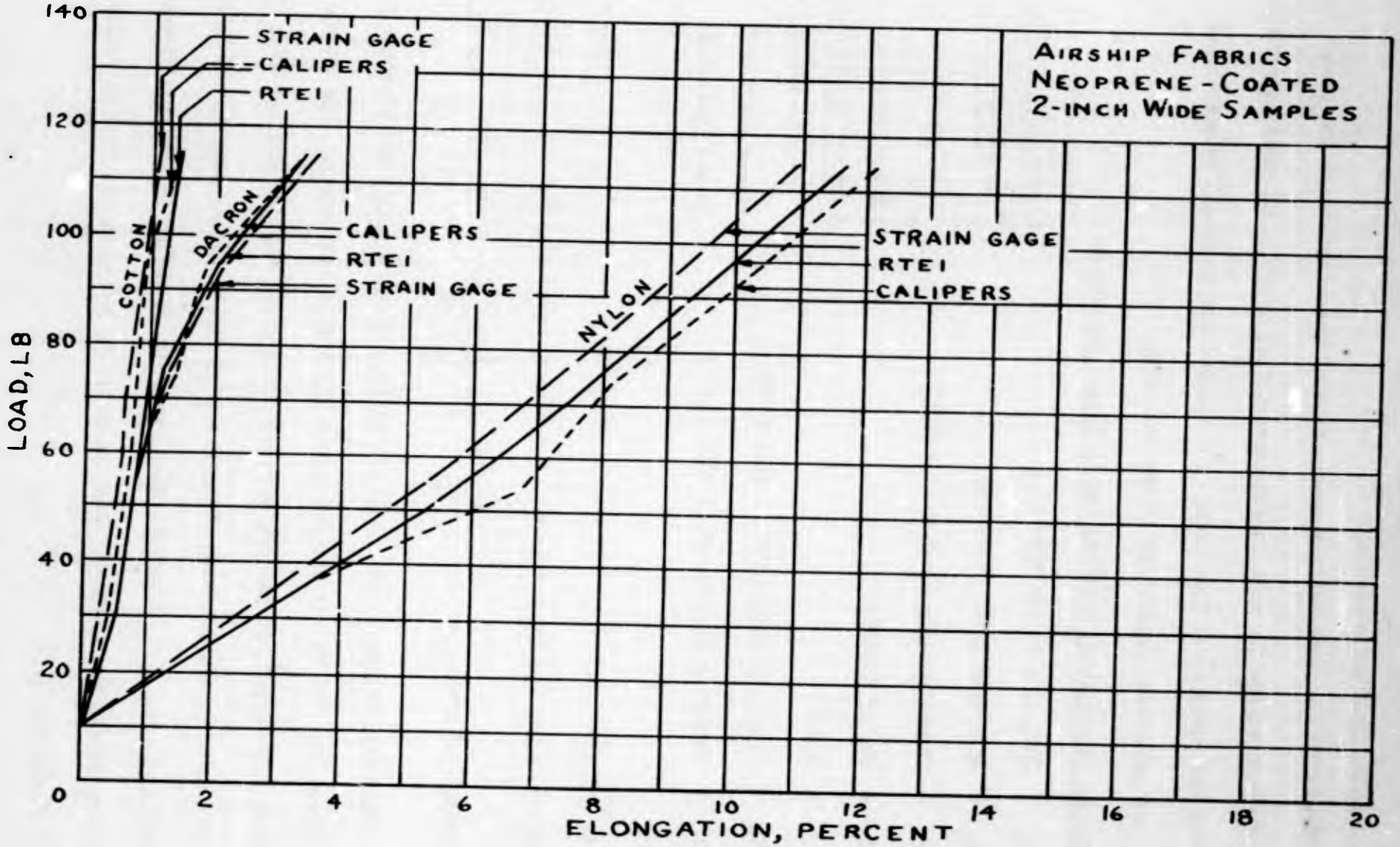

Figure 4.3.13 – Strain Measurement in Airship Fabrics

4.4 Effect of Cloth Stresses on Porosity

Stresses in a cloth cause a combination of thread extension and thread shear both of which change the size of the interstitial openings and thus change the geometry and porosity of the cloth. The changes due to thread extension and shear are calculated separately in the following.

Changes in Interstitial Openings Due to Thread Extension

Let A_1 = Open area before stressing

A_2 = Open area after stressing

a = Thread spacing (both warp & fill)

t = Thread Diameter

c = a - t

Δ_f = Strain in length "a" of fill threads

Δ_w = Strain in length "a" of warp threads

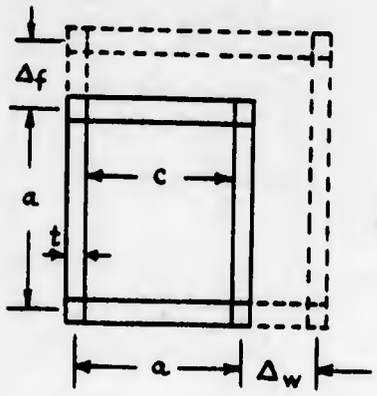

Figure 4.4.1
Thread Extension

Then

$$A_1 = c^2 \qquad (4.4.1)$$

$$A_2 = (c + \Delta_w)(c + \Delta_f) = c^2 + c(\Delta_w + \Delta_f) + \Delta_w \Delta_f \qquad (4.4.2)$$

$$\text{Percentage of areal increase} = \frac{A_2 - A_1}{A_1} 100 = \left[\frac{\Delta_w + \Delta_f}{c} + \frac{\Delta_w \Delta_f}{c^2}\right] 100 \qquad (4.4.3)$$

Numerical values to use in Equations (4.4.1) and (4.4.3) are obtained from Reference 17. The values are for sample 2E, a mock leno weave. This sample weighed 1.92 oz/yd^2, it had 104 warp threads and 112 fill threads per inch (108 is used herein), the breaking strength was 53 lb/in. in the warp direction and 67 lb/in. in the fill direction. When loaded to 20 lb/in. in the warp direction the warp strain was 13.0% and when loaded to 20 lb/in. in the fill direction the fill strain was 8.7%.

For sample 2E: Assume the threads are square in cross-section. On the basis of one square yard of cloth:

Volume of void free cloth = t^2 (36) (108) (36) (2) = 280,000 t^2 cu. in.

Let the specific gravity of void free cloth material = 1.5, then the density = $(\frac{62.4}{1728})$ (1.5) = 0.0541 lb/in^3. Since one square yard weighs 1.92 oz.:

$$280{,}000\ t^2\ (.0541) = 1.92/16$$

or

$$t = 0.00281 \text{ in.}$$

$$a = 1/108 = .00925 \text{ in.}$$

$$c = a - t = .00684 \text{ in.}$$

Let $\Delta_w = 130a$, $\Delta_f = .0870$; this assumes that each deformation takes place independently of the other. Then from Equation (4.4.3) the percentage of areal increase is

$$\left[.217\ (a/c) + (.13)\ (.087)\ (a/c)^2 \right] 100 = 33.5\%$$

Let P_1 = percentage of open area before stressing

P_2 = percentage of open area after stressing

$$P_1 = (c/a)^2\ 100 = 48.5\%$$

Then

$$P_2 = \frac{c^2 + c(\Delta_w + \Delta_f) + \Delta_w \Delta_f}{(a + \Delta_w)\ (a + \Delta_f)}\ (100) = 52.7\%$$

If during a porosity test, stresses and strains of the order of magnitude of those assumed here were realized, there would be a noticeable increase in the porosity as is evidenced by the 33.5% areal increase. However, if the above were permanent, and if a subsequent porosity test were made, the increase in porosity would be small as is evidenced by the change in open area from 48.5% to 52.7%.

In parachutes, stresses as large as 20 lb/in. may occur during the opening phase, but during the steady state they may be less than 1 lb/in. For example, from Section 4.3 the maximum fabric stress in a conical canopy with N = 24, β = 30°, l_s = 22.83 ft, l_c/l_s' = .5339, and x_m = 7.57 ft is $f_1 = 8.9p$ where p is the differential pressure.

If the suspended weight is 200 lb, then $p = 200/\pi\,(7.57)^2 = 1.11$ lb/ft^2 and $f_1 = (8.9)\,(1.11/12) = 0.825$ lb/in. If equal strains are assumed in warp and fill directions and if it is assumed that stress and strain are proportional, then in the cloth above

$$\Delta_w = \Delta_f = \left[(13.0 + 8.7)/2\right](1/100)\,(.825/20)\,(a) = .00448\,a$$

Using Equation (4.4.3), the

$$\text{percentage of areal increase} = \left[2\,\Delta_w/c + (\Delta_w/c)^2\right]100$$

Thus in an inflated canopy in the steady state thread extension causes a negligible change in the porosity of the cloth.

Change in Interstitial Openings Due to Thread Shear

Add to the notation for thread extension γ_{wf} = angle of shear and

$k_1 = f/a$ (see Figure 4.4.2)

$A_1 = (a - t)^2$

$A_2 = (a \cos \gamma_{wf} - t)\,(a - t)$

$$\text{percentage of areal decrease} = \frac{A_1 - A_2}{A_2}\,100$$

$$= \frac{1 - \cos \gamma_{wf}}{1 - k_1}\,100$$

As an example let $k_1 = .00281/.00925 = .304$, and $\gamma_{wf} = 30°$

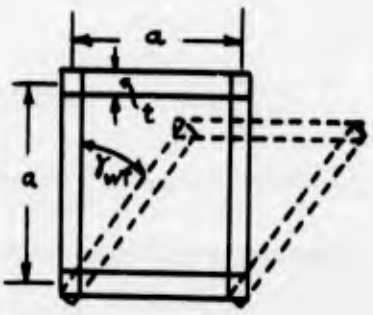

Figure 4.4.2
Thread Shear

Then percentage of areal decrease = 19.3%

P_1 = 48.5% as before

$$P_2 = \frac{k_f^2 - k_1 + (1 - k_1)\cos \gamma_{wf}}{\cos \gamma_{wf}} \; 100 = 45.3\%$$

Stress-strain conditions which result in γ_{wf} = 30% are shown in Figure 4.4.3; σ_1 and σ_2 are the maximum and minimum stresses respectively. Originally σ_1 and σ_2 were at 45° with the warp and fill threads. If $\sigma_1 = 3\,\sigma_2$, and if the strain conditions are such that points in the threads move parallel to principal stress directions, then γ_{wf} = 30° as shown. The equations for these conditions are:

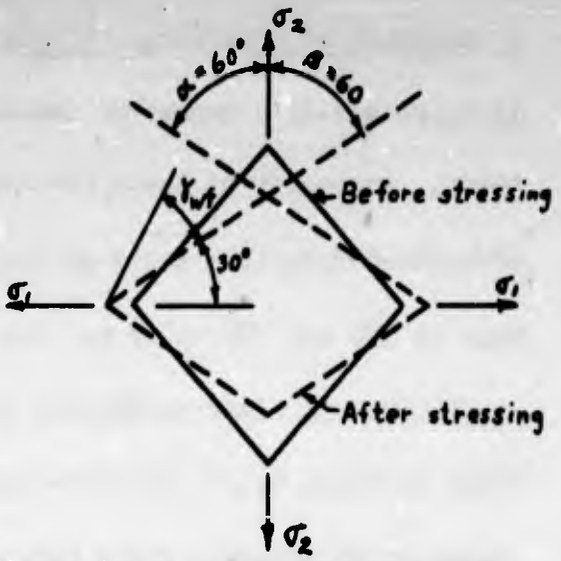

Figure 4.4.3 – Thread Shear with $\sigma_1/\sigma_2 = 3$

$$\cos \alpha / \cos \beta = \cot \theta \quad \text{(Reference 13)}$$

$$\tan \alpha \tan \beta = \sigma_1 / \sigma_2 \quad \text{(Reference 13)}$$

where α and β are angles between the warp and fill threads and σ_2 after thread shear while θ is their value before thread shear; in the example θ = 45°, $\alpha = \beta$ = 60°, $\gamma_{wf} = \alpha + \beta - 90 = 30°$.

As can be seen from the example of thread shear, the absolute magnitudes of the stresses do not affect the deformations, only the ratio of the principal stresses and their directions affect the shear deformations. It is likely then that thread shear would decrease the porosity of a cloth. Even though thread extension accompanies thread shear it is unlikely that increased open area due to thread extension would be large enough to nullify the decreased open area caused by thread shear in a canopy in the steady state. Since changes in porosity are mostly due to thread shear it is reasonable to expect larger changes in canopies with biased gores than with straight gores because thread shear is more predominant in the former.

Examination of Some Porosity Data

In Reference 11 a number of impact tests were made on parachutes on a whirling tower. Accompanying these tests were porosity tests on the canopy fabric and strength-deformation tests of the canopy lines. The whirling tower tests were made at 100 and 200 miles per hour with porosity tests of each panel of the canopy before and after each tower test. Porosity test data for one canopy are shown in Table 4.4.1 while the panel locations are shown in Figure 4.4.4. Examination of the data shows that no lasting changes in porosity are caused by the stresses attained in the whirling tests. In fact the variation in readings from test to test on an individual panel are much greater than the variation in the average values for a complete canopy. Furthermore the changes are erratic, some panels showing increases in porosity while others show decreases.

It had been hoped to obtain from examination of such data an indication of stress magnitudes and distributions, but clearly this is not possible.

Table 4.4.1 - Porosity Measurements on a Canopy of 1.1 oz. Nylon Rip-Stop Spec. MIL-C-7020 Type I. (Reference 26)

Panel No.	a			b			c		
	Speed MPH			Speed MPH			Speed MPH		
	0	100	200	0	100	200	0	100	200
1	108.0	108.9	104.4	82.4	82.4	80.0	105.3	103.5	104.4
2	119.7	125.1	120.6	99.8	96.8	93.7	117.0	113.4	117.9
3	128.4	127.6	125.1	133.2	134.7	93.7	97.9	100.7	117.9
4	110.7	103.5	112.5	109.8	112.5	112.5	115.2	113.4	107.1
5	103.5	97.9	100.7	107.1	109.8	108.9	122.4	132.4	129.2
6	78.8	78.8	82.4	77.6	81.2	80.0	92.6	92.6	91.5
7	94.7	98.9	94.7	92.6	90.4	88.3	90.4	87.1	89.4
8	81.2	88.3	85.9	109.8	115.2	109.8	115.2	114.3	114.3
9	97.9	97.9	96.8	94.7	98.9	107.1	84.7	87.1	83.5
10	89.4	88.3	89.4	95.8	96.8	94.7	90.4	89.4	89.4
11	93.7	91.5	90.4	90.4	88.3	90.4	87.1	82.4	81.2
12	93.7	89.4	92.6	87.1	92.6	90.4	90.4	93.7	92.6
13	100.7	107.1	105.3	99.8	91.5	98.9	111.6	111.6	108.0
14	108.9	103.5	106.2	97.9	96.8	98.9	108.9	108.9	108.9
15	110.7	110.7	106.2	110.7	108.0	117.1	111.6	107.1	113.4
16	102.5	103.5	106.2	112.5	113.4	111.6	111.6	109.8	108.0
17	111.6	109.8	108.0	101.5	97.9	107.1	95.8	88.3	92.6
18	106.2	105.3	103.5	80.0	81.2	90.4	104.4	105.3	101.6
19	107.5	96.8	98.9	95.8	93.7	95.8	78.8	78.8	76.4
20	90.4	90.4	92.6	120.6	124.2	121.5	117.9	126.0	122.4
21	112.5	120.6	115.2	82.4	81.2	83.5	105.3	110.7	108.0
22	109.8	109.8	108.9	93.7	97.9	103.5	112.5	112.5	103.5
23	123.3	122.4	120.6	118.8	122.4	122.4	110.7	109.8	107.1
24	84.7	83.5	82.4	131.6	122.4	116.1	106.2	105.3	103.5
Avg.	102.6	102.5	102.0	101.1	101.3	100.3	103.5	103.5	103.0

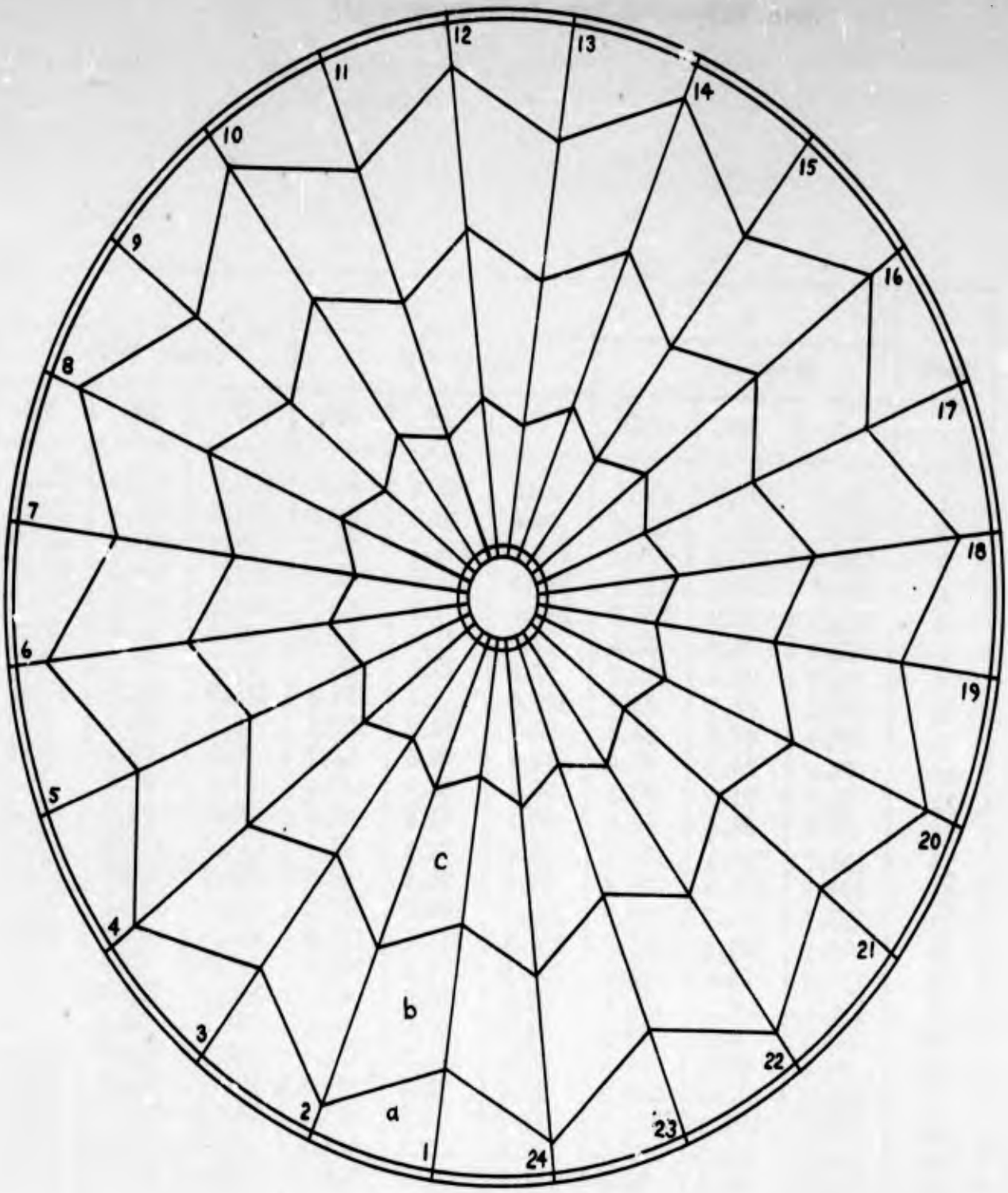

Figure 4.4.4 - Location of Panels for Canopy

Examination of Stresses Occurring During Porosity Tests

Cloth porosity tests are made with the cloth clamped between holders with circular openings. References 18, 19 and 20 give some results of numerous porosity tests of parachute cloths. A rather simple theory of cloth stresses occurring during a porosity test is shown below. The assumptions are: (1) the membrane theory applies, (2) the deflections are small, (3) the material is isotropic, (4) the cloth is taut but not stressed just before the pressure is applied and (5) the cloth assumes a spherical shape after the pressure is applied.

In Figure 4.4.5 let T = tensile stress, lb/in.

p = differential pressure, lb/in.^{2}

E = tensile modulus of elasticity, lb/in.

R = radius of circular opening in holders, in.

ℓ = 2R, in.

$\Delta\ell$ = tensile strain in length , in.

r = radius of spherical shape, in.

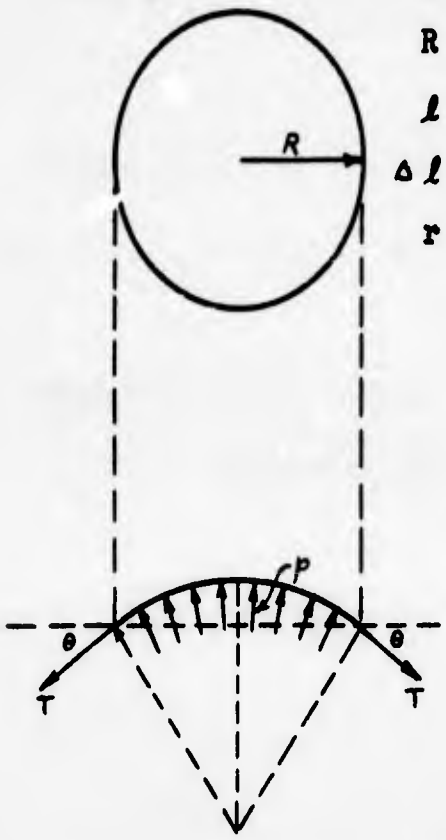

Figure 4.4.5

Spherical Cloth Shape

From statics

$$T \sin\theta\,(2\pi R) = p\pi R^2$$

$$\text{or} \quad T = \frac{pR}{2\sin\theta} \tag{4.4.4}$$

Change in length of a diameter =

$$\Delta R = 2r\theta - 2R \tag{4.4.5}$$

If Poisson's ratio = 0 (see Section 4.2),

$$\Delta\ell = T\ell/E \text{ (Hooke's Law)} \tag{4.4.6}$$

$$\text{then} \quad T = (E/\ell)\,\Delta\ell = (E/R)\,(r\theta - R) \tag{4.4.7}$$

$$\text{and} \quad \frac{pR}{2\sin\theta} = (E/R)\,(r\theta - R) \tag{4.4.8}$$

$$\text{or} \quad (r\theta - R)\sin\theta = pR^2/2E$$

since $r = R/\sin\theta$

$$\theta - \sin\theta = pR/2E \qquad (4.4.9)$$

If the first two terms of the sine series are used in Equation (4.4.9) the error in sin θ is less than $\theta^5/5!$ Therefore in Equation (4.4.9) let sin θ = $\theta - \theta^3/3!$ Then Equation (4.4.9) becomes

$$\theta^3/6 = pR/2E$$

or

$$\theta = \sqrt[3]{3pR/E} \qquad (4.4.10)$$

Equation (4.4.10) can be solved for θ and the result used in Equation (4.4.7) to find T (in Equation (4.4.7) let r = R/sin θ) then

$$T = E\ (\theta/\sin\theta = 1) \qquad (4.4.11)$$

In References 18, 19 and 20, R = 3 in. and pressures up to 50 in. water are used. From Figure 4.3.5,

Rip Stop Nylon Cloth

E = (10) (100)/6.7 = 149 lb/in., for 10 lb/in. in fill direction, variable load in warp direction

E = (10) (100)/8.25 = 121 lb/in., for 10 lb/in. in warp direction, variable load in fill direction.

Use E = ½ (149 + 121) = 135 lb/in.

The solution of Equation (4.4.10) and (4.4.11) are given in Table 4.4.2.

Table 4.4.2 - Cloth Stress During Porosity Test

p		θ				T	
In. Water	Lb/In.^{2}	Radians	Degrees	sin θ	θ/sin θ	Lb/In.	$\Delta_{1/1-T/E}$
1	.036	.13389	7° 40.3'	.13350	1.00292	.394	.00292
20	.720	.36343	20° 49.4'	.35549	1.02234	3.016	.02234
50	1.800	.49324	28° 15.7'	.47350	1.04169	5.678	.04169

By comparing the stresses in the above table with the stresses in a canopy in the steady state, it can be seen that the stresses that occur during a porosity test are much greater; consequently, changes in porosity caused by stresses in a canopy in the steady state of descent are negligible. Since stresses in the opening phase of a descending parachute could be 10 - 100 times those in the steady state, changes in porosity could occur. No data is available concerning the permanence of the large stresses and strains that occur during the opening phase. If such strains lasted as much as, say, 15 minutes, they would affect the porosity during the steady phase. One of the mechanical properties of cloth fibers is that the recovery of large strains is time dependent. A portion of the strain caused by large stresses is instantaneously recoverable. Of the remainder some is permanent and some is recovered after a period of time. If the latter deformation persisted during the steady phase, the porosity would be affected.

5.1 Summary and Conclusions

Analytical methods of predicting the fully inflated shapes of five different types of canopies have been developed. The accuracy of the solutions is indicated by comparisons with photographically determined shapes. The accuracy with which some representative dimensions are predicted is shown in Table 5.1.1.

Table 5.1.1 - Deviations of Theoretical Inflated Canopy Dimensions From Their Photographically Determined Values

Canopy Type	x_{sk}	z_{sk}	θ	x_{gm}	Reference Figure
Flat (T-7)	+1.6%	-0.8%	+1.7%	+4.2%	2.1.5
Extended Skirt (T-10)	+2.0%	+9.0%	+2.5%	+5.0%	2.2.5
Conical	-8.3%	+3.1%	-8.4%	-7.5%	2.3.3
Personnel Guide Surface (C-11)	+0.3%	+2.6%	+0.7%	+6.4%	2.4.4
Conical Ring Slot	+3.2%	-8.9%	+5.7%	+5.5%	2.5.2
Taylor vs Photo T-7	+4.2%	-8.8%	+4.4%	-	2.1.5

The theory for the flat canopy is superior in accuracy to the elementary theory of Stevens and Johns (Reference 2) which predicts a Taylor curve for the cord shape. The Taylor curve remains a very useful approximation, nevertheless, in view of the relative complexity of the new theory. In fact, it forms the basis upon which the new theory was built.

The new theory is applicable, with modifications, to some other types of

canopies, but not to conical canopies, for which an entire new theory was developed. The new theory for the conical canopy checks with photographs less well than does the theory for the flat canopy however.

Table 5.1.2 shows a comparison of the five types of canopies having common l_c, l_s' and N ranking them according to their theoretical load-carrying capacity assuming it to be preportional to the square of the calculated maximum inflated radius (MIR) at any given pressure.

Table 5.1.2 - Comparison of Load-Carrying Capacity of Five Theoretical Canopy Shapes

Section 1.11 - N = 24, l_c/l_s' = 0.6	
1	Personnel Guide Surface
2, 3	Flat, Conical Ring Slot
4	Extended Skirt
5	Conical

As shown in Figure 1.11.1 the personnel guide surface canopy has the largest MIR except for the conical ring slot canopy. The shape of the conical ring slot canopy, however, is determined in Section 1.9 by assuming that it carries the same suspended load as a flat canopy with the same l_c, l_s', and N. Hence the personnel guide surface canopy has the potential to carry the greatest suspended load since it has the largest MIR of the solid canopies. This increased radius is due to the outward force at the pockets of the personnel guide surface canopy.

Table 5.1.3 shows a comparison of the drag characteristics (C_{D_o}) of five similar types of canopies having common cloth area as taken from model tests reported in Reference 24. The flat canopy has the highest drag coefficient (C_{D_o}) of the solid type canopies. For these five canopies the ratio l_c/l_s' varied between 0.47 and 0.54.

Table 5.1.3 - Comparison of Drag Characteristics of Five Canopy Shapes

Reference 24 - Cloth Area = 16,000 Sq. In.	
1	Flat
2	Conical
3	Extended Skirt
4	Personnel Guide Surface
5	Flat Ring Slot

The theoretical comparison does not take into account such items as oscillation, breathing, gliding and cloth porosity which have an important effect on the drag characteristics of the unstable, solid type canopies. All the theoretical shapes have different cloth or sail areas by virtue of assuming a constant l_c. For these reasons a meaningful comparison between Tables 5.1.2 and 5.1.3 cannot be made.

The tensile stresses in the cords are almost constant from apex to risers except in the conical canopy in which the cord stress is zero at the apex. The

cord tension in the conical canopy increases to a maximum at the end of the straight portion, below which it is constant. Cloth stresses vary more or less in the same manner as the cord tensions.

In a straight-cut gore, the cloth stresses are carried almost entirely by the circumferential threads while the "meridonional" threads (actually only the threads parallel to and at the gore centerline are meridional) carry practically no load. In a bias-cut gore the warp and fill threads carry almost equal stresses. Bias gores, therefore, can absorb almost twice as much energy as straight-cut gores, which helps to explain why canopies with bias gores are stronger than those with straight gores.

If, in a flat canopy, the cord length is held constant and the suspension line length varied, both the maximum inflated radius of cord x_m and the vertical distance from the apex to the maximum inflated radius z_m increase as the suspension length is increased. Also the rectangular coordinate x_{sk} of the cord at the skirt increases but z_{sk} decreases with increasing suspension line length. For infinite length of suspension lines the MIR and x_{sk} are coincident. A similar phenomenon occurs when the cone angle of a conical canopy is decreased. As the number of gores is increased, the shape approaches the Taylor curve according to the law $x_m/x_m^T = N/\sqrt{(N+1)(N+2)}$.

Calculations of cloth stresses in an inflated canopy and those occurring during a porosity test indicate that the porosity is negligibly affected by the cloth stresses occurring during the steady descent of a parachute. This may not be true during the opening phase.

The stresses that occur in the fabric, vent reinforcements, seams, and in the cords during steady state descent are relatively small. Probably only stresses occurring during the opening phase are of sufficient magnitude to cause failures.

5.2 Recommendations

An attempt should be made to determine experimentally the shape of the cords over the canopy. Possibly this would show up if black cord lines were used. If not, the coordinates of a cord might be determined in a wind tunnel by a pointer which could be moved in the plane of the cord curve.

Experimental determination of the pattern of threads in an inflated gore should be made by making gores with alternate stripes of colored threads in both warp and fill. These data and those on cord line shape could be used with the intrinsic equation of equilibrium for heavy cords to determine cord tensions and cloth stresses, as suggested in Section 2.7.

Photographs of canopies from directly above or below would be helpful in determining the correct value of $2\alpha_m$, that is, of the central angle of the circular intersection of one gore by the horizontal plane passing through MIR (see Section 1.5).

Further investigation of the effect of cone angle would be desirable in view of the apparent inconsistency of the shapes of conical, conical ring slot, and conical ribbon parachute canopies discussed in Section 1.7.

The results of Section 3.3 suggest a further investigation of the effect of adding extra fullness at the vent in drag parachutes, provided those results are verified by a semi-experimental analysis of cloth stress and cord tension as suggested above.

Biaxial strength and stress-strain data of a kind which can be used for analytical purposes are lacking. Information like that obtained by Haas (Reference 13) for certain airship fabrics, but extended to the ultimate strength, should be sought.

Measurements to determine pressure distributions over the various canopies should be made both to verify the British work and to investigate the importance of canopy shape as a factor.

Because it appears that the opening phase is most important from the structural point of view, it is recommended that an analysis of canopy stresses occurring in this phase be undertaken as soon as possible.

5.3 References

1. Jones, R. "On the Aerodynamic Characteristics of Parachutes". R & M No. 862, June 1953.
2. Stevens, G. W. H. and Johns, T. F. "The Theory of Parachutes with Cords over the Canopy". R & M No. 2320, July 1942.
3. Brown, W. D. "Parachutes". Isaac Pitman & Sons, Ltd., London, 1951.
4. Duncan, W. J., Stevens, G. W. H. and Richards, G. J. "Theory of the Flat Elastic Parachute". R & M No. 2118, March 1942.
5. Beck, E. "The Parachute Considered as a Flexible Shell of Rotation". USAF Translation No. F-TS-3630-RE BR281 of German Report, ATI 32297, November 1942.
6. Reagan, J. F. "A Theoretical Investigation into the Dynamics and Stress Analysis of Parachutes for the Purpose of Determining Design Factors", Daniel Guggenheim Airship Institute Report No. 130, February 1945.
7. Jaeger, J. A., Culver, I. H., and Della-Vedova, R. P. "A Study of the Load Distribution in a Conical Ribbon Type Parachute", Lockheed Aircraft Corporation, Report No. 8641, 22 August 1952.
8. Jahnke, E. and Emde, F. "Tables of Functions with Formulae and Curves," 4th Edition, Dover Publications, New York, 1945.
9. Heinrich, Helmut G. "Aerodynamics, Performance, and Design of Personnel Guide Parachute". Memorandum Report No. WCKE-672-145-A-9-1, Wright Air Development Center, Wright-Patterson AFB, Dayton, Ohio, 21 November 1951.
10. Coe, C. J. "Theoretical Mechanics", MacMillan Co., New York, 1938.
11. Gimalouski, E. A. "Investigation of Impact Load Absorption Through Suspension Line Elongation", WADC TR 52-57, December 1952.

12. Jones, B. "Elements of Practical Aerodynamics", 2nd Edition, John Wiley and Sons, New York, 1939.

13. Haas, R. and Dietzius, A. "The Stretching of the Fabric and Deformation of the Envelope in Non-Rigid Balloons". Springer-Verlag, Berlin, 1912, translated as Report No. 16, Third Annual Report, NACA, 1917, p. 149-271.

14. Coplan, M. J. and Singer, E. "A Study of the Effect of Temperature on Textile Materials", WADC TR No. 53-21, Part 2, July 1953.

15. Booth, H. and Hyde, J. H. "Tests on Balloon Fabrics", R & M No. 57, March 1912, in Report of (British) Advisory Committee for Aeronautics, 1911-12, pp 188-196.

16. Pröll, E. "Experiments with Fabrics for Covering Airplane Wings". Technische Berichte, Vol. 3, No. 3, 1918, p. 57-73. Translated as NACA TN 137, April 1923.

17. McNicholas, H. J. and Hedrick, A. F. "The Structure and Properties of Parachute Cloths". NACA TN 335, March 1930.

18. Goglia, M. J. "Air Permeability of Parachute Cloths". WADC TR 52-283 November 1952.

19. LaVier, H. W. S. "Air Permeability of Parachute Cloths". WADC TR 52-283, Part 2, August 1953.

20. Goglia, M. J., LaVier, H. W. S. and Brown, C. D. "Air Permeability of Parachute Cloths", Textile Research Journal, Volume XXV, April 1955, pp. 296-313.

21. LaVier, H. W. S. "Air Permeability of Parachute Cloths, Part 3. Effect of Loading on Elastic Properties of Parachute Cloths without Air Flow". WADC TR 52-283, Part 3, January 1955.

22. Woo, H. K., and Montgomery, D. J. "Effects of Construction and Fiber Type on Two-Dimensional Stress-Strain Properties of Fabrics". Textile Research Journal, Vol. 23 No. 12, p. 925-929, 1953.

23. Everling, E. "Simplified Characteristic Lines for Wing Covering Fabric". Zeitschrift für Flugtechnik und Motorluftschiffart, Vol. 11, No. 2, January 1920 , pp 23-25. (German)

24. Stimler, F. J. and Ross, R. S. "Drop Tests of 16,000 Sq.-In. Model Parachutes". Volume VIII Summary Report, AFTR-5867, Goodyear Aircraft Corporation, May 1954.